Chemically Fueled Polymer Materials: From Self-Assembly to Functional Devices

Dissertation
zur Erlangung des Grades
„Doktor der Naturwissenschaften“
im Promotionsfach Chemie

am Fachbereich
Chemie, Pharmazie, Geographie und Geowissenschaften
der Johannes Gutenberg-Universität Mainz

Giorgio Fusi
geb. in Varese, Italien

Mainz, October 2024



Abstract

Living organisms are complex systems capable of exhibiting emergent behavior such as sensing, interacting with and adapting to their environment. This behavior is enabled by the spatial, temporal and hierarchical organization of their component processes, which operate out of thermodynamic equilibrium through constant consumption of high-energy input molecules. Such dissipative systems provide a prime example for next-generation materials, capable of dynamic and autonomous operation. One key step in achieving such materials has been employing chemical reaction networks (CRNs) driven by chemical fuels to either directly control material properties or modulate key input stimuli over time. Despite great progress in this regard, the step from autonomously operating, out of equilibrium CRNs and functional devices driven by them remains an open field for exploration. Polymeric materials provide an excellent opportunity, due to the ease with which they can be tailored to a specific application.

This thesis presents the use of chemically fueled CRNs that operate both by a direct activation, active material pathway and to control an out-of-equilibrium active environment. These are employed control the behavior of polymeric materials based on the dually responsive dicarboxylic acid building block aspartic acid *N*-acrylamide (A^3).

The first example employs the carbodiimide-fueled formation of anhydrides to drive the self-assembly of block copolymers (BCPs). This active material CRN relies on direct activation of A^3 by the fuel molecule, with deactivation occurring through hydrolysis of the anhydride. By altering BCP architecture, a range of self-assembled morphologies can be targeted. Altering the ratio of responsive A^3 units to unresponsive hydrophobic units in the responsive segment, fuel efficient self-assembly, arising from reduced fuel requirements for increased self-assembly lifetimes, is demonstrated.

By employing tribromoacetic acid (TBA) as a chemical fuel to drive an active environment CRN, the second example in this thesis demonstrates the use of a one-molecule pH control mechanism to control the self-assembly of BCPs in solution. The CRN is characterized by a rapid pH drop on addition of fuel, which drives BCP self-assembly due to protonation of carboxylate groups in the A^3 unit, and a slow rise back to original pH, during which the polymer assemblies disassemble. The threshold assembly and disassembly pH can be controlled by altering the composition of the pH-responsive BCP segment, and the lifetime and magnitude of the transient pH drop is controlled through the interplay of fuel loading, buffer concentration, and the self-buffering effect of the polymer itself. These results are used to construct a kinetic model capable of accurately predicting the evolution of pH over time in the system.

Finally, the TBA CRN is employed to control the transient deswelling of pH-responsive poly(A^3) hydrogels. The lifetime of the pH drop is tailored to match the kinetics of gel deswelling, and the transiently deswelling hydrogels are coupled to unresponsive gels to obtain bilayer actuators. Both the magnitude and duration of actuation can be controlled by altering fuel loading. Autonomous harpoons capable of object capture and self-locking active interfaces demonstrate the unique benefits of this control mechanism for soft robotic devices. An additional layer of chemomechanical feedback is included by coupling actuating devices to a mechanically-gated urea-urease reaction. By demonstrating the application of this CRN to macroscopic soft robotic devices, a pathway from CRN implementation to functional devices is laid out.

Zusammenfassung

Lebende Organismen sind komplexe Systeme, die emergentes Verhalten zeigen, indem sie ihre Umwelt wahrnehmen, mit dieser interagieren und sich an diese adaptieren. Dieses Verhalten wird durch die räumliche, zeitliche und hierarchische Organisation ihrer Teilprozesse ermöglicht, die durch den ständigen Verbrauch energiereicher Antriebsmoleküle aus dem thermodynamischen Gleichgewicht gebracht werden. Diese dissipativen Systeme sind ein hervorragendes Beispiel für die nächste Generation von Materialien, die zu dynamischem und autonomem Betrieb fähig sind. Ein wichtiger Schritt auf dem Weg zu solchen Materialien ist der Einsatz chemischer Reaktionsnetzwerke (CRN), die durch chemische Treibstoffe angetrieben werden, um entweder die Materialeigenschaften direkt zu steuern oder wichtige Stimuli im Laufe der Zeit zu modulieren. Trotz großer Fortschritte in dieser Hinsicht bleibt der Schritt von autonom arbeitenden, aus dem Gleichgewicht geratenen CRNs zu funktionalen Geräten, die durch sie angetrieben werden, ein offenes Feld für die Erforschung. Polymere Materialien bieten eine hervorragende Gelegenheit, dies zu tun, da sie leicht für eine bestimmte Anwendung zugeschnitten werden können.

In dieser Dissertation werden chemisch angetriebene CRNs vorgestellt, die sowohl über eine direkte Aktivierung als auch über einen aktiven Materialpfad funktionieren und einen Umweltstimulus als aktive Umgebung außerhalb des Gleichgewichts steuern, um das Verhalten von Polymermaterialien auf der Grundlage des doppelt reaktionsfähigen Dicarbonsäure-Bausteins Asparaginsäure-N-Acrylamid (A^3) zu kontrollieren.

Das erste Beispiel nutzt die Carbodiimid-getriebene Bildung von Anhydriden, um die Selbstorganisation von Block-Copolymeren (BCPs) voranzutreiben. Dieses aktive Material CRN beruht auf der direkten Aktivierung von A^3 durch das Antriebsmolekül, wobei die Deaktivierung durch Hydrolyse des Anhydrids erfolgt. Durch Veränderung der BCP-Architektur kann eine Reihe von selbstorganisierenden Morphologien erreicht werden. Durch Veränderung des Verhältnisses von reaktiven A^3-Einheiten zu nicht reaktiven hydrophoben Einheiten im reaktiven Segment wird eine treibstoffeffiziente Selbstorganisation demonstriert, die sich aus einem geringeren Treibstoffbedarf bei längerer Dauer der Selbstorganisation ergibt.

Durch den Einsatz von Tribromessigsäure (TBA) als chemischer Treibstoff zum Antrieb eines aktiven Umgebungs-CRN demonstriert das zweite Beispiel in dieser Dissertation die Verwendung eines Ein-Molekül-pH-Kontrollmechanismus zur Kontrolle der Selbstorganisation von BCPs in Lösung. Das CRN ist durch einen schnellen pH- Abfall bei der Zugabe von Treibstoff gekennzeichnet, der die Selbstorganisation von BCPs aufgrund der Protonierung von Carboxylatgruppen in der A^3-Einheit antreibt, sowie durch einen langsamen Anstieg zurück zum ursprünglichen pH-Wert, während dessen sich die Polymer-Assemblierungen wieder auflösen. Der Grenzwert für den Zusammenbau und den Abfall des pH-Wertes kann durch Änderung der Zusammensetzung, des auf den pH-Wert reagierenden BCP-Segments, gesteuert werden. Die Dauer und das Ausmaß des vorübergehenden pH-Wert-Abfalls werden durch das Zusammenspiel von Treibstoffmenge, Pufferkonzentration und dem Selbstpuffereffekt des Polymers selbst gesteuert. Diese Ergebnisse werden verwendet, um ein kinetisches Modell zu konstruieren, das die Entwicklung des pH-Werts im Laufe der Zeit in dem System genau vorhersagen kann.

Schließlich wird das TBA CRN eingesetzt, um die vorübergehende Abschwellung von auf den pH-responsiven Poly(A^3)-Hydrogelen zu steuern. Die Dauer des pH-Abfalls wird auf die Kinetik

des Abschwellens des Gels abgestimmt, und die vorübergehend abschwellenden Hydrogele werden mit nicht responsiven Gelen gekoppelt, um Doppelschicht-Aktuatoren zu erhalten. Sowohl das Ausmaß als auch die Dauer der Bewegung können durch Veränderung der Treibstoffzufuhr gesteuert werden, und es werden einzigartige Anwendungen demonstriert. Dabei wird die autonome Natur des CRN genutzt, wie z. B. in autonomen Harpunen, die Objekte einfangen können, und selbstsichernde aktive Schnittstellen. Eine zusätzliche Ebene der chemomechanischen Rückkopplung wird durch die Kopplung von Aktuatoren mit einer mechanisch gesteuerten Harnstoff-Urease-Reaktion eingeführt. Durch die Demonstration der Anwendung dieses CRN auf makroskopische Soft-Roboter wird ein Weg vom CRN zu funktionalen Geräten aufgezeigt.

Contents

Abstract iii

Zusammenfassung iv

Contents vi

Abbreviations x

1. Introduction 1

1.1. Motivation 1

1.2. Responsive and Out-Of-Equilibrium Systems 2

1.3. Chemical Fuels for Direct Activation of Materials 5

1.3.1. Methylating Agents 5

1.3.2. Carbodiimide Fuels 7

1.3.3. Building Block Design in Self-Assembling Systems 8

1.3.4. EDC-Fueled Solution-Phase Polymer Systems 10

1.3.5. EDC-Fueled Crosslinked Polymer Systems 12

1.3.6. Other Fuels for Direct Activation of Polymer Materials 13

1.4. Active Environments 16

1.4.1. Redox Oscillators 16

1.4.2. pH oscillators 17

1.4.3. pH Control in Batch Settings 19

1.4.4. Activated Carboxylic Acids 23

1.5. Scope of the Thesis 26

1.6. References 29

2. Chemically-Fueled Self-Assembly of Amphiphilic Copolymers: Targeting Fuel Efficiency Through Polymer Design 36

2.1. Abstract 36

2.2. Introduction 36

2.3. Results and Discussion 38

2.3.1. Design and synthesis of Poly(NAM)-*b*-(A^3-*co*-*t*-BuAm) Copolymers 38

2.3.2. Block Copolymer Self-Assembly 41

2.4. Conclusions 54

2.5. Supplementary Information 54

2.5.1. Materials and Methods 54

2.5.2. Dynamic Light Scattering 60
2.5.3. Transmission Electron Microscopy and Cryo-TEM. 61
2.5.4. Statistical Analysis 61
2.5.5. Supplementary Note: Plate Reader Turbidity Measurements 61
2.5.6. Supplementary Note: Self-Assembly of Methylated Polymers 63
2.6. Acknowledgements 65
2.7. References 65
3. Tribromoacetic Acid as a Chemical Fuel for Self-Assembly of pH-responsive Block Copolymers 70
3.1. Abstract 70
3.2. Introduction 70
3.3. Results and Discussion 72
3.3.1. Synthesis and Characterization of pH-Responsive Block Copolymers 72
3.3.2. Tribromoacetic Acid-Fueled Self-Assembly 74
3.3.3. Modelling the TBA Reaction Cycle 76
3.4. Conclusion 80
3.5. Supplementary Information 81
3.5.1. Materials and Methods 81
3.5.2. Synthesis Procedures 81
3.5.3. Titrations 82
3.5.4. Fueling Experiments (Turbidity) 82
3.5.5. Fueling Experiments (pH) 82
3.5.6. Statistical Analysis 83
3.5.7. Supplementary Note: Additional Turbidity Fueling Experiments 83
3.5.8. Supplementary Note: Measuring pH over the Course of Fueling 84
3.5.9. Supplementary Note: Modelling the TBA Fuel Cycle 85
3.6. Acknowledgements 110
3.7. References 110
4. Autonomous Soft Robots Empowered by Chemical Reaction Networks 114
4.1. Abstract 114
4.2. Introduction 114
4.3. Results and Discussion 115
4.3.1. Coupling a Self-Decarboxylating Acid to a Responsive Hydrogel 115

4.3.2. Exploiting Transient Deswelling for Actuating Elements 117
4.3.3. Temporal Pre-Programming for Fire and Forget Devices 119
4.3.4. Coupling to Urea / Urease Reaction for Chemomechanical Feedback 120
4.4. Conclusion 122
4.5. Supplementary Information 123
4.5.1. Instrumentation and Materials 123
4.5.2. Synthesis Procedures 123
4.5.3. pH measurements 125
4.5.4. Swelling and Fueling Experiments 126
4.5.5. Mechanical Analysis of Gels 127
4.5.6. Statistical Analysis 127
4.6. Acknowledgements 128
4.7. References 128
5. Conclusions 132
5.1. Conclusions 132
5.2. References 134
6. Acknowledgements 136

Abbreviations

A^3	Aspartic acid *N-a*crylamide
AA	Acrylic acid
ABTS	2,2'-azino-bis(3-ethylbenzothiazoline-6-sulfonate)
ACA	Activated carboxylic acid
AIBN	Azobisisobutyronitrile
Am	Acrylamide
AMPS	2-acrylamido-2-methylpropane sulfonic acid
ATP	Adenosine triphosphate
BCP	Block copolymer
BME	β-mercaptoethanol
bpy	Bipyridyl
BSF	Bromate-sulfite-ferrocyanide
BZ	Belousov-Zhabotinsky (reaction)
CMC	Critical micelle concentration
CPDT	2-cyano-2-propyl dodecyl trithiocarbonate
CRC	Chemical reaction cycle
CRN	Chemical reaction network
Cryo-TEM	Cryogenic transmission electron microscopy
CSTR	Continuous stirred tank reactor
CTA	Chain transfer agent
DBU	Diazabicycloundecene
DD	Dormant deactivator
DLS	Dynamic light scattering
DMA-*b*-4VP	Dimethylacrylamide-*b*-4-vinylpyridine
DMAP	Dimethylaminopyridine
DMS	Dimethylsulfate
DNA	Deoxyribonucleic acid
DVP	Divinylpyridine
EDC	*N*-ethyl-*N*'-(3-dimethyl-aminopropyl)carbodiimide
Fmoc	Fluorenylmethoxycarbonyl
GOx	Glucose oxidase

GPC	Gel permeation chromatography
HRP	Horseradish peroxidase
LAP	Lithium phenyl-2,4,6-trimethylbenzoylphosphinate
LCST	Lower critical solution temperature
MALDI-ToF MS	Matrix-assisted laser desorption ionization time-of-flight mass spectrometry
MBH	Morita-Baylis-Hillman (reaction)
MES	2-(N-morpholino)ethanesulfonic acid
MGS	Methylene glycol-sulfite-gluconolactone
MOPS	2-(N-morpholino)propanesulfonic acid
NAM	*N*-acryloylmorpholine
NIPAm	*N*-isopropylacrylamide
NMR	Nuclear magnetic resonance
PAA	Poly(acrylic acid)
PAm	Poly(acrylamide)
PDEAEMA	Poly(diethylaminoethyl methacrylate)
PDI	Polydispersity index
PDMS	Poly(dimethylsiloxane)
PEG	Poly(ethyleneglycol)
PEGDA	Poly(ethyleneglycol) diacrylate
PEG-P2VP	Poly(ethylene glycol)-*b*-poly(2-vinylpyridine)
PEO	Poly(ethylene oxide)
PISA	Polymerization-induced self-assembly
PMAA	Poly(methacrylic acid)
PNAM	Poly(*N*-acryloylmorpholine)
PNDAc	Poly(norbornene dicarboxylic acid)
PNIPAm	Poly(*N*-isopropylacrylamide)
SBML	Systems Biology Markup Language
TBA	Tribromoacetic acid
TRIS	Tris(hydroxymethyl)aminomethane
***t*-BuAm**	*Tert*-Butylacrylamide
TEM	Transmission electron microscopy
UCST	Upper critical solution temperature

Chapter

1 Introduction

1.1. Motivation

A living organism is a complex system composed of interconnected chemical processes that are spatially, temporally, and hierarchically organized. This intricate organization enables living organisms to exhibit behaviors far more complex than the sum of their individual processes. While attempting a general definition of life is fraught with pitfalls, it can be agreed that the fundamental goal of life is reproduction - the process of passing on genetic information to subsequent generations. Indeed, common definitions describe life as a self-sustaining chemical process capable of Darwinian evolution through self-replication.[1-2] To support this goal, a living organism must be capable of maintaining homeostasis and organizing its component processes, which are also frequently included as criteria for life.[3-4] To achieve these functions, an organism interacts with its environment, sensing, adapting to, and responding to external stimuli, through the interface of complex biomaterial systems such as rod and cone cells in the eyes or skin receptors for sensing, muscles for locomotion and neurons for information processing.

Inspired by and attempting to improve on these exceptional properties of natural material systems, the last two centuries have seen an astounding increase in the discovery and manufacture of novel synthetic materials, of which the most ubiquitous are polymers. Since the introduction of Staudinger's macromolecular theory,[5-6] a wide array of synthetic polymers has been introduced for a myriad of applications, based on an equally broad chemical space of repeating units. Advances in polymer design have yielded materials capable of responding to the very same set of stimuli living organisms do,[7-8] be they physical such as temperature,[9] light[10] or mechanical stress,[9] or chemical signals, such as pH.[11-12] It is, however, the integration of stimuli responsive materials into complete systems that allows them to be exploited for real-world and life-like applications.

Two types of systems where stimuli-responsive polymers have been extensively studied are solution-phase self-assembly,[7,13-18] particularly with a view to controlled release in a therapeutic context,[19] and stimuli-responsive hydrogel devices, of particular interest in the realm of non-electronic actuators and soft robotics.[20-25] These two types of systems are effectively two sides of the same coin, being controlled by the balance of polymer-polymer and polymer-solvent interactions, which are modulated by external stimuli. In both examples, polymer architecture is key. In the case of self-assembling systems, part of the polymer must drive the self-assembly process by favoring polymer-polymer interactions, while another part must act to stabilize the assemblies in solution. For this reason, block copolymers (BCPs), composed of two or more such segments, are often employed.[7,15,17,26-31] In systems featuring hydrogel materials as actuating elements, the primary goal is to achieve changes in network swelling, and therefore a volume change that can be exploited for mechanical motion.[32] This places significant importance on the choice of responsive unit based on, for example, factors such as its pK_a in pH-responsive systems

or the lower critical solution temperature (LCST) and desired system temperature range for thermally-responsive systems.

To date, however, the vast majority of such polymer systems are only classically responsive. That is, they respond to a change in the thermodynamic landscape achieving the new lowest-energy equilibrium state. To achieve more lifelike systems capable of intelligent, autonomous operation, more complex, time-defined control over both the stimulus experienced by the material and the material's response to said stimulus must be achieved.[33-34] One approach to this problem is to take inspiration from the out-of-equilibrium systems seen in nature.

The following introduction contains a qualitative discussion of the thermodynamics of out-of-equilibrium systems, focusing on chemically fueled dissipative systems. By discussing key examples from the state of the art, we discuss both active material and active environment systems. In each category, we explore key historical and current examples, leading to those most relevant to the context of this thesis. Namely, carbodiimide fueling in the active material context, and pH modulation in that of active environments. By discussing their operation and application, we highlight their benefits and drawbacks, how they can be applied to polymeric materials, with a particular focus on polymer self-assembly and hydrogels.

1.2. Responsive and Out-Of-Equilibrium Systems

The initial step in achieving the goal of life-like materials is to design a responsive system that can respond to stimuli by switching between two thermodynamically stable states (Figure 1.1a), where these stimuli take the form of two opposing triggers ("on" stimulus/"off" stimulus or stimulus/anti-stimulus). Taking the example of solution phase self-assembly, one can imagine a thermodynamically stable state where the building blocks exist as individual units in solution (State A). Until an appropriate stimulus is provided, no self-assembly will take place. On application of this stimulus, the thermodynamic landscape of the system shifts, and the building blocks are driven to self-assemble (State B). They remain in this state until a reverse stimulus is applied. Self-assembly is driven by the minimization of Gibbs free energy, G,[35] and therefore by entropy maximization and/or enthalpy minimization.[36] When they reside at the global thermodynamic minimum, systems are termed equilibrium self-assemblies. If these systems instead reside at local energy minima, with energetic barriers larger than available kinetic energy, these are termed kinetically trapped assemblies.[37]

More complex behavior, such as autonomous assembly and disassembly with the application of a single stimulus, cannot be achieved by applying stimulus and anti-stimulus contemporaneously, as their effects would cancel out. This can be circumvented by designing a system where the desired "on" state lies out of both thermodynamic equilibrium and any local minima (Figure 1.1b). In such a case, the assembled state can only exist as long as energy is provided to it. Since a constant supply of energy, which is then lost, or dissipated, is required to maintain the desired assembled state, such examples have come to be known as dissipative systems.[38-39]

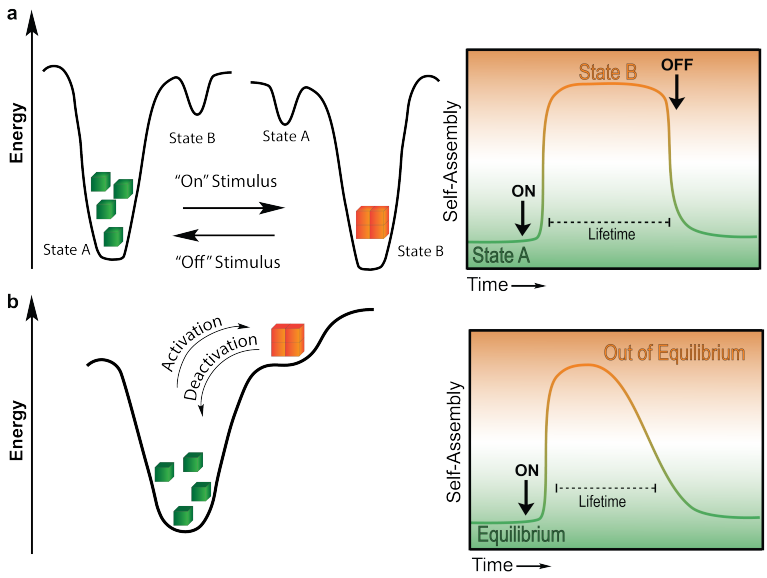

Figure 1.1: Two different cases for stimuli-responsiveness. (a) Static assemblies reside at energetic minima and are stable as long as they are exposed to conditions which bias the energy landscape in their favor. (b) Dissipative assemblies exist in a dynamic quasi-steady state where activation and deactivation reactions are in equilibrium. To sustain this high-energy quasi-steady state, the system constantly consumes chemical fuel as part of the activation reaction. Once fuel is depleted, building blocks are increasingly deactivated until the system returns to equilibrium.

Dissipative systems where energy is provided by a chemical reaction network (CRN), consuming chemical energy in the form of input molecules have been commonly termed chemically fueled systems.[33,38,40-42] While this terminology has proven controversial,[43] it is, at the very least, helpful in identifying the role of components in a CRN and aids in understanding at a conceptual level, and will therefore be employed throughout this thesis.

The simplest possible CRN (Figure 1.2a) is composed of two reactions, the first being an activation reaction, where the substrate is irreversibly converted, consuming energy and forming a self-assembling or otherwise out-of-equilibrium intermediate product. Deactivation occurs as a spontaneous reaction where the high-energy intermediate is consumed to yield the original building block, in most cases additionally a waste product.

Chemically fueled systems can be divided into two broad categories based on their mechanism of activation (Figure 1.2b).[33] In an active material system, energy uptake occurs at the level of individual building blocks by direct reaction with a chemical fuel. Building blocks act as an integral component of the CRN, participating in activation reactions, provided there is fuel available, and deactivation. Because of this concurrent activation and deactivation, there is a turnover in building blocks within assemblies over time, and these systems can exhibit persistent dynamic behaviors, for example self-healing.[44-45] An assembly can be disrupted (for example, mechanically), but due to the constant supply of freshly activated building blocks, can repair where it is damaged.

Active environment systems experience a global, system-wide change in chemical potential driven by the chemical fuel. Like static systems, activation and deactivation is simultaneous for all building blocks but, in this case, it is the stimulus that is autonomous, with a CRN modulating the concentration of some key activating species over time, and building blocks are simply coupled to the stimulus. The building blocks can be thought of as being at a temporary equilibrium with their out-of-equilibrium surroundings. Therefore, these systems tend to lack dynamic character at the

scale of individual building blocks, and are better suited for autonomous control of macroscopic properties, such as gel formation or hydrogel actuation.

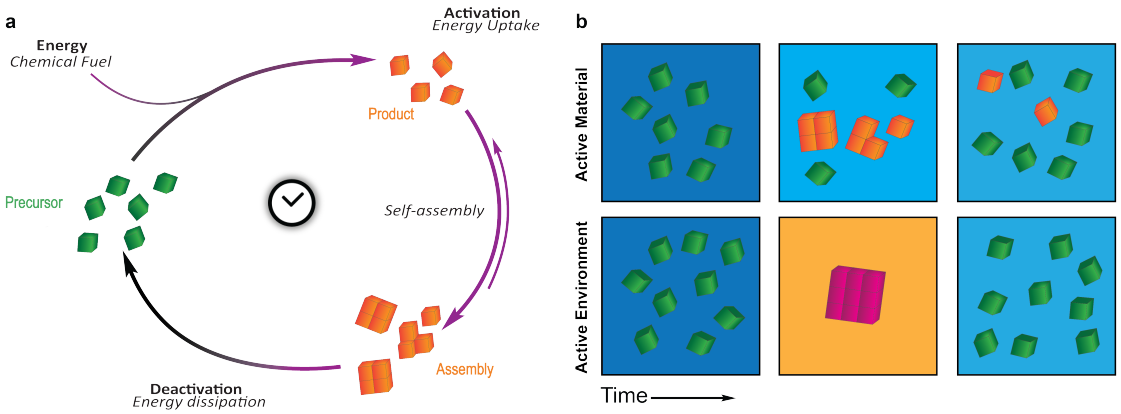

Figure 1.2: Fundamentals of chemically fueled dissipative systems. (a) Minimal reaction cycle necessary for a dissipative system, consisting of activation and deactivation reactions. (b) The two principal types of chemically fueled systems. Active material systems rely on the direct activation of responsive units, with concurrent activation and deactivation reactions. Active environments instead rely on a kinetically decoupled system-wide change, with simultaneous activation and deactivation of each responsive unit.

In both active material and active environment systems the pathways for activation and deactivation must be decoupled to prevent the annihilation of stimuli.[41,46] In active material systems this is achieved by tuning the rate constants of activation and deactivation to obtain a significantly faster activation reaction. This may be improved upon by employing catalysis to increase the rate of activation,[47] or chemo-structural feedback mechanisms to modify the rates of activation and deactivation.[48-50] Active environment systems instead necessitate a built-in temporal separation of activation and deactivation. As will be discussed below, this can be achieved by gating the deactivation reaction such that it can only commence once the activated state is reached,[51] or by generating the deactivating species directly from the consumed fuel.[52-53] Changes in the environment can also be leveraged to tune the catalytic generation of (de)activating species over time, for example in enzymatic systems.[54-55]

1.3. Chemical Fuels for Direct Activation of Materials

Direct activation of materials by a chemical fuel, at its simplest, involves kinetically asymmetrical activation and deactivation reactions. This constraint necessitates the use of highly reactive molecules as fuel. The following is an overview of the most impactful and widespread chemical fuels, with a particular view to applications in polymeric materials.

1.3.1. Methylating Agents

Interest in chemically-fueled systems was first generated by reports from van Esch and coworkers of small-molecule self-assembly fueled by methyl iodide (Figure 1.3a).[38] The dicarboxylate building block dibenzoyl-(L)-cysteine (DBC) reacts with the methyl iodide to yield mono and di-methyl esters. The methylation reaction neutralizes negative charges present in the carboxylate groups, and leads to transient self-assembly of DBC into a fibrous network. Hydrolysis of the esters acts as the deactivating reaction, dissipating chemical energy and returning the building block to its original state. Although the rate of the methylation reaction could be tuned somewhat by tuning the system pH and concentration of fuel, the timescale of activation proved very long (hundreds of hours). To overcome this, dimethylsulfate (DMS), a much stronger methylating agent, can be employed.[56-57] This leads to a significantly faster activation step, and allows system pH to be tuned such that the hydroxide-mediated deactivation reaction also occurs faster, allowing for shorter gel lifetimes when using DBC as a building block (Figure 1.3b).[56] Use of methylating agents as fuel has also been demonstrated in polymeric materials.[57] Colloidal polystyrene particles decorated with an inner shell of hydrophilic poly(*N*-isopropylacrylamide) (PNIPAm) and an outer shell of pH-responsive poly(methacrylic acid) (PMAA) dispersed in alkaline aqueous solution are electrostatically stabilized by the negatively charged PMAA segment. DMS-fueled methylation of the PMAA carboxylate groups removes these stabilizing charges, leading to transient clustering of the particles (Figure 1.3c).[57]

While chemically fueled methylation acts as a prototypal example of a chemical fuel cycle, and initiated interest in the field of fueled self-assembly, it suffers from significant drawbacks as a method. Firstly, methylating agents are by their very nature highly toxic, limiting real-world applications and secondly, the deactivating hydrolysis reaction is impractically slow for any desired lifetimes below the tens of hours.

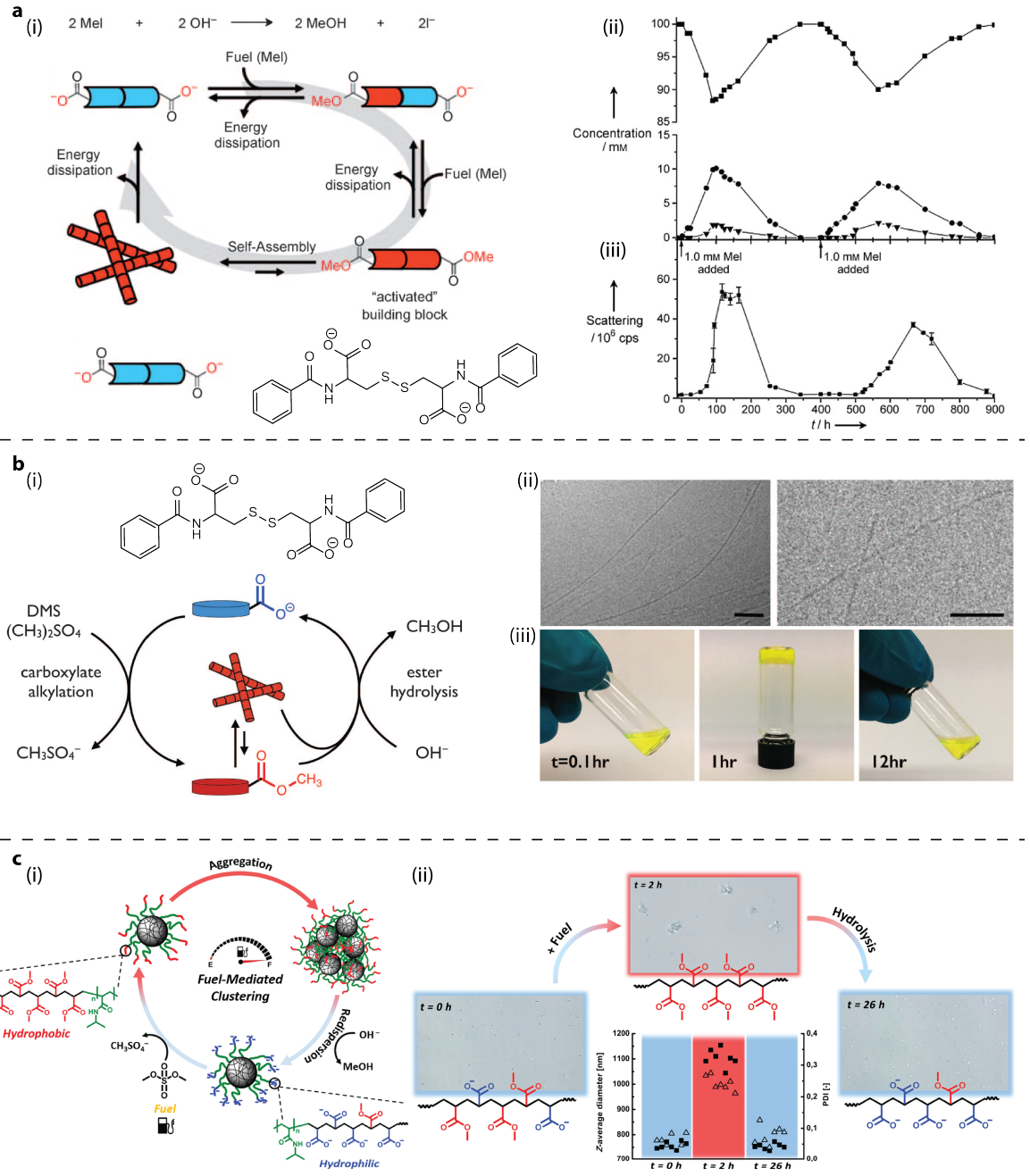

Figure 1.3: Methylating agents as chemical fuels for self-assembly. (a) Use of methyl iodide to fuel assembly of DBC. (i) General scheme for the reaction cycle. (ii) Concentration profiles for DBC (squares) DBC-Ome (circles) and DBC-$(OMe)_2$ (triangles) over the course of two fueling cycles. (iii) Transient aggregation monitored *via* light scattering coincides with increase in methylated species. Adapted from [38] with permission from Wiley. (b) Use of DMS as a fuel to drive the assembly of carboxylate building blocks. (i) General scheme of the reaction cycle. (ii) Cryo-TEM micrographs of fibers formed by methylation of DBC, scale bars = 100 nm. (iii) Vial inversion test demonstrating the formation of a stiff hydrogel by fiber formation. Adapted from [56] with permission from the AAAS. (c) DMS-fueled clustering of polystyrene particles decorated with PNIPAm-PMAA. (i) When in a basic aqueous medium, the PMAA corona on the particle is charged, providing colloidal stability through electrostatic repulsion. Methylation with DMS neutralizes these charges, and additionally renders the PMAA segments hydrophobic, driving aggregation. Hydrolysis of these methyl esters leads to redispersion. (ii) Transient fuel-driven clustering observed by optical microscopy and dynamic light scattering. Adapted from [57] with permission from the American Chemical Society.

1.3.2. Carbodiimide Fuels

To overcome the limitations of methylating agent fuels, the carbodiimide fuel cycle has been developed. The cycle relies on activation of a carboxylate group in the substrate by a carbodiimide to yield an activated *O*-acylurea. The activated *O*-acylurea then reacts with an additional carboxyl group to generate an anhydride (Figure 1.4a). Similarly to methylation of carboxylic acids, anhydride formation both neutralizes any charges present on carboxyl groups and leads to a general decrease in water-solubility, which acts as a driving force for self-assembly and phase-change processes in the fueled systems. Crucially, anhydride formation can be between vicinal carboxylates, leading to building block activation by the formation of a cyclic anhydride, or between carboxylates that are non-neighboring or part of different molecules, which can be used both to generate assembling blocks from two coupled monocarboxylates, or be exploited to form transient crosslinks. As we show in examples below, the former case is particularly useful in self-assembly applications, whereas the latter is most relevant in the context of macroscopic polymer and hydrogel materials.

This first case was demonstrated when the fuel system was pioneered in 2017 by Boekhoven,[58] using short peptides with aspartic (D) and glutamic acid (E) at the C-termini, which on activation by a carbodiimide undergo ring-closure to form five and six-membered anhydrides. Alongside the fluorenylmethoxycarbonyl (Fmoc) functionalized N-termini allowing for hydrophobic interactions, the formation of the anhydrides renders the peptides insoluble in aqueous buffer, driving their self-assembly into a number of structures, ranging from colloidal droplets for Fmoc-E to spherulites for Fmoc-D and fibrillar assemblies in the case of Fmoc-AVD (where A and V are glutamic acid and valine, respectively, Figure 1.4a), which formed weak hydrogels that disassembled on complete hydrolysis of the anhydrides. By enclosing the Fmoc-D peptide into a polyacrylamide hydrogel and applying *N*-ethyl-*N*'-(3-dimethyl-aminopropyl)carbodiimide (EDC) fuel in a pattern, the authors were able to write on the gel as a "self-erasing ink" – areas where EDC was applied turned turbid due to the formation of spherulites, but once again became transparent as the fuel was consumed and the spherulites disassembled (Figure 1.4a).

The use of EDC by the Hartley group the same year illustrated the use of non-neighboring carboxylates to yield crown ether-like macrocycles and linear polymers by coupling oligoethylene glycols featuring terminal carboxylates (Figure 1.4b).[59] Examples by the same authors in polymer systems will be discussed below.

Additional benefits of this fuel system over methylating agents are the increased half-life of EDC in aqueous systems (4 to 35 hours, depending on pH,[60] versus 1.5 hours for DMS), and faster deactivation of the formed anhydrides by water, with a half-life on the order of seconds to a few minutes based on system pH.[58,61] One drawback the system often presents is the requirement for fueling in excess to overcome the rapid deactivation rate.

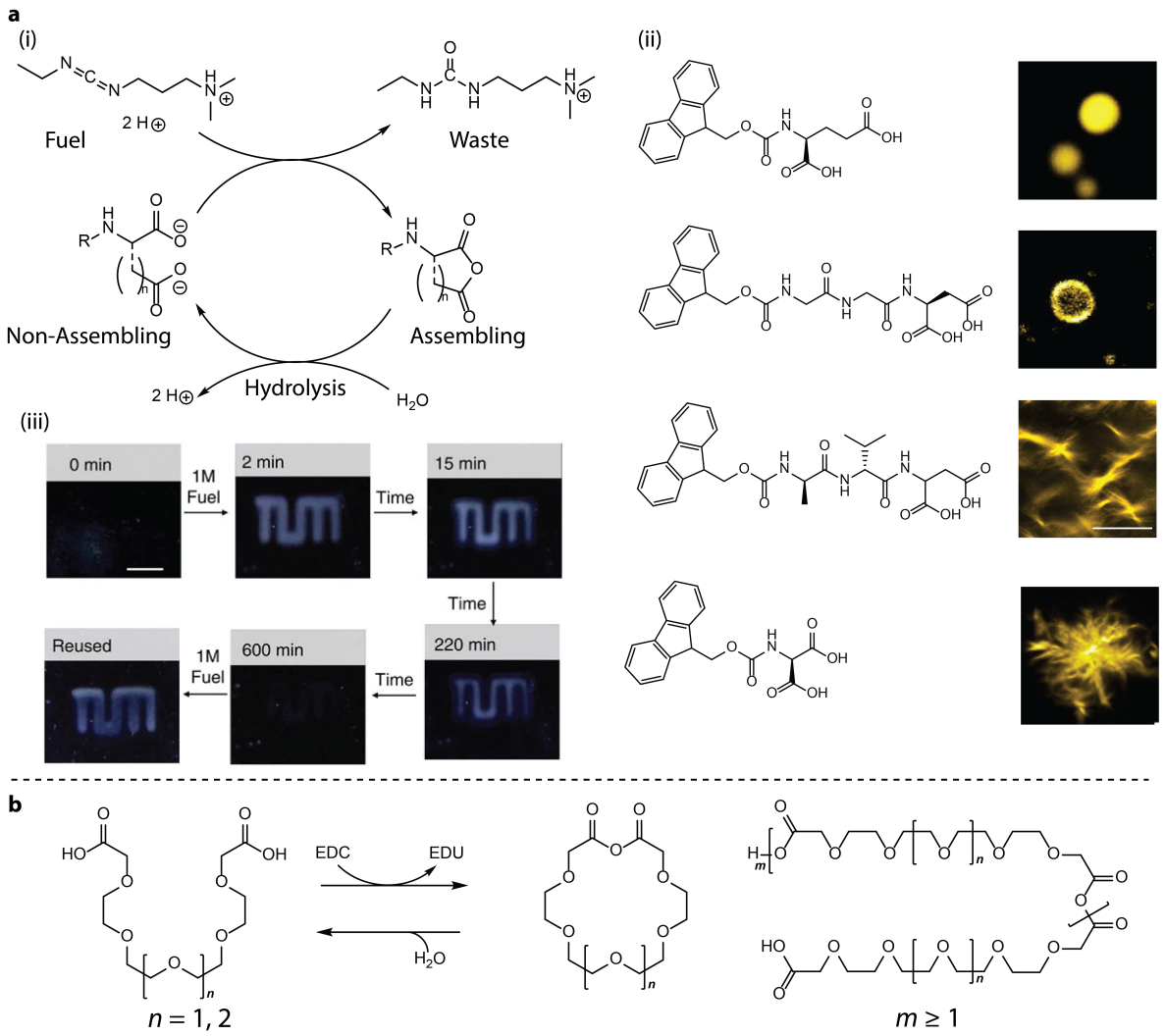

Figure 1.4: Pioneering works in EDC-fueled systems. (a) EDC-fueled assembly of peptides by charge neutralization *via* anhydride ring formation. (i) General scheme for EDC-fueled anhydride formation in dicarboxylate substrates. (ii) Effect of peptide sequence on morphology of fueled assemblies. Top to bottom: Fmoc-E – droplets, Fmoc-GGD – vesicles, Fmoc-AVD – fibers, Fmoc-D – spherulites. (iii) Self-erasing ink composed of Fmoc-D embedded in PAm hydrogel. Application of EDC in a pattern (writing) induces spherulite assembly and increase in local turbidity. When the fuel is exhausted, the spherulites disassemble and the gel returns to transparent. Amino acid one letter codes A, D, E, G and V correspond to alanine, aspartic acid, glutamic acid, glycine and valine, respectively. Adapted from [58], published under CC-BY 4.0 by Springer Nature. (b) EDC-fueled assembly of oligoethylene glycol diacids into macrocyclic and polymeric anhydrides. Relative yields of macrocycles and polymeric species can be controlled by addition of metal ions. Adapted from [59] with permission from the American Chemical Society.

1.3.3. Building Block Design in Self-Assembling Systems

Having established the mechanism and fundamentals of EDC-fueled self-assembly, it is worth considering how control over both the morphology and lifetime of assemblies can be introduced. The EDC fuel cycle leaves little room to tune lifetime on the CRN side beyond simply altering fuel loading or system pH, which modulates both the rate of background fuel hydrolysis and anhydride deactivation. One method to introduce this control is altering the structure of the building blocks. As can be expected, altering peptide sequence in peptide building blocks alters the packing parameters alongside the balance of hydrophobic and hydrogen bonding interactions

between the activated building blocks. Changes in peptide sequence have yielded transiently assembled fibers,[48,50,58,62-63] vesicles,[64] and colloidal droplets.[58,65] The very same changes in interactions that control assembly morphology can be leveraged to control the lifetime of assemblies by achieving kinetic trapping[50] or modulating the rates of (de)activation reactions through chemo-structural feedback (Figure 1.5).

Altering peptide sequence to include additional hydrophobic residues allows for co-assembly of activated (anhydride-terminated) and un-activated peptides.[48] Carboxylate groups present in the unreacted building blocks are able to provide protons in a concerted fashion to EDC, accelerating the formation of anhydrides (Figure 1.5a). At the same time, hydrogen bonding between peptides assembled into fibers enhances the electrophilicity of the anhydride groups, rendering them more susceptible to hydrolysis compared to building blocks that are non-assembled. In this manner, these peptide assemblies simultaneously catalyze their own assembly and disassembly, an important step towards more dynamic and life-like material systems.[34]

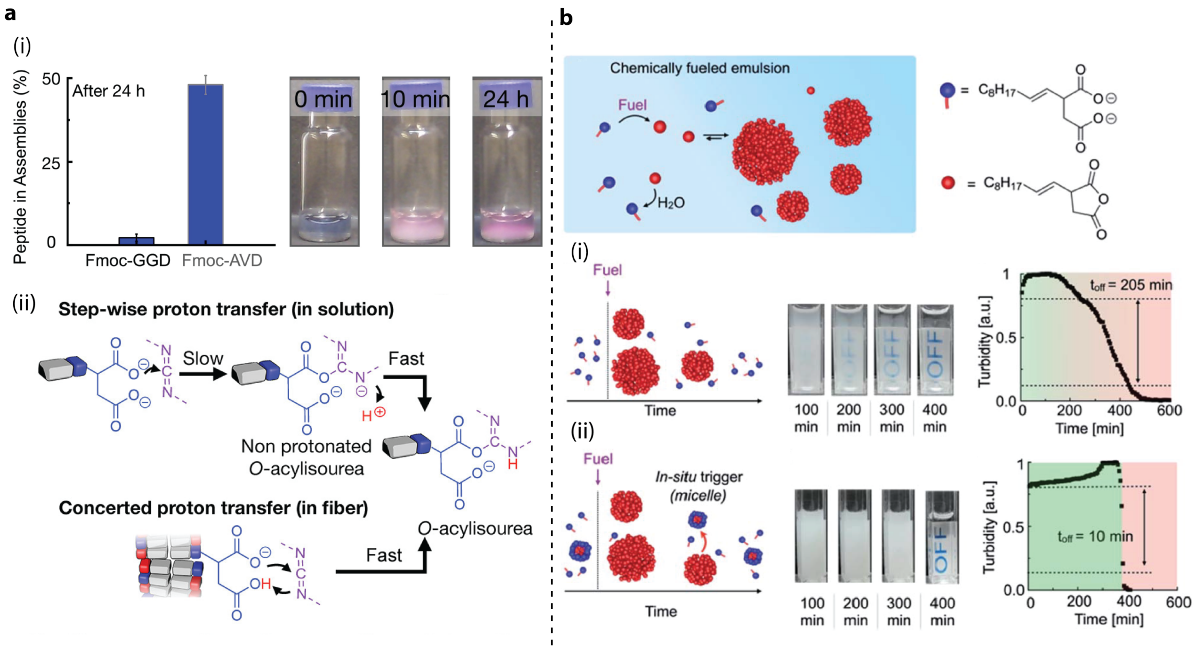

Figure 1.5: Effect of building block design on system behavior. (a)Influence of peptide structure on assembly kinetics. (i) Kinetic trapping of assembled peptide due to fiber formation. Fmoc-AVD forms fibers, in which the microenvironment raises the pK_a of aspartic acid groups, reducing charge density even after anhydride hydrolysis. Left: percentage of peptides in assemblies 24 hours after fueling, determined by ^{1}H NMR. Right: Vial of Fmoc-AVD fueled with EDC, visually demonstrating peptide assemblies persisting past complete consumption of fuel. Fmoc-GGD, which forms vesicles, does not display this behavior. (ii) Mechanism of accelerated activation due to fiber formation. As Fmoc-AVD assembles into fibers, non-activated building blocks are able to provide protons to EDC in a faster, concerted mechanism, increasing the rate of building block reactivation. Adapted from [48,50] with permission from the American Chemical Society and Wiley. (b) Autonomous self-immolation of chemically fueled droplets. (i) When fueling 2-alkeneylsuccinate precursor below its CMC, the system displays typical assembly-disassembly behavior as fuel is consumed. (ii) Fueling above precursor CMC means that as the building blocks are deactivated, they form micelles, which solubilize activated building blocks in the droplets, drastically increasing the rate of hydrolysis. Adapted from [49] published under CC-BY 4.0 by the Royal Society of Chemistry.

A common limitation of chemically-fueled systems is that disassembly is inherently tied to the rate of deactivation, which in directly fueled systems such as these must necessarily be slower than activation. This inherently leads to a slow disassembly as all fuel is consumed and building blocks are gradually deactivated, and precludes the kind of rapid disassembly that may be seen in classically responsive or active environment systems (Figure 1.1, Figure 1.2). This can be overcome by

involving the deactivated building blocks as chemo-structural catalysts for disassembly. A key example of this is seen in systems of 2-alkenylsuccinates assembling into droplets (Figure 1.5b).[49,66-67]

The 2-alkenylsuccinate building blocks feature highly hydrophobic tails, and therefore poor water solubility, even in the un-activated state. Increasing alkene chain length leads to longer lifetimes and slower droplet disassembly arising from the decreased effective rate of anhydride deactivation due to the poorer solubility of long-tailed anhydrides in the surrounding aqueous buffer.[67] The poor water-solubility of the hydrocarbon tails coupled with the hydrophilic succinate groups leads the un-activated building blocks to form micelles in solution when above the critical micelle concentration (CMC). This equilibrium assembly of unfueled building blocks may be exploited to design a system where disassembly of fueled droplets occurs autocatalytically by exploiting precursor micelles to solubilize activated building blocks and increase the rate of deactivation.[49] When fueling at building block concentrations above the CMC, activation into anhydrides leads to their assembly into droplets, and disassembly of micelles. As fuel is consumed, the precursor concentration once again rises above the CMC, and the resulting micelles solubilize the phase-separated droplets, accelerating the hydrolysis of the anhydrides (Figure 1.5b). This allows for similar fueled state lifetimes, while significantly reducing the disassembly time from >200 to 10 minutes, and would be greatly desirable in controlled release applications.

1.3.4. EDC-Fueled Solution-Phase Polymer Systems

The lessons learned from self-assembly of small-molecule or small peptide building blocks can equally be applied to polymers, taking advantage of the additional control polymers offer as materials, namely the ability to precisely control polymer sequence and/or block composition but with considerably greater scalability in synthesis compared to peptides, and the ease of employing polymeric materials in macroscopic systems.

In systems with polymers as the assembling units, polymer structure is equally important and intrinsically linked to the behavior observed on fueling. A homopolymer featuring dicarboxylic acid units will undergo a hydrophilic to hydrophobic transition caused by charge neutralization, driving phase-segregation from solution. Indeed, solutions of poly(norbornene dicarboxylic acid) (PNDAc) have been shown to undergo temporary spinodal decomposition from a homogenous solution to a polymer-rich phase and a polymer-depleted phase when the vicinal carboxylates are converted into a 5-membered anhydride ring on fueling with EDC, significantly increasing the hydrophobicity of the polymer (Figure 1.6a).[68] While this is an important result for understanding the dynamics and driving forces of chemically-fueled phase separation in polymeric systems, for more controlled self-assembly into structures that can be used for further down-stream tasks, a non-responsive hydrophilic block should be included to obtain a switchable amphiphilic BCP. Fueling a block copolymer composed of a hydrophilic poly(ethylene oxide) (PEO) block and a responsive poly(styrene-*alt*-maleic acid) block with EDC activates the maleic acid units to yield the 5-membered maleic anhydride ring, rendering the responsive block hydrophobic, driving the assembly of nanometer-scale polymer micelles (Figure 1.6b).[69] The hydrophobic environment inside these micelles can be exploited to locally concentrate hydrophobic substrates present in the system and catalyze a Diels-Alder addition reaction.

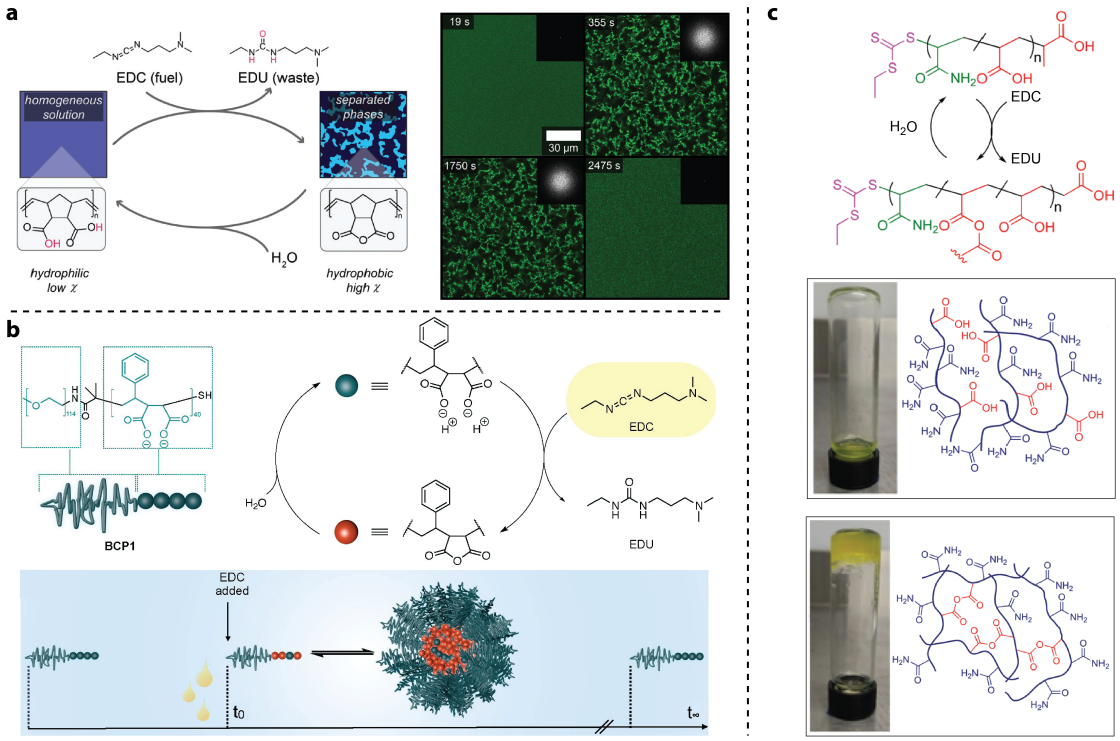

Figure 1.6: EDC fueling of solution-phase polymer systems. (a) Chemically fueled spinodal decomposition of polymer solutions. Left: scheme describing EDC-fueled anhydride formation of poly(norbonene dicarboxylic acid). Right: time-course Confocal Laser Scanning Microscopy images of the polymer solution after addition of 1 equivalent EDC. Adapted from [68] with permission from the Royal Society of Chemistry. (b) EDC-fueled micelle formation in PEO-*b*-poly(styrene-*alt*-maleic acid) BCPs. Adapted from [69], published under CC-BY 4.0 by Wiley. (c) EDC-fueled transient crosslinking of PAm-*co*-PAA copolymer solutions (top image) to form transient hydrogels (bottom). Adapted from [71] with permission from the Royal Society of Chemistry.

In both these systems, lifetime of the self-assembled state is controlled by altering fuel loading, and in the former additionally by changing system pH to control the rate of anhydride hydrolysis. To achieve finer temporal control over polymer assembly into nano-reactors, a variation of the carbodiimide fuel cycle leading to the formation of active esters can be employed. In this case, in addition to EDC fuel, the system contains an electron-poor coupling agent. The *O*-acylurea generated by EDC reacting with the carboxylate substrate reacts with said nucleophile to yield a hydrolytically labile "active" ester. Particularly in the context of polymer self-assembly, this modification provides two advantages. Firstly, charge-neutralization approaches can be employed on substrates where anhydride ring formation is slow, increasing activation rates, or not possible at all, allowing use of a wider array of polymer architectures. Secondly, the choice of coupling agent dictates the stability of the resulting active ester, allowing for much greater temporal control within the same experimental platform by conveniently changing one component. In an important demonstration of this approach, poly(ethylene glycol-*b*-acrylic acid) block copolymers activated with EDC and either *N*-hydroxysuccinimide, *N*-hydroxynorbornenedicarboxylic acid imide, *para*-nitrophenol or pentafluorophenol displayed assembly into micellar nano-reactors with lifetimes dictated by the hydrolytic stability of the resulting active ester.[70]

The above examples show a clear path towards ever more controlled self-assembly behavior in polymer solutions, firstly by transitioning from homopolymer to BCPs, and then by controlling timescale through use of the active ester strategy. However, they lack investigation into the effect

of altering polymer composition within each experimental system on the morphologies and lifetimes of the resultant assemblies, which is the focus of **Chapter 2** of this thesis.

The effect of polymer composition has been explored by the Hartley group not in the context of self-assembly, but rather gel formation from polymer solutions. In the absence of coupling agents, fueling polymers with non-neighboring acid groups leads to inter-chain crosslinking, as carboxylates on different chains form transient anhydride crosslinks (Figure 1.6c). This has been demonstrated in poly(acrylamide-*co*-acrylic acid) (PAm-*co*-PAA) copolymers, which form transient gels with lifetimes in the hundreds of minutes on addition of EDC.[71] The crosslink density, and therefore storage modulus of the gels can be tuned by altering the acrylic acid content of the polymers. This is an important step towards control *via* active-material mechanisms of macroscopic polymer materials, where inter-chain crosslinking can play a significant role.

1.3.5. EDC-Fueled Crosslinked Polymer Systems

In already crosslinked polymer materials, such as microgels and hydrogels, depending on the structure and sequence of the repeating units, either anhydride ring formation or inter-chain anhydride formation may predominate. These two modes of fueling can be exploited to obtain transient (de)swelling in the first case, and modulate mechanical properties in the second.

Fueling of microgels featuring a poly(methacrylic acid) (PMAA) shell leads to formation of 6-membered anhydride rings between neighboring methacrylic acid units. Ring formation leads to charge-neutralization in the microgel shell, and depending on fuel loading, a corresponding volume phase transition as it deswells (Figure 1.7a).[61] Gel deswelling can be exploited at the macroscopic scale to achieve transiently actuating devices.[72] EDC fueling of poly(acrylic acid) (PAA) hydrogels leads to the formation of both 6-membered anhydride rings between neighboring repeat units and inter-chain anhydrides. The resulting charge-neutralization leads to a significant drop in internal osmotic pressure and a corresponding contraction in gel volume. By coupling this gel with a non-responsive poly(dimethylsiloxane) (PDMS) elastomer in a bilayer device, a number of transiently actuating devices such as flowers, plant mimics and grabbers can be obtained (Figure 1.7b).

Chemically fueled inter-chain crosslinking can also be employed to transiently alter the mechanical properties of gels (Figure 1.7c). By applying EDC in patterns to weakly crosslinked polyacrylamide/polyacrylic acid hydrogels, spatially-defined gel reinforcement is achieved by locally increasing the crosslink density *via* the formation of inter-chain anhydride crosslinks, and application of EDC to two individual hydrogels allows them to adhere to each other until the fuel is consumed and the anhydrides hydrolyzed,[45] demonstrating the capacity of active-material mechanisms for dynamic properties such as self-healing. In crosslinked PAm hydrogels perfused with linear PAA, the addition of EDC leads to the transient formation of a second interpenetrating crosslinked network as the activated PAA segments form crosslinks between previously free chains (Figure 1.7d). The resulting dual-network hydrogels display greatly increased mechanical performance over the course of fueling in comparison to their unfueled counterparts, tolerating higher strains and displaying higher fracture energies due to the improved energy dissipation afforded by the secondary network.[73]

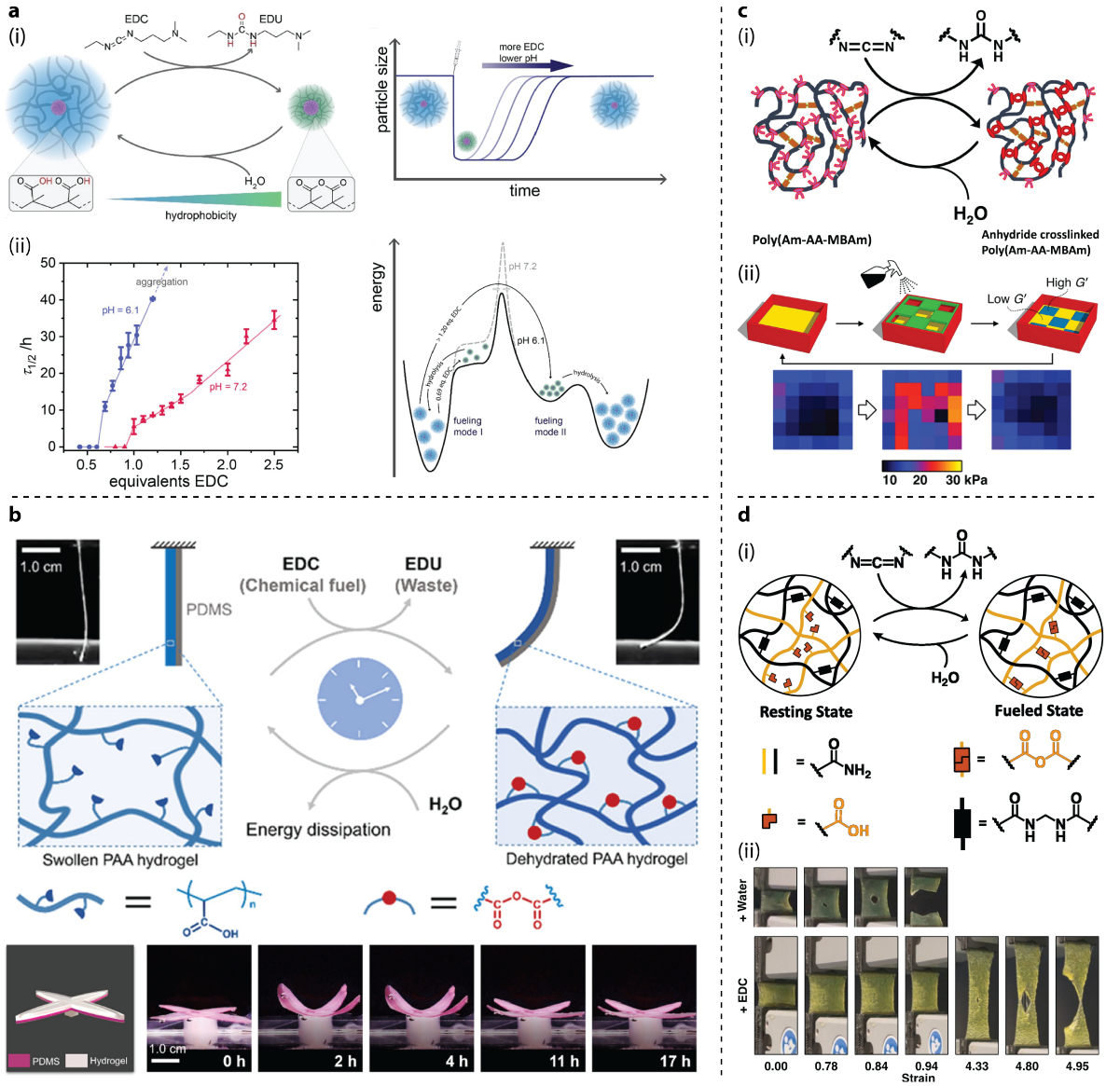

Figure 1.7: EDC fueling to control crosslinked polymeric materials. (a) (i) Chemically fueled volume phase transition of microgels. (ii) pH and fuel-dependent change in fueling mode. Fueling at lower pH leads to increased response to fuel (lower threshold amount) and allows for fuel-dependent aggregation to occur. Adapted from [61] with permission from Wiley. (b) EDC-fueled actuation *via* dehydration of PAA hydrogel. Coupling to a passive PDMS layer allows for the shrinking of the PAA layer to be exploited for transient actuation. Adapted from [72] with permission from the American Chemical Society. (c) (i) Transient reinforcement of a PAA-PAm hydrogel through transient anhydride crosslinks. (ii) Application of EDC through a mask allows for spatially-defined reinforcement and programming of storage modulus (G'). Adapted from [45] with permission from the American Chemical Society. (d) Hydrogel reinforcement through formation of a secondary interpenetrating network. (i) Transient crosslinking of PAA linear polymer within a PAm hydrogel by EDC-fueled anhydride formation. (ii) Comparison of tensile properties of unfueled (top) and fueled hydrogel (bottom). The fueled hydrogel displays greater tensile strength and crack-resistance due to the secondary network. Adapted from [73] with permission from Wiley.

1.3.6. Other Fuels for Direct Activation of Polymer Materials

Approaches using methylating agents, and particularly carbodiimides, as small-molecule chemical fuels to control systems containing polymer materials both feature charge neutralization as a key driving force in both solution-phase self-assembly and control of hydrogel swelling, due to decrease in solubility in the former example and both solubility decrease and primarily reduction in osmotic pressure in the latter. Therefore, a charge-neutralization approach appears the rational

choice for controlling polymeric materials in general. In principle, such an approach can be applied to any system featuring a polyelectrolyte component, the challenge lies in identifying an appropriate CRN so as to achieve temporal control over the process.

The Eelkema group in particular has explored two novel active material CRNs for control of polymeric systems, both of which operate *via* a charge-neutralization mechanism, but with significant differences to the carbodiimide fuel cycle. In the first example, transient acetylation of nitrotyrosine-acrylic acid copolymers is employed to control their conformation in aqueous media.[47] The activation step in this reaction cycle relies on acetic anhydride as the chemical fuel to form a nitrophenol ester with polymer-attached nitrotyrosine groups at slightly basic pH. This leads to charge neutralization of the nitrophenolate anion and a general decrease in hydrophilicity of the nitrotyrosine group, which acts as the driving force for a conformational transition from coil to globule. While this CRN involves direct activation by a fuel molecule and deactivation by solvent, much in the same manner as carbodiimide-fueled systems, it is worth noting that both steps are catalyzed. Activation is necessarily catalyzed by pyridine as an acyl transfer catalyst to overcome the very rapid hydrolysis of acetic anhydride, and the deactivation reaction, the hydrolysis of the nitrophenolate ester, is catalyzed by imidazole *via* a nucleophilic substitution mechanism. Tuning of catalyst loadings allows for the tuning of the active state lifetime over many hours.[47]

The second CRN developed, allowing for exceptional control over polymer materials is that based on the Morita-Baylis-Hillman (MBH) reaction.[74-75] The cycle relies on the formation of a metastable quaternary nitrogen adduct from a tertiary amine substrate and an activated allyl acetate fuel as the activation step, producing acetate as waste. Deactivation relies on the presence of a nucleophile to attack the adduct, yielding a substituted allylic waste product and the original tertiary amine (Figure 1.8a, i). Two modes of operation are possible for this reaction cycle based on the choice of nucleophile (Figure 1.8a, ii). A strong nucleophile, such as β-mercaptoethanol (BME) would immediately attack the quaternary adduct and lead to deactivation, and so must be added after an excess of fuel, allowing for transient signal induced deactivation of the active state. A weaker nucleophile such as threonine reacts far slower with the activated intermediate, and as such can be added as a slow deactivator molecule alongside the fuel, leading to a single, autonomous activation/deactivation cycle.

This reaction network has been successfully applied to polymers containing vinylpyridine groups, were upon activation, the additional charge of the quaternary pyridinium intermediate leads to a significant increase in hydrophilicity. This can be leveraged to control the transient disassembly of dimethylacrylamide-*b*-4-vinylpyridine (DMA-*b*-4VP) BCPs for cargo release[74] and the transient coacervation of DMA-4VP copolymers and polyanions into complex coacervate core micelles.[75] The transient increase in charge density can be leveraged to drive osmotic swelling in crosslinked vinylpyridine-containing hydrogels (Figure 1.8b).[74] In all these examples, both signal-induced deactivation with strong nucleophiles and transient autonomous activation with weak nucleophiles are possible.

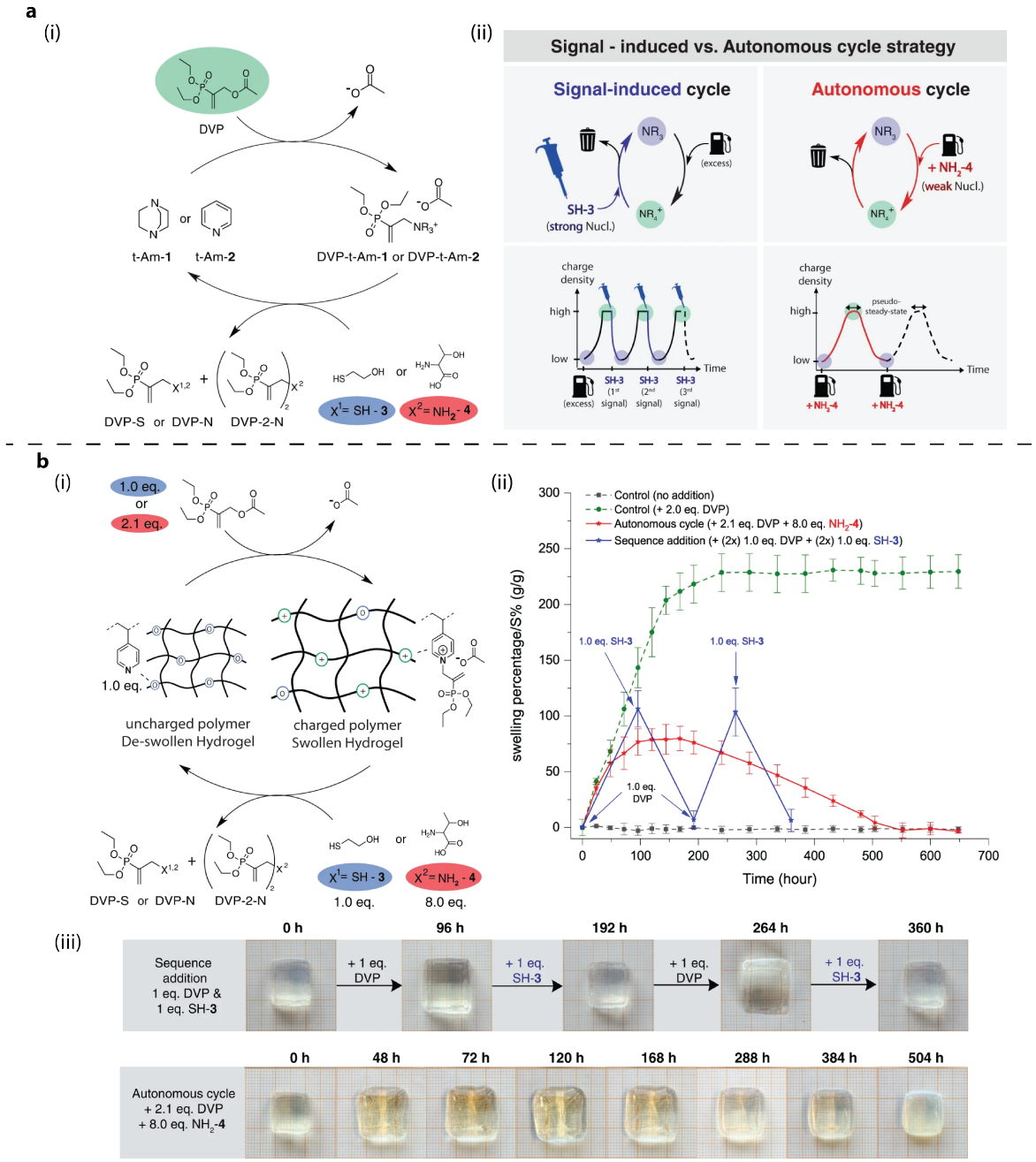

Figure 1.8: Morita-Baylis-Hillman chemical reaction network. (a) General features of the MBH fuel cycle. (i) MBH CRN employed in the study, with diethyl(α-acetoxymethyl) vinylphosphonate (DVP) as fuel, a tertiary amine as the substrate, and BME or threonine as deactivating species. (ii) Modes of CRN operation available based on choice of deactivating nucleophile. Signal-induced cycle: using excess fuel with respect to amine and BME as nucleophile allows for on-demand deactivation upon addition of BME. Excess fuel then reacts with the regenerated amine to achieve another cycle of activation, and so on. Autonomous cycle: addition of a stoichiometric amount of fuel and threonine as a weak nucleophile leads to a single, autonomous activation and deactivation, which may be repeated by addition of further fuel and nucleophile. Adapted from [74], published under CC-BY 4.0 by Springer Nature. (b) MBH CRN applied to vinylpyridine-containing hydrogel. (i) Schematic for reaction cycle, where the tertiary amine is hydrogel-bound pyridyl groups. (ii) Effect of different fueling modes on hydrogel swelling over time. Signal-induced operation (blue trace) leads to swelling that is only negated on addition of MBE. Autonomous operation leads to a single transient swelling and deswelling cycle. (iii) Images of transient hydrogel swelling under both signal-induced and autonomous operation regimes. Adapted from [75], published under CC-BY 3.0 by the Royal Society of Chemistry.

The crucial difference between the MBH reaction cycle and that obtained by using methylating agents or EDC is that it requires an additional deactivator species to complete the deactivation step, which in the aforementioned examples is carried out by solvent molecules. Other systems employing an additional deactivator, sometimes referred to as an additional fuel or "anti-fuel" have been developed, such as those based on saccharide-benzaldehyde hydrogelators reported by the Hermans group.[76-77] In these examples, assembled aldehyde hydrogelators are first oxidized to sulfonic acids by dithionite acting as fuel, which leads to gel disassembly due to electrostatic repulsion. These activated sulfonic acids are stable under experimental conditions, until presented with formaldehyde as the deactivating species, which reduces them once more to the original benzaldehyde. Temporal control over this transient disassembly is obtained by generating formaldehyde *via* an upstream reaction between gluconolactone and hexamethylenetetramine.[76] Additionally, this transient disassembly can be utilized to self-sort different saccharide-benzaldehyde hydrogelators.[77]

1.4. Active Environments

In contrast to dissipative systems where direct activation of the building blocks or material occurs through reaction with a fuel, systems where a simultaneous, system-wide change in chemical potential occurs can be termed active environment systems.[33] In such systems, all responsive units are simultaneously activated, and the equilibrium between forward and backward reactions at the level of individual responsive units is overwhelmingly shifted in favor of the activated species. This allows to conveniently decouple the kinetics of activation and the kinetics of the dissipative process driving the system. The change in chemical potential can come from something as simple as temperature change, light, or sequential addition of acids and bases. While these can in theory be spatially focused on parts of the system and controlled over time, this requires constant external attention – such examples are only classically responsive, and not autonomous. To have autonomous control over chemical potential in an environment, this must be coupled to a CRN that, once initiated, modulates the concentration of key activating species over time.

1.4.1. Redox Oscillators

Oscillating reactions provide a prime example of such active environments. During the latter half of the 20th century, a number of oscillating reactions have been discovered, including the well-known Belousov-Zhabotinsky (BZ)[78] reaction and those based on the "iodine clock",[79-80] of which the Briggs-Rauscher[81] reaction is the most known. These examples are characterized by a non-equilibrium regime where the complex interplay of numerous redox processes leads to the regular variation of key intermediate species in a periodical manner, with the chemical energy originating from an oxidizing species. The oscillations can then be integrated as stimuli for responsive building blocks or materials. In the example of the BZ reaction, this is classically the periodic change in oxidation state of cerium ions, although any metal ion or complex with a sufficiently high redox potential can be employed.[82] Yoshida and coworkers have extensively utilized the BZ reaction to control the oxidation state of $Ru(bpy)_3$ complexes that are included in PNIPAm (Figure 1.9a). The changing oxidation state in turn controls the temperature of the NIPAm lower critical solution temperature (LCST), being above room temperature in the oxidized state and below it when reduced. In this way, periodically oscillating polymers[83-84] and hydrogels[85-93] have been obtained. While coupling materials to the BZ reaction allows for control over material properties in both time and space, it requires significant fine-tuning to achieve oscillations, is

inflexible in tuning the time-domain and volume changes obtained during oscillation are relatively small.

Another noteworthy example of a successfully implemented redox oscillator is that of an iodine clock reaction applied to polymeric solutions as a means of self-assembly control.[94-95] Periodic increases in molecular iodine, which coordinates to the PEG segment of PEG-amino acid BCPs, rendering them hydrophobic and drives assembly into micelles. However, this system likewise suffers from the same drawbacks of the BZ reaction.

1.4.2. pH oscillators

A number of redox CRNs involve protons in the individual reactions that compose the system. Careful design of these can yield examples where protons are a key species, and periodic oscillations in proton concentration, and therefore pH of the system, are achieved. Early examples of these pH-oscillators include the hydrogen peroxide-sodium sulfide[96] and dithionite[97] reactions and the bromate-sulfite-ferrocyanide (BSF) reaction,[98-99] with a wide range of variations developed by altering the nature of the reducing and oxidizing species.[100-101] pH presents the ideal stimulus for an active-environment system, as acid-base equilibria are ubiquitous in biological systems, they are typically very fast, allowing for rapid activation and deactivation, and pH-responsive materials have been extensively studied in the context of classically responsive systems. Indeed, charge neutralization of polyelectrolytes as discussed in the context of active material systems can equally be applied to pH-responsive polymers, albeit through an additional upstream layer for time-defined pH control.

For example, pH-responsive PEG-PAA BCPs can be coupled to the BSF oscillator. The resulting pH oscillations protonate the acrylic acid groups, rendering the polymer segment hydrophobic and driving periodic assembly into micelles.[102] By replacing bromate with iodate, the self-assembly of poly(ethylene oxide)-*b*-poly(2-vinylpyridine) (PEO-P2VP) BCPs can be controlled using the dual stimuli of pH and molecular iodine (Figure 1.9b). In the resting state, above pH 5, the polymers assemble into micelles with the deprotonated P2VP segment in the core. The oscillating reaction generates periodic drops in pH and simultaneous increases in I_2 concentration, which leads to protonation of the P2VP segment and iodine coordination to the PEO units, with the first becoming hydrophilic and the second hydrophobic, leading to a core-shell reversal of the micelles.[103] pH oscillations generated by the hydrogen peroxide-dithionite reaction have been used to control the periodic deswelling of PAA hydrogels (Figure 1.9c).[104-105] Coupling these hydrogels to passive poly(dimethylacrylamide) allows for the construction of bilayer actuators that display periodic motion in time with the pH oscillations of the system.[104] Addition of a pH-responsive tetraphenylethylene chromophore capable of aggregation-induced emission allows for simultaneous shape and color morphing of jellyfish-like actuators.[105]

Recently, non-redox pH oscillators based on organic substrates have been developed, such as the methylene glycol-sulfite-gluconolactone (MGS) reaction,[106-107] which operates at milder conditions than those of classical oscillators involving chemically harsh redox processes.

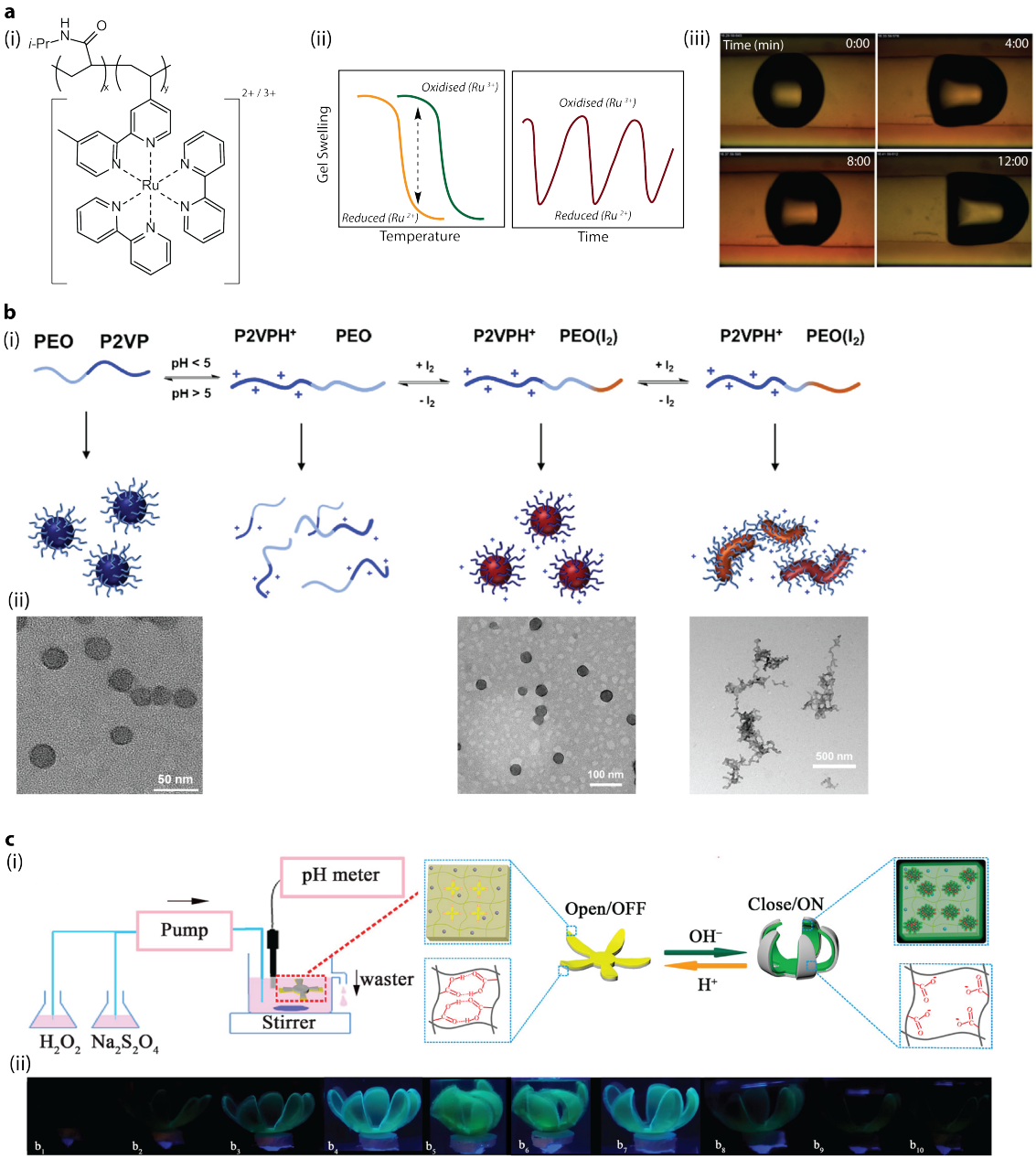

Figure 1.9: Chemical oscillators for control of polymeric materials. (a) Controlling LCST of PNIPAm polymers *via* the BZ reaction. (i) General structure of the PNIPAm-Ru(bpy)$_3$ copolymers employed by the Yoshida group. (ii) Scheme describing how changes in oxidation state of the ruthenium complex control the swelling of PNIPAm hydrogels. The reduced species leads to a lower LCST, and consequently gel deswelling. Cyclical oxidation and reduction lead to travelling swelling and deswelling waves in the gel. (iii) Periodic swelling and deswelling applied to macroscopic materials. Travelling BZ reaction fronts lead to peristalsis of a hydrogel tube, transporting a gas bubble along the length of the tube. Adapted from [85], with permission from Wiley. (b) Dually responsive BCP controlled by an iodine-pH oscillating reaction. (i) At pH above 5, the P2VP groups are deprotonated, and hydrophobic, as the pH drops, they are protonated and the micelles disassemble. As iodine is generated by the oscillating reaction, it coordinates to the PEO segment of the polymer, leading to assembly into first spherical and then worm-like micelles. The overall effect is one of a micelle core-shell reversal. (ii) TEM micrographs of the structures of the assembled polymers at various points in the cycle. Adapted from [103] with permission from Elsevier. (c) A fluorescent hydrogel actuator controlled by a pH oscillator. (i) Scheme of the experimental setup for controlling the peroxide-dithionite pH oscillator and a bilayer hydrogel actuator. The bottom layer is composed of a PAA hydrogel, which swells as pH drops, leading to closure of the flower-shaped device. The top layer contains tetraphenylethylene chromophores which display aggregation-induced emission at high pH. (ii) Time series images of actuator operation over one pH cycle. Adapted from [105] with permission from the American Chemical Society.

However, all pH oscillators suffer from the same set of drawbacks. Namely, oscillations can only be sustained in an open system, in the setting of a continuous stirred tank reactor (CSTR, see Figure 1.9c) or other semi-continuously fed configuration.[108] This significantly increases system complexity by introducing engineering challenges alongside the chemical considerations already present, and means that operation cannot be completely autonomous at the chemical level, as external control of the CSTR is required. Additionally, within the remit of a given oscillating reaction, there is little room to program the timescale or magnitude of oscillations, as there are limited starting conditions that give rise to stable oscillations. Because of these limitations, interest towards time-defined pH control in batch settings has increased.

1.4.3. pH Control in Batch Settings

Given the requirement that there be a time delay between the initial pH change on initiation of the system and the final pH change that returns the system to its starting conditions, time-controlled pH changes in batch settings have proven harder to achieve. The strategies that can be employed to obtain the time separation between activating and deactivating reactions can be grouped into three broad classes; the gating of deactivation behind the activation reaction in promoter/dormant deactivator systems, environmental modulation of the activity of a catalyst generating the activating and/or deactivating species, such as in enzymatic systems, or by employing a single chemical fuel capable of carrying out the activation step and generating the deactivating species in situ, in the case of activated carboxylic acids (ACAs).

Promoter - Dormant Deactivator Systems

The conceptually simplest method of introducing time separation in a pH-control system is to employ the addition of a molecule that instantly alters pH (promoter) and a molecule that will, at the newly introduced pH, degrade to yield a deactivating molecule, the dormant deactivator (DD), and return the pH to its original value. In such a system, the energetic driving force is the instability of the DD with respect to the newly altered pH. This strategy was first demonstrated by the Walther group by using basic tris(hydroxymethyl)aminomethane (TRIS) buffer as promoter and a series of esters as the DD (Figure 1.10a).[51] On addition of the promoter/DD mixture, the system experiences a sharp rise in pH, which encourages the hydrolysis of the ester DD. The resultant carboxylic acid in turn lowers the pH to at or below the starting value. Crucially, timescale control can be introduced by selection of the ester. Gluconic acid δ-lactone rapidly hydrolyzes within minutes, methyl formate within hours, and ε-caprolactone over the course of days (Figure 1.10a). Because of the widespread applicability of pH stimuli, this control mechanism can be coupled to a wide range of substrates such as clustering of nanoparticles with surface-attached phenols, transient gelation of peptides and the self-assembly DNA-functionalized nanoparticles.[109] The self-assembly of BCPs comprised of hydrophilic poly(ethylene oxide) or poly(oligoethyleneoxide methacrylate) block and a pH-responsive poly(diethylaminoethyl methacrylate) (PDEAEMA) block can likewise be controlled (Figure 1.10a). Addition of the promoter/DD mixture deprotonated the PDEAEMA block, rendering it hydrophobic and driving the assembly of BCPs into micelles, which disassemble as the pH once again sinks. This is a particularly relevant example as it is the first demonstration of polymer self-assembly controlled through an active environment CRN.

One downside of employing a promoter/DD strategy is that activation begins immediately on addition of the promoter and cannot be time-programmed. This can be overcome by incorporating an autocatalytic clock reaction as the promoter, allowing for a time-encoded delay before activation. The MGS clock reaction can be used in a batch setting to generate one single rapid spike in pH from ~ 5.5 to ~ 10.5, after an induction period in the order of 10s to 100s of seconds. Addition of lactones as DDs allows for time control of the return to low pH based on DD selection and concentration.[110] This system has been successfully employed in controlling the transient swelling of an *N*-isopropylacrylamide-*co*-*tert*-butylacrylamide hydrogel doped with the pH-responsive monomer dimethylaminopropyl methacrylamide.[110] A variation of this strategy employs 1,3-propanesultone instead of a lactone as the dormant deactivator in a similar CRN to control assembly of perylenediimides into fibers. [111]

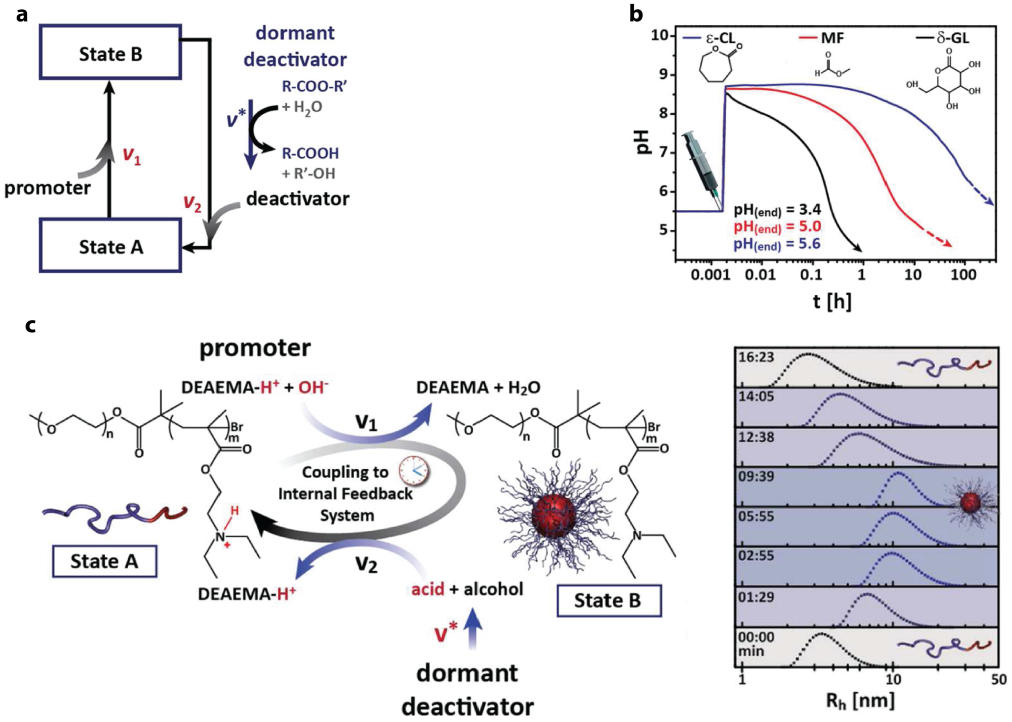

Figure 1.10: Promoter/dormant deactivator strategy for transient pH profiles. First example of Promoter-DD strategy (a) By using a slowly hydrolyzing ester, a transient rise in pH can be achieved. (b) Choice of ester allows for control over the lifetime of the pH profile from under one to hundreds of hours. (c) Application of the pH control mechanism to pH-responsive PEG-DEAEMA BCPs, which transiently assemble into micelles as pH rises, and disassemble as pH once again drops. Transient micelle assembly may be followed by DLS. Adapted from [51] with permission from the American Chemical Society.

Enzymatic Systems

Promoter/DD systems offer convenient control of pH over time, but suffer from background degradation of the DD even in the un-activated state, and difficulty tuning the active state lifetime as it depends on the concentration of promoter, DD and the rate of DD conversion. The latter limitation can be overcome by replacing the self-degrading DD with a stable one that is catalytically converted to a deactivating molecule by an enzymatic reaction, and the former can be mitigated by employing an enzyme with pH-dependent activity such as urease.

In a system controlled by the urea/urease pair, starting pH is basic, at which urease has negligible activity. Promotion is carried out by addition of an acidic buffer, and at low pH urease slowly

converts the DD urea to ammonia, the deactivating molecule. As pH rises, urease activity correspondingly increases, leading to a positive feedback loop until a basic pH is reached and urease activity again decreases (Figure 1.11).[112] This CRN allows for lifetime tuning by simply altering urease concentration, with the additional benefit that it allows for transient decreases in pH, which could not be achieved using ester-based DDs. While the urea/urease reaction has been investigated in the context of CSTRs[112] and reaction-diffusion systems,[113] it was first employed in the context of autonomous materials to control the gelation of solutions of the peptide Fmoc-L-G-COOH. The peptide assembles into nanofibrils at pH < 5.8, and so, on addition of acidic citrate buffer as promoter, forms a hydrogel. As pH subsequently rises, the C-terminus carboxylate is deprotonated, the nanofibrils disassemble, and the gel breaks down (Figure 1.11a).[54]

Enzymatic CRNs capable of regulating a transiently alkaline state have also been reported, employing basic buffer as promoter, glucose as the DD and glucose oxidase (GOx) to convert it to gluconic acid.[114] However, the urea/urease CRN is of particular relevance to polymeric materials and systems due to the large number of applications that have been demonstrated, including photonic bandgap thin films (Figure 1.11b),[115] swelling microgels,[116] catalyst loaded polymersome nanoreactors[117] and bicontinuous enzyme-loaded nanospheres,[118] which can additionally be used to control the actuation of bilayer actuators.[119]

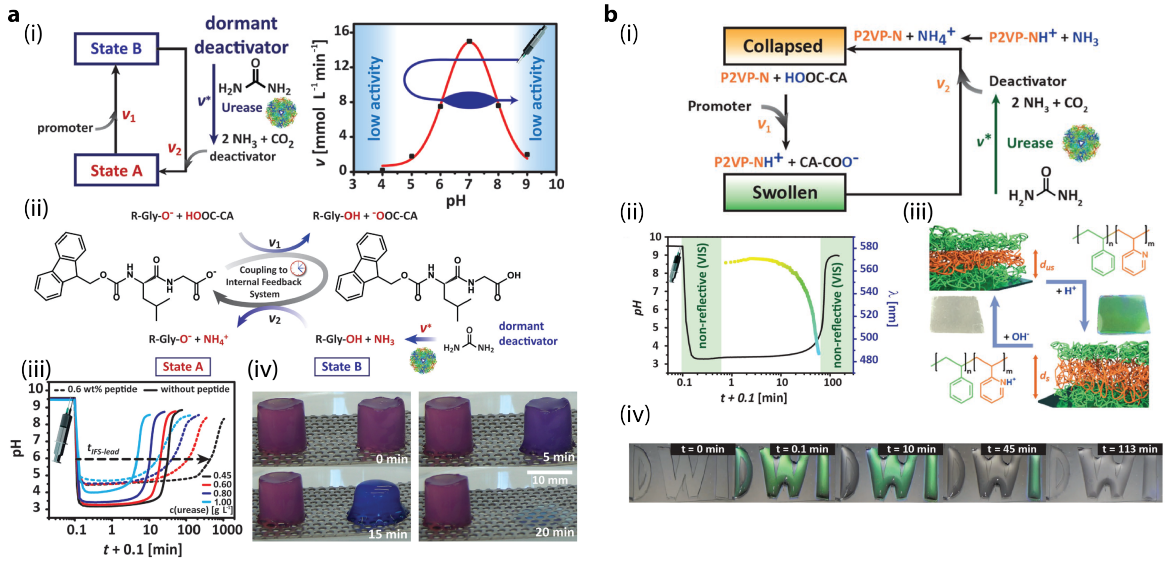

Figure 1.11: Use of the enzymatic urea/urease reaction for pH control. (a) First application of the reaction to control self-assembly of peptide hydrogelators. (i) General scheme for the urea/urease reaction, highlighting the bell-shaped activity of urease over the pH range of the experiment. (ii) Effect of the reaction cycle on peptide gelator. (iii) pH profile of the system over the course of the cycle as a function of urease concentration. Lower urease loadings lead to longer lifetimes of the pH drop. Addition of the peptide leads to self-buffering, lengthening the pH drop additionally. (iv) Demonstration of time-programmed gel materials. Both gels contain urease, citrate and 1 wt% gelator, but only the gel on the right contains urea, and so disassembles as pH rises. Adapted from [54] with permission from Wiley. (b) Photonic device controlled by the urea/urease reaction. (i) Scheme describing the effect of the reaction cycle on the material. Addition of acidic citrate buffer leads to swelling in the P2VP layer, redshifting the photonic stop band, which is subsequently blushifted outside the visible spectrum as pH rises, leading to a transient green structural color (ii) Temporal control over the photonic reflection of the polymer film as a function of pH. (iii) Effect of transient protonation on layer spacing as mechanism for observed photonic reflection. (iv) Demonstration of polymer films programmed with different lifetimes through changes in enzyme concentration. Adapted from [115] with permission from Wiley.

These last three examples, from the van Hest group, all employ polymers featuring the pH-responsive DEAEMA unit. Urease-containing microgels composed of crosslinked poly(oligoethylene glycol methacrylate) and PDEAEMA display time-controlled swelling on addition of urea-containing citrate buffer. As the pH rises, the amine groups are deprotonated and the microgels contract. Inclusion of fluorescein *O*-methacrylate allows for *in situ* pH monitoring by measuring the pH-dependent fluorescence change in fluorescein[116] (Figure 1.12a). This same strategy was employed by us in **Chapter 4** to monitor local urea conversion in a chemo-mechanical feedback system. Polymersomes of pH-responsive PEG-PDEAEMA BCPs loaded with urease likewise show similar swelling behavior controlled by the urea/urease CRN.[117] These swelling changes correspond to changes in membrane permeability, being permeable at low pH, and impermeable at high pH. When also loaded with horseradish peroxidase, these periodic changes in permeability in response to the pH CRN allow for the switching on and off of the secondary enzymatic reaction[117] by allowing or preventing substrate diffusion through the membrane (Figure 1.12b). Permeability effects are also exploited in bicontinuous nanospheres assembled from PEG-PDEAEMA polymers featuring a longer pH-responsive segment (Figure 1.12c).[118-119] These nanospheres show a time lag in permeability changes due to differences between solution pH and that within the nanospheres themselves. This time lag can be exploited to control actuating PAm-PAA hydrogel bilayers with embedded nanospheres.[119] As will be discussed in **Chapter 4**, timescale matching between pH changes and gel (de)swelling is critical to achieve successfully actuating devices. In this example, addition of acidic urea solution leads to initial contraction of the PAA layer, and corresponding bending. Diffusion of acid into the initially impermeable nanospheres is slow, but once protonated, they become permeable to urea and urease activity is triggered, increasing the pH and returning the actuator to the original configuration, with the time delay critical to achieve full actuation. Furthermore, placing the nanospheres in the active PAA layer instead of the passive layer leads to decreased actuation as local pH kept higher than the surrounding environment (Figure 1.12d).[119]

It is worth noting that coupling multiple enzymatic pH-controlling reactions together to obtain a system where both the activator and deactivator are obtained *via* enzymatic conversion is also possible, such as for example the ethyl acetate/esterase and urea/urease pair.[55,120] These systems are important for understanding how to design complex interconnected CRNs inspired by those seen in, for example, cellular metabolism, but the associated increase in complexity limits potential applications, at least for the time being.

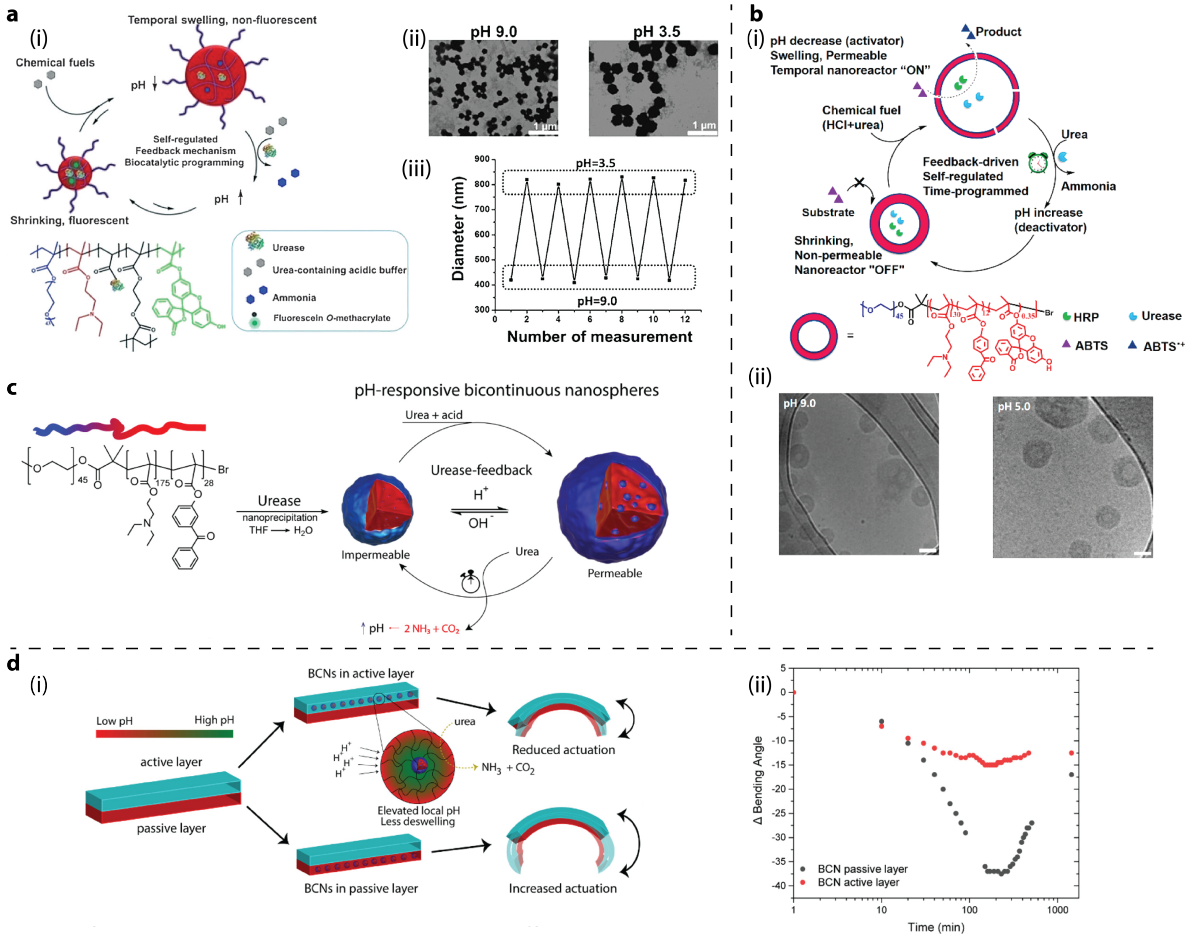

Figure 1.12: Applications of urea/urease CRN and structural feedback in polymeric systems. (a) "Breathing" microgels. (i) As pH increases and the microgels shrink, copolymerized fluorescein increases in fluorescence, acting as an *in-situ* reporter of pH. (ii) TEM micrographs of the microgels shrunk at high pH (left) and swollen at low pH (right). (iii) Diameters of the microgels over a number of fueling cycles, displaying the cyclical breathing behavior. Adapted from [116] with permission from Wiley. (b) Temporal control of nanoreactor polymersomes. (i) At low pH on addition of promoter and urea the polymersomes are permeable, allowing access to the contained enzymes. This allows the enzymatic conversion of 2,2'-azino-bis(3-ethylbenzothiazoline-6-sulfonate) (ABTS) by horseradish peroxidase (HRP). At high pH, they are impermeable, and catalytic activity is halted. (ii) Cryo-TEM micrographs of the polymersomes. Adapted from [117], published under CC-BY-NC 4.0 by the American Chemical Society. (c) pH responsive bicontinuous nanospheres: fabrication and operation of the nanospheres, which display pH-dependent permeability. (d) Control of a PAA-PAm bilayer pH-responsive actuator. (i) Inclusion of urease-containing nanospheres allows for control over actuation by modulating microsphere permeability. (ii) Bending profiles obtained by placing urease-containing nanospheres in different actuator layers. (c-d) Adapted from [119], published under CC-BY 4.0 by the American Chemical Society.

1.4.4. Activated Carboxylic Acids

Seeing how CRNs containing multiple reactions modulating the generation of activating and deactivating species can rapidly balloon in complexity, it would be greatly attractive to design a pH-control CRN where a single chemical fuel could be employed to control the entire cycle, in a manner reminiscent of the role of fuels in some active material systems.

Originating as chemical fuels in supramolecular active material systems,[52,121] activated carboxylic acids (ACAs) have since come into focus as dissipative methods of pH control in aqueous active environment systems. In a typical ACA fuel cycle (Figure 1.13a), the acid is readily deprotonated

in the presence of a basic species, yielding a carboxylate anion that decarboxylates to afford CO_2 and a highly basic carbanion. This carbanion rapidly scavenges a proton, yielding an alkane as waste and returning the system to its original state.

The first example of an ACA used as chemical fuel is 2-cyano-2-phenylpropanoic acid, used by the Di Stefano group to control ring orientation in a pH-responsive catenane (Figure 1.13b).[52,121] Substituting the *para* position on the phenyl ring with a variety of electron withdrawing or donating groups has been shown to control the rate of decarboxylation.[121] Electron withdrawing groups lead to charge stabilization in the resulting carbanion, increasing the observed rate of decarboxylation. Subsequently, trichloroacetic acid was used as fuel to operate a catenane rotary motor and a rotaxane molecular pump.[122] Tribromoacetic acid has likewise been used as fuel in the dissipative assembly of a transient covalent cage from calixarene precursors.[123] It is important to note that in this setting of organic-phase supramolecular systems, ACAs act as chemical fuels, but in the context of an active-material type system. They directly protonate basic groups in the substrates, and the carbanions directly abstract them.

In the setting of aqueous systems however, ACAs act as chemical fuels for an active environment. There is a rapid pH drop on addition of the acid, and a slow rise to the original value as the rate-determining decarboxylation step occurs and the carbanion scavenges protons from solution. Employing ACAs in aqueous media is challenging however, since hydrogen-bonding with water molecules significantly hinders the rate of decarboxylation. The highly activated nitroacetic acid can be used to produce a transient pH drop in aqueous systems.[124] Addition of nitroacetic acid to a basic solution at pH = 12 leads to a large drop to pH = 2, which slowly rises as the resulting carbanion is protonated to yield nitromethane. Some of the generated CO_2 is dissolved, and part of it is converted to carbonic acid. The resulting $H_2CO_3/HCO_3^-/CO_3^{2-}$ equilibria buffer the pH of the solution, meaning pH does not return to the starting value, but remains somewhat below it (Figure 1.13c). Nitroacetic acid has been used to dissipatively control the host-guest complexation of *p*-aminobenzoic acid and *a*-cyclodextrin[124] and pH-responsive DNA nanodevices by controlling triplex to duplex transitions, allowing for controlled release of cargo strands (Figure 1.13c).[125]

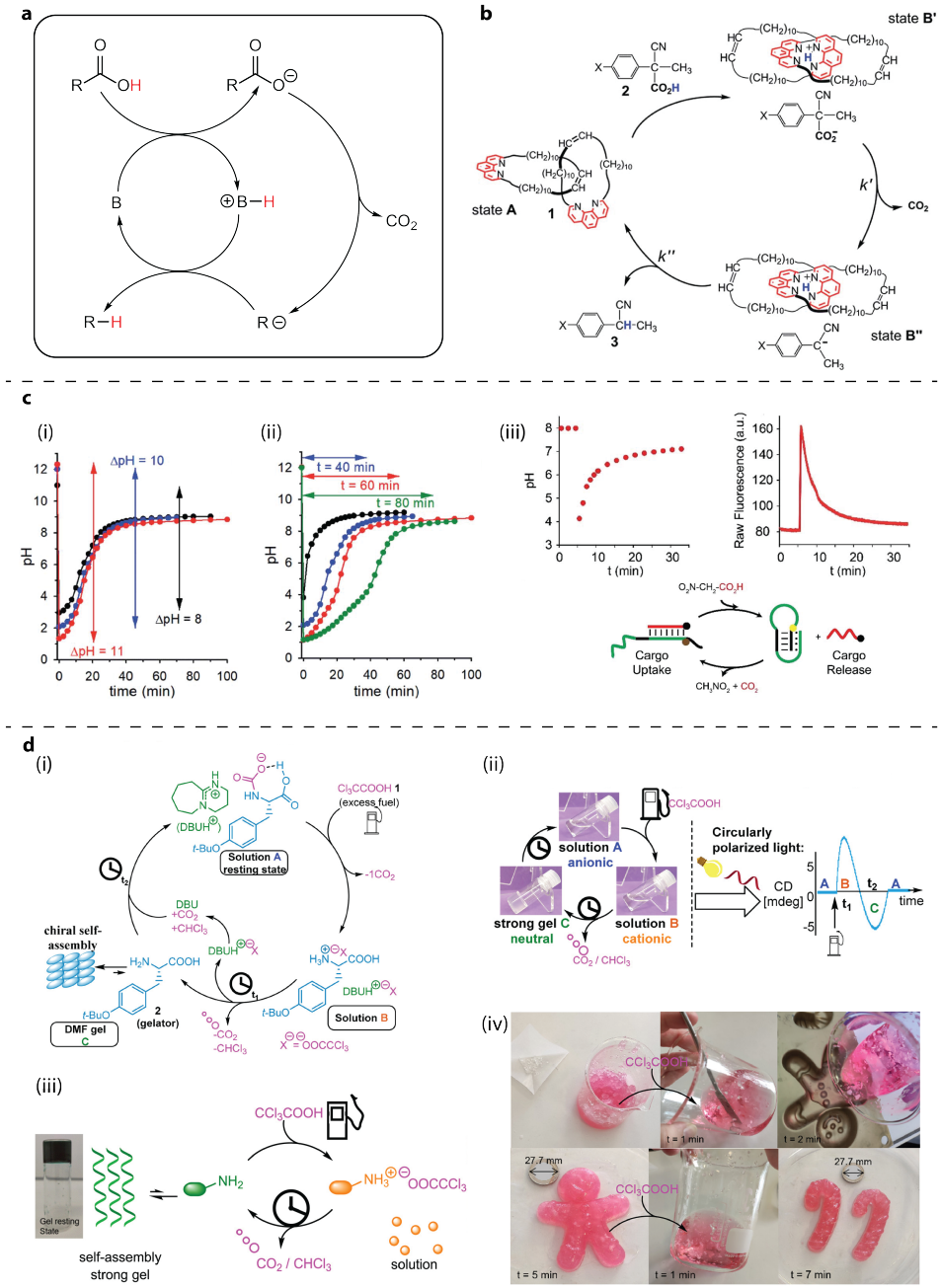

Figure 1.13: Activated carboxylic acids as single-molecule chemical fuels for transient pH drops. (a) General scheme for an ACA reaction cycle. (b) First implementation of ACAs using 2-cyano-2-phenylpropanoic acids as chemical fuels to control ring orientation in catenanes. The X group in the *para* position controls reactivity, with more electron withdrawing groups increasing the rate of decarboxylation. Adapted from [121], published under CC-BY 3.0 by the Royal Society of Chemistry. (c) Control of aqueous pH using ACAs. (i) pH profile of a 0.020 M (red), 0.010 M (blue) and 0.001 M (black) NaOH solution after addition of 0.040 M, 0.020 M and 0.002 M nitroacetic acid. The balance between acid and base influences the magnitude and duration of the pH drop. (ii) pH profile of 0.010 M NaOH solution after addition of 0.010 M (black), 0.020 M (blue), 0.030 M (red) and 0.040 M (green) nitroacetic acid. Increasing acid loading leads to longer and deeper pH drops. (iii) Dissipative release-uptake cycle of a DNA cargo strand controlled by nitroacetic acid. As pH drops, the fluorescent cargo strand is released, before being taken up again as pH rises. Adapted from [124-125], published under CC-BY 3.0 by the Royal Society of Chemistry. (d) Applying ACAs as methods of material control in organogels. (i) Three-stage organogel cycle. On addition of TCA fuel, protonation of the amino-acid residue leads to a significant change in circular dichroism signal. Decarboxylation of TCA, amine deprotonation and loss of carbon dioxide from solution leads to the formation of a stiff organogel. (ii) Gelation and circular dichroism signal over course of fuel cycle. (iii) Transient organogel disassembly. Addition of TCA leads to organogelator protonation, and solubilization as an ion-pair with the trichloroacetate anion. (iv) Application of TCA fueled de-gelation for remoldable materials. Adapted from [126-127] with permission from the American Chemical Society.

ACAs have also been put to use as dissipative fuels to control macroscopic materials, but not in aqueous settings. Trichloroacetic acid can act as a fuel in the sol-gel-sol transition of the pH-responsive organogelator *O-tert*-butyltyrosine,[126] which in the presence of diazabicycloundecene (DBU) as an additive displays three distinct states over the course of the fueling cycle (Figure 1.13d) each featuring different chiroptical properties. Additionally, *O-tert*-butyltyrosine and octadecylamine organogels display a gel-sol-gel transition on fueling with trichloroacetic acid (Figure 1.13d), allowing for remoldable gels, which are stable over many cycles.[127] Since the rate of decarboxylation is strongly solvent dependent, altering the solvent allows for significant tuning of the lifetime of the solution state. These examples clearly illustrate the advantages of ACAs in transient and smart materials, namely the simplicity, cyclability due to reduced waste accumulation, and tunability of ACA systems. However, there have been no reports of coupling of ACAs with synthetic polymers or hydrogels in aqueous active environments to achieve dissipative self-assembly or autonomous devices. These two topics are explored in greater detail in **Chapter 3** and **Chapter 4** respectively.

1.5. Scope of the Thesis

The extensive research carried out in chemically fueled systems has been influenced to a great degree by its origins in the fields of molecular machinery and supramolecular chemistry. Although control of polymer-based systems has been investigated in both active environments and through active material mechanisms, little focus has been placed on examining the interplay of the control method with the design of the polymer itself, and how polymers can be designed to respond to a number of stimuli. Furthermore, chemically-fueled autonomous operation of hydrogel devices has been poorly studied, with only a handful of examples shown to date. To this end, we employ aspartic acid *N*-acrylamide (A^3) as a building block to design polymers capable of controlled self-assembly both through the carbodiimide-fueled direct activation mechanism and an activated carboxylic acid fueled active environment pathway.

As a first example, in **Chapter 2** we investigate the influence of responsive block composition on the EDC-fueled self-assembly of block (Figure 1.14a) composed of a hydrophilic block and a responsive block composed of A^3 and the hydrophobic *tert*-butylacrylamide (*t*-BuAm) in variable ratios. By tuning the composition of the responsive block, we control the fuel threshold assembly concentration, and show that a longer self-assembly response can be achieved by employing a lower fuel concentration, leading to a more fuel-efficient system. By altering the relative lengths of the two blocks in the BCPs, we are further able to target different morphologies for self-assembly, from spherical micelles, to worm-like micelles, to vesicles. The process of self-assembly is followed by *in-situ* dynamic light scattering experiments, which reveal a process of activation, initial assembly, secondary assembly, and finally disassembly in the fueled polymer solutions. These observations are rationalized with the help of a model system of statically self-assembled methylated polymers and confirmed by use of TEM and Cryo-TEM.

Moving to an active-environment system (Figure 1.14b), in **Chapter 3** and **Chapter 4** we exploit the pH-responsiveness of the A^3 building block to control the behavior of polymer materials using tribromoacetic acid as an activated carboxylic acid fuel. In **Chapter 3**, we study the effects of responsive block composition on the self-assembly of BCPs in a mixed water/DMSO solvent system (Figure 1.14c). We first describe the pH-responsiveness of the polymers, revealing significant hysteresis between pH at assembly and disassembly, which we attribute to kinetic

trapping of the self-assembled state in polymers with a large *t*-BuAm content. We employ this result to contextualize the self-assembly duration of polymer solutions on fueling with various concentrations of TBA, which we monitor *via* turbidity and pH measurements over the course of the fueling experiments. Finally, we rationalize the observed behavior by designing a kinetic model of the system capable of accurately predicting the pH over the course of fueling.

In **Chapter 4**, we build on the solution-phase fueling of pH-responsive polymers with tribromoacetic acid to design soft robotic hydrogel actuators capable of autonomous operation (Figure 1.14d). We design an A^3-based hydrogel with a strong (de)swelling response over the relevant pH range (pH 3.0-7.0). By exploiting the understanding gained of the TBA fuel cycle, we are able to carefully tune the lifetime of the pH drop to match the timescale of the gel (de)swelling. After demonstrating this proof-of-concept transient deswelling, we employ the transiently deswelling hydrogel in a bilayer device, demonstrating control over the magnitude and duration of actuation in the device on the basis of increasing fuel loading. We subsequently illustrate the unique benefits of the TBA fuel cycle for the control of soft robotic devices by demonstrating "fire and forget" operation of harpoon devices capable of transient contraction and reswelling for the mechanical lifting of loads and self-recognizing "puzzle piece" active surfaces that can interface upon fueling. Finally, we couple the TBA fuel cycle to the urea-urease reaction to achieve additional chemomechanical feedback. By including a localized urease-containing patch in a bilayer device, and maintaining separation from the urea-containing aqueous phase until the device actuates on fueling with TBA, we demonstrate a device capable of sensing externally present molecules, and locally transducing them into effectors, leading to higher-order control over device operation.

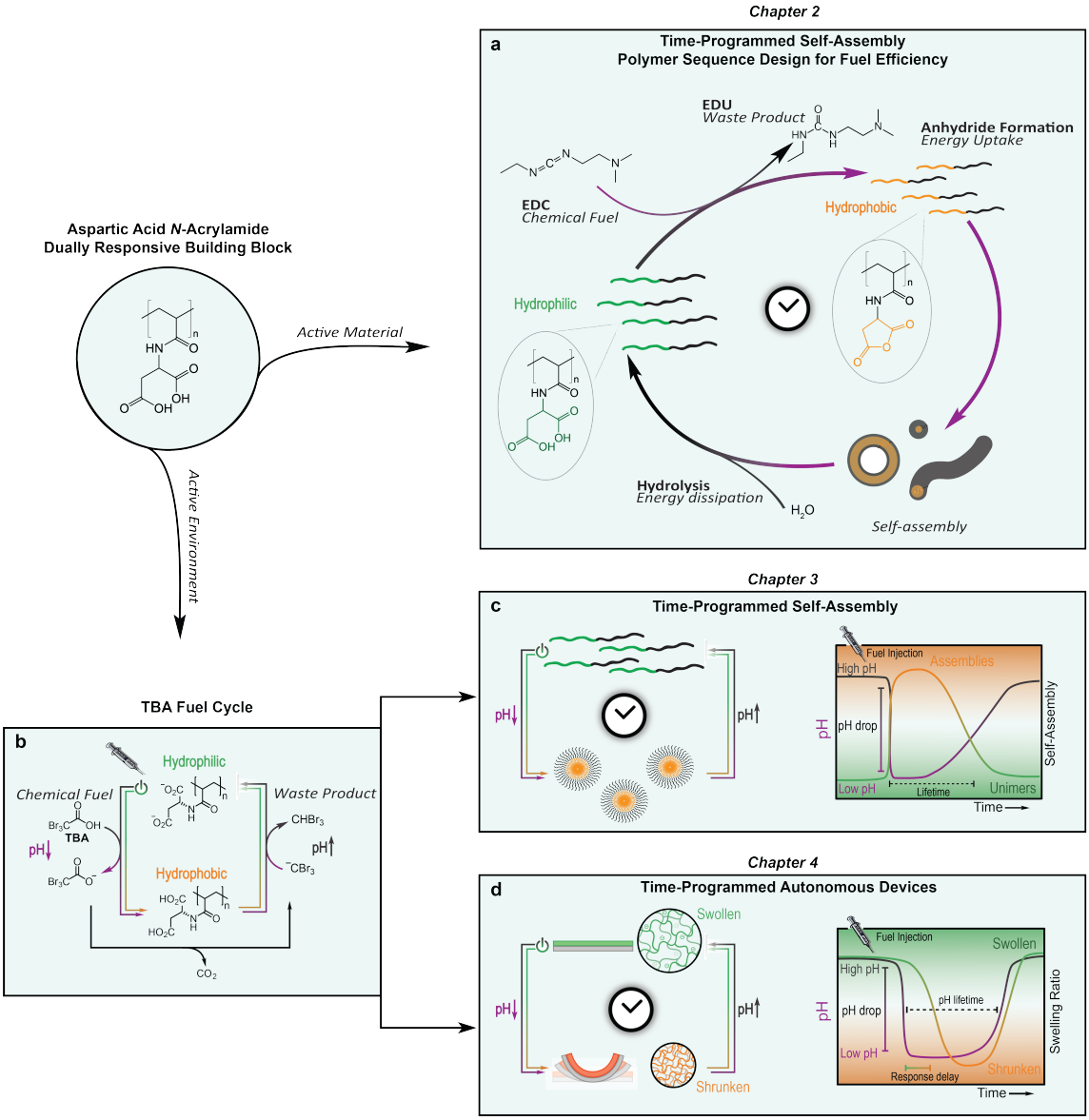

Figure 1.14: Designing a dually responsive polymer platform for active materials and active environments. (a) Time-programmed self-assembly of BCPs by direct activation with EDC. By tuning polymer structure both the morphology and kinetics of self-assembly are controlled. (b) Establishing the tribromoacetic acid fuel cycle as an active environment stimulus for polymer materials. (c) Time-programmed solution-phase self-assembly of BCPs controlled by TBA. (d) Extension of solution-phase work into hydrogels for autonomous hydrogel devices controlled by the TBA fuel cycle. Pre-programmed fueled actuation can be achieved.

1.6. References

[1] C. Sagan, in The Nature of Life: Classical and Contemporary Perspectives from Philosophy and Science, (Eds: M. A. Bedau, C. E. Cleland), Cambridge University Press, Cambridge **2010**.

[2] S. A. Benner, Defining Life, *Astrobiology* **2010**, *10*, 1021.

[3] P. Adamski, M. Eleveld, A. Sood, A. Kun, A. Szilagyi, T. Czaran, E. Szathmary, S. Otto, From Self-Replication to Replicator Systems En Route to De Novo Life, *Nat. Rev. Chem.* **2020**, *4*, 386.

[4] S. Otto, An Approach to the De Novo Synthesis of Life, *Acc. Chem. Res.* **2022**, *55*, 145.

[5] H. Staudinger, Ueber Polymerisation, *Ber. dtsch. Chem. Ges. A/B* **1920**, *53*, 1073.

[6] R. Mulhaupt, Hermann Staudinger and the Origin of Macromolecular Chemistry, *Angew. Chem. Int. Ed.* **2004**, *43*, 1054.

[7] M. A. Stuart, W. T. Huck, J. Genzer, M. Muller, C. Ober, M. Stamm, G. B. Sukhorukov, I. Szleifer, V. V. Tsukruk, M. Urban, F. Winnik, S. Zauscher, I. Luzinov, S. Minko, Emerging Applications of Stimuli-Responsive Polymer Materials, *Nat. Mater.* **2010**, *9*, 101.

[8] M. Wei, Y. Gao, X. Li, M. J. Serpe, Stimuli-Responsive Polymers and Their Applications, *Polym. Chem.* **2017**, *8*, 127.

[9] D. Roy, W. L. Brooks, B. S. Sumerlin, New Directions in Thermoresponsive Polymers, *Chem. Soc. Rev.* **2013**, *42*, 7214.

[10] O. Bertrand, J. F. Gohy, Photo-Responsive Polymers: Synthesis and Applications, *Polym. Chem.* **2017**, *8*, 52.

[11] S. Dai, P. Ravi, K. C. Tam, Ph-Responsive Polymers: Synthesis, Properties and Applications, *Soft Matter* **2008**, *4*, 435.

[12] G. Kocak, C. Tuncer, V. Bütün, Ph-Responsive Polymers, *Polym. Chem.* **2017**, *8*, 144.

[13] A. V. Ruzette, L. Leibler, Block Copolymers in Tomorrow's Plastics, *Nat. Mater.* **2005**, *4*, 19.

[14] N. A. Lynd, A. J. Meuler, M. A. Hillmyer, Polydispersity and Block Copolymer Self-Assembly, *Prog. Polym. Sci.* **2008**, *33*, 875.

[15] Y. Mai, A. Eisenberg, Self-Assembly of Block Copolymers, *Chem. Soc. Rev.* **2012**, *41*, 5969.

[16] N. J. Warren, S. P. Armes, Polymerization-Induced Self-Assembly of Block Copolymer Nano-Objects Via Raft Aqueous Dispersion Polymerization, *J. Am. Chem. Soc.* **2014**, *136*, 10174.

[17] H. Feng, X. Lu, W. Wang, N. G. Kang, J. W. Mays, Block Copolymers: Synthesis, Self-Assembly, and Applications, *Polymers (Basel)* **2017**, *9*.

[18] Y. Lu, J. Lin, L. Wang, L. Zhang, C. Cai, Self-Assembly of Copolymer Micelles: Higher-Level Assembly for Constructing Hierarchical Structure, *Chem. Rev.* **2020**, *120*, 4111.

[19] S. Iqbal, M. Blenner, A. Alexander-Bryant, J. Larsen, Polymersomes for Therapeutic Delivery of Protein and Nucleic Acid Macromolecules: From Design to Therapeutic Applications, *Biomacromolecules* **2020**, *21*, 1327.

[20] G. M. Whitesides, Soft Robotics, *Angew. Chem. Int. Ed.* **2018**, *57*, 4258.

[21] M. Cianchetti, C. Laschi, A. Menciassi, P. Dario, Biomedical Applications of Soft Robotics, *Nat. Rev. Mater.* **2018**, *3*, 143.

[22] S. I. Rich, R. J. Wood, C. Majidi, Untethered Soft Robotics, *Nat. Electron.* **2018**, *1*, 102.

[23] N. El-Atab, R. B. Mishra, F. Al-Modaf, L. Joharji, A. A. Alsharif, H. Alamoudi, M. Diaz, N. Qaiser, M. M. Hussain, Soft Actuators for Soft Robotic Applications: A Review, *Adv. Intell. Syst.* **2020**, *2*, 2000128.

[24] J. Wang, D. Gao, P. S. Lee, Recent Progress in Artificial Muscles for Interactive Soft Robotics, *Adv. Mater.* **2021**, *33*, 2003088.

[25] Y. Zhao, M. Hua, Y. Yan, S. Wu, Y. Alsaid, X. He, Stimuli-Responsive Polymers for Soft Robotics, *Annu. Rev. Control Robot. Auton. Syst.* **2022**, *5*, 515.

[26] T. P. Lodge, Block Copolymers: Past Successes and Future Challenges, *Macromol. Chem. Phys.* **2003**, *204*, 265.

[27] P. Lim Soo, A. Eisenberg, Preparation of Block Copolymer Vesicles in Solution, *J. Polym. Sci., Part B: Polym. Phys.* **2004**, *42*, 923.

[28] S. J. Holder, N. A. J. M. Sommerdijk, New Micellar Morphologies from Amphiphilic Block Copolymers: Disks, Toroids and Bicontinuous Micelles, *Polym. Chem.* **2011**, *2*, 1018.

[29] P. Pramanik, D. Ray, V. K. Aswal, S. Ghosh, Supramolecularly Engineered Amphiphilic Macromolecules: Molecular Interaction Overrules Packing Parameters, *Angew. Chem. Int. Ed.* **2017**, *56*, 3516.

[30] M. Karayianni, S. Pispas, Block Copolymer Solution Self-Assembly: Recent Advances, Emerging Trends, and Applications, *J. Polym. Sci.* **2021**, *59*, 1874.

[31] S. D. P. Fielden, Kinetically Controlled and Nonequilibrium Assembly of Block Copolymers in Solution, *J. Am. Chem. Soc.* **2024**.

[32] X. Peng, H. Wang, Shape Changing Hydrogels and Their Applications as Soft Actuators, *J. Polym. Sci., Part B: Polym. Phys.* **2018**, *56*, 1314.

[33] R. Merindol, A. Walther, Materials Learning from Life: Concepts for Active, Adaptive and Autonomous Molecular Systems, *Chem. Soc. Rev.* **2017**, *46*, 5588.

[34] A. Walther, Viewpoint: From Responsive to Adaptive and Interactive Materials and Materials Systems: A Roadmap, *Adv. Mater.* **2020**, *32*, e1905111.

[35] L. Magnus, in *Application of Thermodynamics to Biological and Materials Science*, (Ed: T. Mizutani), **2011**, Chapter 11.

[36] B. A. Grzybowski, C. E. Wilmer, J. Kim, K. P. Browne, K. J. M. Bishop, Self-Assembly: From Crystals to Cells, *Soft Matter* **2009**, *5*.

[37] Y. Yan, J. Huang, B. Z. Tang, Kinetic Trapping - a Strategy for Directing the Self-Assembly of Unique Functional Nanostructures, *Chem. Commun.* **2016**, *52*, 11870.

[38] J. Boekhoven, A. M. Brizard, K. N. Kowlgi, G. J. Koper, R. Eelkema, J. H. van Esch, Dissipative Self-Assembly of a Molecular Gelator by Using a Chemical Fuel, *Angew. Chem. Int. Ed.* **2010**, *49*, 4825.

[39] A. Arango-Restrepo, D. Barragan, J. M. Rubi, Self-Assembling Outside Equilibrium: Emergence of Structures Mediated by Dissipation, *Phys. Chem. Chem. Phys.* **2019**, *21*, 17475.

[40] G. Ragazzon, L. J. Prins, Energy Consumption in Chemical Fuel-Driven Self-Assembly, *Nat. Nanotechnol.* **2018**, *13*, 882.

[41] N. Singh, G. J. M. Formon, S. De Piccoli, T. M. Hermans, Devising Synthetic Reaction Cycles for Dissipative Nonequilibrium Self-Assembly, *Adv. Mater.* **2020**, *32*, e1906834.

[42] M. Weißenfels, J. Gemen, R. Klajn, Dissipative Self-Assembly: Fueling with Chemicals Versus Light, *Chem* **2021**, *7*, 23.

[43] I. Aprahamian, S. M. Goldup, Non-Equilibrium Steady States in Catalysis, Molecular Motors, and Supramolecular Materials: Why Networks and Language Matter, *J. Am. Chem. Soc.* **2023**, *145*, 14169.

[44] J. Rodon-Fores, M. A. Wurbser, M. Kretschmer, B. Riess, A. M. Bergmann, O. Lieleg, J. Boekhoven, A Chemically Fueled Supramolecular Glue for Self-Healing Gels, *Chem. Sci.* **2022**, *13*, 11411.

[45] C. W. H. Rajawasam, C. Tran, M. Weeks, K. S. McCoy, R. Ross-Shannon, O. J. Dodo, J. L. Sparks, C. S. Hartley, D. Konkolewicz, Chemically Fueled Reinforcement of Polymer Hydrogels, *J. Am. Chem. Soc.* **2023**, *145*, 5553.

[46] L. Heinen, A. Walther, Celebrating Soft Matter's 10th Anniversary: Approaches to Program the Time Domain of Self-Assemblies, *Soft Matter* **2015**, *11*, 7857.

[47] M. P. van der Helm, C. L. Wang, B. Fan, M. Macchione, E. Mendes, R. Eelkema, Organocatalytic Control over a Fuel-Driven Transient-Esterification Network, *Angew. Chem. Int. Ed.* **2020**, *59*, 20604.

[48] B. A. K. Kriebisch, A. Jussupow, A. M. Bergmann, F. Kohler, H. Dietz, V. R. I. Kaila, J. Boekhoven, Reciprocal Coupling in Chemically Fueled Assembly: A Reaction Cycle Regulates Self-Assembly and Vice Versa, *J. Am. Chem. Soc.* **2020**, *142*, 20837.

[49] P. S. Schwarz, L. Tebcharani, J. E. Heger, P. Muller-Buschbaum, J. Boekhoven, Chemically Fueled Materials with a Self-Immolative Mechanism: Transient Materials with a Fast on/Off Response, *Chem. Sci.* **2021**, *12*, 9969.

[50] B. A. K. Kriebisch, C. M. E. Kriebisch, A. M. Bergmann, C. Wanzke, M. Tena-Solsona, J. Boekhoven, Tuning the Kinetic Trapping in Chemically Fueled Self-Assembly, *ChemSystemsChem* **2022**, *5*.

[51] T. Heuser, A. K. Steppert, C. M. Lopez, B. Zhu, A. Walther, Generic Concept to Program the Time Domain of Self-Assemblies with a Self-Regulation Mechanism, *Nano Lett.* **2015**, *15*, 2213.

[52] J. A. Berrocal, C. Biagini, L. Mandolini, S. Di Stefano, Coupling of the Decarboxylation of 2-Cyano-2-Phenylpropanoic Acid to Large-Amplitude Motions: A Convenient Fuel for an Acid-Base-Operated Molecular Switch, *Angew. Chem. Int. Ed.* **2016**, *55*, 6997.

[53] C. Biagini, S. Di Stefano, Abiotic Chemical Fuels for the Operation of Molecular Machines, *Angew. Chem. Int. Ed.* **2020**, *59*, 8344.

[54] T. Heuser, E. Weyandt, A. Walther, Biocatalytic Feedback-Driven Temporal Programming of Self-Regulating Peptide Hydrogels, *Angew. Chem. Int. Ed.* **2015**, *54*, 13258.

[55] L. Heinen, T. Heuser, A. Steinschulte, A. Walther, Antagonistic Enzymes in a Biocatalytic Ph Feedback System Program Autonomous DNA Hydrogel Life Cycles, *Nano Lett.* **2017**, *17*, 4989.

[56] J. Boekhoven, W. E. Hendriksen, G. J. Koper, R. Eelkema, J. H. van Esch, Transient Assembly of Active Materials Fueled by a Chemical Reaction, *Science* **2015**, *349*, 1075.

[57] B. G. P. van Ravensteijn, W. E. Hendriksen, R. Eelkema, J. H. van Esch, W. K. Kegel, Fuel-Mediated Transient Clustering of Colloidal Building Blocks, *J. Am. Chem. Soc.* **2017**, *139*, 9763.

[58] M. Tena-Solsona, B. Riess, R. K. Grotsch, F. C. Lohrer, C. Wanzke, B. Kasdorf, A. R. Bausch, P. Muller-Buschbaum, O. Lieleg, J. Boekhoven, Non-Equilibrium Dissipative Supramolecular Materials with a Tunable Lifetime, *Nat. Commun.* **2017**, *8*, 15895.

[59] L. S. Kariyawasam, C. S. Hartley, Dissipative Assembly of Aqueous Carboxylic Acid Anhydrides Fueled by Carbodiimides, *J. Am. Chem. Soc.* **2017**, *139*, 11949.

[60] M. A. Gilles, A. Q. Hudson, C. L. J. Borders, Stability of Water-Soluble Carbodiimides in Aqueous Solution, *Anal. Biochem.* **1990**, *184*, 244.

[61] J. Heckel, S. Loescher, R. T. Mathers, A. Walther, Chemically Fueled Volume Phase Transition of Polyacid Microgels, *Angew. Chem. Int. Ed.* **2021**, *60*, 7117.

[62] K. Dai, J. R. Fores, C. Wanzke, B. Winkeljann, A. M. Bergmann, O. Lieleg, J. Boekhoven, Regulating Chemically Fueled Peptide Assemblies by Molecular Design, *J. Am. Chem. Soc.* **2020**, *142*, 14142.

[63] Z. F. Yao, Y. Kuang, P. Kohl, Y. Li, H. A. M. Ardoña, Carbodiimide-Fueled Assembly of Π-Conjugated Peptides Regulated by Electrostatic Interactions, *ChemSystemsChem* **2023**, *5*.

[64] C. Wanzke, A. Jussupow, F. Kohler, H. Dietz, V. R. I. Kaila, J. Boekhoven, Dynamic Vesicles Formed by Dissipative Self-Assembly, *ChemSystemsChem* **2019**, *2*.

[65] B. Riess, C. Wanzke, M. Tena-Solsona, R. K. Grotsch, C. Maity, J. Boekhoven, Dissipative Assemblies That Inhibit Their Deactivation, *Soft Matter* **2018**, *14*, 4852.

[66] M. Tena-Solsona, J. Janssen, C. Wanzke, F. Schnitter, H. Park, B. Riess, J. M. Gibbs, C. A. Weber, J. Boekhoven, Accelerated Ripening in Chemically Fueled Emulsions, *ChemSystemsChem* **2021**, *3*.

[67] B. J. Niebuur, H. Hegels, M. Tena-Solsona, P. S. Schwarz, J. Boekhoven, C. M. Papadakis, Droplet Formation by Chemically Fueled Self-Assembly: The Role of Precursor Hydrophobicity, *J. Phys. Chem. B* **2021**, *125*, 13542.

[68] J. Heckel, F. Batti, R. T. Mathers, A. Walther, Spinodal Decomposition of Chemically Fueled Polymer Solutions, *Soft Matter* **2021**, *17*, 5401.

[69] M. A. Würbser, P. Schwarz, J. Heckel, A. M. Bergmann, A. Walther, J. Boekhoven, Chemically Fueled Block Copolymer Self-Assembly into Transient Nanoreactor, *ChemSystemsChem* **2021**, *3*, e2100015

[70] X. Lang, U. Thumu, L. Yuan, C. Zheng, H. Zhang, L. He, H. Zhao, C. Zhao, Chemical Fuel-Driven Transient Polymeric Micelle Nanoreactors toward Reversible Trapping and Reaction Acceleration, *Chem. Commun.* **2021**, *57*, 5786.

[71] B. Zhang, I. M. Jayalath, J. Ke, J. L. Sparks, C. S. Hartley, D. Konkolewicz, Chemically Fueled Covalent Crosslinking of Polymer Materials, *Chem. Commun.* **2019**, *55*, 2086.

[72] H. Xu, S. Bai, G. Gu, Y. Gao, X. Sun, X. Guo, F. Xuan, Y. Wang, Bioinspired Self-Resettable Hydrogel Actuators Powered by a Chemical Fuel, *ACS Appl. Mater. Interfaces* **2022**, *14*, 43825.

[73] C. W. H. Rajawasam, C. Tran, J. L. Sparks, W. H. Krueger, C. S. Hartley, D. Konkolewicz, Carbodiimide-Driven Toughening of Interpenetrated Polymer Networks, *Angew. Chem. Int. Ed.* **2024**, *63*, e202400843.

[74] B. Klemm, R. W. Lewis, I. Piergentili, R. Eelkema, Temporally Programmed Polymer - Solvent Interactions Using a Chemical Reaction Network, *Nat. Commun.* **2022**, *13*, 6242.

[75] R. W. Lewis, B. Klemm, M. Macchione, R. Eelkema, Fuel-Driven Macromolecular Coacervation in Complex Coacervate Core Micelles, *Chem. Sci.* **2022**, *13*, 4533.

[76] N. Singh, B. Lainer, G. J. M. Formon, S. De Piccoli, T. M. Hermans, Re-Programming Hydrogel Properties Using a Fuel-Driven Reaction Cycle, *J. Am. Chem. Soc.* **2020**, *142*, 4083.

[77] N. Singh, A. Lopez-Acosta, G. J. M. Formon, T. M. Hermans, Chemically Fueled Self-Sorted Hydrogels, *J. Am. Chem. Soc.* **2022**, *144*, 410.

[78] A. N. Zaikin, A. M. Zhabotinsky, Concentration Wave Propagation in Two-Dimensional Liquid-Phase Self-Oscillating System, *Nature* **1970**, *225*, 535.

[79] E. C. Edblom, M. Orban, I. R. Epstein, A New Iodate Oscillator: The Landolt Reaction with Ferrocyanide in a Cstr, *J. Am. Chem. Soc.* **1986**, *108*, 2826.

[80] H. N. Alyea, The Old Nassau Reaction, *J. Chem. Educ.* **1977**, *54*.

[81] T. S. Briggs, W. C. Rauscher, An Oscillating Iodine Clock, *J. Chem. Educ.* **1973**, *50*.

[82] R. Yoshida, T. Ueki, Evolution of Self-Oscillating Polymer Gels as Autonomous Polymer Systems, *NPG Asia Mater.* **2014**, *6*, e107.

[83] T. Ueki, M. Shibayama, R. Yoshida, Self-Oscillating Micelles, *Chem. Commun.* **2013**, *49*, 6947.

[84] R. Yoshida, T. Sakai, S. Ito, T. Yamaguchi, Self-Oscillation of Polymer Chains with Rhythmical Soluble-Insoluble Changes, *J. Am. Chem. Soc.* **2002**, *124*, 8095.

[85] Y. Shiraki, R. Yoshida, Autonomous Intestine-Like Motion of Tubular Self-Oscillating Gel, *Angew. Chem. Int. Ed.* **2012**, *51*, 6112.

[86] R. Yoshida, Self-Oscillating Gels Driven by the Belousov-Zhabotinsky Reaction as Novel Smart Materials, *Adv. Mater.* **2010**, *22*, 3463.

[87] Y. Murase, S. Maeda, S. Hashimoto, R. Yoshida, Design of a Mass Transport Surface Utilizing Peristaltic Motion of a Self-Oscillating Gel, *Langmuir* **2009**, *25*, 483.

[88] D. Suzuki, T. Sakai, R. Yoshida, Self-Flocculating/Self-Dispersing Oscillation of Microgels, *Angew. Chem. Int. Ed.* **2008**, *47*, 917.

[89] S. Shinohara, T. Seki, T. Sakai, R. Yoshida, Y. Takeoka, Photoregulated Wormlike Motion of a Gel, *Angew. Chem. Int. Ed.* **2008**, *47*, 9039.

[90] S. Maeda, Y. Hara, R. Yoshida, S. Hashimoto, Peristaltic Motion of Polymer Gels, *Angew. Chem. Int. Ed.* **2008**, *47*, 6690.

[91] S. Maeda, Y. Hara, T. Sakai, R. Yoshida, S. Hashimoto, Self-Walking Gel, *Adv. Mater.* **2007**, *19*, 3480.

[92] Y. Takeoka, M. Watanabe, R. Yoshida, Self-Sustaining Peristaltic Motion on the Surface of a Porous Gel, *J. Am. Chem. Soc.* **2003**, *125*, 13320.

[93] R. Yoshida, T. Takahashi, T. Yamaguchi, H. Ichijo, Self-Oscillating Gel, *J. Am. Chem. Soc.* **1996**, *118*, 5134.

[94] G. Wang, J. Sun, L. An, S. Liu, Fuel-Driven Dissipative Self-Assembly of a Supra-Amphiphile in Batch Reactor, *Biomacromolecules* **2018**, *19*, 2542.

[95] G. Wang, B. Tang, Y. Liu, Q. Gao, Z. Wang, X. Zhang, The Fabrication of a Supra-Amphiphile for Dissipative Self-Assembly, *Chem. Sci.* **2016**, *7*, 1151.

[96] M. R. Hoffmann, Kinetics and Mechanism of Oxidation of Hydrogen-Sulfide by Hydrogen-Peroxide in Acidic Solution, *Environ. Sci. Technol.* **1977**, *11*, 61.

[97] K. M. Kovács, G. Rábai, Large Amplitude Ph Oscillations in the Hydrogen Peroxide−Dithionite Reaction in a Flow Reactor, *J. Phys. Chem. A* **2001**, *105*, 9183.

[98] G. Rabai, K. Kustin, I. R. Epstein, A Systematically Designed Ph Oscillator: The Hydrogen Peroxide-Sulfite-Ferrocyanide Reaction in a Continuous-Flow Stirred Tank Reactor, *J. Am. Chem. Soc.* **1989**, *111*, 3870.

[99] E. C. Edblom, Y. Luo, M. Orban, K. Kustin, I. R. Epstein, Systematic Design of Chemical Oscillators. 45. Kinetics and Mechanism of the Oscillatory Bromate-Sulfite-Ferrocyanide Reaction, *J. Phys. Chem.* **1989**, *93*, 2722.

[100] G. Rabai, M. Orban, I. R. Epstein, Systematic Design of Chemical Oscillators. 64. Design of Ph-Regulated Oscillators, *Acc. Chem. Res.* **1990**, *23*, 258.

[101] G. Rabai, I. Hanazaki, Ph Oscillations in the Bromate-Sulfite-Marble Semibatch and Flow Systems, *J. Phys. Chem.* **1996**, *100*, 10615.

[102] G. Wang, Y. Liu, Y. Liu, N. Xia, W. Zhou, Q. Gao, S. Liu, The Non-Equilibrium Self-Assembly of Amphiphilic Block Copolymers Driven by a Ph Oscillator, *Colloids Surf. A: Physicochem. Eng. Asp* **2017**, *529*, 808.

[103] X. Li, G. Wang, Q. Zhang, Y. Liu, T. Sun, S. Liu, Dissipative Self-Assembly of a Dual-Responsive Block Copolymer Driven by a Chemical Oscillator, *J. Colloid Interface Sci.* **2022**, *615*, 732.

[104] C. Yang, F. Su, Y. Liang, W. Xu, S. Li, E. Liang, G. Wang, N. Zhou, Q. Wan, X. Ma, Fabrication of a Biomimetic Hydrogel Actuator with Rhythmic Deformation Driven by a Ph Oscillator, *Soft Matter* **2020**, *16*, 2928.

[105] C. Yang, F. Su, Y. Xu, Y. Ma, L. Tang, N. Zhou, E. Liang, G. Wang, J. Tang, Ph Oscillator-Driven Jellyfish-Like Hydrogel Actuator with Dissipative Synergy between Deformation and Fluorescence Color Change, *ACS Macro Lett.* **2022**, *11*, 347.

[106] K. Kovacs, R. E. McIlwaine, S. K. Scott, A. F. Taylor, Ph Oscillations and Bistability in the Methylene Glycol-Sulfite-Gluconolactone Reaction, *PCCP* **2007**, *9*, 3711.

[107] K. Kovacs, R. E. McIlwaine, S. K. Scott, A. F. Taylor, An Organic-Based Ph Oscillator, *J. Phys. Chem. A* **2007**, *111*, 549.

[108] E. Poros, V. Horvath, K. Kurin-Csorgei, I. R. Epstein, M. Orban, Generation of Ph-Oscillations in Closed Chemical Systems: Method and Applications, *J. Am. Chem. Soc.* **2011**, *133*, 7174.

[109] L. Heinen, A. Walther, Temporal Control of I-Motif Switch Lifetimes for Autonomous Operation of Transient DNA Nanostructures, *Chem. Sci.* **2017**, *8*, 4100.

[110] E. Tóth-Szeles, J. Horváth, G. Holló, R. Szűcs, H. Nakanishi, I. Lagzi, Chemically Coded Time-Programmed Self-Assembly, *Mol. Syst. Des. Eng.* **2017**, *2*, 274.

[111] G. Panzarasa, A. L. Torzynski, T. Sai, K. Smith-Mannschott, E. R. Dufresne, Transient Supramolecular Assembly of a Functional Perylene Diimide Controlled by a Programmable Ph Cycle, *Soft Matter* **2020**, *16*, 591.

[112] G. Hu, J. A. Pojman, S. K. Scott, M. M. Wrobel, A. F. Taylor, Base-Catalyzed Feedback in the Urea-Urease Reaction, *J. Phys. Chem. B* **2010**, *114*, 14059.

[113] M. M. Wrobel, T. Bansagi, Jr., S. K. Scott, A. F. Taylor, C. O. Bounds, A. Carranza, J. A. Pojman, Ph Wave-Front Propagation in the Urea-Urease Reaction, *Biophys. J.* **2012**, *103*, 610.

[114] X. Fan, A. Walther, Ph Feedback Lifecycles Programmed by Enzymatic Logic Gates Using Common Foods as Fuels, *Angew. Chem. Int. Ed.* **2021**, *60*, 11398.

[115] T. Heuser, R. Merindol, S. Loescher, A. Klaus, A. Walther, Photonic Devices out of Equilibrium: Transient Memory, Signal Propagation, and Sensing, *Adv. Mater.* **2017**, *29*, 1606842.

[116] H. Che, B. C. Buddingh, J. C. M. van Hest, Self-Regulated and Temporal Control of a "Breathing" Microgel Mediated by Enzymatic Reaction, *Angew. Chem. Int. Ed.* **2017**, *56*, 12581.

[117] H. Che, S. Cao, J. C. M. van Hest, Feedback-Induced Temporal Control of "Breathing" Polymersomes to Create Self-Adaptive Nanoreactors, *J. Am. Chem. Soc.* **2018**, *140*, 5356.

[118] W. P. van den Akker, H. Wu, P. L. W. Welzen, H. Friedrich, L. Abdelmohsen, R. van Benthem, I. K. Voets, J. C. M. van Hest, Nonlinear Transient Permeability in Ph-Responsive Bicontinuous Nanospheres, *J. Am. Chem. Soc.* **2023**, *145*, 8600.

[119] W. P. van den Akker, R. van Benthem, I. K. Voets, J. C. M. van Hest, Dampened Transient Actuation of Hydrogels Autonomously Controlled by Ph-Responsive Bicontinuous Nanospheres, *ACS Appl. Mater. Interfaces* **2024**, *16*, 19642.

[120] X. Fan, A. Walther, Autonomous Transient Ph Flips Shaped by Layered Compartmentalization of Antagonistic Enzymatic Reactions, *Angew. Chem. Int. Ed.* **2021**, *60*, 3619.

[121] C. Biagini, S. Albano, R. Caruso, L. Mandolini, J. A. Berrocal, S. Di Stefano, Variations in the Fuel Structure Control the Rate of the Back and Forth Motions of a Chemically Fuelled Molecular Switch, *Chem. Sci.* **2018**, *9*, 181.

[122] S. Erbas-Cakmak, S. D. P. Fielden, U. Karaca, D. A. Leigh, C. T. McTernan, D. J. Tetlow, M. R. Wilson, Rotary and Linear Molecular Motors Driven by Pulses of a Chemical Fuel, *Science* **2017**, *358*, 340.

[123] V. W. Liyana Gunawardana, T. J. Finnegan, C. E. Ward, C. E. Moore, J. D. Badjic, Dissipative Formation of Covalent Basket Cages, *Angew. Chem. Int. Ed.* **2022**, *61*, e202207418.

[124] D. Del Giudice, E. Spatola, M. Valentini, C. Bombelli, G. Ercolani, S. Di Stefano, Time-Programmable Ph: Decarboxylation of Nitroacetic Acid Allows the Time-Controlled Rising of Ph to a Definite Value, *Chem. Sci.* **2021**, *12*, 7460.

[125] D. Mariottini, D. Del Giudice, G. Ercolani, S. Di Stefano, F. Ricci, Dissipative Operation of Ph-Responsive DNA-Based Nanodevices, *Chem. Sci.* **2021**, *12*, 11735.

[126] E. Olivieri, G. Quintard, J. V. Naubron, A. Quintard, Chemically Fueled Three-State Chiroptical Switching Supramolecular Gel with Temporal Control, *J. Am. Chem. Soc.* **2021**, *143*, 12650.

[127] E. Olivieri, B. Gasch, G. Quintard, J. V. Naubron, A. Quintard, Dissipative Acid-Fueled Reprogrammable Supramolecular Materials, *ACS Appl. Mater. Interfaces* **2022**, *14*, 24720.

Chapter

2 Chemically-Fueled Self-Assembly of Amphiphilic Copolymers: Targeting Fuel Efficiency Through Polymer Design

2.1. Abstract

Amphiphilic copolymers capable of self-assembly offer a diverse and versatile platform for the development of advanced materials and responsive nanostructures with tailored properties. By coupling a copolymer with a hydrophilic to hydrophobic switchable block with carbodiimide-mediated chemical fueling, we explore the interplay of copolymer structure and composition on the dynamics of the fuel cycle and the resulting transient self-assembly. By altering the length of the passive block, we are able to target different morphologies of self-assembled structures, and show that altering the composition of the switchable block allows us to achieve longer-lasting self-assembly while consuming less chemical fuel, a feature we term fuel efficiency.

2.2. Introduction

Driven by the pursuit of materials with tailored properties,[1-2] the capacity to organize molecular building blocks into well-defined structures through a bottom-up approach and the wide chemical space available to explore in macromolecular chemistry, the field of polymer self-assembly has witnessed significant advancements in past decades.[3] Block copolymers (BCPs), polymer chains composed of at least two discrete blocks, each with different chemical properties based on its composition[4] are of particular relevance. By incorporating dissimilar polymer segments, polymer-polymer and polymer-solvent interactions can be controlled to form a wide variety of structures in a solution-phase environment,[5] with applications ranging from nanostructured materials[6] to drug delivery systems and therapeutics.[7]

Approaches to direct the solution-phase assembly of BCPs include spherical and worm-like micelles, as well as vesicle formation by solvent exchange from a favorable solvent to one capable of solvating only one of the polymer segments,[8-9] temperature-induced self-assembly exploiting lower critical solution temperature (LCST) and upper critical solution temperature (UCST) behavior of BCPs [10-11] as well as polymerization-induced self-assembly (PISA).[12-13] Control over self-assembly of BCPs may also be achieved by employing chemical stimuli, such as pH,[14-15] redox reactions[16] and small molecules.[17] These stimuli can be used to both trigger self-assembly and modulate assembly morphology, but are limited in their ability to control the system in the time domain.[18]

More complex control can be achieved by employing a fuel-driven chemical reaction network (CRN),[19] in which the reaction between a fuel molecule and the building block(s) primes them for self-assembly, and a deactivation reaction returns them to their original state. These two competing reactions allow for temporal control over building block activation, and therefore transient self-

assembly.[20] Examples of employed reaction cycles include ATP-driven systems[21-22], enzymatic[23] and non-enzymatic[24] pH cycles, transient methylation[25-26] and the Morita-Baylis-Hillman allylic substitution.[23-24] These last two have been employed in polymeric systems to control the clustering of BCP colloids[27] and self-assembly of poly(vinylpyridine)-containing polymers into micelles[28] and to guide the formation of complex core coacervate micelles.[29]

Carbodiimide-fueled anhydride formation, specifically employing 1-ethyl-3-(3-dimethylaminopropyl) carbodiimide (EDC), has arguably become the most widespread CRN for controlling self-assembled systems. First pioneered by Boekhoeven[30] and Hartley,[31] the cycle relies on the activation of a carboxyl group by the carbodiimide fuel to yield an activated *O*-acylurea, which further reacts with an additional carboxyl group to generate an anhydride. Self-assembly is generally achieved by charge-neutralization of the negatively charged carboxyl group in the building block allowing for assembly,[32] and this strategy has been applied numerous times to peptide systems, yielding transient gels,[30] fibers,[33-34] vesicles[35] and complex coacervate droplets[36-39] as well as small molecules to yield phase-separated droplets.[40-41] EDC fueling has also been employed to control polymer-solvent interactions, leading to the spinodal decomposition of polymer solutions[42] and assembly of copolymers into transient micelles.[43]

While general considerations for designing systems responsive to EDC fueling are now well known, polymeric systems have to date relied on the complete reaction of each monomer unit, leading to significant waste accumulation and the associated loss of efficiency.

Herein, we target fuel efficiency in the EDC-fueled assembly of block copolymers by controlling the composition of the responsive block (Figure 2.1a). By including a non-responsive, highly hydrophobic co-monomer in the responsive segment, we are able to bring the polymer to the brink of the hydrophilic to hydrophobic transition, such that on fueling (Figure 2.1b), longer-lasting self-assembly can be achieved while employing significantly lower fuel concentrations (Figure 2.1c). To this end, we systematically explore the effect of polymer composition and relative block length on the fuel efficiency and self-assembled morphologies of a library of block copolymers.

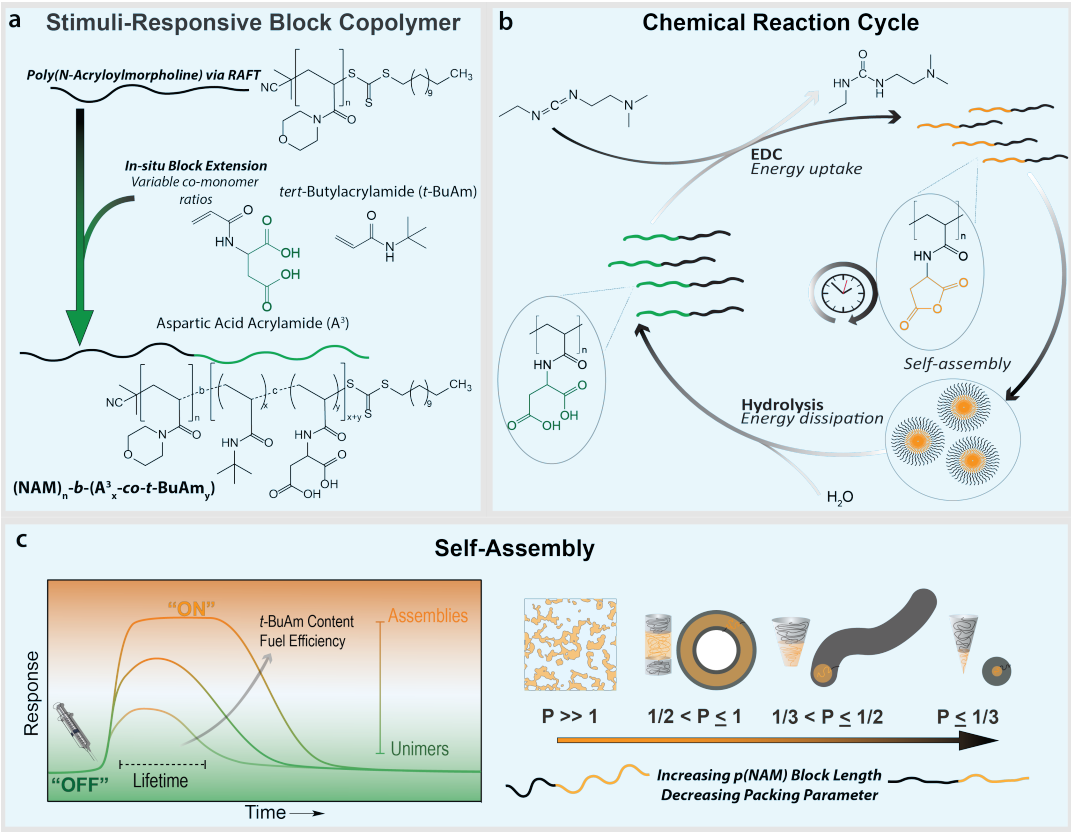

Figure 2.1: From monomer building blocks to transient self-assembly. (a) Synthesis of block copolymers with varying second block composition *via* RAFT. (b) Chemical reaction cycle of EDC-fueled anhydride formation leads in switch to amphiphilic BCP and resulting time-controlled self-assembly. (c) Self-assembly response of the polymers can be controlled both in duration and morphology by altering the length of the first block and the monomer ratio in the second.

2.3. Results and Discussion

2.3.1. Design and synthesis of Poly(NAM)-*b*-(A^3-*co*-*t*-BuAm) Copolymers

To obtain a polymer that displays the desired fuel-responsive self-assembly behavior, we designed and synthesized *via* RAFT polymerization a BCP composed of a hydrophilic first block composed of poly(*N*-acryloylmorpholine) (poly(NAM)), and a second block composed of A^3 and *t*-BuAm in varying ratios. Poly(NAM) was selected due to the highly hydrophilic nature of the polymer, comparable to poly(ethyleneglycol).[44-45] RAFT polymerization of poly(NAM) has been well established,[46-47] and by synthesizing the poly(NAM) block and extending it in situ, the block length can easily be tailored on demand.

We employ the hydrophilic aspartic acid *N*-acrylamide (A^3) in the responsive block due to the formation of a 5-memebered anhydride ring on EDC fueling. This structural motif has been employed in numerous peptide and small molecule systems, leading to a robust understanding of the fueling process.[33,48] The A^3 unit is weakly acidic,[49] and therefore ideal for employing a charge-neutralization strategy at range 5.0-7.0 commonly associated with EDC fueling. *Tert*-butylacrylamide (*t*-BuAm) is included in the second block as a hydrophobic co-monomer to tune the overall water-solubility of the responsive block. This brings the responsive block closer to the hydrophilic/hydrophobic transition, and therefore reduces the threshold fuel concentration

required for assembly. Additionally, the RAFT copolymerization of NAM and *t*-BuAm has been previously established in the synthesis of non-responsive polymer surfactants.[47]

The polymers were synthesized by RAFT polymerization, employing 2-cyano-2-propyl dodecyl trithiocarbonate (CPDT) as the chain transfer agent (CTA) and azobisisobutyronitrile (AIBN) as the initiator in a two-step, one-pot synthesis as outlined in Figure 2.2a. In the first step we synthesized poly(NAM) with monomer to CTA ratios of 50:1 and 100:1, respectively (Figure 2.2b-d). The poly(NAM) blocks obtained show a controlled polymerization (Figure 2.2b), yielding polymers with a tight dispersity (Figure 2.2c,d). We subsequently extended the first block *in situ* through the addition of $A^3$and *t*-BuAm (Figure 2.2e-f).The ratio of A^3 to *t*-BuAm monomers was systematically varied, spanning the range from 0:100 to 50:50, with a target of 100 repeat units. This approach allowed us to systematically synthesize 8 block copolymers. The *in-situ* block extension was confirmed by GPC in all cases (Figure 2.2e, Section 2.5.1). The final polymers were analyzed by ^{1}H-NMR to determine their monomer makeup (Figure 2.2f, Section 2.5.1), which was found to be in good agreement with the theoretical ratios. We synthesized 5 polymer samples with a poly(NAM) block of 35-40 units and two with longer NAM segments of 107 and 111 units, respectively. Finally, we synthesized a gradient BCP containing a short initial NAM block of 39 units, with additional units incorporated into the A^3/*t*-BuAm switchable block. A summary of polymer characterization data is reported in Table 2.1.

Table 2.1: Summary of Polymer Samples

Polymer Sample	Repeat Units (^{1}H-NMR)			*Đ* (GPC)		$M_{n\ (GPC)}$
	NAM	A^3	*t*-BuAm	First Block	Final Copolymer	kg mol^1
NAM_{37}-*b*-(A^3_8-*co*-*t*-$BuAm_{96}$)	37	8	96	1.12	1.20	26.2
NAM_{38}-*b*-(A^3_{19}-*co*-*t*-$BuAm_{81}$)	38	19	81	1.23	1.21	22.7
NAM_{39}-*b*-(A^3_{27}-*co*-*t*-$BuAm_{76}$)	39	27	76	1.24	1.17	23.9
NAM_{37}-*b*-(A^3_{36}-*co*-*t*-$BuAm_{66}$)	37	36	66	1.25	1.18	22.4
NAM_{35}-*b*-(A^3_{43}-*co*-*t*-$BuAm_{57}$)	35	43	57	1.16	1.20	23.0
NAM_{107}-*b*-(A^3_{17}-*co*-*t*-$BuAm_{74}$)	107	17	74	1.25	1.14	18.0
NAM_{111}-*b*-(A^3_{28}-*co*-*t*-$BuAm_{77}$)	111	28	77	1.28	1.18	18.7
NAM_{39}-*b*-(NAM_{57}-*co*-A^3_9-*co*-*t*-$BuAm_{80}$)	96*	9	80	1.1	1.21	18.5

* NAM_{39}-*b*-(NAM_{57}-*co*-A^3_9-*co*-*t*-$BuAm_{80}$) has an initial poly(NAM) block of 39 units, with the remaining 57 incorporated into the second block.

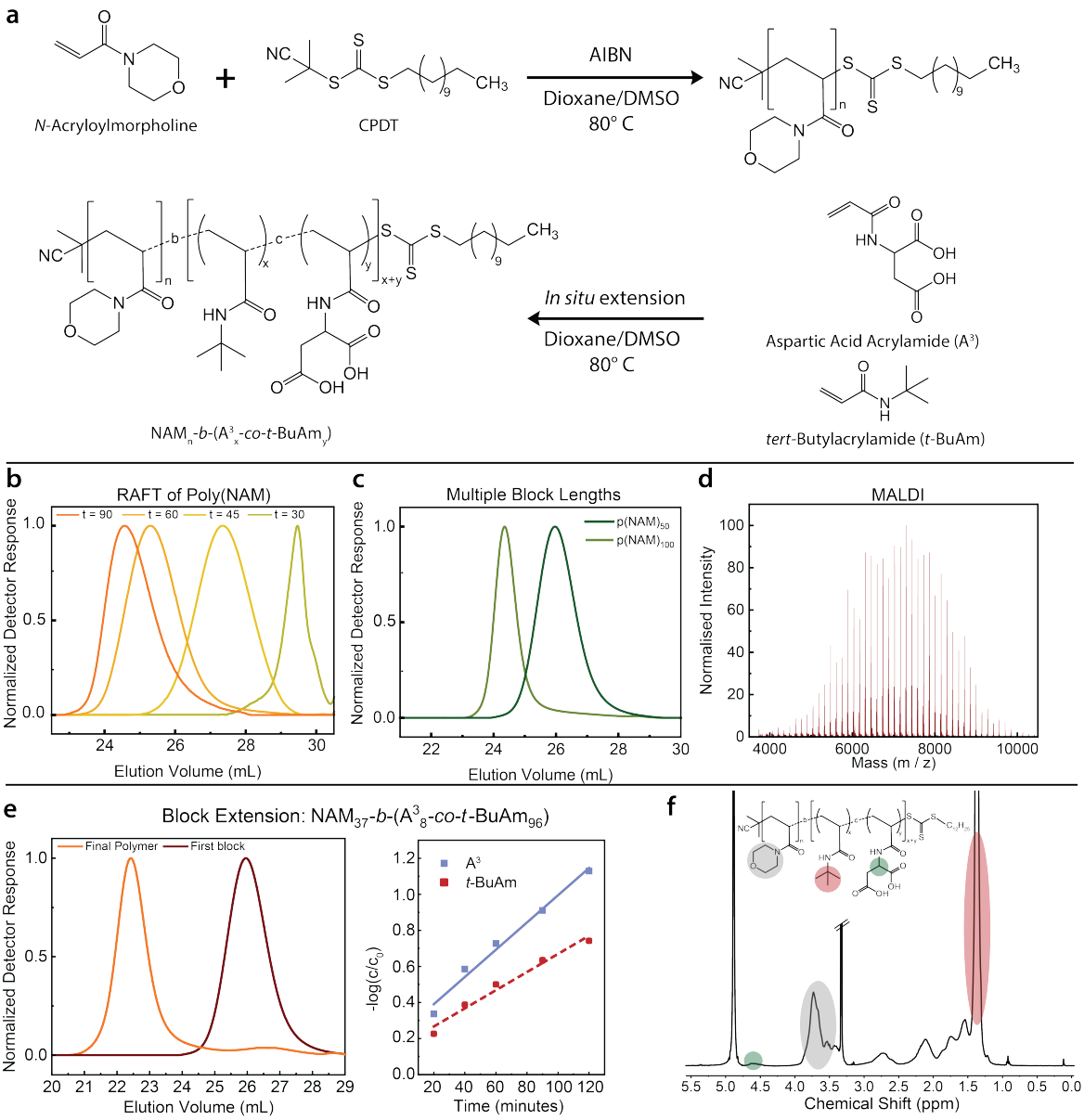

Figure 2.2: Synthesis of (NAM)-b-(A³-co-*t*-BuAm) Copolymers. (a) Scheme describing the two-step synthesis, beginning with RAFT polymerization of NAM and in situ block extension to afford the final block copolymers. (b) GPC elugram of a first block polymerization of poly(NAM) with a NAM to CTA ratio of 100:1 at varying reaction times, displaying tight dispersity during chain growth. (c) GPC elugrams of completed poly(NAM) with a NAM to CTA ratio of 50:1 (M_n(GPC) = 3285 g mol^{-1}, $Đ$ = 1.12) and 100:1 (M_n (GPC) = 7720 g mol^{-1}, $Đ$ = 1.20) (d) Matrix-assisted laser desorption ionization (MALDI) mass spectrogram of a representative sample of poly(NAM) (first block of NAM_{37}-*b*-(A^3_8-*co*-*t*-$BuAm_{96}$)), prior to chain extension, M_n = 6943 g mol^{-1}, $Đ$ = 1.05. (e) In situ block extension of poly(NAM) (M_n(GPC) = 3285 g mol^{-1}, $Đ$ = 1.12) to afford NAM_{37}-b-(A^3_8-*co*-*t*-$BuAm_{96}$) (M_n (GPC) = 26.2 kg mol^{-1}, $Đ$ = 1.20). The final polymer is methylated to allow for effective analysis in THF GPC. (f) NMR of NAM_{37}-*b*-(A^3_8-*co*-*t*-$BuAm_{96}$), indicating the regions used for the determination of the monomer makeup in the final polymer chain.

2.3.2. Block Copolymer Self-Assembly

Plate Reader Absorbance Studies

To study the effect of polymer architecture on EDC-fueled self-assembly of the BCPs, we conducted a series of fueling experiments at polymer concentrations of 5 g L^{-1} in 100 mM 2-(N-morpholino)ethanesulfonic acid (MES) buffer at pH 6.2 with 100 mM NaCl. EDC was added from a buffered stock solution as 25-200 equivalents with respect to carboxyl groups in the polymer. Upon addition of EDC, the optical density of the polymer solutions at 440 nm was monitored to observe the evolution of the fueled self-assembly (Figure 2.3, see Section 2.5.5).

NAM_{37}-*b*-(A^3_8-*co*-*t*-$BuAm_{96}$), NAM_{38}-*b*-(A^3_{19}-*co*-*t*-$BuAm_{81}$), NAM_{39}-*b*-(A^3_{27}-*co*-*t*-$BuAm_{76}$), NAM_{37}-*b*-(A^3_{36}-*co*-*t*-$BuAm_{66}$) and NAM_{35}-*b*-(A^3_{43}-*co*-*t*-$BuAm_{57}$) were fueled with 200 equivalents EDC (with respect to carboxyl groups) to explore the effect of polymer composition on fueled behavior (Figure 2.3a). All polymers displayed a rapid response to fueling, with each solution becoming turbid within 5 minutes of fuel addition, indicative of self-assembly taking place.

NAM_{37}-*b*-(A^3_8-*co*-*t*-$BuAm_{96}$) (A^3/*t*-BuAm molar ratio of 0.08) displays a self-assembly lifetime (defined as the time taken for optical density to return to ½OD_{max}) of 1085 minutes, which decreases to 496 minutes for NAM_{38}-*b*-(A^3_{19}-*co*-*t*-$BuAm_{81}$), with a A^3/*t*-BuAm ratio of 0.23. Further increasing the A^3/*t*-BuAm ratio in NAM_{39}-*b*-(A^3_{27}-*co*-*t*-$BuAm_{76}$) (A^3/*t*-BuAm = 0.36), NAM_{36}-*b*-(A^3_{36}-*co*-*t*-$BuAm_{66}$) (A^3/*t*-BuAm = 0.54) and NAM_{35}-*b*-(A^3_{43}-*co*-*t*-$BuAm_{57}$) (A^3/*t*-BuAm = 0.75) leads to shorter lifetimes of 152, 45 and 26 minutes respectively. This trend illustrates how decreasing A^3 content in the responsive block allows for longer self-assembly to take place, while requiring lower fuel concentrations (Figure 2.3a, insert).

Each polymer also shows a fuel-dependent self-assembly response, with increasing fuel loading leading to longer assembly lifetimes. For example, NAM_{37}-*b*-(A^3_8-*co*-*t*-$BuAm_{96}$) (Figure 2.3b) shows increasing self-assembly lifetimes with increased EDC loading. 25 equivalents of EDC (107.5 mM) cause the polymer to self-assemble for 90 minutes. Increasing EDC loading to 50 equivalents (215 mM) and 100 equivalents (430 mM) increases the lifetime to 181 minutes and 372 minutes, doubling lifetime as fuel concentration doubles. It is worth noting that loading with 200 equivalents of EDC (860 mM) leads however to a far longer lifetime of the fueled state, at 1085 minutes. It is likely that kinetic trapping of the fueled state, as has been reported in peptide systems[33] may influence this lifetime increase.

NAM_{107}-*b*-(A^3_{17}-*co*-*t*-$BuAm_{74}$), NAM_{111}-*b*-(A^3_{28}-*co*-*t*-$BuAm_{77}$), NAM_{39}-*b*-(NAM_{57}-*co*-A^3_9-*co*-*t*-$BuAm_{80}$), with a larger poly(NAM) content, display a similar trend based on the A^3 content of their responsive block (Figure 2.3c). When fueled with 200 equivalents EDC, NAM_{107}-*b*-(A^3_{17}-*co*-*t*-$BuAm_{74}$) (A^3/*t*-BuAm = 0.23) displays a self-assembly lifetime of 686 minutes, NAM_{111}-*b*-(A^3_{28}-*co*-*t*-$BuAm_{77}$) (A^3/*t*-BuAm = 0.36) of 181 minutes and NAM_{39}-*b*-(NAM_{57}-*co*-A^3_9-*co*-*t*-$BuAm_{80}$) (A^3/*t*-BuAm 0.11) shows a far longer lifetime of 1814 minutes. NAM_{39}-*b*-(NAM_{57}-*co*-A^3_9-*co*-*t*-$BuAm_{80}$) (Figure 2.3d), when fueled with 25, 50, 100 and 200 EDC equivalents (90, 180, 360 and 720 mM EDC), self-assembles for periods of 129, 336, 800 and 1814 minutes, showing how self-assembly lifetime scales with fuel loading for polymers with larger poly(NAM) content.

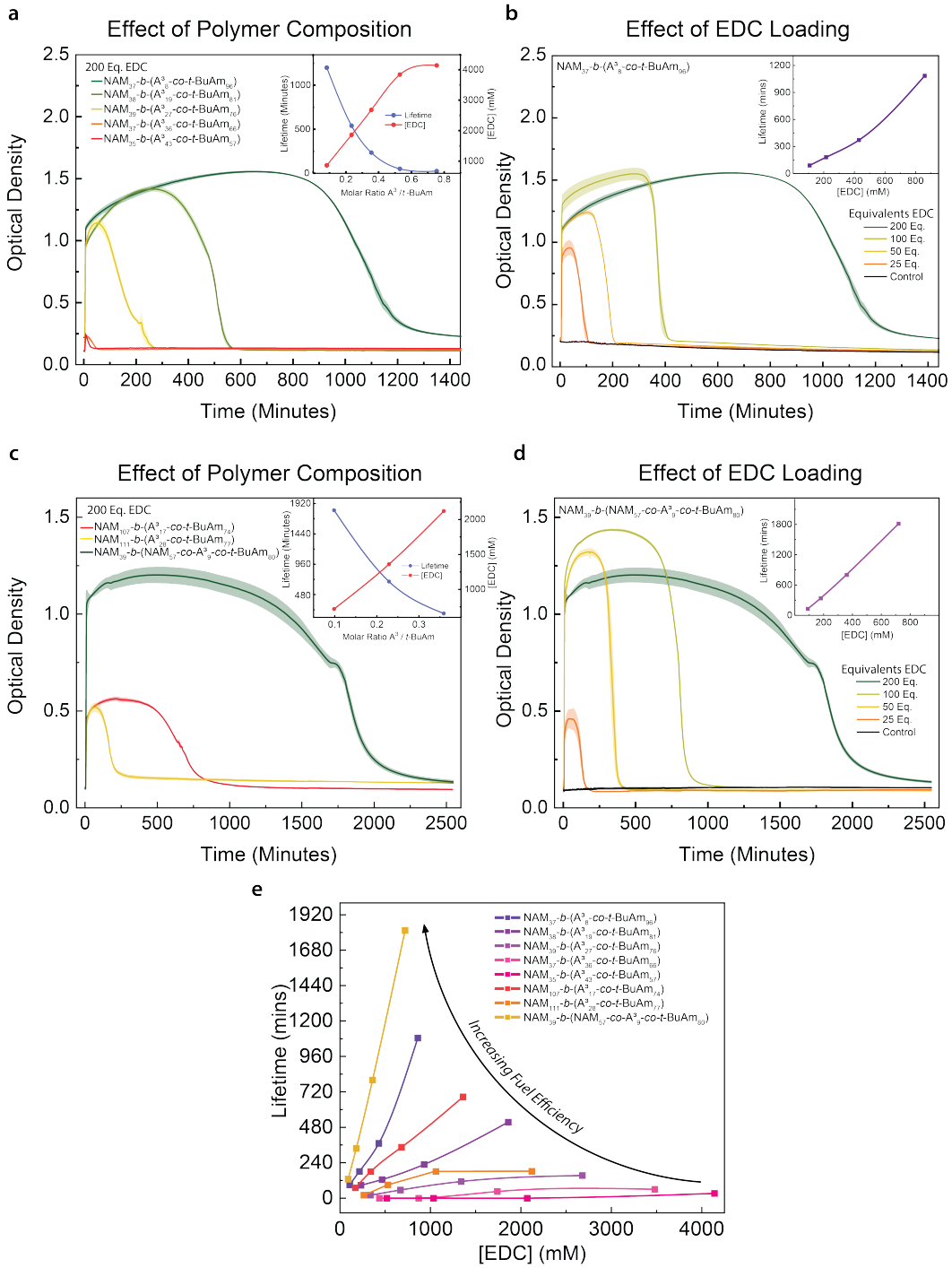

Figure 2.3: Screening of polymer fueling behavior. (a) Effect of polymer composition on optical density and lifetime of fueled state for short poly(NAM) segment polymers, with 200 equivalents of EDC with respect to carboxyl groups. Insert: lifetime of fueled state and EDC concentration corresponding to 200 equivalents for each A^3/*t*-BuAm monomer ratio. (b) Effect of increasing EDC equivalents on fueling behavior of NAM_{37}-*b*-(A^3_8-*co*-*t*-$BuAm_{96}$). Insert: Lifetime of fueled state versus concentration of EDC. (c) Effect of polymer composition on optical density and lifetime of fueled state for polymers with high NAM content, with 200 equivalents of EDC with respect to carboxyl groups. Insert: lifetime of fueled state and EDC concentration corresponding to 200 equivalents for each A^3/*t*-BuAm monomer ratio. (d) Effect of increasing EDC equivalents on fueling behavior of NAM_{39}-b-(NAM_{57}-co-A^3_9-*co*-*t*-$BuAm_{80}$). Insert: Lifetime of fueled state versus concentration of EDC. (e) Comparison of fueled state lifetimes for each polymer in relation to the concentration of EDC. Polymers with steeper curves display longer lifetimes while requiring less fuel, and are therefore termed more fuel efficient. Conditions for all experiments are 5 mg mL^{-1} polymer, 100 mM MES buffer, pH 6.2, with added 100 mM NaCl. Error contours show the standard error for measurements, with **n** = 3. Plots for all measured fuel equivalents for all polymers are available in Section 2.5.5

By comparing NAM$_{38}$-*b*-(A$^3_{19}$-*co*-*t*-BuAm$_{81}$) and NAM$_{39}$-*b*-(A$^3_{27}$-*co*-*t*-BuAm$_{76}$) to NAM$_{107}$-*b*-(A$^3_{17}$-*co*-*t*-BuAm$_{74}$) and NAM$_{111}$-*b*-(A$^3_{28}$-*co*-*t*-BuAm$_{77}$), which have comparable A^3/*t*-BuAm ratios, the effect of increasing poly(NAM) segment length on fueling behavior is determined. Self-assembly duration (given the same fueling stoichiometry) is governed largely by the molar ratio of A^3 to *t*-BuAm in the responsive block, with only a minor increase in lifetime due to the increase in poly(NAM) block length.

NAM$_{38}$-*b*-(A$^3_{19}$-*co*-*t*-BuAm$_{81}$) and NAM$_{107}$-*b*-(A$^3_{17}$-*co*-*t*-BuAm$_{74}$) (with A^3/*t*-BuAm = 0.23 and 0.23) show lifetimes of 496 and 686 minutes respectively. Likewise, NAM$_{39}$-*b*-(A$^3_{27}$-*co*-*t*-BuAm$_{76}$) and NAM$_{111}$-*b*-(A$^3_{28}$-*co*-*t*-BuAm$_{77}$) (A^3/*t*-BuAm = 0.36 and 0.36) display lifetimes of 152 and 181 minutes respectively. However, comparing NAM$_{37}$-*b*-(A$^3_{8}$-*co*-*t*-BuAm$_{96}$) and NAM$_{39}$-*b*-(NAM$_{57}$-*co*-A$^3_{9}$-*co*-*t*-BuAm$_{80}$), both with a similar A^3/*t*-BuAm ratio of 0.08 and 0.11, the effect of altered polymer architecture is marked. When both are fueled with 200 equivalents of EDC, NAM$_{39}$-*b*-(NAM$_{57}$-*co*-A$^3_{9}$-*co*-*t*-BuAm$_{80}$) displays a much longer self-assembly lifetime (1814 vs 1085 minutes), while requiring 720 compared to 860 mM EDC. This can be attributed to the unique architecture of this polymer, with a small initial poly(NAM) segment and a gradient of poly(NAM) into the second block, altering the packing parameter, and therefore structure of self-assembly taking place.

Plotting the fueled state lifetimes of each polymer versus the concentration of EDC required for each experiment (Figure 2.3e) clearly illustrates the effect of polymer design on fuel requirements. As the ratio of A^3 to *t*-BuAm decreases, the polymers become increasingly sensitive to EDC. Self-assembly requires a lower absolute EDC concentration while displaying a longer lifetime, a feature we term fuel-efficiency.

Methylated Polymers as a Model System

With the fuel-mediated response of the polymers, as well as the relationship between polymer composition, fuel concentration and self-assembly lifetimes established, we further probe the polymers through dynamic light scattering (DLS) and transmission electron microscopy (TEM) to establish the interplay between responsive block composition and passive block length in regulating the nature of self-assembly.

While DLS allows for the convenient, non-destructive and time-dependent monitoring of both the number of objects in a sample volume, their hydrodynamic radii, R_h, and the distribution thereof, it cannot conclusively determine the morphology of non-spherical or high aspect ratio objects with a single scattering angle.[50-51] Rather, the sphere-equivalent hydrodynamic radius, R_h is obtained from diffusion coefficients, *D,* extracted from the measured autocorrelation function, and transformed to R_h according to the Einstein-Stokes equation.[52] We therefore employ TEM to directly image the shape and size of the assembled structures, thus providing empirical evidence to validate our DLS measurements.

We first employ a model system composed of statically-assembled polymers to probe the effect of polymer composition on self-assembly in an idealized system where A^3 unit activation is complete, deactivation due to hydrolysis is absent, and exclude changes in self-assembly over time. To achieve this, all polymers were exhaustively methylated at their carboxyl groups by addition of trimethylsilyl diazomethane, rendering the A^3/*t*-BuAm block hydrophobic. These methylated polymers, denoted as NAM$_x$-*b*-(MeA^3_y-*co*-*t*-BuAm$_z$), were assembled *via* solvent exchange from

THF to water to achieve self-assembled structures, with a final polymer mass fraction of 1 mg mL^{-1}. Further details regarding the process are available in Section 2.5.6.

NAM$_{38}$-*b*-(MeA$^3_{19}$-*co*-*t*-BuAm$_{81}$) (Figure 2.4a) assembles into two populations of spherical objects with TEM radii, R_{TEM} of 27-35 nm, and R_{TEM} = 50-65 nm. A hollow lumen can be observed in some of the latter particles (Figure 2.4a, right panel). The spherical particles further assemble into chained structures, and larger aggregate structures (which are not observed in DLS, and are likely artefacts of drying the sample for TEM imaging). The sample presents a mean R_{TEM} = 47.1 nm, and a DLS hydrodynamic radius of $R_{h\,(DLS)}$ = 50.5 nm. NAM$_{39}$-*b*-(MeA$^3_{27}$-*co*-*t*-BuAm$_{76}$) (Figure 2.4b) likewise assembles into spherical objects, although these are larger, with a primary population of R_{TEM} = 60-70 nm, and a second population of hollow spherical vesicles of R_{TEM} = 100-150 nm. Assembly of the spherical objects into chained structures is also observed. DLS measurement yields $R_{h\,(DLS)}$ = 101.4 nm, in line with the mean R_{TEM} = 94.6 nm.

NAM$_{107}$-*b*-(MeA$^3_{17}$-*co*-*t*-BuAm$_{74}$) (Figure 2.4c) displays a clear bimodal size distribution, including small circular objects of R_{TEM} = 10-20 nm and long, worm-like micelles, some of which display branching (Figure 2.4c, middle panel), and others reaching lengths over 1 μm (Figure 2.4c, rightmost panel), with short axes on the scale of the smaller objects. However, the overwhelming majority of objects observed in TEM belong to the smaller population, reflected in a mean R_{TEM} = 38.0. The average $R_{h(DLS)}$ = 52.6 nm is noticeably larger due to the contribution of the long worm-like micelles.

NAM$_{39}$-*b*-(NAM$_{57}$-*co*-MeA$^3_9$-*co*-*t*-BuAm$_{80}$) displays formation of thin, worm-like structures which further assemble into circularized structures with R_{TEM} = 50-120 nm (Figure 2.4d, middle panel) and groupings of branched, network-like structures (Figure 2.4d, right panel). A small number of small, circular objects of R_{TEM} = 10-20 nm are additionally visible. Additionally, we observe a small number of non-circularized worm-like micelles. (Figure 2.4d, right panel).

The model system employed evidences the effect of poly(NAM) segment length on the self-assembly of the polymers, with increasing relative length of the hydrophilic block leading from vesicles to elongated, worm-like structures. This is in line with general expectations regarding the effect of block lengths on the packing parameter of polymer amphiphiles (Figure 2.1c), and therefore morphology of their assemblies in solution, and informs the expected morphologies of fueled assemblies. The number distributions obtained *via* TEM and the intensity-weighted DLS size distributions are, given their different weighting, in good agreement, validating our approach for monitoring self-assembly in solution. It is worth noting that the intensity of scattered light, I, scales according to $I \propto r^6$.[53] DLS is therefore increasingly sensitive as object radius increases, and a small number of large objects can significantly skew measured size distributions.[54] This is not, however, entirely disadvantageous, as it enables detection and monitoring of larger assembled structures.

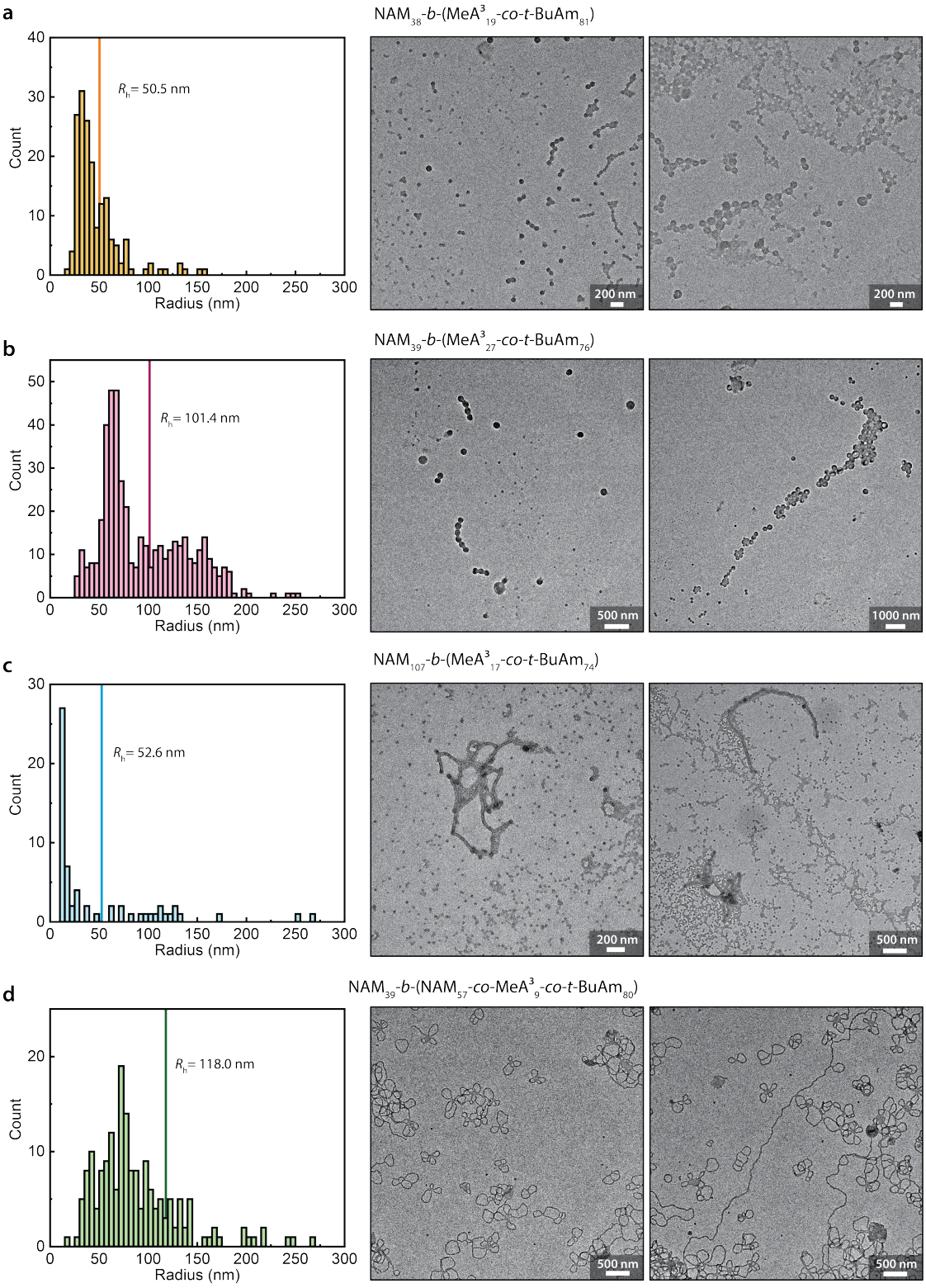

Figure 2.4: Self-assembly of methylated polymers *via* solvent exchange. (a) Left: Size distribution for NAM_{38}-*b*-(MeA^3_{19}-*co*-*t*-$BuAm_{81}$). Histogram represents number distribution from TEM micrographs, straight line indicates the intensity-weighted mean R_h. Average R_{TEM} = 47.1 nm (PDI = 0.27), weighted mean R_h = 50.5 nm (PDI = 0.49) Right: TEM Micrographs of the polymer sample. (b) NAM_{39}-*b*-(MeA^3_{27}-*co*-*t*-$BuAm_{76}$), average R_{TEM} = 94.6 nm (PDI = 0.21), weighted mean R_h = 101.4 nm (PDI = 0.53). (c) NAM_{107}-*b*-(MeA^3_{17}-*co*-*t*-$BuAm_{74}$) average R_{TEM} = 38.0 nm (PDI = 1.88), weighted mean R_h = 52.6 nm (PDI = 0.64). (d) NAM_{39}-*b*-(NAM_{57}-*co*-MeA^3_9-*co*-*t*-$BuAm_{80}$) average R_{TEM} = 91.7 nm (PDI = 0.51), weighted mean R_h = 118.0 nm (PDI = 0.88). Conditions for all DLS measurements are 1 mg mL^{-1} polymer in DI water. DLS and TEM data for the remaining polymers is available in Section 2.5.6.

Monitoring EDC-Fueled Self-Assembly of Polymers via Dynamic Light Scattering

To observe fueled self-assembly, polymer solutions at 1 g L^{-1} in 100 mM MES buffer (pH 6.2, with 100 mM NaCl) are fueled with 25-200 equivalents of EDC (with respect to carboxyl groups). Upon fueling, the polymer samples display an increase in count rate, indicating the transition from polymer unimers to nanometer-scale structures. Even at this lower polymer mass fraction, samples also display corresponding increases in turbidity. The laser intensity used for measurements is necessarily adjusted from sample to sample, and count rate is therefore reported as a scaled count rate (count rate divided by laser power, in kHz/mW) to allow for meaningful comparison.

Polymers with a short NAM block are each fueled with increasing equivalents of EDC (25, 75, 100 and 200 equivalents, respectively, Figure 2.5a). As with turbidity measurements above, the A^3 mole fraction in the polymer increases, the lifetime (taken as time for scaled count rate to return to ½ of maximum value) of the self-assembled state decreases. NAM_{37}-*b*-(A^3_8-*co*-*t*-$BuAm_{96}$), at an absolute EDC concentration of 22.5 mM, displays a self-assembly lifetime of 900 minutes. NAM_{38}-*b*-(A^3_{19}-*co*-*t*-$BuAm_{81}$), NAM_{39}-*b*-(A^3_{27}-*co*-*t*-$BuAm_{76}$) and NAM_{37}-*b*-(A^3_{36}-*co*-*t*-$BuAm_{66}$) follow this trend, showing self-assembly lifetimes of 220, 110 and 90 minutes at EDC concentrations of 142.5, 270 and 700 mM respectively (as summarized in Figure 2.5a, inset). At this polymer concentration of 1 g L^{-1}, NAM_{35}-*b*-(A^3_{43}-*co*-*t*-$BuAm_{57}$), displays no measurable assembly response to EDC fueling. This can be attributed to the higher A^3 content in this polymer, which even on conversion to the anhydride maintains the water-solubility of the responsive block, preventing self-assembly.

Size distributions of the fueled polymer solutions (Figure 2.5b-e) show a trend in decreasing size of the objects as A^3 mole fraction in the polymer increases. NAM_{37}-*b*-(A^3_8-*co*-*t*-$BuAm_{96}$) displays two populations of objects, one at R_h > 2000 nm, indicating the formation of large aggregate structures, and another population of objects is present, centered around R_h = 76 nm (PDI = 0.07). NAM_{38}-*b*-(A^3_{19}-*co*-*t*-$BuAm_{81}$) shows a broad peak centered at 140 nm, tailing towards larger radii (PDI = 1.14, with a weighted average R_h of 270 nm), indicating the presence of a small number of large objects. NAM_{39}-*b*-(A^3_{27}-*co*-*t*-$BuAm_{76}$) displays two peaks, at R_h = 46 nm (PDI = 0.05) and 155 nm (PDI = 0.24), and NAM_{37}-*b*-(A^3_{36}-*co*-*t*-$BuAm_{66}$) assembles into far smaller objects at 31 nm (PDI = 0.54).

The fueling behavior of individual polymers with respect to the amount of EDC supplied also follows a trend similar to the one observed with turbidity measurements. When fueled with increasing equivalents of EDC, NAM_{38}-*b*-(A^3_{19}-*co*-*t*-$BuAm_{81}$) (Figure 2.5f-g) displays an increase in count rate and fueled lifetime. When fueled with 50 equivalents of EDC (95 mM), the system shows a self-assembly lifetime of 100 minutes, with peak intensity at R_h = 42 nm (average R_h = 75 nm, PDI = 1.03). This closely resembles the size distribution for the methylated analogue displayed in Figure 2.4a, albeit with significantly more tailing, indicating the formation of a larger number of secondary assemblies. Increasing to 75 equivalents (142.5 mM) likewise increases R_h to 140 nm (average R_h = 277, PDI = 1.16) and lifetime to 220 minutes. The larger R_h observed indicates that at this fuel loading, secondary assemblies predominate, and large aggregates begin to appear, as indicated by tailing towards larger radii. 100 and 150 equivalents of EDC (190 and 285 mM, respectively) leads to lifetimes of 320 and 450 minutes, with R_h of 890 nm (average R_h = 1394 nm PDI = 0.92) and 1030 nm (average R_h = 1588 nm, PDI = 0.76) respectively. These fueling

experiments exhibit much larger hydrodynamic radii, as the polymer assembles predominantly into larger, ill-defined aggregates, likely similar in morphology to those seen in Figure 2.4a above.

NAM_{39}-*b*-($A^3{}_{27}$-*co*-*t*-$BuAm_{76}$) also displays similar changes in self-assembly in response to increasing amounts of EDC (Figure 2.5h-l). At a mass fraction of 1 g L^{-1}, no measurable assembly occurs with less than 75 equivalents of EDC, which leads to self-assembly with a lifetime of 60 minutes. Fueling with 100 equivalents of EDC leads to a significant increase in lifetime to 100 minutes and an increase in the number of scattering events, from 48 to 540 kHz/mw. 125 equivalents of EDC yield a self-assembly lifetime of 170 minutes, 150 equivalents 220 minutes and 200 equivalents 330 minutes. The size of self-assemblies also increases with EDC loading (Figure 2.5i-l). 75 equivalents of EDC (not shown) yield a single population of objects at R_h = 35 nm, with some tailing towards higher radii (PDI = 0.63). 100 Equivalents of EDC (Figure 2.5i) lead to self-assembly into two well-defined populations centered at R_h = 48 and 156 nm, with PDI 0.05 and 0.23, respectively. These can be compared to the model system in Figure 2.4b, which displays similar populations in TEM micrographs. Large aggregates are also present, as evidenced by a small, broad peak past R_h > 1000 nm. Increasing to 125 equivalents of EDC (Figure 2.5j), the smaller population disappears, and a narrow peak at R_h = 130 (PDI = 0.03) is observed, indicating the disappearance of singular spherical objects in favor of secondary assemblies, similar to those observed in Figure 2.4b. A larger contribution from aggregates at R_h > 2000 nm in also observed. A further increase to 150 equivalents (Figure 2.4k) shifts the narrow peak from 130 nm to R_h = 190 nm (PDI = 0.06), with a more prominent aggregate peak. Fueling with 200 equivalents of EDC (Figure 2.5l) shifts the peak further to 280 nm, indicating the further assembly of the discrete units formed at lower fueling amounts into increasingly large secondary assemblies. Likewise, the aggregate peak additionally shifts to larger radii, past R_h > 3000 nm.

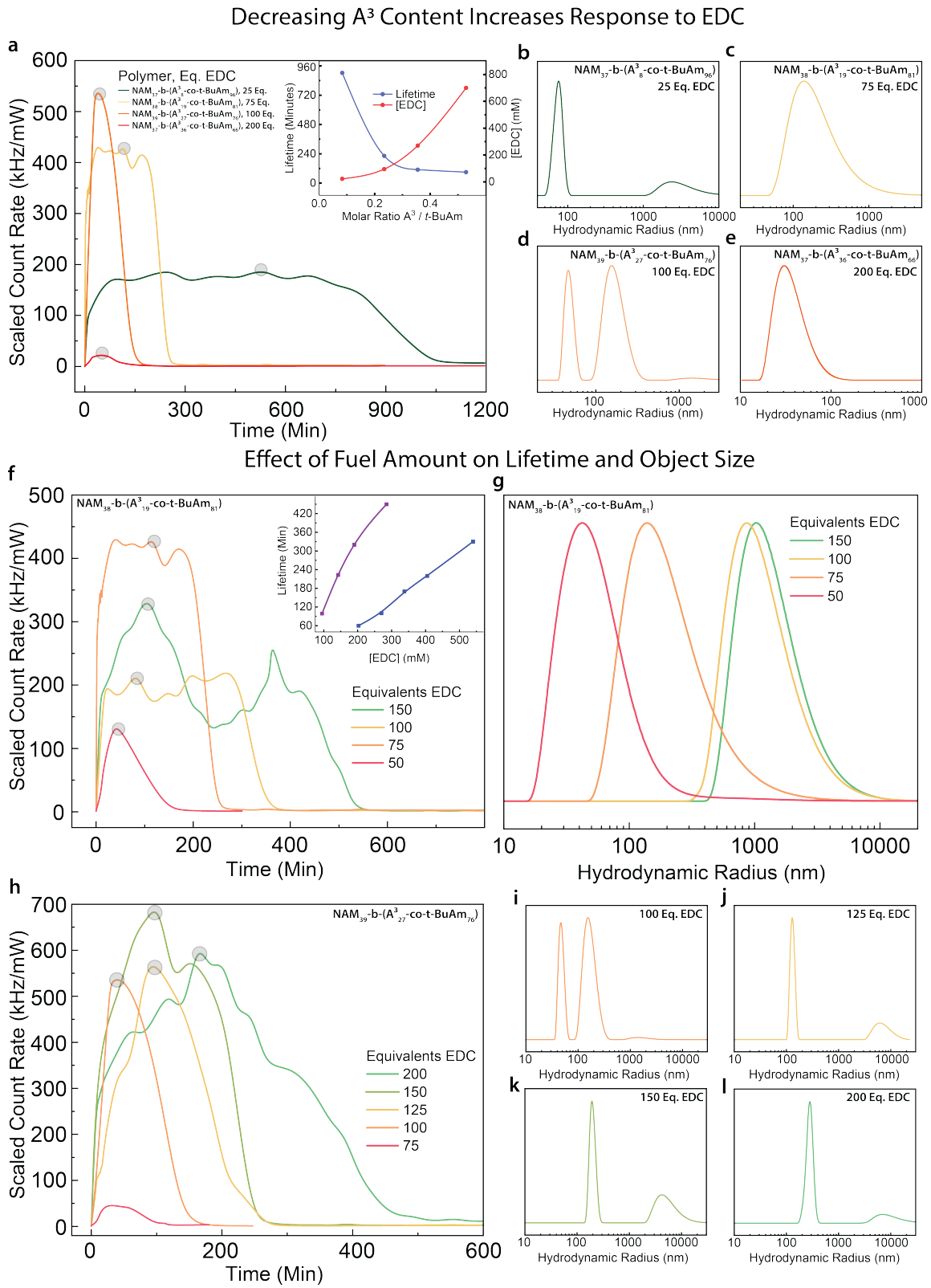

Figure 2.5: Probing self-assembly by dynamic light scattering. (a) DLS measurements of copolymers 1-5 over time. Each polymer is fueled with increasing equivalents of EDC, with the fueled state displaying a shorter lifetime. Grey circles indicate timepoints in which size distributions in panels b-e were taken. Insert: Lifetime of each fueled state (taken as time for scaled count rate to return to ½ of maximum value) and EDC concentration for each polymer, based on the molar A³/*t*-BuAm ratio of the responsive segment. (b)-(e) Intensity-weighted size distributions of each sample in (a) at the timepoint indicated by the grey circle. Average size of the assemblies can be seen to decrease drastically from NAM$_{37}$-*b*-(A$^3_8$-*co*-*t*-BuAm$_{96}$) to NAM$_{37}$-*b*-(A$^3_{36}$-*co*-*t*-BuAm$_{66}$), although there is a corresponding

increase in EDC concentration. (f) DLS measurements of NAM_{38}-*b*-(A^3_{19}-*co*-*t*-$BuAm_{81}$) fueled with different amounts of EDC. Grey circles indicate timepoints at which size distributions shown in (g) were measured. Insert: fueled state lifetimes of NAM_{38}-*b*-(A^3_{19}-*co*-*t*-$BuAm_{81}$) (purple) and NAM_{39}-*b*-(A^3_{27}-*co*-*t*-$BuAm_{76}$) (blue) at varying EDC concentrations. A clear difference in fuel response trends can be seen. (g) Intensity-weighted size distributions for NAM_{38}-*b*-(A^3_{19}-*co*-*t*-$BuAm_{81}$) when fueled with increasing amounts of EDC. Assemblies change in apparent radius from R_h = 50 nm to over 1000 nm as EDC concentration triples, indicating a significant shift in the nature of the self-assembly taking place. (h) DLS measurements of NAM_{39}-*b*-(A^3_{27}-*co*-*t*-$BuAm_{76}$) fueled with different amounts of EDC. Grey circles indicate timepoints at which size distributions shown in (i)-(l) were obtained. (i)-(l) Intensity-weighted size distributions for NAM_{39}-*b*-(A^3_{27}-*co*-*t*-$BuAm_{76}$) when fueled with 100, 125, 150 and 200 equivalents of EDC respectively. Conditions for all experiments are 1 mg mL^{-1} polymer in 100 mM MES buffer with 100 mM NaCl, pH 6.2. Due to large differences in turbidity between samples, laser power is varied to achieve reliable results. Count rate is therefore reported as scaled count rate (kHz/mW) for meaningful comparison between samples. Size distributions were generated using the CORENN algorithm.

With the effect of both A^3/*t*-BuAm ratio on the fuel efficiency trend in polymers, and the effect of altering EDC loading on individual polymer's self-assembly established by DLS measurements, we further investigated self-assembly of NAM_{107}-*b*-(A^3_{17}-*co*-*t*-$BuAm_{74}$) and NAM_{39}-*b*-(NAM_{57}-*co*-A^3_9-*co*-*t*-$BuAm_{80}$). $(NAM)_{107}$-*b*-(A^3_{17}-*co*-*t*-$BuAm_{74}$) displays fueling trends similar to previously observed polymers (Figure 2.6a). Fueling with 75 equivalents leads to an assembly response with a lifetime of 255 minutes, and a broad size distribution with a single, tailing peak at R_h = 13 nm with PDI = 1.08 (Figure 2.6b). Increasing to 100 equivalents EDC, lifetime likewise increases to 365 minutes, with a size distribution showing two peaks (Figure 2.6c), at R_h = 23 and 80 nm, with PDI = 0.09 and 0.23, respectively.

The count rate trace for 150 equivalents of EDC displays one peak at 120 minutes, which gradually declines until *t* = 400 minutes, before rising again to a second peak at 590 minutes. We attribute this behavior to the assembly of objects immediately upon fueling, which gradually decrease in number as fuel is consumed. Subsequently, they separate into multiple objects of smaller size, and finally disassemble as the count rate returns to baseline. This is supported by the size distribution data at these three timepoints, shown in Figure 2.6d. At *t* = 120 minutes, we observe a peak at R_h = 28 nm (PDI = 0.14) and a second, smaller and broader peak at 133 nm (PDI = 0.32), with an overall average R_h of 39 nm. A similar size distribution is observed at *t* = 400 minutes, with peaks at 35 nm (PDI = 0.21) and at 272 nm (PDI = 0.39), and overall average R_h = 39 nm. The bimodal size distributions at these timepoints indicate a similar assembly morphology to that observed when fueled with 100 equivalents of EDC. As the count rate rises, and fuel is exhausted, the larger population of worm-like micelles disassembles, and at *t* = 590 minutes, we observe two narrow peaks, at R_h = 16 nm (PDI = 0.01) and R_h = 38 nm (PDI = 0.04), and a smaller average R_h of 31 nm.

On fueling with 200 equivalents of EDC, fueled self-assembly lasts 640 minutes, and apart from initial assembly and final disassembly, a large change in count rate over the course of the experiment is not observed. Alongside the size distributions, shown in Figure 2.6e, this points to a change in the nature of the self-assembly taking place. At *t* = 80 minutes, peaks at R_h = 9 nm (PDI = 0.01) and R_h = 80 nm (PDI = 0.02) are observed, alongside a peak at R_h = 570 nm (PDI = 0.05). This is very similar to what is observed at *t* = 505 minutes, with peaks at R_h = 10 nm (PDI = 0.01), 80 nm (PDI 0.02) and R_h = 660 nm (PDI = 0.03). The size distribution at the intermediate timepoint *t* = 400 minutes shows a shift of the 10 nm peak to R_h = 27 nm (PDI = 0.01), with the second peak at R_h = 95 (PDI = 0.05). An additional peak at R_h = 510 nm (PDI = 0.08) is also present. The overall average hydrodynamic radius of the objects only slightly decreases from 92 nm at *t* = 80, to 91 nm at *t* = 400 and 89 nm at *t* = 505 minutes. This, alongside the low PDI of

the individual peaks, points to assembly into separate populations of discrete sizes rather than high aspect-ratio worm-like micelles as observed in the previous samples and the methylated analogue. Rather, as cryo-TEM results (below) show, the polymer assembles into spherical polymersomes.

We subsequently investigated the structural changes EDC fueling brings to the self-assembly of NAM_{39}-*b*-(NAM_{57}-*co*-A^3_9-*co*-*t*-$BuAm_{80}$) (Figure 2.6f-j), given the large response to EDC fueling observed in screening experiments. When fueled with 100, 150, 175 and 200 equivalents of EDC, the polymer displays self-assembly lifetimes of 543, 940, 1025 and 975 minutes respectively. The shorter lifetime when fueled with 200 compared to 175 equivalents of EDC can be attributed to the larger peak count rate at 200 equivalents of EDC, with lifetime taken as time for scaled count rate to return to ½ of maximum value. Nevertheless, it is worth noting that under these experimental conditions, lifetime plateaus at higher fuel loading for both NAM_{107}-*b*-(A^3_{17}-*co*-*t*-$BuAm_{74}$) and NAM_{39}-*b*-(NAM_{57}-*co*-A^3_9-*co*-*t*-$BuAm_{80}$) (Figure 2.6a, inset).

The count rate for fueled samples of NAM_{39}-*b*-(NAM_{57}-*co*-A^3_9-*co*-*t*-$BuAm_{80}$) displays multiple peaks over time in all experiments. Fueling with 100 equivalents of EDC, count rate rises to a maximum at 235 minutes, before rapidly falling off to a local minimum at 335 minutes, reaching a second, smaller maximum at 465 minutes. Self-assembly behavior mirrors that displayed in NAM_{107}-*b*-(A^3_{17}-*co*-*t*-$BuAm_{74}$), as described above. Size distribution data (Figure 2.6g) shows how the polymer self-assembles on fueling into objects with a peak R_h = 62 nm (PDI = 0.85, intensity-weighted average R_h = 80 nm). As the count rate decreases to the minimum at t = 335 minutes, peak R_h decreases to 50 nm, with intensity-weighted average R_h = 73 nm. While the overall size of the objects decreases, the distribution at this timepoint is far broader (PDI = 1.2), reflecting the gradual disassembly of the larger objects into smaller ones, which are observed at the second count rate maximum at t = 465 minutes. At the second maximum, the size distribution displays a maximum at R_h = 40 nm, with a weighted average R_h of 53 nm, and PDI = 0.85.

When fueled with 150 equivalents of EDC (Figure 2.6f, h), the count rate rises quickly, then dips slightly to t = 70 minutes, at which point the system displays a bimodal size distribution, featuring a peak at R_h = 16 nm (PDI = 0.05) and a broader peak at 230 nm (PDI = 0.86), with an overall average R_h = 223 nm. Count rate then peaks and drops again at t = 360 minutes. The bimodal distribution displays peaks at R_h = 18nm (PDI = 0.06), and R_h = 205 nm (PDI = 0.62), with the intensity-weighted R_h decreasing to 197 nm. At t = 760 minutes, count rate reaches its maximum, where the size distribution reflects the decreasing size of objects before the count rate rapidly drops. Peaks are observed at R_h = 21 nm (PDI = 0.12) and R_h = 166 nm (PDI = 1.17), with a marked decrease in the intensity-weighted hydrodynamic radius to 166 nm.

Fueling NAM_{39}-*b*-(NAM_{57}-*co*-A^3_9-*co*-*t*-$BuAm_{80}$) with larger amounts of EDC alters the progression of self-assembly to feature initial assembly of objects, coalescence of these objects into larger ones, and subsequent disassembly. When fueled with 175 equivalents of EDC, count rate rapidly increases to a maximum at 30 minutes, before decreasing to a steady value until rising again to a second maximum at 950 minutes, before rapidly returning to the pre-fueling baseline. Size distributions illustrate how objects form, coalesce, and disassemble. At t = 30 minutes, a bimodal distribution with a narrow peak at R_h = 7 nm (PDI = 0.02) is observed, along with a peak at 188 nm (PDI = 1.34) which displays significant tailing towards larger radii. As count rate drops, at t = 460 minutes, the first peak remains at R_h = 7 nm (PDI = 0.06), with a second, broad, peak present at 230 nm (PDI = 1.44), which presents significant tailing towards larger hydrodynamic radii. At

t = 950, when count rate rises to a second maximum, a peak at R_h = 7 nm (PDI = 0.07) is observed again, with the second peak shifting to R_h = 88 nm (PDI = 2.0), again with a very large degree of tailing towards larger hydrodynamic radii. Monitoring the intensity-weighted average R_h of the system further underscores the evolution of the assemblies over time, as it changes from 256 nm at t = 30 minutes, rising to 301 nm at 460 minutes, and falling to 150 nm at 950 minutes. At all of these timepoints, the second peak at larger R_h displays a large PDI, indicative of significant heterogeneity in the species composing it.

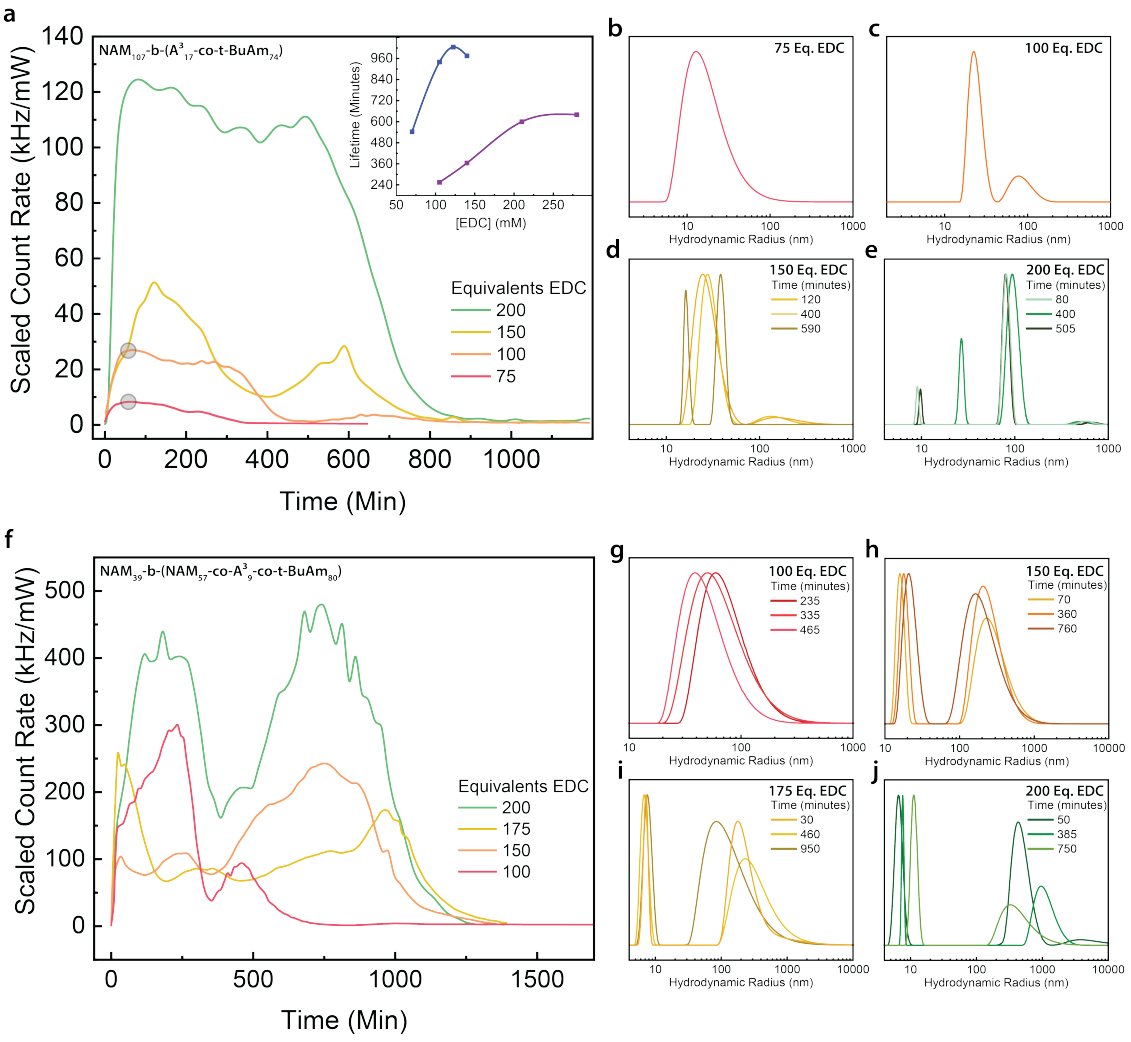

Figure 2.6: Monitoring self-assembly of polymers with larger NAM content by DLS. (a) Count rate of NAM$_{107}$-*b*-(A$^3_{17}$-*co*-*t*-BuAm$_{74}$) when fueled with 75-200 equivalents of EDC. Insert: fueled state lifetimes of NAM$_{107}$-*b*-(A$^3_{17}$-*co*-*t*-BuAm$_{74}$) (purple) and NAM$_{39}$-*b*-(NAM$_{57}$-*co*-A$^3_9$-*co*-*t*-BuAm$_{80}$) (blue) at EDC concentrations measured. (b)-(e) Size distributions of experiments in (a) at given timepoints indicated by grey circles. (f) Count rate of NAM$_{39}$-*b*-(NAM$_{57}$-*co*-A$^3_9$-*co*-*t*-BuAm$_{80}$) when fueled with 100-200 equivalents EDC. (g)-(j) Size distributions for count rate traces shown in (f). Since the traces display multiple peaks, size distributions are plotted for multiple timepoints, given in the figure legends. Conditions for all experiments are 1mg mL^{-1} polymer in 100 mM MES buffer with 100 mM NaCl, pH 6.2. Count rate is reported as scaled count rate (kHz/mW) for meaningful comparison between samples. Size distributions were generated using the CORENN algorithm.

Similar behavior is observed when fueling with 200 equivalents of EDC. On addition of fuel, the count rate increases rapidly to a maximum at t = 50 minutes, decreases to a minimum at t = 385, and rises again to a second maximum at t = 750 minutes, before rapidly decaying to baseline. Over

the course of the fueling lifetime of 975 minutes, objects assemble, grow and disassemble, as shown in Figure 2.6j. At t = 50 minutes, peaks at R_h = 6nm (PDI = 0.07) and 445 nm (PDI = 0.31) are observed, indicating high-aspect ratio objects similar to those observed in the previous experiment. An additional small, broad peak centered at 3000 nm (PDI = 1.76) indicative of aggregates is observed. The intensity-weighted average R_h = 682 nm. At t = 385 minutes, the peak at R_h = 7 nm (PDI = 0.01) remains, with the long axis peak visible at 1010 nm (PDI = 0.43). At t = 750 minutes, count rate rises, indicating an increase in the number of objects in the sample volume. A peak at 11 nm (PDI = 0.04) is present, with the peak at larger radii shifting to 320 nm and broadening significantly (PDI = 1.41), indicating a wide variation in the long axis of the assembled objects, due to their ongoing disassembly. The intensity-weighted average progresses from 682 nm at t = 50 minutes to 883 nm at 385 minutes, before dropping to 280 nm at 750 minutes. Our observations regarding object formation, growth and disassembly resemble those made in EDC-fueled droplet formation by small molecules.[41]

The significant change in mean R_h over the course of the fueling experiments with 175 and 200 equivalents of EDC, alongside the bimodal distributions observed throughout featuring a constant peak at low R_h is indicative of high-aspect ratio objects with a variable long axis, which form, grow and finally disassemble over the course of the fueling experiment, and a second population of small, circular objects at $R_{h(DLS)}$ = 7-11 nm.

This interpretation is further supported by comparison to the TEM micrographs of statically assembled polymer NAM$_{39}$-*b*-(NAM$_{57}$-*co*-MeA$^3_9$-*co*-*t*-BuAm$_{80}$) (Figure 2.4d, above), as a population of small, spherical assemblies is present alongside the worm-like micelles. We attribute the lack of a population of circularized objects at 50-100 nm in fueled experiments to the additional equilibration time of the methylated analogue, which was dialyzed for 2 days between assembly and measurement to remove non-aqueous solvent. It is worth noting the worm-like micelles display a diameter in the order of 12-18 nm, which coincides with that of the small peak observed in DLS measurements of fueled self-assembly (Figure 2.6h-j), and that therefore the population of small objects may be in equilibrium with the worm-like micelles.

Cryo-Transmission Electron Microscopy of Fueled Polymer Assemblies

To confirm our DLS observations of fueled self-assembly, we imaged fueled samples of NAM$_{107}$-*b*-(A$^3_{17}$-*co*-*t*-BuAm$_{74}$) and NAM$_{39}$-*b*-(NAM$_{57}$-*co*-A$^3_9$-*co*-*t*-BuAm$_{80}$) *via* cryo-TEM. NAM$_{107}$-*b*-(A$^3_{17}$-*co*-*t*-BuAm$_{74}$), fueled with 200 equivalents of EDC (Figure 2.7a) displays assembly into spherical vesicles. These can be separated into a smaller population, with radii of 10-20 nm, and a lower quantity of larger objects with a radius of 50-70 nm, along with a very small number of objects of radius 80-100 nm. NAM$_{39}$-*b*-(NAM$_{57}$-*co*-A$^3_9$-*co*-*t*-BuAm$_{80}$), fueled with 175 equivalents of EDC (Figure 2.7b) displays assembly into thin, worm-like structures which further form networks. The individual threads display a diameter in the order of 10-15 nm, in line with our observations of the model system in Figure 2.4. They exhibit long axes in the order of 200-500 nm; however, their unclear interconnectivity renders exact measurement difficult. Additionally, small circular objects 20 nm in diameter can be seen, which may be in equilibrium with the worm-like micelles as we propose above. However, more observations over multiple timepoints will be required to conclusively state this. DLS data displays a similar size distribution to that observed in other fueling experiments of NAM$_{39}$-*b*-(NAM$_{57}$-*co*-A$^3_9$-*co*-*t*-BuAm$_{80}$), featuring a population at $R_{h(DLS)}$ = 16 nm,

and a broad second peak at $R_{h(DLS)}$ = 180 nm, and is, given the limitations of the technique, in line with the observations in the micrographs.

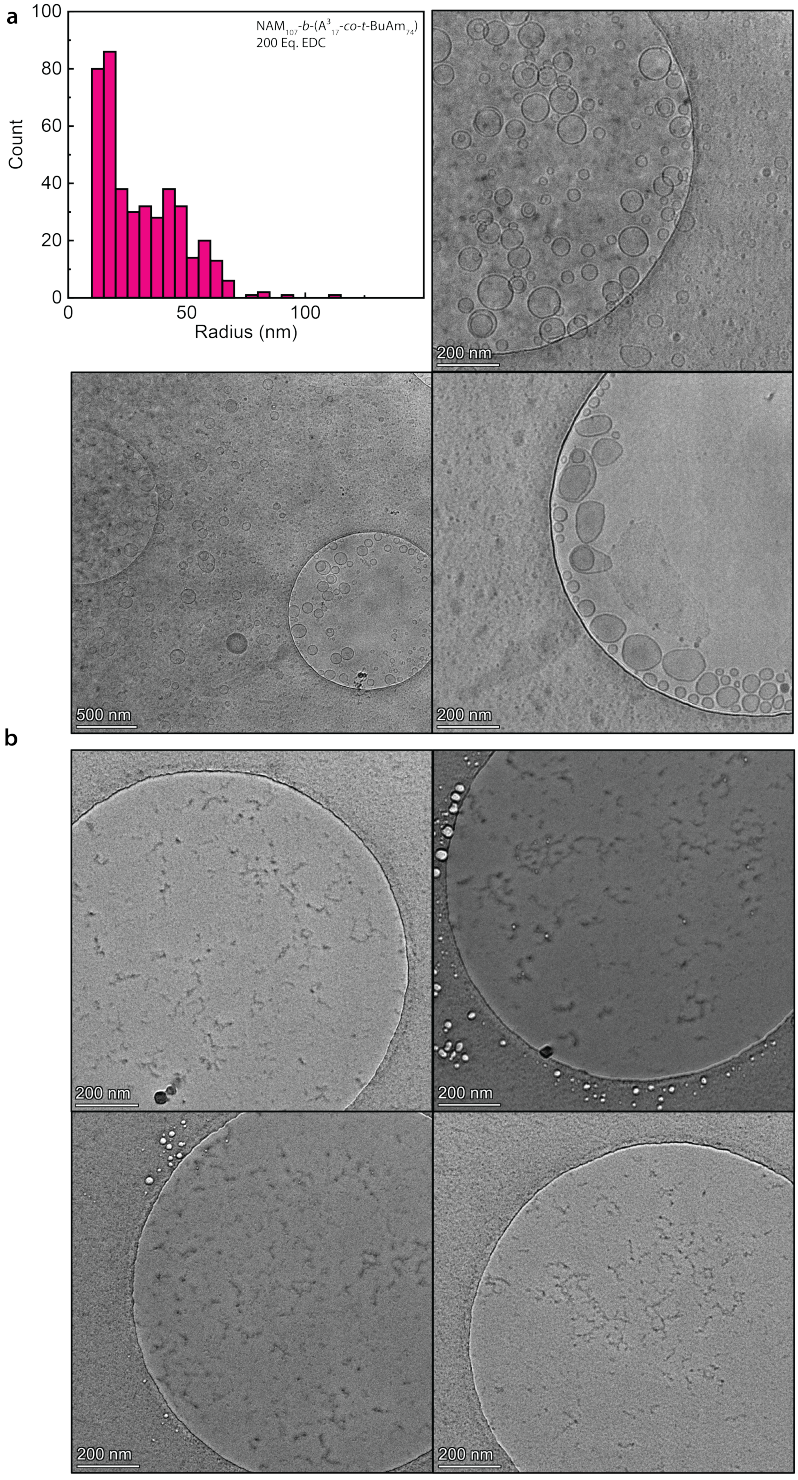

Figure 2.7: Cryo-TEM imaging of fueled polymer assemblies. (a) NAM_{107}-*b*-(A^3_{17}-*co*-*t*-$BuAm_{74}$), fueled with 200 equivalents of EDC. Cryo-TEM images display circular vesicles, with both single and double membranes. R_{TEM} = 31 nm. (b) NAM_{39}-*b*-(NAM_{57}-*co*-A^3_9-*co*-*t*-$BuAm_{80}$), fueled with 175 equivalents of EDC. TEM radii where not determined given their ill-defined connectivity. Strands are 10-15 nm across. Both samples are at 1 mg mL^{-1} polymer mass fraction, in MES buffer, pH 6.2, with 100 mM NaCl. Both samples are imaged at t = 300 minutes. These samples comprise separate fueling experiments to those shown in Figure 2.6.

2.4. Conclusions

In this study, we have synthesized a library of responsive block copolymers and explored their fuel-mediated self-assembly into nanoscale structures. In contrast to previous studies on EDC-fueled copolymer self-assembly[43,55], we examined the effects of multiple parameters on the lifetime and morphology of the resulting structures. By carefully altering the ratio of A^3 to *t*-BuAm within the switchable block, we are able to control the threshold concentration of EDC required for self-assembly, and show that significantly longer self-assembly lifetimes can be obtained with lowered fuel consumption, which we term fuel efficiency. We further explored the relationship between responsive block composition and morphology of assembled structures, and found that the composition of the polymer affects the dynamic evolution of the structures during the course of fueling. We additionally showed that by altering the relative lengths of the polymer blocks, we are able to target specific morphologies that to our knowledge have not so far been reported in EDC-fueled systems, such as worm-like micelles and polymersomes.

Given the great interest in out of equilibrium self-assembly generally,[56] and chemically-fueled self-assembly specifically,[57-58] we expect our findings on the effect of polymer architecture in the fueling response, and therefore system-wide behavior to offer further guidance in designing the next generation of polymers for ever more complex self-assembling systems.

2.5. Supplementary Information

2.5.1. Materials and Methods

Instrumentation

NMR spectra were measured on a Bruker 400 MHz spectrometer.

Gel permeation chromatography (GPC) was performed using an Agilent 1260 Infinity II system equipped with a 1260 series isocratic pump and refractive index detector. A MZ-gel SD Plus e5/e3/100 column assembly (MZ-Analysentechnik GmbH) was employed as stationary phase. Measurements were conducted in THF with a flowrate of 1 mL min^{-1}. Narrowly distributed poly(methyl methacrylate) standards were used for calibration (Polymer Standards Service).

Matrix-assisted laser-desorption-ionization time of flight mass spectrometry (MALDI-ToF MS) measurements were performed using matrix consisting of 2,5-dihydroxybenzoic acid with potassium trifluoroacetate as cationization agent. The measurements were conducted on an Autoflex maX MALDI-TOF-MS from Bruker.

Plate reader experiments were carried out on a Byonoy Absorbance 96. Dynamic light scattering (DLS) measurements were carried out on a LS Instruments Nanolab 3D (λ = 638 nm, 90° scattering angle). Transmission electron microscopy (TEM) imaging was carried out on a Tecnai Spirit G2 120 kV electron microscope. Cryo-TEM imaging was carried out using a Krios G4 Cryo-TEM Electron microscope.

Materials

Azobisisobutyronitrile (AIBN) (98%) was purchased from Acros Organics. Acryloyl chloride (97%) and aspartic acid (99%) were purchased from Alfa Aesar. 1-ethyl-3-(3-dimethylaminopropyl)carbodiimide hydrochloride (EDC) (99%) was purchased from Carbolution Chemicals GmbH. DMSO (≥99%), diethyl ether, methanol, NaOH (99%), THF, toluene and

(trimethylsilyl)diazomethane (2.0 M in hexanes) were purchased from Fischer Scientific. N-acryloylmorpholine (NAM) (>98%), morpholinoethane sulfonic acid (MES) (99%) and *tert*-butyl acrylamide (*t*-BuAm) (99%) were purchased from TCI Europe. 2-Cyano-2-propyldodecyltrithiocarbonate (CPDT) was purchased from Sigma Aldrich. All chemicals were used as received, except for AIBN and *t*-BuAm, which were recrystallized before use, and NAM, which was passed through a basic alumina plug to remove inhibitors.

Synthesis of Aspartic Acid N-Acrylamide Monomer

Aspartic acid *N*-acrylamide was synthesized as previously described.[49] In brief, aspartic acid (30 g, 225 mmol) and NaOH (31.5 g, 788 mmol) were dissolved in water (300 mL). The mixture was stirred vigorously and cooled to 0 °C, at which point acryloyl chloride (20 mL, 247 mmol) was added dropwise over the course of 30 minutes. The reaction was stirred at 0 °C for 3 hours, and then at room temperature for a further 4 hours. The aqueous mixture was extracted with EtOAc (3 × 500 mL). The aqueous phase was then adjusted to pH = 2 with conc. HCl and extracted with further EtOAc (9 × 500 mL). The combined organic layers were dried over $MgSO_4$, and their volume reduced in vacuo. A minimum amount of solvent was left to stand overnight for the product to crystallize. The product was separated by filtration and washed once with minimum ice-cold EtOAc. The product was recovered as an off-white solid (27.2 g, 145 mmol, 64% yield).

^{1}H NMR (400 MHz, D_2O, 25 °C, TMS): δ = 6.14 – 5.96 ppm (m, 2H; CH_2), 5.57 ppm (dd, ^3J = 9.7, 1.8 Hz, 1H; CH), 4.62 ppm (t, ^3J = 5.9 Hz, 1H, CH), 2.75 ppm (d, ^3J = 6.1 Hz, 2H; CH_2)

Synthesis of Polymers

General Experimental Remarks

NMR conversion data during polymerization experiments was obtained by comparing the monomer acrylamide -CH- and -CH_2 signals to a 1,3,5-trioxane internal standard. Final monomer ratios were determined by the ratio of unique signals originating from each monomer.

Generalized RAFT Polymerization Procedure

NAM (847 mg, 755 µL, 6 mmol), CPDT (41.4 or 20.74 mg, depending on desired NAM block length, 1.2 and 0.6 mmol respectively), 1,3,5-trioxane (100 mg) and AIBN (1.00 or 0.50 mg respectively, always in a 1:0.05 ratio with CPDT) are dissolved in 2.10 mL of 20/80 v/v DMSO / dioxane. The mixture is thoroughly degassed by carrying out 4 freeze-pump-thaw cycles with dry N_2. The reaction flask is then immersed in an 80°C oil bath for 60 – 180 minutes, until NAM conversion has reached >90% by NMR.

In a separate flask, A^3 and *t*-BuAm (in a variable molar ratio from 0/100 to 50/50, with a total monomer : CTA ratio of 100:1) are dissolved in 20/80 v/v DMSO / dioxane by gentle heating in a hot water bath, and the mixture thoroughly degassed by carrying out 4 freeze-pump-thaw cycles. This mixture is then added to the NAM RAFT polymerization to carry out *in situ* block extension. Once conversion of the added A^3 and *t*-BuAm plateaus around 80-90%, the reaction flask is taken off the heat and the polymer precipitated in diethyl ether. A 5 mg sample of the recovered crude polymer is methylated, for GPC analysis. The remaining polymer is dissolved in 100 mM NaOH and dialyzed against MilliQ water in 6-8 or 12-14 kDa MWCO tubing (depending on target length of the polymer) for 2 days. The purified copolymers were obtained as yellow powders after freeze drying. The conditions for all polymer samples synthesized are summarized in table 2.

Table 2: Summary of polymer synthesis conditions

Polymer Sample	NAM: CTA Ratio	NAM Conversion (NMR)	Block Extension			M_n (theoretical)
			A^3:*t*-BuAm Ratio[a]	Conversion (A^3)	Conversion (*t*-BuAm)	kg mol^{-1}
NAM_{37}-*b*-(A^3_8-*co*-*t*-$BuAm_{96}$)	50	99 %	10:90	83 %	76 %	17.5
NAM_{38}-*b*-(A^3_{19}-*co*-*t*-$BuAm_{81}$)	50	99 %	20:80	93 %	91 %	19.7
NAM_{39}-*b*-(A^3_{27}-*co*-*t*-$BuAm_{76}$)	50	99 %	30:70	91 %	89 %	20.0
NAM_{37}-*b*-(A^3_{36}-*co*-*t*-$BuAm_{66}$)	50	99 %	40:60	91 %	89 %	20.6
NAM_{35}-*b*-(A^3_{43}-*co*-*t*-$BuAm_{57}$)	50	99 %	50:50	87 %	86%	20.6
NAM_{107}-*b*-(A^3_{17}-*co*-*t*-$BuAm_{74}$)	100	95 %	20:80	84 %	79 %	24.6
NAM_{111}-*b*-(A^3_{28}-*co*-*t*-$BuAm_{77}$)	100	95 %	30:70	93 %	89 %	26.7
NAM_{39}-*b*-(NAM_{57}-*co*-A^3_9-*co*- *t*-$BuAm_{80}$)	100	99 %	10:90	89 %	76 %	24.2

a) The monomer to CTA ratio is always set at 100:1 for block extensions.

Characterization of polymers

Average relative molecular weights and polydispersity of the polymers were determined by GPC with a sample concentration of 1 mg mL^{-1}, relative to PMMA standards in THF (Figure 2.8). Polymers containing carboxylate groups were methylated prior to measurement by dissolving in 3/1 v/v toluene/MeOH and adding an excess of (trimethylsilyl)diazomethane.

The absolute molecular weights of select poly(NAM) first blocks were determined by MALDI (Figure 2.9). Samples were prepared through the "vortex" method.[59] Briefly, 1 mg of analyte polymer, 90 mg of 2,5-DHB matrix and 0.5 mg of K-TFA cationization agent were added to a glass vial along with two glass boiling beads. The vials were vortexed at high speed for 1 minute, and a thin film applied to the target plate.

All polymers were characterized by ^{1}H NMR (Figure 2.10) to determine the final incorporation ratio of monomers. This was achieved by comparing the integrals of the peaks at 4.40-4.10 ppm, 3.90-3.00 ppm and 1.33-1.00 ppm, corresponding to the aspartic acid -C*H*-, the *N*-acryloylmorpholine ring protons, and *t*-BuAm *tert*-butyl protons respectively. By taking the percentage conversion of the A^3 monomer and comparing the A^3 integral to those originating from the other monomers, a composition of the final recovered polymers could be calculated.

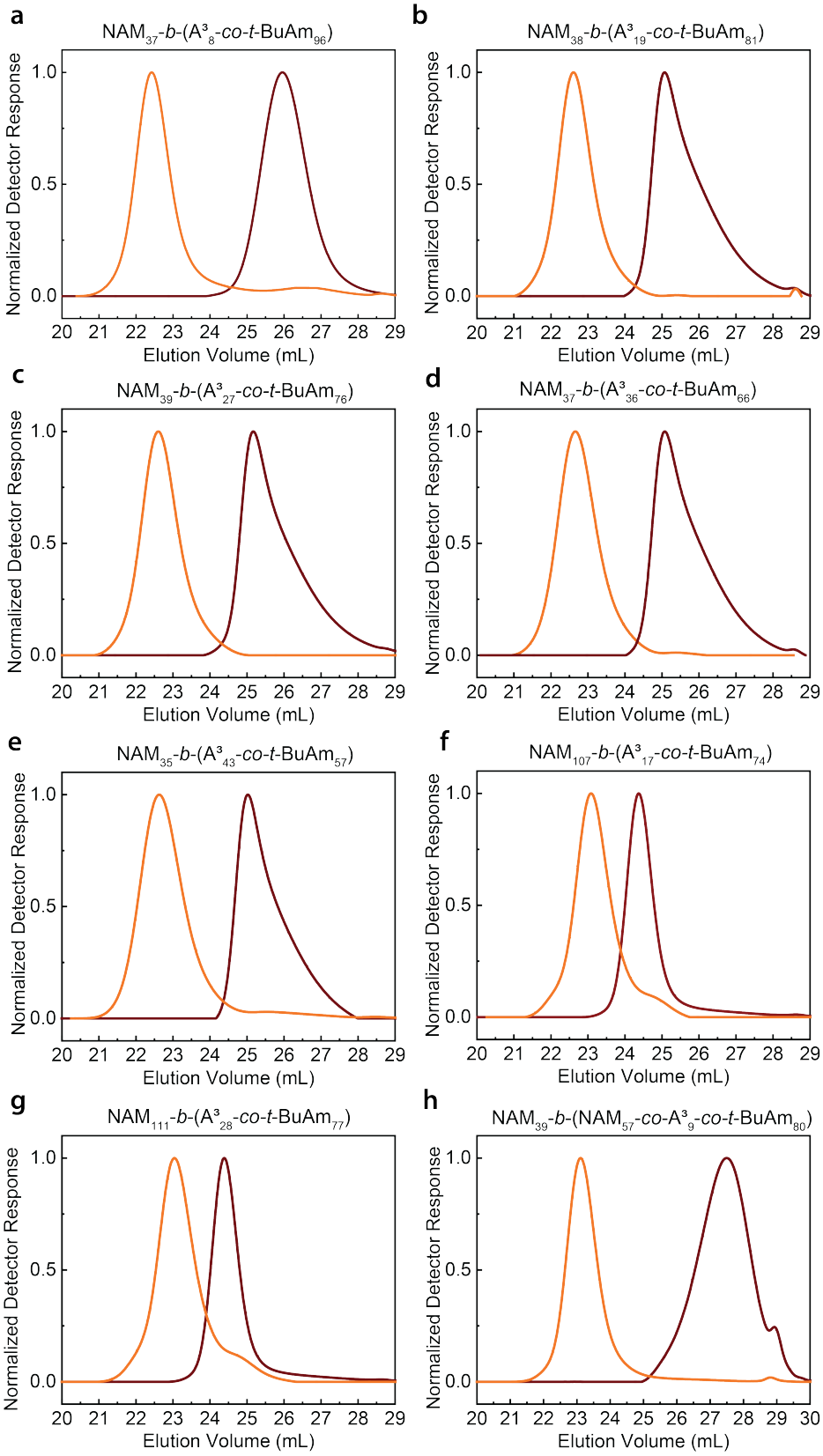

Figure 2.8: Summary of GPC traces of polymer samples synthesized, with each pair of samples showing extension from the poly(NAM) first block (maroon) to the final copolymer after block extension (orange). All measurements taken in THF with toluene as internal standard. Final polymers were methylated prior to measurement.

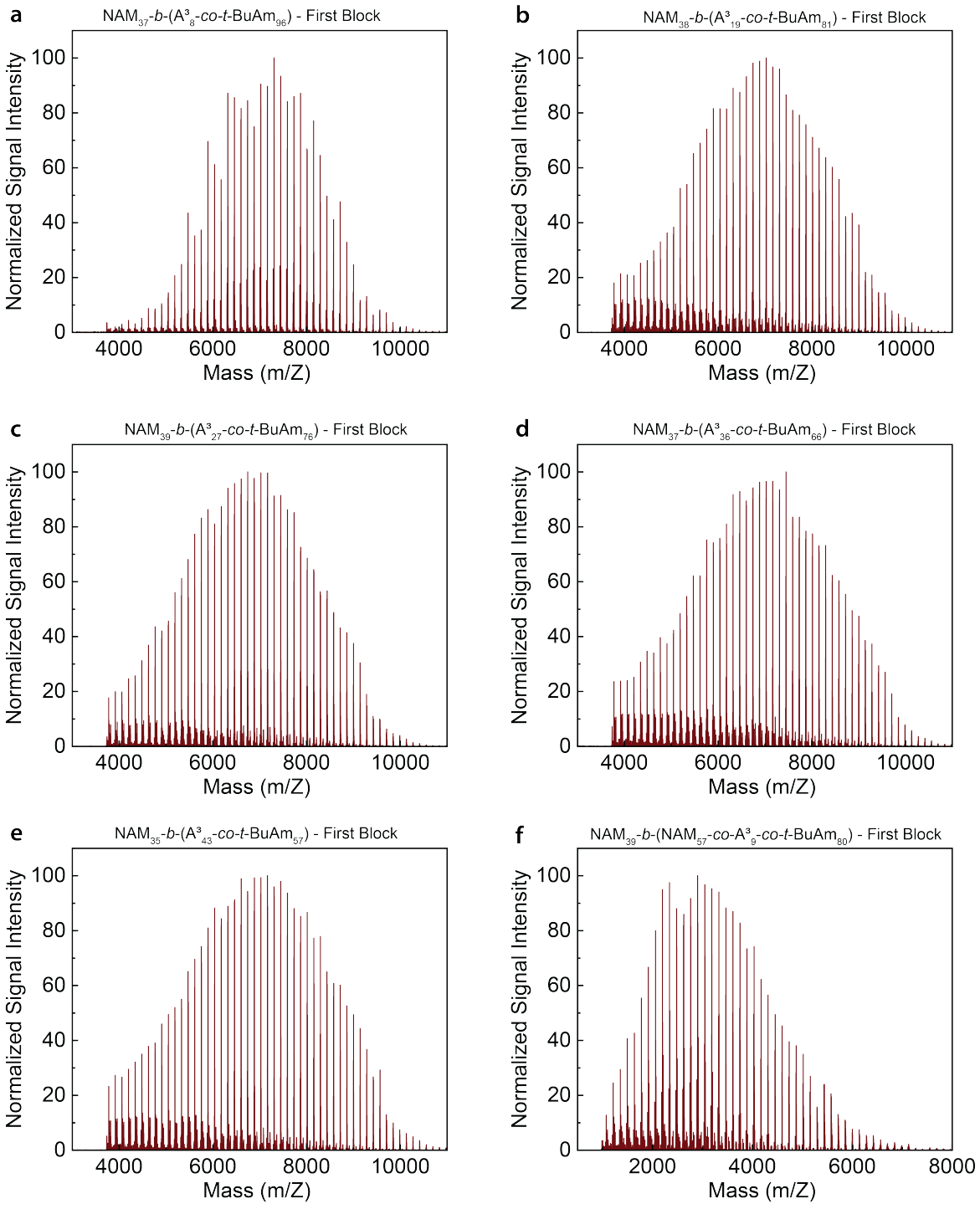

Figure 2.9: MALDI-ToF Mass spectra of p(NAM) first blocks of select copolymers. (a) M_n = 6943, M_w = 7306 g mol^{-1}, $Đ$ = 1.05. (b) M_n = 6710, M_w = 7059 g mol^{-1}, $Đ$ = 1.05. (c) M_n = 6754, M_w = 7105 g mol^{-1}, $Đ$ = 1.05. (d) M_n = 6768, M_w = 7125 g mol^{-1}, $Đ$ = 1.06. (e) M_n = 6728, M_w = 7041 g mol^{-1}, $Đ$ = 1.05. (f) M_n = 3282, M_w = 3775 g mol^{-1}, $Đ$ = 1.15.

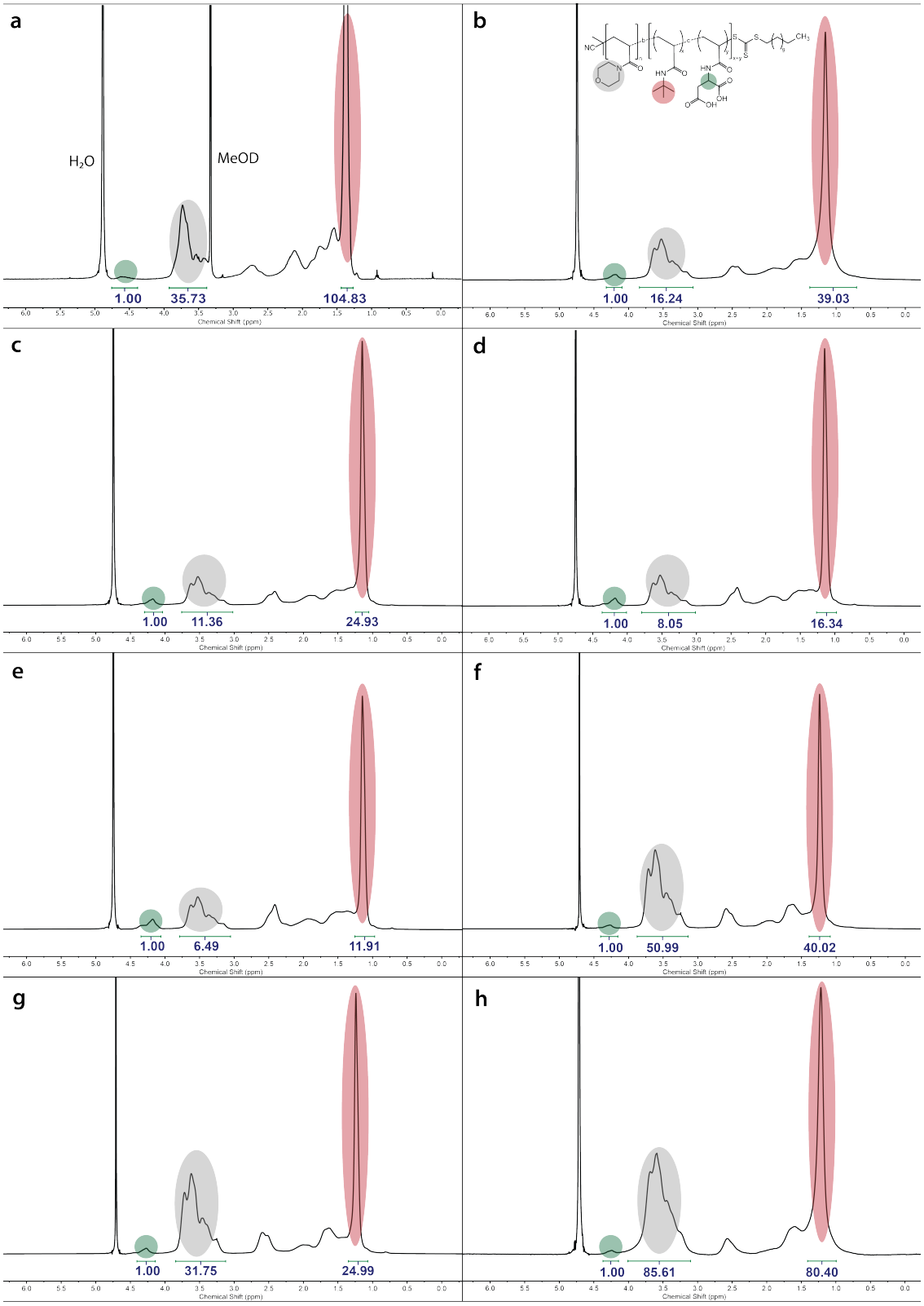

Figure 2.10: ^{1}H-NMR Spectra of (a) NAM_{37}-*b*-(A^{3}_{8}-*co*-*t*-$BuAm_{96}$), (b) NAM_{38}-*b*-(A^{3}_{19}-*co*-*t*-$BuAm_{81}$), (c) NAM_{39}-*b*-(A^{3}_{27}-*co*-*t*-$BuAm_{76}$), (d) NAM_{37}-*b*-(A^{3}_{36}-*co*-*t*-$BuAm_{66}$), (e) NAM_{39}-*b*-(A^{3}_{43}-*co*-*t*-$BuAm_{57}$), (f) NAM_{107}-*b*-(A^{3}_{17}-*co*-*t*-$BuAm_{74}$), (g) NAM_{111}-*b*-(A^{3}_{28}-*co*-*t*-$BuAm_{78}$), (h) NAM_{39}-*b*-(NAM_{57}-*co*-A^{3}_{9}-*co*-*t*-$BuAm_{80}$), (a) Measured in D_2O/MeOD, (b)-(h) measured in D_2O with 100 mM NaOD. Signals and integrals pertaining to each repeat unit have been highlighted in red (*t*-BuAm), green (A^{3}) and grey (NAM). These integrals were used to calculate the monomer ratio of the polymers. Signals between 3.0 and 1.5 ppm arise from the polymer backbone and aspartic group CH_2.

Plate Reader Measurements

Polymer solutions (in 100 mM MES buffer, pH 6.2 with 100 mM added NaCl) were placed in a 96-well plate, and an unfueled baseline measured for 5 minutes. The samples were then fueled with EDC as a 4M stock solution in the same buffer. Samples were then measured in transmission mode at 405 nm. All samples were made up to the same final polymer concentration (5 mg mL^{-1}) and volume (200 μL) by addition of 100 mM MES buffer. All samples were measured as triplicates, with duplicate unfueled polymer controls and EDC stock controls.

2.5.2. Dynamic Light Scattering

General remarks

Before all measurements, a blank water or buffer sample, as appropriate, was measured to ensure the absence of dust in the cuvette. All measurements were carried out in a quartz cuvette of volume 0.8 mL, path length 8 mm. Experiments were carried out using 3D cross-correlation to suppress multiple scattering events. Samples displayed a large variability in turbidity on fueling, therefore laser intensity was manually set to ensure an appropriate count rate for reliable data acquisition. For this reason, count rates are reported as scaled count rates in kHz / mW to allow for meaningful comparison.

Size distributions are given at select timepoints to highlight the nature of structures over the course of the fueling experiments. The size distribution of objects was determined using the CORENN algorithm provided in the instrument software. This algorithm employs a modified version of the non-negative least squares approach used in CONTIN, and benefits from higher tolerance to experimental noise.[60] Peaks in these size distributions were analyzed to determine the polydispersity index (PDI), given by the equation:

$$PDI = (\frac{\sigma}{a})^2$$

Where σ is the standard deviation of the peak, and a the average R_h. It is important to distinguish this from the dispersity in molecular weights of a polymer mixture, denoted by $Đ$. In a theoretical perfectly monodisperse polymer mixture, $Đ = 1$. In a theoretically monodisperse sample of particles, $\sigma = 0$, and therefore PDI = 0.

Overall intensity-weighted average of these size distributions was also computed according to the following equation:

$$R_{avg} = \frac{\sum(S \cdot R_x)}{\sum S}$$

Where R_{avg} is the intensity-weighted average, R_x is a given hydrodynamic radius and S is the scattered intensity at this given radius.

Methylated Polymers

Methylated polymers were dissolved in THF to achieve a concentration of 10 mg mL^{-1}. Deionized water was then slowly added to achieve a final polymer concentration of 1 mg mL^{-1}, and the sample dialyzed against water for 2 days (MWCO of 100 kDa) before measurement.

EDC Fueled Self-Assembly

Polymer stock solutions (10 mg mL^{-1} in 100 mM MES buffer, pH 6.2 with 100 mM added NaCl) were filtered through 0.25 μm PVDF membrane syringe filters and diluted with freshly filtered buffer. A baseline unfueled measurement was taken, and freshly filtered EDC stock solution added to achieve the required EDC concentration, and a final polymer concentration of 1 mg mL^{-1}. The sample was then measured at regular intervals.

2.5.3. Transmission Electron Microscopy and Cryo-TEM.

TEM samples were prepared by first cleaning a carbon-coated copper grid with O_2 plasma for 30 seconds. 3 μL of sample solution was then dropped onto the grid and incubated for 120 seconds before being blotted away.

Cryo-TEM samples were prepared by placing 3 μL of sample solution on cleaned carbon grids before blotting and plunging into liquid ethane.

TEM and cryo-TEM micrographs were analyzed with the FIJI software package. TEM radii reported were determined by averaging the semimajor and semiminor axes of particles and aggregates.

2.5.4. Statistical Analysis

Data was gathered using the methods outlined above. All data points featuring statistical analysis are presented as mean ± standard error. The sample size for each statistical analysis is reported in the relevant figure legend. Statistical analysis was carried out using Microsoft Excel and Origin Pro 2020.

2.5.5. Supplementary Note: Plate Reader Turbidity Measurements

To identify samples of interest, we screened the fueling behavior of all polymers synthesized for this study. Lifetime of the fueled states was calculated according to the equation:

$$Lifetime(t) \equiv t\left(OD = \frac{OD_{max}}{2}\right)$$

Figure 2.11 displays comparisons of polymers when fueled with the same stoichiometric equivalents of EDC. A very clear relationship between the A^3 content of the polymer and its response to EDC fueling exists – polymers with a low A^3 mole fraction display higher optical densities for longer, while requiring a lower overall EDC concentration, as illustrated in the inset graphs of lifetime and absolute EDC concentration versus A^3/*t*-BuAm ratio.

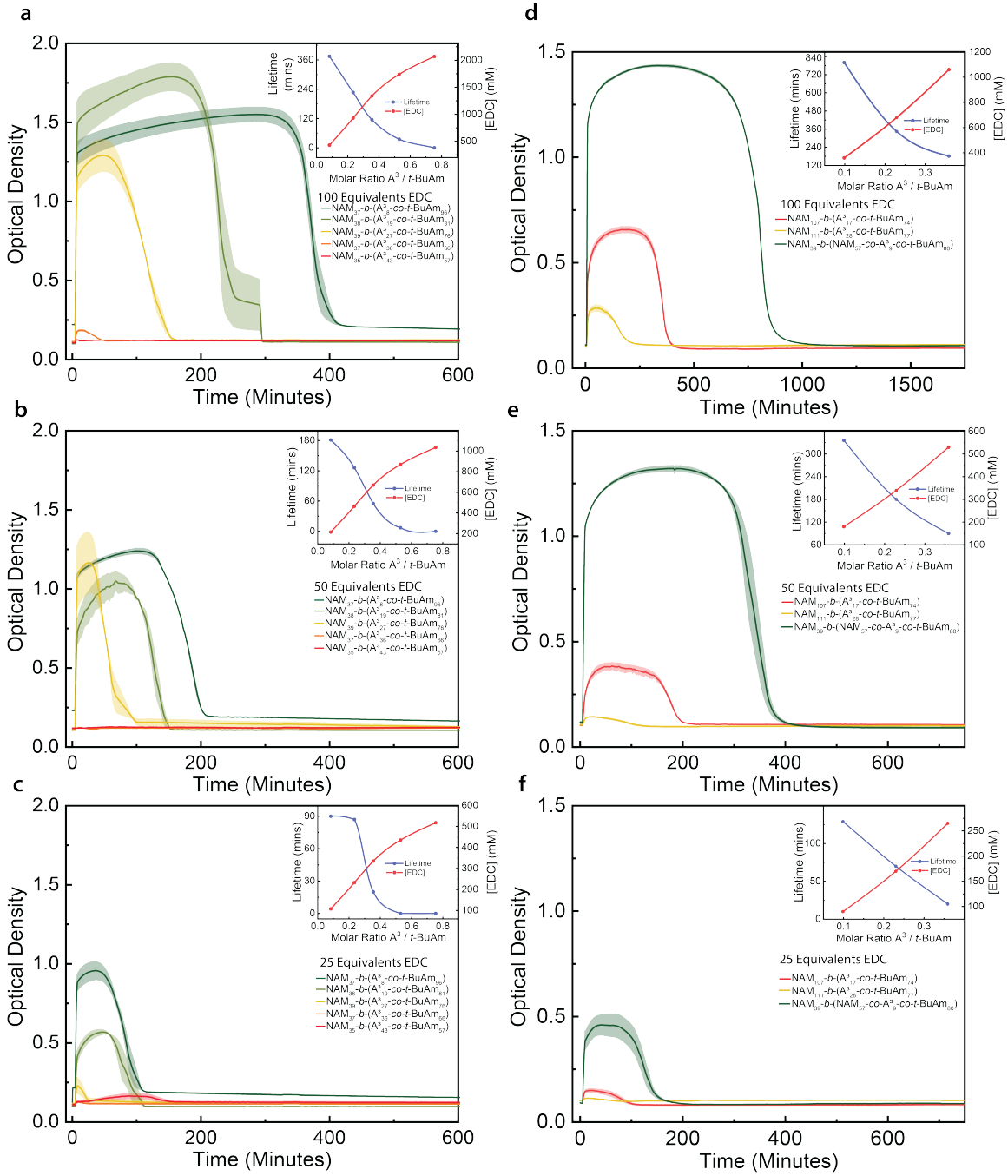

Figure 2.11: Turbidity of fueled polymer solutions. Plots arranged to display fueling response of each polymer to a set equivalent of EDC. (a) Polymers with short poly(NAM) segments, on fueling with 100 equivalents EDC. Inset: Fueled state lifetime (blue) and EDC concentration (red) for each polymer, based on A^3/*t*-BuAm molar ratio in responsive group. (b) Polymers with short poly(NAM) segment on fueling with 100 equivalents EDC. (c) Fueling with 25 equivalents EDC. (d) Polymers with long poly(NAM) segments, on fueling with 100 equivalents EDC. (e) Fueling with 50 equivalents of EDC. (f) Fueling with 25 equivalents EDC. Conditions for all measurements are 5 mg mL^{-1} polymer in 100 mM MES buffer, pH 6.2 with added 100 mM NaCl. Shaded contours display ± standard error, n = 3. Fueling experiments with 200 equivalents of EDC are shown Figure 2.3.

All BCPs display a response to fueling with 200 equivalents of EDC (Figure 2.3), and as EDC loading is decreased, polymers with a larger A^3/*t*-BuAm ratio display no measurable response. NAM$_{37}$-*b*-(A$^3_8$-*co*-*t*-BuAm$_{96}$) and NAM$_{38}$-*b*-(A$^3_{19}$-*co*-*t*-BuAm$_{81}$) display a fueling response to all equivalents of EDC measured (Figure 2.11a-c), with NAM$_{39}$-*b*-(A$^3_{27}$-*co*-*t*-BuAm$_{76}$) weakly responding to 25 equivalents of EDC. NAM$_{37}$-*b*-(A$^3_{36}$-*co*-*t*-BuAm$_{66}$) very weakly responds to 200

and 100 equivalents of EDC, with self-assembly lifetimes of 60 and 45 minutes, respectively. NAM_{35}-*b*-(A^3_{43}-*co*-*t*-$BuAm_{57}$) displays a self-assembly lifetime of 30 minutes when fueled with 200 equivalents of EDC, and does not display self-assembly at lower fuel loadings. This can be attributed to the increased A^3 content (and corresponding decrease in *t*-BuAm) increasing the overall solubility of the responsive segment, such that even on fueling there is an insufficient decrease in water-solubility to afford self-assembly. NAM_{107}-*b*-(A^3_{17}-*co*-*t*-$BuAm_{74}$), NAM_{111}-*b*-(A^3_{28}-*co*-*t*-$BuAm_{77}$) and NAM_{39}-*b*-(NAM_{57}-*co*-A^3_{9}-*co*-*t*-$BuAm_{80}$) follow similar trends in response to fueling, based on their A^3/*t*-BuAm ratio. It is worth noting that NAM_{107}-*b*-(A^3_{17}-*co*-*t*-$BuAm_{74}$) and NAM_{111}-*b*-(A^3_{28}-*co*-*t*-$BuAm_{77}$), with comparable A^3/*t*-BuAm ratios to NAM_{38}-*b*-(A^3_{19}-*co*-*t*-$BuAm_{81}$) and NAM_{39}-*b*-(A^3_{27}-*co*-*t*-$BuAm_{76}$), display longer self-assembly lifetimes, while requiring lower absolute EDC concentrations at a given mass fraction.

2.5.6. Supplementary Note: Self-Assembly of Methylated Polymers

Due to the highly dynamic nature of the EDC-fueled transient self-assembly, EDC-fueled assemblies of the polymers could not be directly imaged *via* TEM. To gain further insight into the nature of the self-assembly, methylated polymers, denoted as NAM_x-*b*-(MeA^3_y-*co*-*t*-$BuAm_z$), self-assembled *via* solvent exchange (as described above) were imaged. The initial formation of structures was confirmed by the appearance of the characteristic blue-hued turbidity of polymer micelles, which persisted after dialysis. These assemblies were imaged by TEM and analyzed by DLS (Figure 2.4, Figure 2.12). Observations by these two techniques show good agreement, and illustrate general trends in the morphology of the polymer assemblies based on the structural composition of the polymers.

NAM_{37}-*b*-(MeA^3_8-*co*-*t*-$BuAm_{96}$) (Figure 2.12a) assembles primarily into spherical objects of radius R_{TEM} = 25-50 nm, with some larger vesicles with R_{TEM} = 50-70 nm displaying a hollow center. The DLS hydrodynamic radius, $R_{h(DLS)}$ of 54.6 nm is in good agreement. NAM_{37}-*b*-(MeA^3_{36}-*co*-*t*-$BuAm_{66}$) (Figure 2.12b) similarly shows assembly of a small population, with R_{TEM} below 50 nm, and a significantly larger number of larger vesicles at R_{TEM} = 50-80 nm. Both populations display secondary assembly into chained structures, and this is reflected in the $R_{h(DLS)}$ = 82.6 nm. NAM_{35}-*b*-(MeA^3_{43}-*co*-*t*-$BuAm_{57}$)displays assembly into spherical micelles with no visible hollow core, with a tight distribution around R_{TEM} = 60 nm, $R_{h(DLS)}$ = 55.8 nm and some ill-defined aggregates are additionally visible. NAM_{111}-*b*-(MeA^3_{28}-*co*-*t*-$BuAm_{77}$) (Figure 2.12c) displays assembly into very small spherical micelles of R_{TEM} = 10-20 nm, along with some larger micelles with R_{TEM} = 20-50 nm (Figure 2.12d). Long, worm-like micelles are also visible, and these compose a small minority of the objects observed by TEM. Given the previously discussed sensitivity of DLS to larger objects, they are over-represented in the resultant $R_{h(DLS)}$ = 47.5 nm. As for the samples discussed in the main text, our TEM observations are in agreement with DLS measurements.

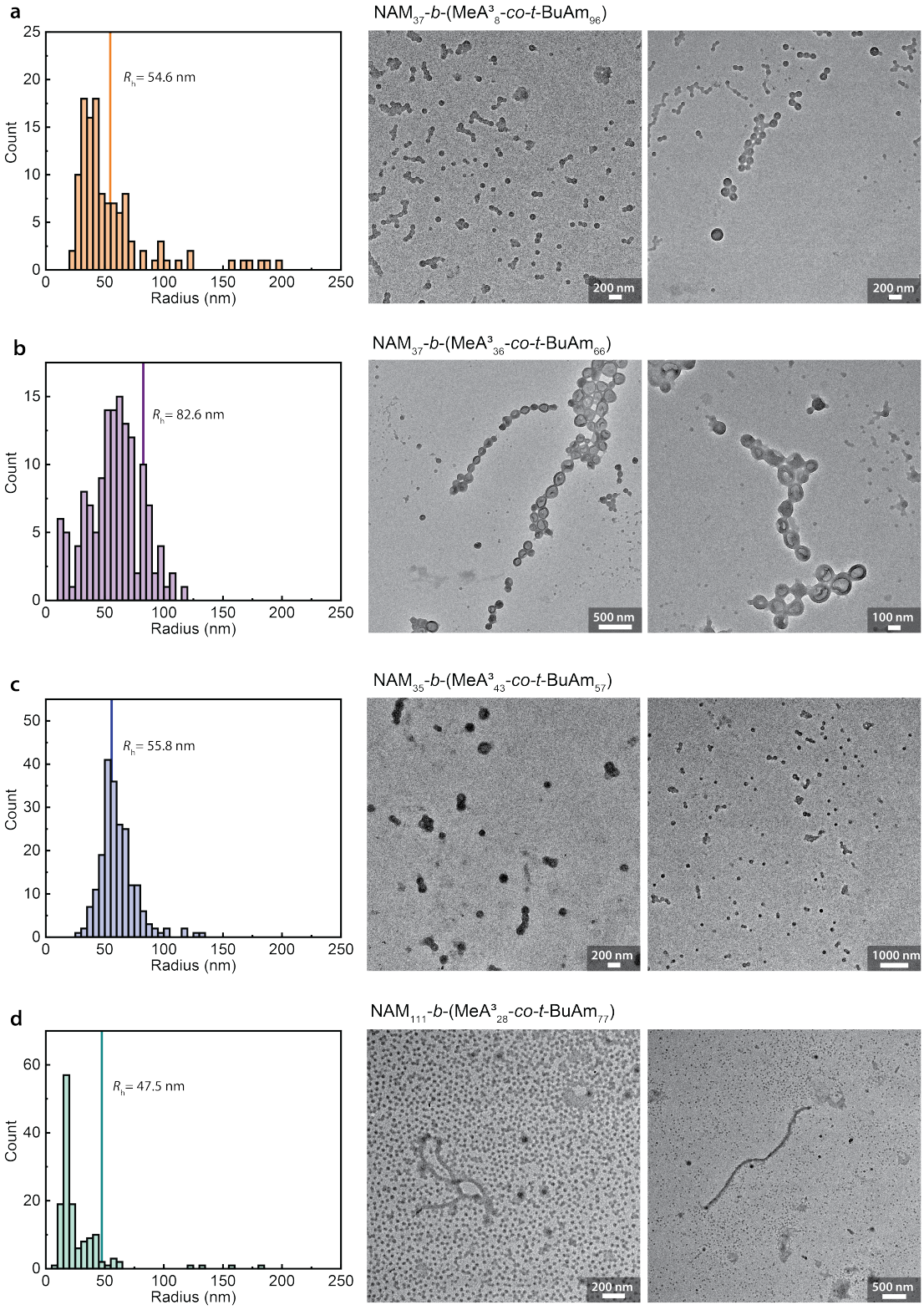

Figure 2.12: Self-assembly of methylated polymers *via* solvent exchange. (**a**) Left: Size distribution for NAM_{37}-*b*-(MeA^3_8-*co*-*t*-$BuAm_{96}$). Histogram represents number distribution from TEM micrographs, straight line indicates the intensity-weighted mean $R_{h(DLS)}$. Average R_{TEM} = 55.7 nm (PDI = 0.46), weighted mean $R_{h(DLS)}$ = 54.6 (PDI = 0.77) Right: TEM micrographs of the polymer sample. (**b**) NAM_{37}-*b*-(A^3_{36}-*co*-*t*-$BuAm_{66}$), average R_{TEM} = 58.1 nm (PDI = 0.15), weighted mean $R_{h(DLS)}$ = 82.6 (PDI = 0.79). (**c**) NAM_{35}-*b*-(A^3_{43}-*co*-*t*-$BuAm_{57}$), average R_{TEM} = 60.6 nm (PDI = 0.07), weighted mean $R_{h(DLS)}$ = 55.8 (PDI = 0.54). (**d**) NAM_{111}-*b*-(A^3_{28}-*co*-*t*-$BuAm_{77}$), average R_{TEM} = 27.8 nm (PDI = 0.75), weighted mean $R_{h(DLS)}$ = 47.5 (PDI = 0.44)

2.6. Acknowledgements

We acknowledge funding from the European Union's Horizon 2020 research and innovation program under the Marie Skłodowska-Curie grant agreement no. 812868. AW acknowledges funding via a Gutenberg Research Professorship underpinning his Life-Like Materials Program.

GF would like to thank Dr. Aritra Sarkar for carrying out MALDI-ToF measurements, Dr. Ingo Lieberwirth for carrying out Cryo-TEM imaging, Dr. Avik Samanta for advice regarding TEM measurements and Dr. Elena Berger-Nicoletti for fruitful discussion regarding GPC and MALDI-ToF sample preparation.

2.7. References

[1] A. V. Ruzette, L. Leibler, Block Copolymers in Tomorrow's Plastics, *Nat. Mater.* **2005**, *4*, 19.

[2] T. P. Lodge, Block Copolymers: Past Successes and Future Challenges, *Macromol. Chem. Phys.* **2003**, *204*, 265.

[3] Y. Mai, A. Eisenberg, Self-Assembly of Block Copolymers, *Chem. Soc. Rev.* **2012**, *41*, 5969.

[4] H. Feng, X. Lu, W. Wang, N. G. Kang, J. W. Mays, Block Copolymers: Synthesis, Self-Assembly, and Applications, *Polymers (Basel)* **2017**, *9*.

[5] S. J. Holder, N. A. J. M. Sommerdijk, New Micellar Morphologies from Amphiphilic Block Copolymers: Disks, Toroids and Bicontinuous Micelles, *Polym. Chem.* **2011**, *2*, 1018.

[6] A. H. Groschel, A. H. Muller, Self-Assembly Concepts for Multicompartment Nanostructures, *Nanoscale* **2015**, *7*, 11841.

[7] S. Iqbal, M. Blenner, A. Alexander-Bryant, J. Larsen, Polymersomes for Therapeutic Delivery of Protein and Nucleic Acid Macromolecules: From Design to Therapeutic Applications, *Biomacromolecules* **2020**, *21*, 1327.

[8] P. Lim Soo, A. Eisenberg, Preparation of Block Copolymer Vesicles in Solution, *J. Polym. Sci., Part B: Polym. Phys.* **2004**, *42*, 923.

[9] L. Zhang, A. Eisenberg, Morphogenic Effect of Added Ions on Crew-Cut Aggregates of Polystyrene-B-Poly(Acrylic Acid) Block Copolymers in Solutions, *Macromolecules* **1996**, *29*, 8805.

[10] G. Wanka, H. Hoffmann, W. Ulbricht, Phase Diagrams and Aggregation Behavior of Poly(Oxyethylene)-Poly(Oxypropylene)-Poly(Oxyethylene) Triblock Copolymers in Aqueous Solutions, *Macromolecules* **1994**, *27*, 4145.

[11] J. E. Chung, M. Yokoyama, T. Aoyagi, Y. Sakurai, T. Okano, Effect of Molecular Architecture of Hydrophobically Modified Poly(N-Isopropylacrylamide) on the Formation of Thermoresponsive Core-Shell Micellar Drug Carriers, *J. Controlled Release* **1998**, *53*, 119.

[12] X. Zhang, S. Boissé, W. Zhang, P. Beaunier, F. D'Agosto, J. Rieger, B. Charleux, Well-Defined Amphiphilic Block Copolymers and Nano-Objects Formed in Situ Via Raft-Mediated Aqueous Emulsion Polymerization, *Macromolecules* **2011**, *44*, 4149.

[13] N. J. Warren, S. P. Armes, Polymerization-Induced Self-Assembly of Block Copolymer Nano-Objects Via Raft Aqueous Dispersion Polymerization, *J. Am. Chem. Soc.* **2014**, *136*, 10174.

[14] T. J. Martin, K. Procházka, P. Munk, S. E. Webber, Ph-Dependent Micellization of Poly(2-Vinylpyridine)-Block-Poly(Ethylene Oxide), *Macromolecules* **1996**, *29*, 6071.

[15] H. Dou, M. Jiang, H. Peng, D. Chen, Y. Hong, Ph-Dependent Self-Assembly: Micellization and Micelle-Hollow-Sphere Transition of Cellulose-Based Copolymers, *Angew. Chem. Int. Ed.* **2003**, *42*, 1516.

[16] J. C. Eloi, D. A. Rider, G. Cambridge, G. R. Whittell, M. A. Winnik, I. Manners, Stimulus-Responsive Self-Assembly: Reversible, Redox-Controlled Micellization of Polyferrocenylsilane Diblock Copolymers, *J. Am. Chem. Soc.* **2011**, *133*, 8903.

[17] X. Li, Y. Wang, Q. Yan, Cyanine Polymersomes Inbreathe Gas Signaling Molecule: So(2) -Driven Bilayer Tubular Deformation for Transmembrane Traffic Regulation, *Angew. Chem. Int. Ed.* **2023**, *62*, e202305290.

[18] M. Karayianni, S. Pispas, Block Copolymer Solution Self-Assembly: Recent Advances, Emerging Trends, and Applications, *J. Polym. Sci.* **2021**, *59*, 1874.

[19] S. De, R. Klajn, Dissipative Self-Assembly Driven by the Consumption of Chemical Fuels, *Adv. Mater.* **2018**, *30*, e1706750.

[20] L. Heinen, A. Walther, Celebrating Soft Matter's 10th Anniversary: Approaches to Program the Time Domain of Self-Assemblies, *Soft Matter* **2015**, *11*, 7857.

[21] A. Sorrenti, J. Leira-Iglesias, A. Sato, T. M. Hermans, Non-Equilibrium Steady States in Supramolecular Polymerization, *Nat. Commun.* **2017**, *8*, 15899.

[22] L. Heinen, A. Walther, Programmable Dynamic Steady States in Atp-Driven Nonequilibrium DNA Systems, *Sci. Adv.* **2019**, *5*, eaaw0590.

[23] T. Heuser, E. Weyandt, A. Walther, Biocatalytic Feedback-Driven Temporal Programming of Self-Regulating Peptide Hydrogels, *Angew. Chem. Int. Ed.* **2015**, *54*, 13258.

[24] J. A. Berrocal, C. Biagini, L. Mandolini, S. Di Stefano, Coupling of the Decarboxylation of 2-Cyano-2-Phenylpropanoic Acid to Large-Amplitude Motions: A Convenient Fuel for an Acid-Base-Operated Molecular Switch, *Angew. Chem. Int. Ed.* **2016**, *55*, 6997.

[25] J. Boekhoven, A. M. Brizard, K. N. Kowlgi, G. J. Koper, R. Eelkema, J. H. van Esch, Dissipative Self-Assembly of a Molecular Gelator by Using a Chemical Fuel, *Angew. Chem. Int. Ed.* **2010**, *49*, 4825.

[26] J. Boekhoven, W. E. Hendriksen, G. J. Koper, R. Eelkema, J. H. van Esch, Transient Assembly of Active Materials Fueled by a Chemical Reaction, *Science* **2015**, *349*, 1075.

[27] B. G. P. van Ravensteijn, W. E. Hendriksen, R. Eelkema, J. H. van Esch, W. K. Kegel, Fuel-Mediated Transient Clustering of Colloidal Building Blocks, *J. Am. Chem. Soc.* **2017**, *139*, 9763.

[28] B. Klemm, R. W. Lewis, I. Piergentili, R. Eelkema, Temporally Programmed Polymer - Solvent Interactions Using a Chemical Reaction Network, *Nat. Commun.* **2022**, *13*, 6242.

[29] R. W. Lewis, B. Klemm, M. Macchione, R. Eelkema, Fuel-Driven Macromolecular Coacervation in Complex Coacervate Core Micelles, *Chem. Sci.* **2022**, *13*, 4533.

[30] M. Tena-Solsona, B. Riess, R. K. Grotsch, F. C. Lohrer, C. Wanzke, B. Kasdorf, A. R. Bausch, P. Muller-Buschbaum, O. Lieleg, J. Boekhoven, Non-Equilibrium Dissipative Supramolecular Materials with a Tunable Lifetime, *Nat. Commun.* **2017**, *8*, 15895.

[31] L. S. Kariyawasam, C. S. Hartley, Dissipative Assembly of Aqueous Carboxylic Acid Anhydrides Fueled by Carbodiimides, *J. Am. Chem. Soc.* **2017**, *139*, 11949.

[32] P. S. Schwarz, M. Tena-Solsona, K. Dai, J. Boekhoven, Carbodiimide-Fueled Catalytic Reaction Cycles to Regulate Supramolecular Processes, *Chem. Commun.* **2022**, *58*, 1284.

[33] B. A. K. Kriebisch, C. M. E. Kriebisch, A. M. Bergmann, C. Wanzke, M. Tena-Solsona, J. Boekhoven, Tuning the Kinetic Trapping in Chemically Fueled Self-Assembly, *ChemSystemsChem* **2022**, *5*.

[34] K. Dai, J. R. Fores, C. Wanzke, B. Winkeljann, A. M. Bergmann, O. Lieleg, J. Boekhoven, Regulating Chemically Fueled Peptide Assemblies by Molecular Design, *J. Am. Chem. Soc.* **2020**, *142*, 14142.

[35] C. Wanzke, A. Jussupow, F. Kohler, H. Dietz, V. R. I. Kaila, J. Boekhoven, Dynamic Vesicles Formed by Dissipative Self-Assembly, *ChemSystemsChem* **2019**, *2*.

[36] F. Spath, A. S. Maier, M. Stasi, A. M. Bergmann, K. Halama, M. Wenisch, B. Rieger, J. Boekhoven, The Role of Chemically Innocent Polyanions in Active, Chemically Fueled Complex Coacervate Droplets, *Angew. Chem. Int. Ed.* **2023**, *62*, e202309318.

[37] C. Donau, F. Spath, M. Stasi, A. M. Bergmann, J. Boekhoven, Phase Transitions in Chemically Fueled, Multiphase Complex Coacervate Droplets, *Angew. Chem. Int. Ed.* **2022**, *61*, e202211905.

[38] F. Spath, C. Donau, A. M. Bergmann, M. Kranzlein, C. V. Synatschke, B. Rieger, J. Boekhoven, Molecular Design of Chemically Fueled Peptide-Polyelectrolyte Coacervate-Based Assemblies, *J. Am. Chem. Soc.* **2021**, *143*, 4782.

[39] C. Donau, F. Spath, M. Sosson, B. A. K. Kriebisch, F. Schnitter, M. Tena-Solsona, H. S. Kang, E. Salibi, M. Sattler, H. Mutschler, J. Boekhoven, Active Coacervate Droplets as a Model for Membraneless Organelles and Protocells, *Nat. Commun.* **2020**, *11*, 5167.

[40] M. Tena-Solsona, J. Janssen, C. Wanzke, F. Schnitter, H. Park, B. Riess, J. M. Gibbs, C. A. Weber, J. Boekhoven, Accelerated Ripening in Chemically Fueled Emulsions, *ChemSystemsChem* **2021**, *3*.

[41] B. J. Niebuur, H. Hegels, M. Tena-Solsona, P. S. Schwarz, J. Boekhoven, C. M. Papadakis, Droplet Formation by Chemically Fueled Self-Assembly: The Role of Precursor Hydrophobicity, *J. Phys. Chem. B* **2021**, *125*, 13542.

[42] J. Heckel, F. Batti, R. T. Mathers, A. Walther, Spinodal Decomposition of Chemically Fueled Polymer Solutions, *Soft Matter* **2021**, *17*, 5401.

[43] M. A. Würbser, P. Schwarz, J. Heckel, A. M. Bergmann, A. Walther, J. Boekhoven, Chemically Fueled Block Copolymer Self-Assembly into Transient Nanoreactor, *ChemSystemsChem* **2021**, *3*, e2100015

[44] Y. S. Jo, A. J. van der Vlies, J. Gantz, S. Antonijevic, D. Demurtas, D. Velluto, J. A. Hubbell, Raft Homo- and Copolymerization of N-Acryloyl-Morpholine, Piperidine, and Azocane and Their Self-Assembled Structures, *Macromolecules* **2008**, *41*, 1140.

[45] J. I. Solomun, L. Martin, P. Mapfumo, E. Moek, E. Amro, F. Becker, S. Tuempel, S. Hoeppener, K. L. Rudolph, A. Traeger, Ph-Sensitive Packaging of Cationic Particles by an Anionic Block Copolymer Shell, *J. Nanobiotechnology* **2022**, *20*, 336.

[46] T. Boursier, S. Georges, M. Mosquet, D. Rinaldi, F. D'Agosto, Synthesis of Poly(N-Acryloylmorpholine) Macromonomers Using Raft and Their Copolymerization with Methacrylic Acid for the Design of Graft Copolymer Additives for Concrete, *Polym. Chem.* **2016**, *7*, 917.

[47] B. de Lambert, M.-T. Charreyre, C. Chaix, C. Pichot, Poly(N-Tert-Butyl Acrylamide-B-N-Acryloylmorpholine) Amphiphilic Block Copolymers Via Raft Polymerization: Synthesis, Purification and Characterization, *Polymer* **2007**, *48*, 437.

[48] F. Schnitter, J. Boekhoven, A Method to Quench Carbodiimide-Fueled Self-Assembly, *ChemSystemsChem* **2020**, *3*.

[49] G. Fusi, D. Del Giudice, O. Skarsetz, S. Di Stefano, A. Walther, Autonomous Soft Robots Empowered by Chemical Reaction Networks, *Adv. Mater.* **2023**, *35*, e2209870.

[50] K. Fischer, M. Schmidt, Pitfalls and Novel Applications of Particle Sizing by Dynamic Light Scattering, *Biomaterials* **2016**, *98*, 79.

[51] J. Stetefeld, S. A. McKenna, T. R. Patel, Dynamic Light Scattering: A Practical Guide and Applications in Biomedical Sciences, *Biophys. Rev.* **2016**, *8*, 409.

[52] A. Einstein, Über Die Von Der Molekularkinetischen Theorie Der Wärme Geforderte Bewegung Von in Ruhenden Flüssigkeiten Suspendierten Teilchen, *Ann. Phys. (Berl.)* **1905**, *322*, 549.

[53] C. M. Sorensen, in *Light Scattering and Absorption by Particles*, IOP Publishing **2022**, 6.

[54] B. J. Berne, R. Pecora, *Dynamic Light Scattering with Applications to Chemistry, Biology, and Physics*, John Wiley & Sons, Inc., **2000**.

[55] X. Lang, U. Thumu, L. Yuan, C. Zheng, H. Zhang, L. He, H. Zhao, C. Zhao, Chemical Fuel-Driven Transient Polymeric Micelle Nanoreactors toward Reversible Trapping and Reaction Acceleration, *Chem. Commun.* **2021**, *57*, 5786.

[56] R. Merindol, A. Walther, Materials Learning from Life: Concepts for Active, Adaptive and Autonomous Molecular Systems, *Chem. Soc. Rev.* **2017**, *46*, 5588.

[57] K. Das, L. Gabrielli, L. J. Prins, Chemically Fueled Self-Assembly in Biology and Chemistry, *Angew. Chem. Int. Ed.* **2021**, *60*, 20120.

[58] N. Singh, G. J. M. Formon, S. De Piccoli, T. M. Hermans, Devising Synthetic Reaction Cycles for Dissipative Nonequilibrium Self-Assembly, *Adv. Mater.* **2020**, *32*, e1906834.

[59] S. D. Hanton, D. M. Parees, Extending the Solvent-Free Maldi Sample Preparation Method, *J. Am. Soc. Mass. Spectrom.* **2005**, *16*, 90.

[60] *Dls Data Analysis: The Corenn Method,* Available online: https://lsinstruments.ch/en/theory/dynamic-light-scattering-dls/dls-data-analysis-the-corenn-method Accessed: 27/03/2024

Chapter

3 Tribromoacetic Acid as a Chemical Fuel for Self-Assembly of pH-responsive Block Copolymers

3.1. Abstract

Stimuli-responsive polymers are of great interest in developing smart and programmable materials for applications ranging from controlled drug delivery to in-material sensing and reporting. pH is an attractive and widely used stimulus due to its simplicity and ubiquity in biological contexts. Here, we report the use of tribromoacetic acid as a chemical fuel to control the pH of polymer systems over time, overcoming drawbacks of classical pH switching systems. We show that controlling block copolymer architecture affords differing responses to this chemical fuel through engineered assembly thresholds and kinetic trapping. With the aid of a kinetic model, we further study the interplay of the numerous acid-base equilibria at play to provide general guidelines for designing chemically fueled pH-responsive systems, and accurately predict the evolution of the system over time.

3.2. Introduction

Self-assembling polymers[1-2] have in recent years found a number of applications[3] such as rheological modifiers,[4] carriers for controlled drug release[5] and nanoreactors.[6-8] pH is an attractive control stimulus for polymeric systems, due to the relative simplicity of acid-base chemistry, the wide variety of pH-responsive monomers that can be incorporated. Furthermore, the reversibility of acid-base equilibria allows for reversible self-assembly, often over many cycles. As such, pH alteration found early adoption as a control mechanism for polymer assembly.[4,9-11] In such systems, pH acts as a switch stimulus, precluding any change in system properties until more acid or base is added. However, if the pH stimulus is further modulated over time by an upstream process, temporal control of pH can be achieved, and therefore the timescale of the (dis)assembly of polymers in solution, allowing for more complex autonomous behavior.[12]

To this end, a number of pH control mechanisms have been developed. Oscillating clock reactions, such as the bromate-sulfite-ferrocyanide system[13] have been successfully coupled to polymers.[14-15] Small-molecule based chemical reaction networks can employ dormant deactivators to effect a pH change for a pre-programmed time, and have been successfully coupled to polymer self-assembly.[16] Enzymatic networks have also been successfully employed for temporal control of pH, such as in the now ubiquitous urea-urease reaction.[17] These can further be coupled to additional enzymatic or small-molecule based reaction cycles to yield systems of increasing complexity.[18-21] The key advantage of these approaches over oscillating and clock reactions is the ability to arbitrarily pre-program the lifetime and magnitude of the pH change by altering the starting conditions.

Another class of small-molecule systems are those employing activated carboxylic acids (ACAs) as chemical fuels. These acids readily release protons in solution and subsequently slowly decarboxylate, yielding a carbanion that recaptures protons from solution, the net effect being a rapid pH drop followed by a gradual recovery to higher pH. Originally employed to control out of equilibrium supramolecular assembly in non-aqueous solvents,[22-25] ACAs have also been used to control reversible gelation of organogels.[26-27] Recent advances have shown that more reactive ACAs can be used in aqueous media[28] to drive the dissipative operation of DNA nanodevices.[29]

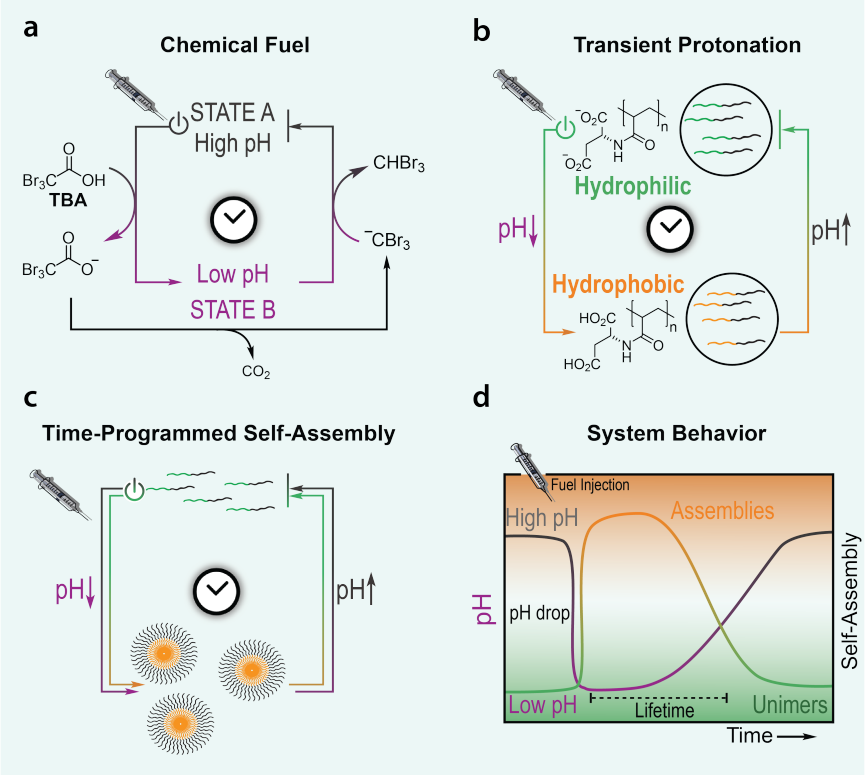

Figure 3.1: Coupling an autonomous pH cycle to responsive copolymers. (a) Chemistry of the transient pH drop achieved through the tribromoacetic acid fuel cycle. (b) Transient pH drop coupled to a pH-responsive copolymer leads to transient hydrophilic to hydrophobic switch. (c) Protonated copolymers assemble for a pre-programmed duration based on fuel loading. (d) Overall system behavior, where fuel addition leads to a pH drop (purple line), quickly followed by assembly of copolymers.

Here, we report the use of tribromoacetic acid (TBA) as a chemical fuel to drive the out of equilibrium self-assembly of block copolymers (BCPs) (Figure 3.1) composed of a hydrophilic and a pH-responsive segment. We show that control over the lifetime and magnitude of the pH drop can be tuned by altering the amount of fuel added. We are further able to alter the pH-responsiveness of the BCPs by altering the ratio of pH-responsive to hydrophobic monomers in the responsive block, and explore the interplay of these effects on the self-assembly properties of the BCPs. With the aid of a kinetic model, we further discuss the interplay of the numerous of acid-base equilibria in the system and how they give rise to the exhibited behavior.

3.3. Results and Discussion

3.3.1. Synthesis and Characterization of pH-Responsive Block Copolymers

To obtain block copolymers that display the desired pH-responsive behavior, we designed and synthesized, as described in **Chapter 2** above, BCPs comprising a hydrophilic first block composed of poly(*N*-acryloylmorpholine) (poly(NAM)), and a second block composed of aspartic acid *N*-acrylamide (A^3) and *tert*-butylacrylamide (*t*-BuAm) in varying ratios *via* RAFT polymerization. Poly(NAM) was selected due to the highly hydrophilic nature of the polymer, comparable to poly(ethyleneglycol).[30-31] RAFT polymerization of poly(NAM) has been well established,[32-33] and by synthesizing the poly(NAM) block and extending it in situ, the block length can easily be tailored on demand. We employ A^3 as a pH-responsive building block for the responsive polymer segment, as it can be easily copolymerized with the other acrylamide monomers included in the study, and poly(A^3) has a pK_a in the range of 5.0-6.0, which is relevant for TBA fueling. *t*-BuAm is included as a co-monomer, as poly(*t*-BuAm) is insoluble in both water and DMSO (which we employ as a co-solvent in fueling experiments) and is therefore ideal to modulate the density of carboxyl groups in the responsive segment of the BCP and bring the responsive segment to the brink of insolubility. A summary of the BCPS synthesized is included in Table 3.1.

Table 3.1: Summary of Polymer Samples

Polymer Sample	Repeat Units (^{1}H-NMR)			*Đ* (GPC)		M_n (GPC)
	NAM	A^3	*t*-BuAm	First Block	Final Copolymer	(kg mol^{-1})
NAM_{37}-*b*-(A^3_8-*co*-*t*-$BuAm_{96}$)	37	8	96	1.12	1.20	26.2
NAM_{38}-*b*-(A^3_{19}-*co*-*t*-$BuAm_{81}$)	38	19	81	1.23	1.21	22.7
NAM_{39}-*b*-(A^3_{27}-*co*-*t*-$BuAm_{76}$)	39	27	76	1.24	1.17	23.9
NAM_{37}-*b*-(A^3_{36}-*co*-*t*-$BuAm_{66}$)	37	36	66	1.25	1.18	22.4
NAM_{35}-*b*-(A^3_{43}-*co*-*t*-$BuAm_{57}$)	35	43	57	1.16	1.20	23.0
NAM_{107}-*b*-(A^3_{17}-*co*-*t*-$BuAm_{74}$)	107	17	74	1.25	1.14	18.0
NAM_{111}-*b*-(A^3_{28}-*co*-*t*-$BuAm_{77}$)	111	28	77	1.28	1.18	18.7
NAM_{39}-*b*-(NAM_{57}-*co*-A^3_9-*co*-*t*-$BuAm_{80}$)	96*	9	80	1.1	1.21	18.5

We first explore the pH-responsive behavior of the BCPs. The apparent pK_a of each BCP was determined by conductimetric titration (Figure 3.2a, b) of solutions of 3 mg mL^{-1} BCP in water, adjusted to pH 11 with NaOH. All BCPs display a pK_a between 5.7 and 5.2. In the shorter BCPs with a total NAM content below 40 units, the sample with the lowest A^3 content, NAM_{37}-*b*-(A^3_8-*co*-*t*-$BuAm_{96}$), displays a slightly higher apparent pK_a of 5.5. Likewise, NAM_{35}-*b*-(A^3_{43}-*co*-*t*-$BuAm_{57}$), with the highest A^3 content displays a slightly lower pK_a of 5.2, with the remaining BCPs' pK_a = 5.3. The longer BCPs, NAM_{107}-*b*-(A^3_{17}-*co*-*t*-$BuAm_{74}$), NAM_{111}-*b*-(A^3_{28}-*co*-*t*-$BuAm_{77}$) and NAM_{39}-*b*-(NAM_{57}-*co*-A^3_9-*co*-*t*-$BuAm_{80}$) display slightly higher pK_a of 5.6, 5.6 and 5.7 respectively. This discrepancy can be attributed to the lower overall ionic strength of these polymer solutions, given the lower effective A^3 concentration.

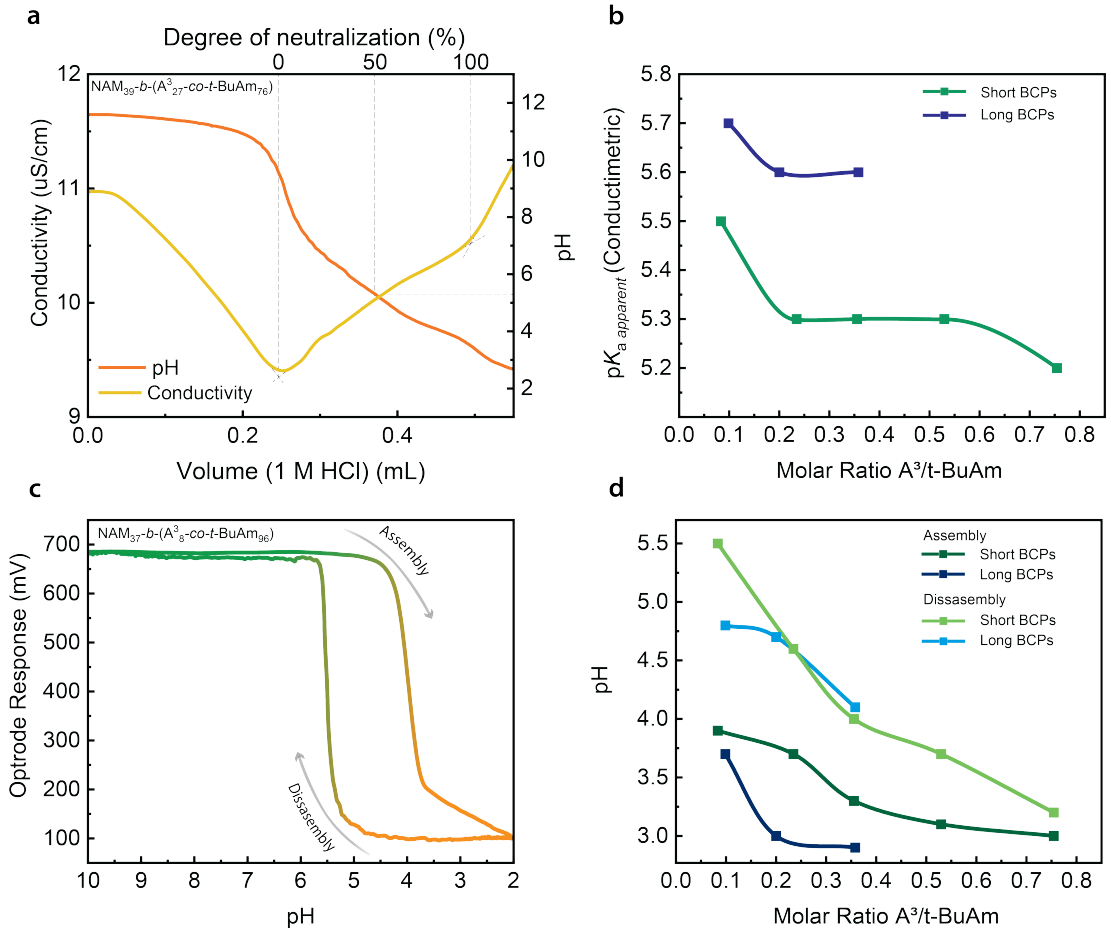

Figure 3.2: Characterizing the pH responsiveness of BCPs. (a) Representative conductimetric titration of NAM_{39}-*b*-(A^3_{27}-*co*-*t*-$BuAm_{76}$), showing a single protonation step. (b) pK_a of all copolymers determined by conductimetric titration. Short BCPs are those with < 40 total NAM units. (c) Turbidimetric titration reveals hysteresis in pH-responsive assembly and disassembly of copolymers. NAM_{37}-*b*-(A^3_8-*co*-*t*-$BuAm_{96}$) assembles as pH drops below 3.9, remaining in an assembled state until pH rises past 5.5. (d) Assembly and disassembly pH of all BCPs. The relationship between increasing A^3 content, decreasing (dis)assembly pH and reduced hysteresis can be clearly seen. Conditions for all measurements are 3 mg mL^{-1} copolymer in water. pH adjusted using 1M NaOH and 1M HCl, with maximum addition rates of 0.05 mL min^{-1}.

As the A^3 units in the BCPs are protonated during titration, the solutions become turbid (Figure 3.2c), indicating assembly into structures. For each BCP, the pH at which assembly commences is lower than that at which the assemblies re-solubilize, leading to significant hysteresis in their assembly (Figure 3.2c, d). BCPs with lower A^3/*t*-BuAm ratios display higher assembly and disassembly pH, as well as a greater hysteresis. This is evident in the shorter BCPs, with NAM_{37}-*b*-(A^3_8-*co*-*t*-$BuAm_{96}$) displaying an assembly pH (Figure 3.2d, dark green) of 3.9, a disassembly pH of 5.5 (light green), and therefore a ΔpH of 1.6 pH units. In comparison, NAM_{35}-*b*-(A^3_{43}-*co*-*t*-$BuAm_{57}$) assembles at pH = 3.0 and disassembles at pH = 3.2. Given that pK_a values are similar, we attribute the difference in assembly onset to the lowered overall solubility (irrespective of acid group ionization) when a larger fraction of the second block is composed of the insoluble *t*-BuAm, such that even partial protonation of the carboxyl groups is sufficient to drive a hydrophilic to hydrophobic transition. The trend in hysteresis we instead attribute to kinetic trapping of the assemblies in a highly hydrophobic environment, where deprotonation of the acid groups is hindered by the lack of mediating solvent molecules. To exclude the influence of rapid pH changes

and slower equilibration kinetics, titrations were carried out with the limited rate of 0.05 mL min^{-1}.

3.3.2. Tribromoacetic Acid-Fueled Self-Assembly

With the effect of A^3/*t*-BuAm block composition on the pH-responsive behavior of the BCPs established, we couple these BCPs to the TBA fuel cycle to control their self-assembly over time.

On addition to aqueous solution, TBA rapidly releases a proton, and the resulting carboxylate anion slowly decarboxylates. This decarboxylation step generates CO_2, which is partially dissolved in water affording carbonic acid, which dissociates into the HCO_3^- / H^+ buffer pair. The complete cycle leads to a swift drop in pH as TBA dissociates, followed by a gradual rise as the rate-determining decarboxylation step occurs, and the produced Br_3C^- scavenges the previously released protons (Figure 3.1a), yielding bromoform. Due to the presence of added carbonate buffer from the CO_2, the pH does not return to its initial value, but remains buffered slightly below it.

To investigate the self-assembly of the BCPs as coupled to the TBA cycle, we carried out a series of fueling experiments at a BCP concentration of 3 g L^{-1} in 10 mM 3-(*N*-morpholino) propanesulfonic acid (MOPS) buffer at pH 7.0, with the addition of 5 mM NaCl in 30 / 70 vol / vol DMSO / H_2O. Tribromoacetate decarboxylates very slowly in pure water[34] due to hydrogen-bonding stabilization of the anion, as will be discussed in greater detail in **Chapter 4**. Addition of DMSO as a co-solvent greatly increases the rate of decarboxylation, while minimally impacting the acid / base chemistry and solubility of the remaining components in the system. Upon addition of TBA, the optical density of the solutions at 440 nm was monitored to observe BCP self-assembly (Figure 3.3)

To explore the effect of responsive block composition on fueled behavior, NAM_{37}-*b*-(A^3_8-*co*-*t*-$BuAm_{96}$), NAM_{38}-*b*-(A^3_{19}-*co*-*t*-$BuAm_{81}$), NAM_{39}-*b*-(A^3_{27}-*co*-*t*-$BuAm_{76}$), NAM_{37}-*b*-(A^3_{36}-*co*-*t*-$BuAm_{66}$) and NAM_{35}-*b*-(A^3_{43}-*co*-*t*-$BuAm_{57}$) were fueled with 10 mM TBA (Figure 3a).

Solutions of the first three BCPs displayed a rapid response to TBA addition, becoming turbid within 5 minutes, with a significant variation in the lifetime of the self-assembly, defined as the time taken for optical density to return to $½OD_{max}$.

It can be clearly seen that assembly lifetime is inversely proportional to the A^3 content of the BCP. NAM_{37}-*b*-(A^3_8-*co*-*t*-$BuAm_{96}$), with the lowest carboxyl group content, correspondingly displays the longest assembly lifetime of 2620 minutes, followed by NAM_{38}-*b*-(A^3_{19}-*co*-*t*-$BuAm_{81}$) with 985 minutes and NAM_{39}-*b*-(A^3_{27}-*co*-*t*-$BuAm_{76}$) with 155 minutes. NAM_{37}-*b*-(A^3_{36}-*co*-*t*-$BuAm_{66}$) and NAM_{35}-*b*-(A^3_{43}-*co*-*t*-$BuAm_{57}$), with the greatest A^3 content, display no measurable response on addition of 10 mM TBA. This can be rationalized by considering the greater effective concentration of carboxylate groups in solution, which are largely deprotonated at the starting pH, and therefore act to buffer the acid-induced pH drop, leading to a smaller overall drop in pH (see Section 3.5.8). Furthermore, the increased A^3 content in the responsive block affords greater overall solubility, even in the protonated state. These two effects in tandem greatly reduce the assembly response of A^3-rich polymers.

Examining the effect of altering TBA concentration on the same BCP, we observe the expected increase in assembly lifetime on increasing TBA loading (Figure 3.3b). NAM_{38}-*b*-(A^3_{19}-*co*-*t*-$BuAm_{81}$), fueled with 5 mM TBA, displays a lifetime of 208 minutes, and 985 minutes when loaded with 10 mM TBA, and fueling with 20 mM TBA leads to a lifetime of 2790 minutes. This general trend of increased assembly lifetime holds true for the remaining samples (Figure 3.3c).

BCPs containing a larger fraction of poly(NAM), NAM_{107}-*b*-(A^3_{17}-*co*-*t*-$BuAm_{74}$), NAM_{111}-*b*-(A^3_{28}-*co*-*t*-$BuAm_{77}$) and NAM_{39}-*b*-(NAM_{57}-*co*-A^3_9-*co*-*t*-$BuAm_{80}$) all display an assembly response at 10 mM TBA, with lifetimes of 1740, 1200 and 1770 minutes respectively (Figure 3.3d), and the trend of increasing lifetime with decreasing A^3 content is observed. Likewise, addition of increasing amounts of TBA leads to a longer period of measured turbidity. NAM_{39}-*b*-(NAM_{57}-*co*-A^3_9-*co*-*t*-$BuAm_{80}$), on addition of 5, 10 and 20 mM TBA (Figure 3.3e) displays lifetimes of 740, 1770 and 3330 minutes, respectively. Again, this trend holds for the remaining BCPs (Figure 3.3f).

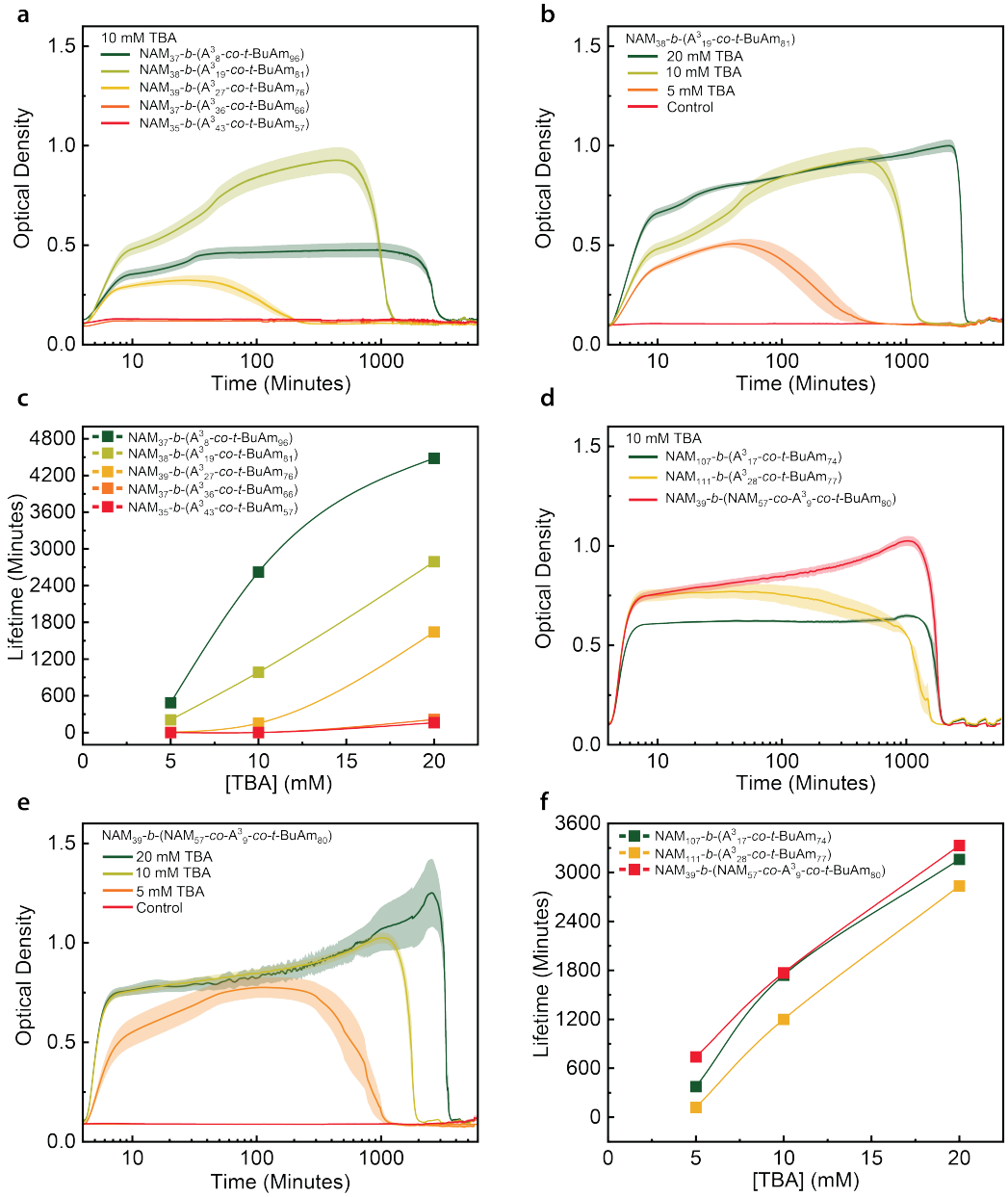

Figure 3.3: Exploring fueled self-assembly of BCPs. (a) Effect of BCP composition on optical density and lifetime of fueled state for short poly(NAM) segment BCPs, with 10 mM TBA. (b) Effect of increasing TBA concentration on self-assembly of NAM_{38}-*b*-(A^3_{19}-*co*-*t*-$BuAm_{81}$). (c) Lifetime of self-assembled state as a function of BCP sample and TBA concentration for BCPs with short poly(NAM) segments. (d) Effect of copolymer composition on optical density and lifetime of the fueled state for BCPs with long poly(NAM) segments. (e) Effect of increasing TBA concentration on the self-assembly of NAM_{39}-*b*-(NAM_{57}-*co*-A^3_9-*co*-*t*-$BuAm_{80}$). (f) Lifetime of the self-assembled state as a function of BCP sample and TBA concentration, for BCPs with long poly(NAM) segments. Conditions for all measurements are 3 mg mL^{-1} BCP in 10 mM MOPS buffer, 10 mM NaCl, in 30/70 v/v DMSO/H_2O. Error contours show the standard error for measurements, with **n** = 3. Additional plots for all BCPs and TBA concentrations are included in Figure 3.5.

3.3.3. Modelling the TBA Reaction Cycle

To gain a deeper understanding of the evolution of the system over the course of fueling, we design a kinetic model of the reaction cycle. As discussed above, the core of the fuel cycle is comprised of two reaction sequences that modulate the pH; firstly, the dissociation of TBA to afford a proton and the corresponding carboxylate anion, followed by its spontaneous decarboxylation to Br_3C^-, and proton capture to yield bromoform and secondly, the dissolution of released CO_2, leading to the H_2CO_3 / HCO_3^- / CO_3^{2-} buffer system. In all fueling experiments MOPS buffer is employed to set the starting system pH, and accordingly this buffer pair must be taken into account. Additionally, when fueling BCP solutions, the sequential (de)protonation of carboxyl groups in the A^3 monomer must also be considered. The reactions involved in the fuel cycle are summarized in Figure 3.4a.

Although many, these processes serve to modulate the concentration of H^+ in solution as a series of acid-base equilibria, and as such are easily modeled if the respective equilibrium constants are known. We designed a simple kinetic model of the TBA fuel cycle and implemented it in the COPASI software package,[35] assuming that the system remains homogeneous throughout, all acid/base equilibria occur much faster than the process of decarboxylation, and that pK_a values in the mixed DMSO/water solvent system do not appreciably deviate from those in pure water. Acid-base equilibria were implemented as reversible mass action processes with equilibrium constants equivalent to their respective K_a values, and decarboxylation as an irreversible process with a first order dependency on the concentration of the tribromoacetate anion. Table 3.2 displays a summary of the pK_a values used in modeling these acid-base pairs (Figure 3.4a).

Table 3.2: Summary of Parameters Employed in Kinetic Model

K_1 (s^{-1})	2.25×10^{-5}	Decarboxylation of tribromoacetate
pK_{a1}	1.00	pK_a of TBA
pK_{a2}	13.17	pK_a of bromoform
pK_{a3}	6.35	Apparent pK_a of $CO_{2\,(aq)}$ (hydration and dissociation)
pK_{a4}	10.33	pK_a of HCO_3^-
pK_{a5}	7.20	pK_a of MOPS Buffer
pK_{a6} = pK_{a7}	5.20 - 5.70	pK_a of aspartate groups, varies by BCP, refer to Figure 3.2

In mathematical terms, the concentrations of all species in the model are described by a set of ordinary differential equations, which can be grouped by reactions sequences of the system as outlined in Figure 3.4a.

The decarboxylation is described as follows:

$$\frac{\partial[\mathrm{TBAH}]}{\partial t} = -K_{\mathrm{a1}}[\mathrm{TBAH}] + \frac{[\mathrm{TBA^-}][\mathrm{H^+}]}{K_{\mathrm{a1}}}$$

$$\frac{\partial[\mathrm{TBA^-}]}{\partial t} = K_{\mathrm{a1}}[\mathrm{TBAH}] - \frac{[\mathrm{TBA^-}][\mathrm{H^+}]}{K_{\mathrm{a1}}} - K_1[\mathrm{TBA^-}]$$

$$\frac{\partial[\mathrm{Br_3C^-}]}{\partial t} = K_1[\mathrm{TBA^-}] - \frac{[\mathrm{Br_3C^-}][\mathrm{H^+}]}{K_{\mathrm{a2}}}$$

$$\frac{\partial[\mathrm{Br_3CH}]}{\partial t} = K_{\mathrm{a2}}[\mathrm{Br_3C^-}][\mathrm{H^+}]$$

The decarboxylation rate constant, K_1, was determined by fitting the measured pH of fueling experiments with 5, 10 and 20 mM, with 10 mM MOPS buffer in the absence of polymer to the model, and found to be 2.25×10^{-5} s^{-1} (Figure 3.4b-c). To the best of our knowledge, no value for this rate constant has been published to date.

Since the decarboxylating species is the deprotonated tribromoacetate, it is possible that very large tribromoacetic acid concentrations, and therefore low pH, would lead to negative feedback and a corresponding drop in decarboxylation rate. The model considers this eventuality, but we find that the concentration of undissociated acid is always negligible at the pH values reached in our experiments.

The off-gassing of dissolved CO_2 is a complex process dependent on a wide number of factors including the complex viscosity of the medium, number of nucleation sites in the reaction vessel[36] and partial CO_2 pressure in the vessel headspace[37] and therefore, the nature of the vessel itself. We modeled this as an irreversible mass action process with a first order rate constant, K_{gas}, left as a fitted parameter, with the additional constraint that $[CO_{2(aq)}]$ not exceed the saturation concentration of 1.45 g L^{-1} (equivalent to 30 mM). This is a reasonable compromise that allows for accurate modelling of pH over time while avoiding additional complexity. In all cases, this rate constant was on the order of 10^{-4} s^{-1}. Additionally, the dissolution of CO_2 was modeled according to the commonly employed apparent pK_a of dissolved CO_2 in aqueous solution, combining the hydration of CO_2 to carbonic acid and the dissociation of carbonic acid into one step. With these considerations, the behavior of CO_2 in the system is described as follows:

$$\frac{\partial[\mathrm{CO_{2(aq)}}]}{\partial t} = K_1[\mathrm{TBA^-}] - K_{\mathrm{a3}}[\mathrm{CO_{2(aq)}}][\mathrm{H_2O}] + \frac{[\mathrm{HCO_3^-}][\mathrm{H^+}]}{K_{\mathrm{a3}}} - K_{\mathrm{gas}}[\mathrm{CO_{2(aq)}}]$$

$$\frac{\partial[\mathrm{HCO_3^-}]}{\partial t} = K_{\mathrm{a3}}[\mathrm{CO_{2(aq)}}][\mathrm{H_2O}] - \frac{[\mathrm{HCO_3^-}][\mathrm{H^+}]}{K_{\mathrm{a3}}} - K_{\mathrm{a4}}[\mathrm{HCO_3^-}] + \frac{[\mathrm{CO_3^{2-}}][\mathrm{H^+}]}{K_{\mathrm{a4}}}$$

$$\frac{\partial[\mathrm{CO_3^{2-}}]}{\partial t} = K_{\mathrm{a4}}[\mathrm{HCO_3^-}] - \frac{[\mathrm{CO_3^{2-}}][\mathrm{H^+}]}{K_{\mathrm{a4}}}$$

$$\frac{\partial[\mathrm{CO_{2(g)}}]}{\partial t} = K_{\mathrm{gas}}[\mathrm{CO_{2(aq)}}]$$

The buffering behavior of the MOPS buffer and any aspartic groups in the BCPs is described as follows:

$$\frac{\partial[\mathrm{MOPSH}]}{\partial t} = \frac{[\mathrm{MOPS}][\mathrm{H^+}]}{K_{a5}} - K_{\mathrm{a5}}[\mathrm{MOPSH}]$$

$$\frac{\partial[\mathrm{MOPS}]}{\partial t} = K_{\mathrm{a5}}[\mathrm{MOPSH}] - \frac{[\mathrm{MOPS}][\mathrm{H^+}]}{K_{\mathrm{a5}}}$$

$$\frac{\partial[\mathrm{AspHH}]}{\partial t} = -K_{\mathrm{a6}}[\mathrm{AspHH}] + \frac{[\mathrm{AspH^-}][\mathrm{H^+}]}{K_{\mathrm{a6}}}$$

$$\frac{\partial[\mathrm{AspH^-}]}{\partial t} = +K_{\mathrm{a6}}[\mathrm{AspHH}] - \frac{[\mathrm{AspH^-}][\mathrm{H^+}]}{K_{\mathrm{a6}}} - K_{\mathrm{a7}}[\mathrm{AspH^-}] + \frac{[\mathrm{Asp^{2-}}][\mathrm{H^+}]}{K_{\mathrm{a7}}}$$

$$\frac{\partial[\mathrm{Asp^{2-}}]}{\partial t} = K_{\mathrm{a7}}[\mathrm{AspH^-}] - \frac{[\mathrm{Asp^{2-}}][\mathrm{H^+}]}{K_{\mathrm{a7}}}$$

Where AspHH denotes the doubly protonated aspartic acid group, $AspH^-$ the singly deprotonated one, and Asp^{2-} the doubly dissociated aspartate. The rate constants for these steps were taken from the measured pK_a for each polymer. The starting conditions for the ratio of protonated and deprotonated species is calculated according to the Henderson-Hasselbach equation, using the initial pH of the system.

The above equations can be combined to derive an equation describing the evolution of $[H^+]$, and therefore pH, over time:

$$\begin{aligned}\frac{\partial[\mathrm{H^+}]}{\partial t} = {} & K_{\mathrm{a1}}[\mathrm{TBAH}] - \frac{[\mathrm{TBA^-}][\mathrm{H^+}]}{K_{\mathrm{a1}}} - \frac{[\mathrm{Br_3C^-}][\mathrm{H^+}]}{K_{\mathrm{a2}}} \\ & + K_{\mathrm{a3}}\left[\mathrm{CO_{2(aq)}}\right][\mathrm{H_2O}] - \frac{[\mathrm{HCO_3^-}][\mathrm{H^+}]}{K_{\mathrm{a3}}} \\ & + K_{\mathrm{a4}}[\mathrm{HCO_3^-}] - \frac{[\mathrm{CO_3^{2-}}][\mathrm{H^+}]}{K_{\mathrm{a4}}} \\ & + K_{\mathrm{a5}}[\mathrm{MOPSH}] - \frac{[\mathrm{MOPS}][\mathrm{H^+}]}{K_{\mathrm{a5}}} \\ & + K_{\mathrm{a6}}[\mathrm{AspHH}] - \frac{[\mathrm{AspH^-}][\mathrm{H^+}]}{K_{\mathrm{a6}}} \\ & + K_{\mathrm{a7}}[\mathrm{AspH^-}] - \frac{[\mathrm{Asp^{2-}}][\mathrm{H^+}]}{K_{\mathrm{a7}}}\end{aligned}$$

The complete set of differential equations is solved over the time-course of the experiment to derive the concentration of each species over the course of the TBA fuel cycle. Additional information on the model and the full XML code in the Systems Biology Markup Language (SBML) standard are available in Section 3.5.9.

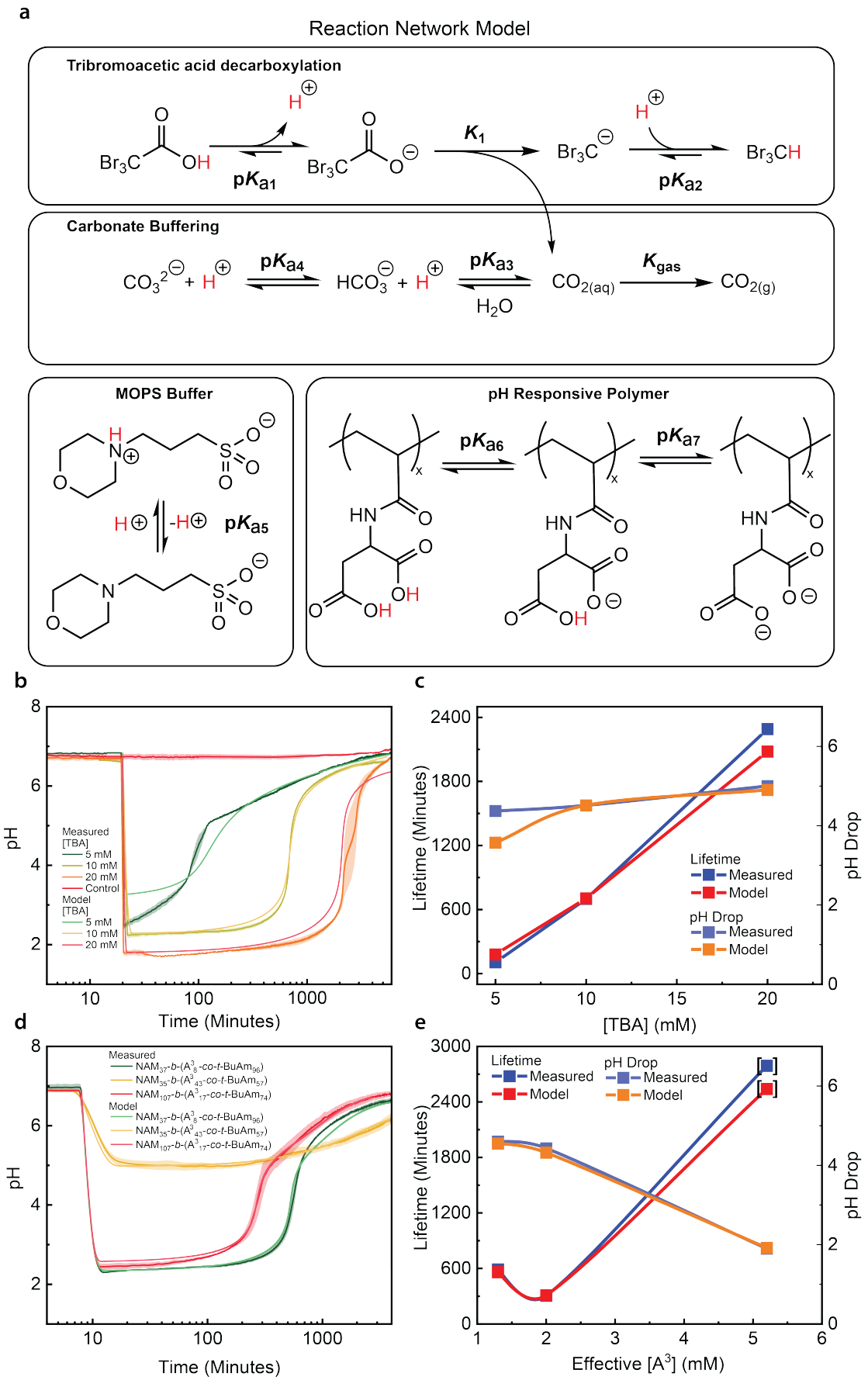
a
Reaction Network Model
Tribromoacetic acid decarboxylation
Br3C
OH
pKa1
Br3C
K1
Br3C
pKa2
Br3CH
Carbonate Buffering
CO3 2
pKa4
HCO3
pKa3
H2O
CO2(aq)
Kgas
CO2(g)
MOPS Buffer
pKa5
pH Responsive Polymer
pKa6
pKa7
b
pH
Measured
[TBA]
5 mM
10 mM
20 mM
Control
Model
[TBA]
5 mM
10 mM
20 mM
Time (Minutes)
c
Lifetime (Minutes)
pH Drop
Lifetime
Measured
Model
pH Drop
Measured
Model
[TBA] (mM)
d
pH
Measured
NAM37-b-(A3 8-co-t-BuAm96)
NAM35-b-(A3 43-co-t-BuAm57)
NAM107-b-(A3 17-co-t-BuAm74)
Model
NAM37-b-(A3 8-co-t-BuAm96)
NAM35-b-(A3 43-co-t-BuAm57)
NAM107-b-(A3 17-co-t-BuAm74)
Time (Minutes)
e
Lifetime (Minutes)
pH Drop
Lifetime
Measured
Model
pH Drop
Measured
Model
Effective [A3] (mM)

Figure 3.4: Modelling the tribromoacetic acid fuel cycle. (a) Scheme of the reactions involved in the TBA fuel cycle, with relevant rate constants and steps involving H^+ highlighted. K_1 is fitted according to the measured data as $K_1 = 2.25 \times 10^{-5}$ s^{-1}. (b) Measured and fitted pH traces for fuel loadings of 5, 10 and 20 mM TBA in 10 mM MOPS, 10 mM NaCl in 30/70 v/v DMSO/H_2O, in the absence of any polymer sample. Shaded contours indicate standard error, **n** = 3 for measured traces. (c) Lifetimes of measured and fitted traces from (b), displaying very close agreement. Lifetime for pH drop taken as time for pH to recover half of pH drop. (d) Measured and modeled pH traces for fueling experiments of select BCPs. Conditions for all experiments are 3 g L^{-1} BCP, 10 mM MOPS, 10 mM NaCl in 30/70 v/v DMSO/H_2O, with a fuel loading of 10 mM TBA. Shaded contours indicate standard error, **n** = 3 for measured traces. (e) Lifetimes of measured and fitted traces from (d). Lifetime for pH drop taken as time for pH to recover half of pH drop, leading the small pH drop observed for high A^3 content BCP display as an artificially large lifetime.

We subsequently apply the model, with the fitted value of K_1, to pH measurements carried out in solutions with 3 g L^{-1} BCP, 10 mM MOPS with 10 mM added NaCl, fueled with 10 mM TBA (Figure 3.4d). The model allows for accurate prediction of the magnitude and duration the pH drop, even with the additional effect of polymer in solution (Figure 3.4e). The magnitude of the pH drop on addition of TBA is influenced by the effective concentration of the A^3 monomer in the solution, as the carboxylate groups, which are deprotonated at the starting pH, act as a buffer to absorb the protons released by TBA. This leads to a decreased drop in pH as effective A^3 concentration increases. The lifetime of the pH drop also decreases with increasing A^3 concentration, as can be seen with NAM_{37}-*b*-(A^3_8-*co*-*t*-$BuAm_{96}$) and NAM_{107}-*b*-(A^3_{17}-*co*-*t*-$BuAm_{74}$), with respective lifetimes of 590 and 305 minutes (Figure 3.4d-e). However, NAM_{37}-*b*-(A^3_{43}-*co*-*t*-$BuAm_{57}$), with an effective A^3 concentration of 6.2 mM (equivalent to 12.4 mM carboxyl groups) contains enough carboxylate groups to effectively buffer the added fuel. The pH drop is greatly hindered and remains in the buffering range of the A^3 units in the BCP, and the pH range at which dissolved CO_2 readily converts to hydrogencarbonate, further increasing the buffering capacity of the system. This leads to a modified pH curve (Figure 3.4d, yellow trace) where the pH returns only very slowly to its original value, and an artificially long lifetime (Figure 3.4e) as a result. By taking into account the behavior of CO_2 in the system, the kinetic model is capable of accurately predicting this change in behavior.

3.4. Conclusion

In this study, we have employed tribromoacetic acid as a fuel to drive the pH-responsive self-assembly of a family of block copolymers. By altering the ratio of monomers in the responsive block, we were able to exhibit differing threshold pH values for assembly and disassembly, and show control over the kinetic trapping of the assembled state, driven by increased hydrophobicity of the responsive chain segment. These results are confirmed by turbidimetric measurements of fueled BCP solutions. We developed a kinetic model to accurately describe and predict the evolution of pH over time, accounting for the additional effect of the BCPs on the system. Such results will hopefully aid in understanding the numerous processes at play in pH-mediated fueled self-assembly, and provide a guide in broadening the applications of activated carboxylic acids to other polymeric systems.

3.5. Supplementary Information

3.5.1. Materials and Methods

Instrumentation

pH measurements in solution-phase experiments were carried out with 12-channel pH station (EA Instruments). Titrations were carried out on a Metrohm 907 Titrando auto-titrator equipped with a glass electrode for potentiometric pH determination, a conductivity module and an Optrode Turbidimeter. pH measurements for calibrations were carried out with a Mettler Toledo SevenCompact pH meter**.**

NMR spectra were measured on a Bruker 400 MHz spectrometer. Gel permeation chromatography (GPC) was performed using an Agilent 1260 Infinity II system equipped with a 1260 series isocratic pump and refractive index detector. A MZ-gel SD Plus e5/e3/100 column assembly (MZ-Analysentechnik GmbH) was employed as stationary phase. Measurements were conducted in THF with a flowrate of 1 mL min^{-1}. Narrowly distributed poly(methylmethacrylate) standards were used for calibration (Polymer Standards Service).

Matrix-assisted laser-desorption-ionization time of flight mass spectrometry (MALDI-ToF MS) measurements were performed using matrix consisting of 2,5-dihydroxybenzoic acid with potassium trifluoroacetate as cationization agent. The measurements were conducted on an Autoflex maX MALDI-TOF-MS from Bruker.

Fueled turbidity measurements were carried out on a Byonoy Absorbance 96 plate reader.

Materials

Azobisisobutyronitrile (AIBN) (98%) was purchased from Acros Organics. Acryloyl chloride (97%) and aspartic acid (99%) were purchased from Alfa Aesar. THF, toluene, (trimethylsilyl)diazomethane (2.0 M in hexanes), DMSO (≥99%), and NaOH (99%) were purchased from Fischer Scientific. were purchased from Fischer Scientific. N-acryloylmorpholine (NAM) (>98%), *tert*-butyl acrylamide (*t*-BuAm) (99%) and morpholinopropane sulfonic acid (MOPS) (99%) were purchased from TCI Europe. Cyano-2-propyldodecyltrithiocarbonate (CPDT) and Tribromoacetic acid were purchased from Sigma Aldrich. All chemicals were used as received, except for AIBN and *t*-BuAm, which were recrystallized before use, and NAM, which was passed through a basic alumina plug to remove inhibitors.

3.5.2. Synthesis Procedures

Synthesis of aspartic acid N-acrylamide (A^3)

In a typical procedure, aspartic acid (30 g, 225 mmol) and NaOH (31.5 g, 788 mmol) were dissolved in water (300 mL). The mixture was stirred vigorously and cooled to 0 °C, at which point acryloyl chloride (20 mL, 247 mmol) was added dropwise over the course of 30 minutes. The reaction was stirred at 0 °C for 3 hours, and then at room temperature for a further 4 hours. The aqueous mixture was extracted with EtOAc (3 × 500 mL). The aqueous phase was then adjusted to pH = 2 with conc. HCl and extracted with further EtOAc (9 × 500 mL). The combined organic layers were dried over MgSO4, and their volume reduced in vacuo. A minimum amount of solvent was left to stand overnight for the product to crystallize from. The product was separated by filtration

and washed once with minimum ice-cold EtOAc. The product was recovered as an off-white to faint pink solid (27.2 g, 145 mmol, 64% yield).

^{1}H NMR (400 MHz, D_2O, 25 °C, TMS): δ = 6.14 – 5.96 ppm (m, 2H; CH_2), 5.57 ppm (dd, ^3J = 9.7, 1.8 Hz, 1H; CH), 4.62 ppm (t, ^3J = 5.9 Hz, 1H, CH), 2.75 ppm (d, ^3J = 6.1 Hz, 2H; CH_2)

Generalized RAFT Polymerization Procedure

NAM (847 mg, 755 µL, 6 mmol), CPDT (41.4 or 20.74 mg, depending on desired NAM block length, 1.2 and 0.6 mmol respectively), 1,3,5-trioxane (100 mg) and AIBN (1.00 or 0.50 mg respectively, always in a 1:0.05 ratio with CPDT) are dissolved in 2.10 mL of 20/80 v/v DMSO / dioxane. The mixture is thoroughly degassed by carrying out 4 freeze-pump-thaw cycles with dry N_2. The reaction flask is then immersed in an 80°C oil bath for 60 – 180 minutes, until NAM conversion has reached >90% by NMR.

In a separate flask, A^3 and *t*-BuAm (in a variable molar ratio from 0/100 to 50/50) are dissolved in 20/80 v/v DMSO / dioxane by gentle heating in a hot water bath, and the mixture thoroughly degassed by carrying out 4 freeze-pump-thaw cycles. This mixture is then added to the NAM RAFT polymerization to carry out *in situ* block extension. Once conversion of the added A^3 and *t*-BuAm plateaus around 80-90%, the reaction flask is taken off the heat and the polymer precipitated in diethyl ether. A 5 mg sample of the recovered crude polymer is methylated, for GPC analysis. The remaining polymer is dissolved in 100 mM NaOH and dialyzed against MilliQ water in 6-8 or 12-14 kDa MWCO tubing (depending on target length of the polymer) for 2 days. The purified copolymers were obtained as yellow powders after freeze drying.

3.5.3. Titrations

Polymers were dissolved to a concentration of 3 mg mL^{-1} in deionized water. Titrations were carried out from high to low pH to ensure the complete dissolution of the polymers. Polymer solutions were adjusted to pH 11 with 1M NaOH, and titrated to pH 2 with 1M HCl with a maximum flowrate of 0.05 mL min^{-1}. Potentiometric pH measurements and conductimetric measurements were carried out in parallel, and the apparent pK_a of the polymers determined conductimetrically. Transmission measurements at λ = 600 nm were taken simultaneously to determine the assembly pH of the polymers. A second set of low pH to high pH titrations, under the same conditions, were carried out to determine the disassembly pH of the polymers.

3.5.4. Fueling Experiments (Turbidity)

Polymer solutions (3 mg mL^{-1} in 10 mM MOPS buffer, pH 7.0 with 10 mM NaCl in 30% v/v DMSO / H_2O) were added to a 96-well plate and a baseline measured for 5 minutes. Tribromoacetic acid (250 mM, in the same buffer) was added to give the desired concentration. The plate was sealed with an airtight film to prevent evaporation, and the samples mixed by orbital shaking. Samples were measured in transmission mode at 440 nm. All samples were measured as triplicates, with duplicate unfueled controls and TBA stock controls.

3.5.5. Fueling Experiments (pH)

Polymer stock solutions (5 mg mL^{-1} in 10 mM MOPS buffer, pH 7.0 with 10 mM added NaCl in 30% DMSO) were added to individual vials and diluted with the same buffer to a polymer concentration of 3.125 mg mL^{-1}. pH was measured for 10 minutes to obtain a baseline pH.

Tribromoacetic acid (250 mM, in the same buffer) was added, such that a final polymer concentration of 3 mg mL^{-1} and TBA concentration of 10 mM was obtained. The pH of the samples was then measured under constant vigorous stirring.

3.5.6. Statistical Analysis

Data was gathered using the methods outlined above. All data points featuring statistical analysis are presented as mean ± standard error. The sample size for each statistical analysis is reported in the relevant figure legend. Statistical analysis was carried out using Microsoft Excel and Origin Pro 2020.

3.5.7. Supplementary Note: Additional Turbidity Fueling Experiments

The fueling behavior of BCPs was explored by addition of TBA at final concentrations of 10 mM (Figure 3.3) and 5 and 20 mM (Figure 3.5). At a loading of 5 mM TBA (Figure 3.5a), NAM_{37}-*b*-(A^3_8-*co*-*t*-$BuAm_{96}$) and NAM_{38}-*b*-(A^3_{19}-*co*-*t*-$BuAm_{81}$) show assembly lifetimes of 487 and 208 minutes respectively, while the remaining polymers with a larger A^3 content show no appreciable increase in turbidity, due to the increased buffering capacity afforded by an increased concentration of carboxyl groups in the polymer. On fueling with 20 mM of TBA (Figure 3.5b), the same BCPs all show an assembly response. NAM_{37}-*b*-(A^3_8-*co*-*t*-$BuAm_{96}$) and NAM_{38}-*b*-(A^3_{19}-*co*-*t*-$BuAm_{81}$) show assembly lifetimes of 4480 and 2790 minutes respectively, followed by NAM_{39}-*b*-(A^3_{27}-*co*-*t*-$BuAm_{76}$) with 1640 minutes. NAM_{37}-*b*-(A^3_{36}-*co*-*t*-$BuAm_{66}$) and NAM_{35}-*b*-(A^3_{43}-*co*-*t*-$BuAm_{57}$) show shorter assembly lifetimes of 215 and 160 minutes respectively. This can again be attributed to the increased concentration of carboxylates in the BCPs.

Similar behavior is observed in solutions of the BCPs with larger poly(NAM) content (Figure 3.5c,d). Fueling with 5 mM TBA, BCPs NAM_{39}-*b*-(NAM_{57}-*co*-A^3_9-*co*-*t*-$BuAm_{80}$), NAM_{107}-*b*-(A^3_{17}-*co*-*t*-$BuAm_{74}$) and NAM_{111}-*b*-(A^3_{28}-*co*-*t*-$BuAm_{77}$) display assembly lifetimes of 740, 375 and 120 minutes respectively (Figure 3.5c). In line with expectations, fueling with 20 mM TBA leads to assembly durations of 3330, 3160 and 2835 minutes (Figure 3.5d).

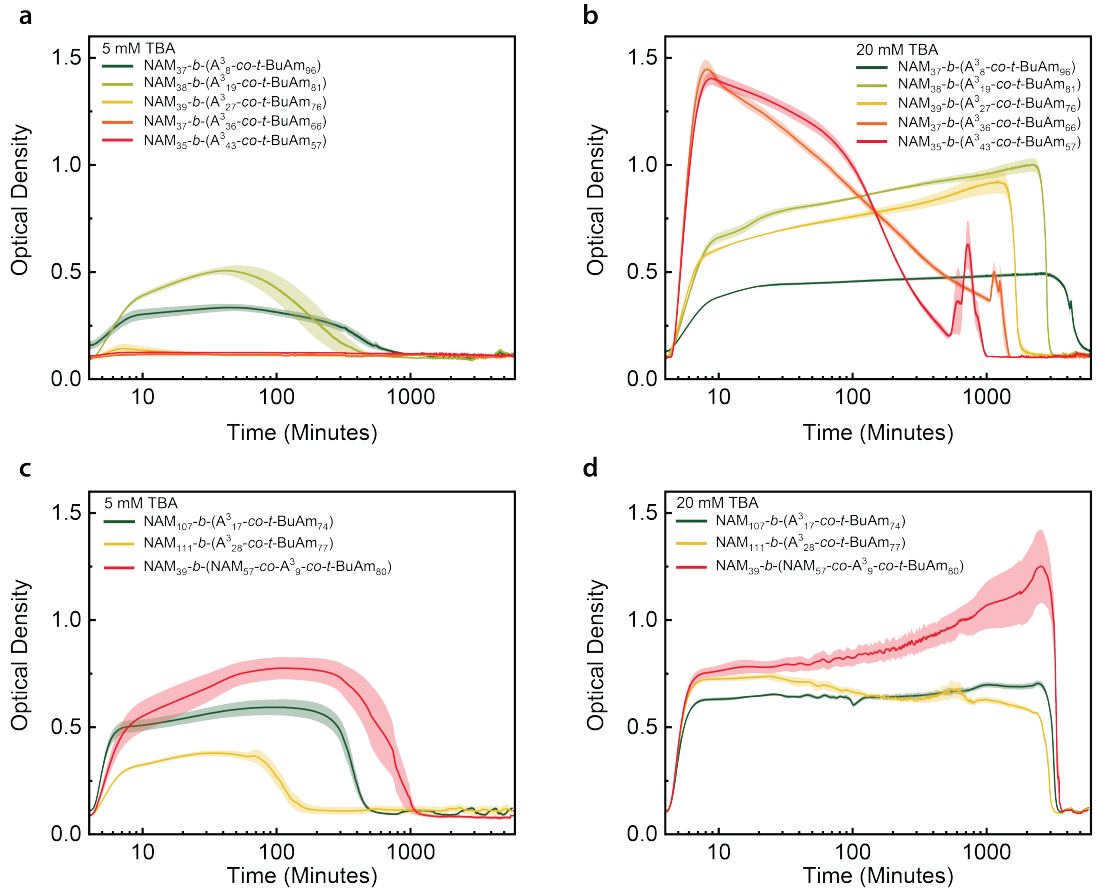

Figure 3.5: Fueled self-assembly of copolymers followed by turbidity measurements. Effect of copolymer composition on optical density and lifetime of the fueled state for short poly(NAM) segment BCPs fueled with (a) 5 mM TBA and (b) 20 mM TBA. Effect of copolymer composition on optical density and lifetime of the fueled state for long poly(NAM) segment BCPs fueled with (c) 5 mM TBA and (d) 20 mM TBA. Conditions for all measurements are 3 mg mL^{-1} BCP in 10 mM MOPS buffer, 10 mM NaCl, in 30/70 v/v DMSO/H_2O. Error contours show the standard error for measurements, with n = 3.

3.5.8. Supplementary Note: Measuring pH over the Course of Fueling

The pH of BCP solutions fueled with 10 mM TBA was followed over the course of 72 hours (Figure 3.6) to determine the effect of BCP composition on the progression of the TBA reaction cycle. As expected, the pH drop is directly correlated to the effective A^3 composition in the BCP solution, and the solution pH is buffered by these additional carboxylate groups. Lifetime of the pH drop, defined as the time for pH to recover half of the initial pH drop, is equally linked to the effective A^3 concentration in the solution. A trend of decreasing lifetime is observed as A^3 concentration rises, as the additional carboxyl groups remove protons provided by TBA from solution. As A^3 concentration goes over 4 mM (Figure 3.6c), the additional buffering capacity is such that the pH drop is far smaller, and remains within the buffering range of the polymer. Additionally, at these pH values of 4.5-6, CO_2 generated by the TBA is readily converted into HCO_3^-, such that the effective rate of off-gassing is reduced, and a greater effect of carbonate buffering is observed. This leads to the higher lifetimes observed, both because of the smaller pH drop, and the slower return to initial pH caused by additional buffering.

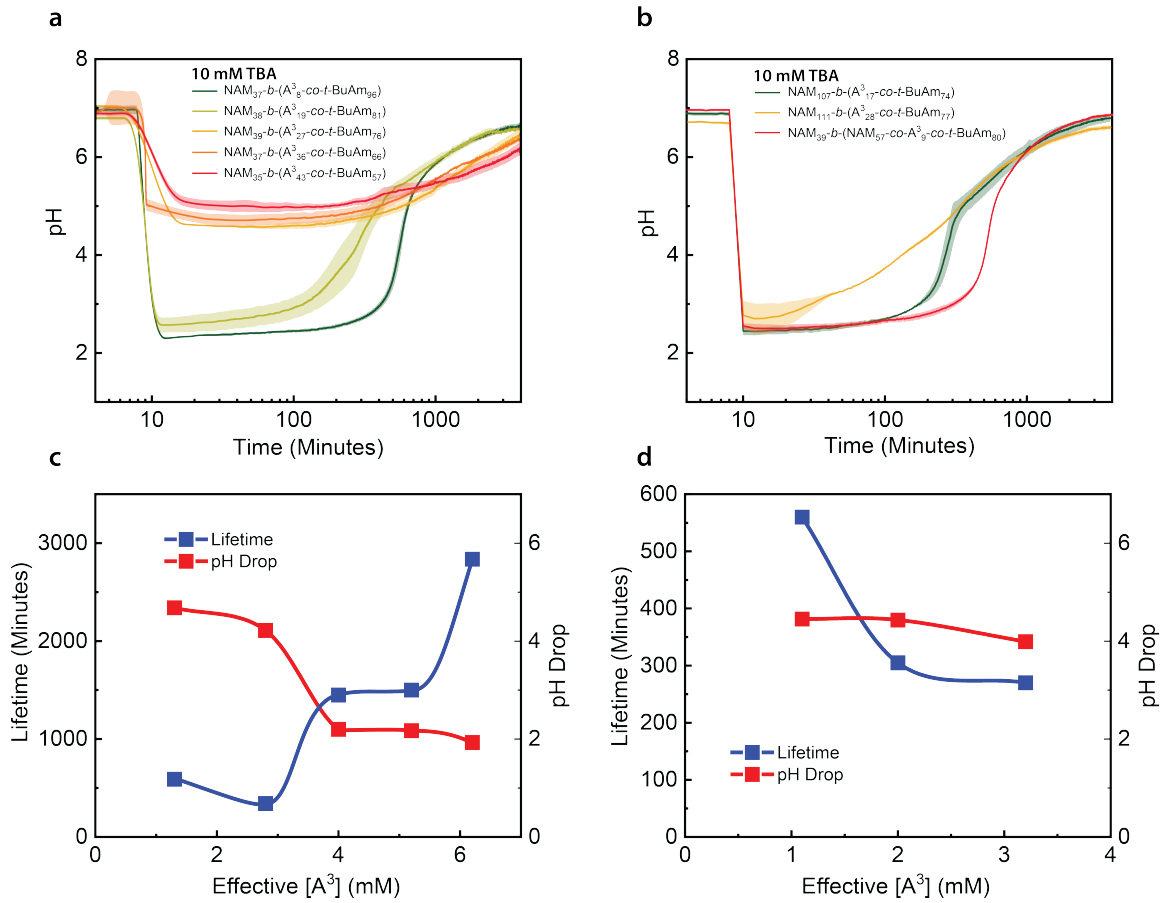

Figure 3.6: Evolution of pH in BCP solutions. (a)-(b) pH traces of BCP solutions on addition of 10 mM TBA. The effect of increased A^3 concentration on pH drop and lifetime can be seen. (c)-(d) Lifetime (blue lines) and pH drop (red lines) as a function of effective A^3 concentration in the BCP solutions. Artificially long lifetimes are observed for high A^3 concentrations due to the increased buffering. Lines serve to guide the eye. Conditions for all measurements are 3 g L^{-1} BCP in 10 mM MOPS buffer with 10 mM added NaCl, fueled with 10 mM TBA. Shaded contours indicate standard error, n =3.

3.5.9. Supplementary Note: Modelling the TBA Fuel Cycle

We designed a simple kinetic model of the TBA fuel cycle, comprising the reactions outlined in Figure 3.4a. We implemented this model in the COPASI software package,[35] which is a stand-alone program that supports models in the Systems Biology Markup Language (SBML) standard. Reactions in the model were implemented as sets of ordinary differential equations, which were solved using the LSODA solver. The decarboxylation rate constant, K_1, was determined by fitting the measured pH of fueling experiments with 5, 10 and 20 mM, with 10 mM MOPS buffer in the absence of polymer to the model using the Levenberg-Marquardt non-linear least squares method.

The transcribed XML code for the kinetic model in the SBML standard is included below.

<?xml version="1.0" encoding="UTF-8"?>
<!-- Created by GIORGIO FUSI // COPASI version 4.43 (Build 288) // on 2024-04-20 15:54 with libSBML version 5.20.0. -->
<!-- First Designed and implemented in the COPASI software Package by Giorgio Fusi for "Tribromoacetic Acid as a Chemical Fuel for Self-Assembly of pH-responsive Block Copolymers" by G. Fusi and A. Walther. Comments by G. Fusi -->
<!-- If you use this model for your scientific work, please give proper credit to the source -->

<sbml xmlns="http://www.sbml.org/sbml/level3/version1/core" xmlns:layout="http://www.sbml.org/sbml/level3/version1/layout/version1" xmlns:render="http://www.sbml.org/sbml/level3/version1/render/version1" level="3" version="1" layout:required="false" render:required="false">
 <model metaid="COPASI0" id="TBA_fuelling_of_Copolymers" name="TBA fuelling of Copolymers" substanceUnits="substance" timeUnits="time" volumeUnits="volume" areaUnits="area" lengthUnits="length" extentUnits="substance">
  <annotation>
   <copasi:COPASI xmlns:copasi="http://www.copasi.org/static/sbml">
    <rdf:RDF xmlns:dcterms="http://purl.org/dc/terms/" xmlns:rdf="http://www.w3.org/1999/02/22-rdf-syntax-ns#" xmlns:vCard="http://www.w3.org/2001/vcard-rdf/3.0#">
     <rdf:Description rdf:about="#COPASI0">
      <dcterms:created>
       <rdf:Description>
        <dcterms:W3CDTF>2024-04-13T16:27:18Z</dcterms:W3CDTF>
       </rdf:Description>
      </dcterms:created>
      <dcterms:creator>
       <rdf:Description>
        <vCard:N>
         <rdf:Description>
          <vCard:Family>Fusi</vCard:Family>
          <vCard:Given>Giorgio</vCard:Given>
         </rdf:Description>
        </vCard:N>
       </rdf:Description>
      </dcterms:creator>
     </rdf:Description>
    </rdf:RDF>
   </copasi:COPASI>
   <rdf:RDF xmlns:rdf="http://www.w3.org/1999/02/22-rdf-syntax-ns#" xmlns:dcterms="http://purl.org/dc/terms/" xmlns:vCard="http://www.w3.org/2001/vcard-rdf/3.0#" xmlns:vCard4="http://www.w3.org/2006/vcard/ns#" xmlns:bqbiol="http://biomodels.net/biology-qualifiers/" xmlns:bqmodel="http://biomodels.net/model-qualifiers/">
    <rdf:Description rdf:about="#COPASI0">
     <dcterms:creator>
      <rdf:Bag>
       <rdf:li rdf:parseType="Resource">
        <vCard:N rdf:parseType="Resource">
         <vCard:Family>Fusi</vCard:Family>
         <vCard:Given>Giorgio</vCard:Given>
        </vCard:N>
       </rdf:li>
      </rdf:Bag>
     </dcterms:creator>
     <dcterms:created rdf:parseType="Resource">
      <dcterms:W3CDTF>2024-04-13T16:27:18Z</dcterms:W3CDTF>
     </dcterms:created>
     <dcterms:modified rdf:parseType="Resource">
      <dcterms:W3CDTF>2024-04-13T16:27:18Z</dcterms:W3CDTF>

```
      </dcterms:modified>
    </rdf:Description>
  </rdf:RDF>
 </annotation>
 <listOfFunctionDefinitions>
  <functionDefinition metaid="COPASI71" id="Constant_flux__reversible" name="Constant flux (reversible)">
   <math xmlns="http://www.w3.org/1998/Math/MathML">
    <lambda>
     <bvar>
      <ci> v </ci>
     </bvar>
     <ci> v </ci>
    </lambda>
   </math>
  </functionDefinition>
 </listOfFunctionDefinitions>
 <listOfUnitDefinitions>
  <unitDefinition id="length" name="length">
   <listOfUnits>
    <unit kind="metre" exponent="1" scale="0" multiplier="1"/>
   </listOfUnits>
  </unitDefinition>
  <unitDefinition id="area" name="area">
   <listOfUnits>
    <unit kind="metre" exponent="2" scale="0" multiplier="1"/>
   </listOfUnits>
  </unitDefinition>
  <unitDefinition id="volume" name="volume">
   <listOfUnits>
    <unit kind="litre" exponent="1" scale="0" multiplier="1"/>
   </listOfUnits>
  </unitDefinition>
  <unitDefinition id="time" name="time">
   <listOfUnits>
    <unit kind="second" exponent="1" scale="0" multiplier="1"/>
   </listOfUnits>
  </unitDefinition>
  <unitDefinition id="substance" name="substance">
   <listOfUnits>
    <unit kind="mole" exponent="1" scale="0" multiplier="1"/>
   </listOfUnits>
  </unitDefinition>
 </listOfUnitDefinitions>
 <listOfCompartments>
  <compartment metaid="COPASI1" id="Vial" name="Vial" spatialDimensions="3" size="1" units="volume"
constant="true">
   <notes>
    <body xmlns="http://www.w3.org/1999/xhtml">
     <pre>This is the compartment the reaction(s) run in.
Given this system occurs in homogenous solution, only one compartment is necessary. As concentrations for
species are defined below, the size is also arbitrary.
Units should be kept to litres, as changing to mL will additionally change all the concentration units.</pre>
    </body>
   </notes>
  </compartment>
 </listOfCompartments>
 <listOfSpecies>
```

<species metaid="COPASI2" id="MOPS" name="MOPS" compartment="Vial" initialConcentration="0.00386863179666335" substanceUnits="substance" hasOnlySubstanceUnits="false" boundaryCondition="false" constant="false">
<notes>
<body xmlns="http://www.w3.org/1999/xhtml">
<pre>Species:
Deprotonated MOPS buffer molecule.
Initial concentration is a function of [buffer], pKa and starting pH according to Henderson-Hasselbach equation</pre>
</body>
</notes>
</species>
<species metaid="COPASI3" id="TBA" name="TBA-" compartment="Vial" initialConcentration="0" substanceUnits="substance" hasOnlySubstanceUnits="false" boundaryCondition="false" constant="false">
<notes>
<body xmlns="http://www.w3.org/1999/xhtml">
<pre>Tribromoacetate anion. This is the species that decarboxylates.</pre>
</body>
</notes>
</species>
<species metaid="COPASI4" id="Br3C" name="Br3C-" compartment="Vial" initialConcentration="0" substanceUnits="substance" hasOnlySubstanceUnits="false" boundaryCondition="false" constant="false">
<notes>
<body xmlns="http://www.w3.org/1999/xhtml">
<pre>Species:
Tribromomethyl carbanion generated from decarboxylation</pre>
</body>
</notes>
</species>
<species metaid="COPASI5" id="Br3CH" name="Br3CH" compartment="Vial" initialConcentration="0" substanceUnits="substance" hasOnlySubstanceUnits="false" boundaryCondition="false" constant="false">
<notes>
<body xmlns="http://www.w3.org/1999/xhtml">
<pre>Species:
Bromoform, waste product of TBA cycle</pre>
</body>
</notes>
</species>
<species metaid="COPASI6" id="H2O" name="H2O" compartment="Vial" initialConcentration="55.5999999999997" substanceUnits="substance" hasOnlySubstanceUnits="false" boundaryCondition="true" constant="true">
<notes>
<body xmlns="http://www.w3.org/1999/xhtml">
<pre>Species:
Water. The system is modelled as being in pure water to simplify assumptions on water concentration (Kept constant as 55.6 M). This does not impact modelling.</pre>
</body>
</notes>
</species>
<species metaid="COPASI7" id="MOPSH" name="MOPSH" compartment="Vial" initialConcentration="0.00613136820333665" substanceUnits="substance" hasOnlySubstanceUnits="false" boundaryCondition="false" constant="false">
<notes>
<body xmlns="http://www.w3.org/1999/xhtml">
<pre>Species:
Protonated buffer molecule
Intial concentration is a function of [buffer], pKa and starting pH according to Henderson-Hasselbach equation</pre>

```
      </body>
     </notes>
    </species>
    <species metaid="COPASI8" id="H" name="H+" compartment="Vial" initialConcentration="1e-07"
substanceUnits="substance" hasOnlySubstanceUnits="false" boundaryCondition="false" constant="false">
     <notes>
      <body xmlns="http://www.w3.org/1999/xhtml">
       <pre>Species:
Proton concentration in solution.</pre>
      </body>
     </notes>
    </species>
    <species metaid="COPASI9" id="TBA_0" name="TBA" compartment="Vial" initialConcentration="0.02"
substanceUnits="substance" hasOnlySubstanceUnits="false" boundaryCondition="false" constant="false">
     <notes>
      <body xmlns="http://www.w3.org/1999/xhtml">
       <pre>Tribromoacetic acid as an undissociated molecule. This is the chemical fuel.</pre>
      </body>
     </notes>
    </species>
    <species metaid="COPASI10" id="AspH" name="AspH" compartment="Vial" initialConcentration="0"
substanceUnits="substance" hasOnlySubstanceUnits="false" boundaryCondition="false" constant="false">
     <notes>
      <body xmlns="http://www.w3.org/1999/xhtml">
       <pre>Species:
Sinlgy deprotonated aspartic acid group appended to a polymer.</pre>
      </body>
     </notes>
    </species>
    <species metaid="COPASI11" id="AspHH" name="AspHH" compartment="Vial" initialConcentration="0"
substanceUnits="substance" hasOnlySubstanceUnits="false" boundaryCondition="false" constant="false">
     <notes>
      <body xmlns="http://www.w3.org/1999/xhtml">
       <pre>Species:
Aspartic acid group appended to a polymer. Fully protonated.</pre>
      </body>
     </notes>
    </species>
    <species metaid="COPASI12" id="CO3" name="CO3" compartment="Vial" initialConcentration="0"
substanceUnits="substance" hasOnlySubstanceUnits="false" boundaryCondition="false" constant="false">
     <notes>
      <body xmlns="http://www.w3.org/1999/xhtml">
       <pre>Species:
Carbonate anion in solution</pre>
      </body>
     </notes>
    </species>
    <species metaid="COPASI13" id="HCO3" name="HCO3" compartment="Vial" initialConcentration="0"
substanceUnits="substance" hasOnlySubstanceUnits="false" boundaryCondition="false" constant="false">
     <notes>
      <body xmlns="http://www.w3.org/1999/xhtml">
       <pre>Species:
Hydrogencarbonate anion</pre>
      </body>
     </notes>
    </species>
    <species metaid="COPASI14" id="CO2" name="CO2" compartment="Vial" initialConcentration="1.7e-05"
substanceUnits="substance" hasOnlySubstanceUnits="false" boundaryCondition="false" constant="false">
```

```
      <notes>
        <body xmlns="http://www.w3.org/1999/xhtml">
          <pre>Species:
CO2 in solution as dissolved gas</pre>
        </body>
      </notes>
    </species>
    <species metaid="COPASI15" id="CO2g" name="CO2g" compartment="Vial" initialConcentration="0"
substanceUnits="substance" hasOnlySubstanceUnits="false" boundaryCondition="false" constant="false">
      <notes>
        <body xmlns="http://www.w3.org/1999/xhtml">
          <pre>Species:
CO2 that has offgassed from solution. It is kept in the same compartment to simplify the model, once CO2 becomes
CO2g, it is functionally ignored by the model.</pre>
        </body>
      </notes>
    </species>
    <species metaid="COPASI16" id="OH" name="OH-" compartment="Vial" initialConcentration="1e-07"
substanceUnits="substance" hasOnlySubstanceUnits="false" boundaryCondition="false" constant="false">
      <notes>
        <body xmlns="http://www.w3.org/1999/xhtml">
          <pre>Hydroxide ion. Concentration is defined according to Kw</pre>
        </body>
      </notes>
    </species>
    <species metaid="COPASI17" id="Asp" name="Asp" compartment="Vial" initialConcentration="0"
substanceUnits="substance" hasOnlySubstanceUnits="false" boundaryCondition="false" constant="false">
      <notes>
        <body xmlns="http://www.w3.org/1999/xhtml">
          <pre>Species:
Doubly deprotonated aspartic acid group appended to a polymer.</pre>
        </body>
      </notes>
    </species>
    <species metaid="COPASI18" id="H2CO3" name="H2CO3" compartment="Vial" initialConcentration="0"
substanceUnits="substance" hasOnlySubstanceUnits="false" boundaryCondition="false" constant="false">
      <notes>
        <body xmlns="http://www.w3.org/1999/xhtml">
          <pre>Species:
CO2 in solution in the form of carbonic acid. Leftover from previous implementation of model where there was a
two step hydration and dissociation process. That approach was discarded due to unreliability of lit. data on the
rate constants. One step process led to simpler model and more accurate predictions.</pre>
        </body>
      </notes>
    </species>
    <species metaid="COPASI19" id="diTBA" name="diTBA" compartment="Vial" initialConcentration="0"
substanceUnits="substance" hasOnlySubstanceUnits="false" boundaryCondition="false" constant="false">
      <notes>
        <body xmlns="http://www.w3.org/1999/xhtml">
          <pre>Species:
Hydrogen bonded dimer of TBA. This was included originally as H-Bonding dimerization was thought to maybe
play a large role in decarb kinetics at low pH. This is not the case however.
Kept in in case someone wants to use this model with a weaker acid.</pre>
        </body>
      </notes>
    </species>
    <species metaid="COPASI20" id="Check" name="Check" compartment="Vial" initialConcentration="0"
substanceUnits="substance" hasOnlySubstanceUnits="false" boundaryCondition="true" constant="false">
```

```
      <notes>
       <body xmlns="http://www.w3.org/1999/xhtml">
        <pre>This is a check function to check that the defining of the intial concentration of the three Asp species is occuring without error.</pre>
       </body>
      </notes>
     </species>
     <species metaid="COPASI21" id="Check_T" name="Check(T)" compartment="Vial" initialConcentration="0" substanceUnits="substance" hasOnlySubstanceUnits="false" boundaryCondition="true" constant="false">
      <notes>
       <body xmlns="http://www.w3.org/1999/xhtml">
        <pre>This is a check function to check that the concentrations of the three Asp species are correct over time.</pre>
       </body>
      </notes>
     </species>
    </listOfSpecies>
    <listOfParameters>
     <parameter metaid="COPASI22" id="K1" name="K1" value="6.30957344e-08" constant="true"/>
     <parameter metaid="COPASI23" id="K1f" name="K1f" value="10000000" constant="true"/>
     <parameter metaid="COPASI24" id="K1b" name="K1b" value="158489319366730" constant="false"/>
     <parameter metaid="COPASI25" id="K2" name="K2" value="0.1" constant="true"/>
     <parameter metaid="COPASI26" id="K2f" name="K2f" value="10000" constant="true"/>
     <parameter metaid="COPASI27" id="K2b" name="K2b" value="100000" constant="false"/>
     <parameter metaid="COPASI28" id="K3" name="K3" value="1.99e-06" constant="true">
      <notes>
       <body xmlns="http://www.w3.org/1999/xhtml">
        <pre>pKa of first deprotonation of aspartic acid</pre>
       </body>
      </notes>
     </parameter>
     <parameter metaid="COPASI29" id="K3f" name="K3f" value="10000" constant="true"/>
     <parameter metaid="COPASI30" id="K3b" name="K3b" value="5025125628.1407" constant="false"/>
     <parameter metaid="COPASI31" id="K4" name="K4" value="6.76082975391982e-14" constant="true"/>
     <parameter metaid="COPASI32" id="K4f" name="K4f" value="10000" constant="true"/>
     <parameter metaid="COPASI33" id="K4b" name="K4b" value="1.47910838816821e+17" constant="false"/>
     <parameter metaid="COPASI34" id="K5" name="K5" value="4.67e-11" constant="true"/>
     <parameter metaid="COPASI35" id="K5f" name="K5f" value="10000" constant="true"/>
     <parameter metaid="COPASI36" id="K5b" name="K5b" value="214132762312634" constant="false"/>
     <parameter metaid="COPASI37" id="K6" name="K6" value="4.46e-07" constant="true"/>
     <parameter metaid="COPASI38" id="K6f" name="K6f" value="10000" constant="true"/>
     <parameter metaid="COPASI39" id="K6b" name="K6b" value="22421524663.6771" constant="false"/>
     <parameter metaid="COPASI40" id="K7" name="K7" value="2e-05" constant="true"/>
     <parameter metaid="COPASI41" id="K8" name="K8" value="300000000000" constant="true"/>
     <parameter metaid="COPASI42" id="K8f" name="K8f" value="0" constant="true"/>
     <parameter metaid="COPASI43" id="K8b" name="K8b" value="0" constant="false"/>
     <parameter metaid="COPASI44" id="pH" name="pH" value="7" constant="false">
      <notes>
       <body xmlns="http://www.w3.org/1999/xhtml">
        <pre>Calculating pH from [H+]</pre>
       </body>
      </notes>
     </parameter>
     <parameter metaid="COPASI45" id="KWf" name="Kdf" value="0" constant="true"/>
     <parameter metaid="COPASI46" id="KWb" name="Kdb" value="0" constant="false"/>
     <parameter metaid="COPASI47" id="Kw" name="Kd" value="1" constant="true">
      <notes>
       <body xmlns="http://www.w3.org/1999/xhtml">
```

```
      <pre>Dimerization constant for TBA</pre>
     </body>
    </notes>
   </parameter>
   <parameter metaid="COPASI48" id="t_Min" name="t(Min)" value="0" constant="false">
    <notes>
     <body xmlns="http://www.w3.org/1999/xhtml">
      <pre>Converting time in seconds to time in minutes for simpler plotting outputs.</pre>
     </body>
    </notes>
   </parameter>
   <parameter metaid="COPASI49" id="K9" name="K9" value="1.99e-06" constant="true">
    <notes>
     <body xmlns="http://www.w3.org/1999/xhtml">
      <pre>pKa of second deprotonation of aspartic acid</pre>
     </body>
    </notes>
   </parameter>
   <parameter metaid="COPASI50" id="K9f" name="K9f" value="10000" constant="true"/>
   <parameter metaid="COPASI51" id="K9b" name="K9b" value="5025125628.1407" constant="false"/>
   <parameter metaid="COPASI52" id="Start_pH" name="Start pH" value="7" constant="true">
    <notes>
     <body xmlns="http://www.w3.org/1999/xhtml">
      <pre>Input value. The inital measured pH</pre>
     </body>
    </notes>
   </parameter>
   <parameter metaid="COPASI53" id="_Buffer" name="[Buffer]" value="0.01" constant="true">
    <notes>
     <body xmlns="http://www.w3.org/1999/xhtml">
      <pre>Overall MOPS buffer concentration.

Used to determine the starting concentrations of MOPSH and MOPS based on starting pH, buffer pKa and the Henderson-Hasselbach equation.</pre>
     </body>
    </notes>
   </parameter>
   <parameter metaid="COPASI54" id="HA_A" name="HA/A" value="1.5848931936673" constant="false">
    <notes>
     <body xmlns="http://www.w3.org/1999/xhtml">
      <pre>Used to determine the starting concentrations of MOPSH and MOPS based on starting pH, buffer pKa and the Henderson-Hasselbach equation.</pre>
     </body>
    </notes>
   </parameter>
   <parameter metaid="COPASI55" id="Kw_Check" name="Kw Check" value="1e-14" constant="false">
    <notes>
     <body xmlns="http://www.w3.org/1999/xhtml">
      <pre>Recalculating Kw from [H+] and [OH-]

Value used to check that something isn&amp;apos;t going wrong with aqueous acid-base chemistry. Should remain constant at the value of Kw</pre>
     </body>
    </notes>
   </parameter>
   <parameter metaid="COPASI56" id="_A3" name="[A3]" value="0" constant="true">
    <notes>
     <body xmlns="http://www.w3.org/1999/xhtml">
```

<pre>The overall concentration of A3 units in solution.

Used to determine the starting concentrations of AspHH, AspH and Asp based on starting pH, polymer pKa and the Henderson-Hasselbach equation.</pre>
</body>
</notes>
</parameter>
<parameter metaid="COPASI57" id="AspHH_AspH" name="AspHH/AspH" value="0.050251256281407" constant="false">
<notes>
<body xmlns="http://www.w3.org/1999/xhtml">
<pre>Used to determine the starting concentrations of AspHH, AspH and Asp based on starting pH, polymer pKa and the Henderson-Hasselbach equation.</pre>
</body>
</notes>
</parameter>
<parameter metaid="COPASI58" id="AspH_initial" name="AspH(initial)" value="0" constant="false">
<notes>
<body xmlns="http://www.w3.org/1999/xhtml">
<pre>Used to determine the starting concentrations of AspHH, AspH and Asp based on starting pH, polymer pKa and the Henderson-Hasselbach equation.</pre>
</body>
</notes>
</parameter>
<parameter metaid="COPASI59" id="AspH_Asp" name="AspH/Asp" value="0.050251256281407" constant="false">
<notes>
<body xmlns="http://www.w3.org/1999/xhtml">
<pre>Used to determine the starting concentrations of AspHH, AspH and Asp based on starting pH, polymer pKa and the Henderson-Hasselbach equation.</pre>
</body>
</notes>
</parameter>
<parameter id="Metabolite_9" name="Initial for AspHH" value="0" constant="true">
<annotation>
<initialValue xmlns="http://copasi.org/initialValue" parent="AspHH" type="InitialConcentration"/>
</annotation>
</parameter>
<parameter id="Metabolite_8" name="Initial for AspH" value="0" constant="true">
<annotation>
<initialValue xmlns="http://copasi.org/initialValue" parent="AspH" type="InitialConcentration"/>
</annotation>
</parameter>
<parameter id="Metabolite_15" name="Initial for Asp" value="0" constant="true">
<annotation>
<initialValue xmlns="http://copasi.org/initialValue" parent="Asp" type="InitialConcentration"/>
</annotation>
</parameter>
<parameter id="Metabolite_6" name="Initial for H+" value="1e-07" constant="true">
<annotation>
<initialValue xmlns="http://copasi.org/initialValue" parent="H" type="InitialConcentration"/>
</annotation>
</parameter>
<parameter id="ModelValue_0" name="Initial for K1" value="6.30957344e-08" constant="true">
<annotation>
<initialValue xmlns="http://copasi.org/initialValue" parent="K1" type="InitialValue"/>
</annotation>
</parameter>

```
<parameter id="ModelValue_1" name="Initial for K1f" value="10000000" constant="true">
 <annotation>
  <initialValue xmlns="http://copasi.org/initialValue" parent="K1f" type="InitialValue"/>
 </annotation>
</parameter>
<parameter id="ModelValue_3" name="Initial for K2" value="0.1" constant="true">
 <annotation>
  <initialValue xmlns="http://copasi.org/initialValue" parent="K2" type="InitialValue"/>
 </annotation>
</parameter>
<parameter id="ModelValue_4" name="Initial for K2f" value="10000" constant="true">
 <annotation>
  <initialValue xmlns="http://copasi.org/initialValue" parent="K2f" type="InitialValue"/>
 </annotation>
</parameter>
<parameter id="ModelValue_6" name="Initial for K3" value="1.99e-06" constant="true">
 <annotation>
  <initialValue xmlns="http://copasi.org/initialValue" parent="K3" type="InitialValue"/>
 </annotation>
</parameter>
<parameter id="ModelValue_7" name="Initial for K3f" value="10000" constant="true">
 <annotation>
  <initialValue xmlns="http://copasi.org/initialValue" parent="K3f" type="InitialValue"/>
 </annotation>
</parameter>
<parameter id="ModelValue_9" name="Initial for K4" value="6.76082975391982e-14" constant="true">
 <annotation>
  <initialValue xmlns="http://copasi.org/initialValue" parent="K4" type="InitialValue"/>
 </annotation>
</parameter>
<parameter id="ModelValue_10" name="Initial for K4f" value="10000" constant="true">
 <annotation>
  <initialValue xmlns="http://copasi.org/initialValue" parent="K4f" type="InitialValue"/>
 </annotation>
</parameter>
<parameter id="ModelValue_12" name="Initial for K5" value="4.67e-11" constant="true">
 <annotation>
  <initialValue xmlns="http://copasi.org/initialValue" parent="K5" type="InitialValue"/>
 </annotation>
</parameter>
<parameter id="ModelValue_13" name="Initial for K5f" value="10000" constant="true">
 <annotation>
  <initialValue xmlns="http://copasi.org/initialValue" parent="K5f" type="InitialValue"/>
 </annotation>
</parameter>
<parameter id="ModelValue_15" name="Initial for K6" value="4.46e-07" constant="true">
 <annotation>
  <initialValue xmlns="http://copasi.org/initialValue" parent="K6" type="InitialValue"/>
 </annotation>
</parameter>
<parameter id="ModelValue_16" name="Initial for K6f" value="10000" constant="true">
 <annotation>
  <initialValue xmlns="http://copasi.org/initialValue" parent="K6f" type="InitialValue"/>
 </annotation>
</parameter>
<parameter id="ModelValue_19" name="Initial for K8" value="300000000000" constant="true">
 <annotation>
  <initialValue xmlns="http://copasi.org/initialValue" parent="K8" type="InitialValue"/>
```

```
    </annotation>
   </parameter>
   <parameter id="ModelValue_20" name="Initial for K8f" value="0" constant="true">
    <annotation>
     <initialValue xmlns="http://copasi.org/initialValue" parent="K8f" type="InitialValue"/>
    </annotation>
   </parameter>
   <parameter id="ModelValue_27" name="Initial for K9" value="1.99e-06" constant="true">
    <annotation>
     <initialValue xmlns="http://copasi.org/initialValue" parent="K9" type="InitialValue"/>
    </annotation>
   </parameter>
   <parameter id="ModelValue_28" name="Initial for K9f" value="10000" constant="true">
    <annotation>
     <initialValue xmlns="http://copasi.org/initialValue" parent="K9f" type="InitialValue"/>
    </annotation>
   </parameter>
   <parameter id="ModelValue_25" name="Initial for Kd" value="1" constant="true">
    <annotation>
     <initialValue xmlns="http://copasi.org/initialValue" parent="Kw" type="InitialValue"/>
    </annotation>
   </parameter>
   <parameter id="ModelValue_23" name="Initial for Kdf" value="0" constant="true">
    <annotation>
     <initialValue xmlns="http://copasi.org/initialValue" parent="KWf" type="InitialValue"/>
    </annotation>
   </parameter>
   <parameter id="ModelValue_34" name="Initial for [A3]" value="0" constant="true">
    <annotation>
     <initialValue xmlns="http://copasi.org/initialValue" parent="_A3" type="InitialValue"/>
    </annotation>
   </parameter>
  </listOfParameters>
  <listOfInitialAssignments>
   <initialAssignment symbol="MOPS">
    <math xmlns="http://www.w3.org/1998/Math/MathML">
     <apply>
      <divide/>
      <ci> _Buffer </ci>
      <apply>
       <plus/>
       <cn> 1 </cn>
       <ci> HA_A </ci>
      </apply>
     </apply>
    </math>
   </initialAssignment>
   <initialAssignment symbol="MOPSH">
    <math xmlns="http://www.w3.org/1998/Math/MathML">
     <apply>
      <minus/>
      <ci> _Buffer </ci>
      <ci> MOPS </ci>
     </apply>
    </math>
   </initialAssignment>
   <initialAssignment symbol="H">
    <math xmlns="http://www.w3.org/1998/Math/MathML">
```

```
    <apply>
     <power/>
     <cn> 10 </cn>
     <apply>
      <minus/>
      <ci> Start_pH </ci>
     </apply>
    </apply>
   </math>
  </initialAssignment>
  <initialAssignment symbol="AspH">
   <math xmlns="http://www.w3.org/1998/Math/MathML">
    <apply>
     <divide/>
     <apply>
      <times/>
      <ci> AspH_Asp </ci>
      <ci> AspH_initial </ci>
     </apply>
     <apply>
      <plus/>
      <cn> 1 </cn>
      <ci> AspH_Asp </ci>
     </apply>
    </apply>
   </math>
  </initialAssignment>
  <initialAssignment symbol="AspHH">
   <math xmlns="http://www.w3.org/1998/Math/MathML">
    <apply>
     <divide/>
     <apply>
      <times/>
      <ci> AspHH_AspH </ci>
      <ci> _A3 </ci>
     </apply>
     <apply>
      <plus/>
      <cn> 1 </cn>
      <ci> AspHH_AspH </ci>
     </apply>
    </apply>
   </math>
  </initialAssignment>
  <initialAssignment symbol="OH">
   <math xmlns="http://www.w3.org/1998/Math/MathML">
    <apply>
     <power/>
     <cn> 10 </cn>
     <apply>
      <minus/>
      <apply>
       <minus/>
       <cn> 14 </cn>
       <ci> pH </ci>
      </apply>
     </apply>
    </apply>
```

```
  </math>
</initialAssignment>
<initialAssignment symbol="Asp">
  <math xmlns="http://www.w3.org/1998/Math/MathML">
    <apply>
      <minus/>
      <ci> AspH_initial </ci>
      <ci> AspH </ci>
    </apply>
  </math>
</initialAssignment>
<initialAssignment symbol="Metabolite_9">
  <math xmlns="http://www.w3.org/1998/Math/MathML">
    <ci> AspHH </ci>
  </math>
</initialAssignment>
<initialAssignment symbol="Metabolite_8">
  <math xmlns="http://www.w3.org/1998/Math/MathML">
    <ci> AspH </ci>
  </math>
</initialAssignment>
<initialAssignment symbol="Metabolite_15">
  <math xmlns="http://www.w3.org/1998/Math/MathML">
    <ci> Asp </ci>
  </math>
</initialAssignment>
<initialAssignment symbol="Metabolite_6">
  <math xmlns="http://www.w3.org/1998/Math/MathML">
    <ci> H </ci>
  </math>
</initialAssignment>
<initialAssignment symbol="ModelValue_0">
  <math xmlns="http://www.w3.org/1998/Math/MathML">
    <ci> K1 </ci>
  </math>
</initialAssignment>
<initialAssignment symbol="ModelValue_1">
  <math xmlns="http://www.w3.org/1998/Math/MathML">
    <ci> K1f </ci>
  </math>
</initialAssignment>
<initialAssignment symbol="ModelValue_3">
  <math xmlns="http://www.w3.org/1998/Math/MathML">
    <ci> K2 </ci>
  </math>
</initialAssignment>
<initialAssignment symbol="ModelValue_4">
  <math xmlns="http://www.w3.org/1998/Math/MathML">
    <ci> K2f </ci>
  </math>
</initialAssignment>
<initialAssignment symbol="ModelValue_6">
  <math xmlns="http://www.w3.org/1998/Math/MathML">
    <ci> K3 </ci>
  </math>
</initialAssignment>
<initialAssignment symbol="ModelValue_7">
  <math xmlns="http://www.w3.org/1998/Math/MathML">
```

```
    <ci> K3f </ci>
  </math>
</initialAssignment>
<initialAssignment symbol="ModelValue_9">
  <math xmlns="http://www.w3.org/1998/Math/MathML">
    <ci> K4 </ci>
  </math>
</initialAssignment>
<initialAssignment symbol="ModelValue_10">
  <math xmlns="http://www.w3.org/1998/Math/MathML">
    <ci> K4f </ci>
  </math>
</initialAssignment>
<initialAssignment symbol="ModelValue_12">
  <math xmlns="http://www.w3.org/1998/Math/MathML">
    <ci> K5 </ci>
  </math>
</initialAssignment>
<initialAssignment symbol="ModelValue_13">
  <math xmlns="http://www.w3.org/1998/Math/MathML">
    <ci> K5f </ci>
  </math>
</initialAssignment>
<initialAssignment symbol="ModelValue_15">
  <math xmlns="http://www.w3.org/1998/Math/MathML">
    <ci> K6 </ci>
  </math>
</initialAssignment>
<initialAssignment symbol="ModelValue_16">
  <math xmlns="http://www.w3.org/1998/Math/MathML">
    <ci> K6f </ci>
  </math>
</initialAssignment>
<initialAssignment symbol="ModelValue_19">
  <math xmlns="http://www.w3.org/1998/Math/MathML">
    <ci> K8 </ci>
  </math>
</initialAssignment>
<initialAssignment symbol="ModelValue_20">
  <math xmlns="http://www.w3.org/1998/Math/MathML">
    <ci> K8f </ci>
  </math>
</initialAssignment>
<initialAssignment symbol="ModelValue_27">
  <math xmlns="http://www.w3.org/1998/Math/MathML">
    <ci> K9 </ci>
  </math>
</initialAssignment>
<initialAssignment symbol="ModelValue_28">
  <math xmlns="http://www.w3.org/1998/Math/MathML">
    <ci> K9f </ci>
  </math>
</initialAssignment>
<initialAssignment symbol="ModelValue_25">
  <math xmlns="http://www.w3.org/1998/Math/MathML">
    <ci> Kw </ci>
  </math>
</initialAssignment>
```

```
  <initialAssignment symbol="ModelValue_23">
    <math xmlns="http://www.w3.org/1998/Math/MathML">
      <ci> KWf </ci>
    </math>
  </initialAssignment>
  <initialAssignment symbol="ModelValue_34">
    <math xmlns="http://www.w3.org/1998/Math/MathML">
      <ci> _A3 </ci>
    </math>
  </initialAssignment>
</listOfInitialAssignments>
<listOfRules>
  <assignmentRule variable="K3b">
    <math xmlns="http://www.w3.org/1998/Math/MathML">
      <apply>
        <divide/>
        <ci> ModelValue_7 </ci>
        <ci> ModelValue_6 </ci>
      </apply>
    </math>
  </assignmentRule>
  <assignmentRule variable="Check_T">
    <math xmlns="http://www.w3.org/1998/Math/MathML">
      <apply>
        <plus/>
        <ci> Asp </ci>
        <ci> AspH </ci>
        <ci> AspHH </ci>
      </apply>
    </math>
  </assignmentRule>
  <assignmentRule variable="Check">
    <math xmlns="http://www.w3.org/1998/Math/MathML">
      <apply>
        <plus/>
        <ci> Metabolite_15 </ci>
        <ci> Metabolite_8 </ci>
        <ci> Metabolite_9 </ci>
      </apply>
    </math>
  </assignmentRule>
  <assignmentRule variable="K4b">
    <math xmlns="http://www.w3.org/1998/Math/MathML">
      <apply>
        <divide/>
        <ci> ModelValue_10 </ci>
        <ci> ModelValue_9 </ci>
      </apply>
    </math>
  </assignmentRule>
  <assignmentRule variable="KWb">
    <math xmlns="http://www.w3.org/1998/Math/MathML">
      <apply>
        <divide/>
        <ci> ModelValue_23 </ci>
        <ci> ModelValue_25 </ci>
      </apply>
    </math>
```

```
</assignmentRule>
<assignmentRule variable="K5b">
  <math xmlns="http://www.w3.org/1998/Math/MathML">
    <apply>
      <divide/>
      <ci> ModelValue_13 </ci>
      <ci> ModelValue_12 </ci>
    </apply>
  </math>
</assignmentRule>
<assignmentRule variable="K8b">
  <math xmlns="http://www.w3.org/1998/Math/MathML">
    <apply>
      <divide/>
      <ci> ModelValue_20 </ci>
      <ci> ModelValue_19 </ci>
    </apply>
  </math>
</assignmentRule>
<assignmentRule variable="t_Min">
  <math xmlns="http://www.w3.org/1998/Math/MathML">
    <apply>
      <divide/>
      <csymbol encoding="text" definitionURL="http://www.sbml.org/sbml/symbols/time"> time </csymbol>
      <cn> 60 </cn>
    </apply>
  </math>
</assignmentRule>
<assignmentRule variable="pH">
  <math xmlns="http://www.w3.org/1998/Math/MathML">
    <apply>
      <minus/>
      <apply>
        <log/>
        <logbase>
          <cn type="integer"> 10 </cn>
        </logbase>
        <ci> H </ci>
      </apply>
    </apply>
  </math>
</assignmentRule>
<assignmentRule variable="HA_A">
  <math xmlns="http://www.w3.org/1998/Math/MathML">
    <apply>
      <divide/>
      <ci> Metabolite_6 </ci>
      <ci> ModelValue_0 </ci>
    </apply>
  </math>
</assignmentRule>
<assignmentRule variable="Kw_Check">
  <math xmlns="http://www.w3.org/1998/Math/MathML">
    <apply>
      <times/>
      <ci> H </ci>
      <ci> OH </ci>
    </apply>
```

```
  </math>
</assignmentRule>
<assignmentRule variable="K9b">
  <math xmlns="http://www.w3.org/1998/Math/MathML">
    <apply>
      <divide/>
      <ci> ModelValue_28 </ci>
      <ci> ModelValue_27 </ci>
    </apply>
  </math>
</assignmentRule>
<assignmentRule variable="K6b">
  <math xmlns="http://www.w3.org/1998/Math/MathML">
    <apply>
      <divide/>
      <ci> ModelValue_16 </ci>
      <ci> ModelValue_15 </ci>
    </apply>
  </math>
</assignmentRule>
<assignmentRule variable="AspHH_AspH">
  <math xmlns="http://www.w3.org/1998/Math/MathML">
    <apply>
      <divide/>
      <ci> Metabolite_6 </ci>
      <ci> ModelValue_6 </ci>
    </apply>
  </math>
</assignmentRule>
<assignmentRule variable="AspH_Asp">
  <math xmlns="http://www.w3.org/1998/Math/MathML">
    <apply>
      <divide/>
      <ci> Metabolite_6 </ci>
      <ci> ModelValue_27 </ci>
    </apply>
  </math>
</assignmentRule>
<assignmentRule variable="AspH_initial">
  <math xmlns="http://www.w3.org/1998/Math/MathML">
    <apply>
      <minus/>
      <ci> ModelValue_34 </ci>
      <ci> Metabolite_9 </ci>
    </apply>
  </math>
</assignmentRule>
<assignmentRule variable="K2b">
  <math xmlns="http://www.w3.org/1998/Math/MathML">
    <apply>
      <divide/>
      <ci> ModelValue_4 </ci>
      <ci> ModelValue_3 </ci>
    </apply>
  </math>
</assignmentRule>
<assignmentRule variable="K1b">
  <math xmlns="http://www.w3.org/1998/Math/MathML">
```

```
        <apply>
          <divide/>
          <ci> ModelValue_1 </ci>
          <ci> ModelValue_0 </ci>
        </apply>
      </math>
    </assignmentRule>
  </listOfRules>
  <listOfReactions>
    <reaction metaid="COPASI60" id="MOPS_Dissociation" name="MOPS Dissociation" reversible="true" fast="false">
      <notes>
        <body xmlns="http://www.w3.org/1999/xhtml">
          <pre>Dissociation of the MOPS buffer. Ka is K1</pre>
        </body>
      </notes>
      <listOfReactants>
        <speciesReference species="MOPSH" stoichiometry="1" constant="true"/>
      </listOfReactants>
      <listOfProducts>
        <speciesReference species="MOPS" stoichiometry="1" constant="true"/>
        <speciesReference species="H" stoichiometry="1" constant="true"/>
      </listOfProducts>
      <kineticLaw>
        <math xmlns="http://www.w3.org/1998/Math/MathML">
          <apply>
            <times/>
            <ci> Vial </ci>
            <apply>
              <minus/>
              <apply>
                <times/>
                <ci> K1f </ci>
                <ci> MOPSH </ci>
              </apply>
              <apply>
                <times/>
                <ci> K1b </ci>
                <ci> MOPS </ci>
                <ci> H </ci>
              </apply>
            </apply>
          </apply>
        </math>
      </kineticLaw>
    </reaction>
    <reaction metaid="COPASI61" id="TBA_dissociation" name="TBA dissociation" reversible="true" fast="false">
      <notes>
        <body xmlns="http://www.w3.org/1999/xhtml">
          <pre>Dissociation of TBA acid. Ka is K2</pre>
        </body>
      </notes>
      <listOfReactants>
        <speciesReference species="TBA_0" stoichiometry="1" constant="true"/>
      </listOfReactants>
      <listOfProducts>
        <speciesReference species="TBA" stoichiometry="1" constant="true"/>
        <speciesReference species="H" stoichiometry="1" constant="true"/>
```

```
      </listOfProducts>
      <kineticLaw>
       <math xmlns="http://www.w3.org/1998/Math/MathML">
        <apply>
         <times/>
         <ci> Vial </ci>
         <apply>
          <minus/>
          <apply>
           <times/>
           <ci> K2f </ci>
           <ci> TBA_0 </ci>
          </apply>
          <apply>
           <times/>
           <ci> K2b </ci>
           <ci> TBA </ci>
           <ci> H </ci>
          </apply>
         </apply>
        </apply>
       </math>
      </kineticLaw>
    </reaction>
    <reaction metaid="COPASI62" id="Asp_1st_Dissociation" name="Asp 1st pKa" reversible="true" fast="false">
      <notes>
       <body xmlns="http://www.w3.org/1999/xhtml">
        <pre>The first pKa of the polymer aspartic acid groups. The Ka is K3, from which forward and backward values are derived by arbitrarily setting K3forward to be 10000.
K3 is set according to measured conductimetric pKa of the polymers.

K3 and K9 should be the same number.</pre>
       </body>
      </notes>
      <listOfReactants>
       <speciesReference species="AspHH" stoichiometry="1" constant="true"/>
      </listOfReactants>
      <listOfProducts>
       <speciesReference species="AspH" stoichiometry="1" constant="true"/>
       <speciesReference species="H" stoichiometry="1" constant="true"/>
      </listOfProducts>
      <kineticLaw>
       <math xmlns="http://www.w3.org/1998/Math/MathML">
        <apply>
         <times/>
         <ci> Vial </ci>
         <apply>
          <minus/>
          <apply>
           <times/>
           <ci> K3f </ci>
           <ci> AspHH </ci>
          </apply>
          <apply>
           <times/>
           <ci> K3b </ci>
           <ci> AspH </ci>
           <ci> H </ci>
```

```
            </apply>
           </apply>
          </apply>
         </math>
        </kineticLaw>
      </reaction>
      <reaction metaid="COPASI63" id="Bromoform_Dissociation" name="Bromoform Dissociation" reversible="true" fast="false">
        <notes>
         <body xmlns="http://www.w3.org/1999/xhtml">
          <pre>The dissociation of bromoform to the tribromomethyl anion. Ka is K4</pre>
         </body>
        </notes>
        <listOfReactants>
         <speciesReference species="Br3CH" stoichiometry="1" constant="true"/>
        </listOfReactants>
        <listOfProducts>
         <speciesReference species="Br3C" stoichiometry="1" constant="true"/>
         <speciesReference species="H" stoichiometry="1" constant="true"/>
        </listOfProducts>
        <kineticLaw>
         <math xmlns="http://www.w3.org/1998/Math/MathML">
          <apply>
           <times/>
           <ci> Vial </ci>
           <apply>
            <minus/>
            <apply>
             <times/>
             <ci> K4f </ci>
             <ci> Br3CH </ci>
            </apply>
            <apply>
             <times/>
             <ci> K4b </ci>
             <ci> Br3C </ci>
             <ci> H </ci>
            </apply>
           </apply>
          </apply>
         </math>
        </kineticLaw>
      </reaction>
      <reaction metaid="COPASI64" id="Bicarb_Dissoc" name="Bicarb Dissoc" reversible="true" fast="false">
        <notes>
         <body xmlns="http://www.w3.org/1999/xhtml">
          <pre>The dissociation of bicarbonate to carbonate. K5 is the Ka of the process.</pre>
         </body>
        </notes>
        <listOfReactants>
         <speciesReference species="HCO3" stoichiometry="1" constant="true"/>
        </listOfReactants>
        <listOfProducts>
         <speciesReference species="CO3" stoichiometry="1" constant="true"/>
         <speciesReference species="H" stoichiometry="1" constant="true"/>
        </listOfProducts>
        <kineticLaw>
         <math xmlns="http://www.w3.org/1998/Math/MathML">
```

```
          <apply>
           <times/>
           <ci> Vial </ci>
           <apply>
            <minus/>
            <apply>
             <times/>
             <ci> K5f </ci>
             <ci> HCO3 </ci>
            </apply>
            <apply>
             <times/>
             <ci> K5b </ci>
             <ci> CO3 </ci>
             <ci> H </ci>
            </apply>
           </apply>
          </apply>
         </math>
        </kineticLaw>
      </reaction>
      <reaction metaid="COPASI65" id="CO2_Hydration" name="CO2 Hydration" reversible="true" fast="false">
        <notes>
          <body xmlns="http://www.w3.org/1999/xhtml">
            <pre>Reaction for the hydration and dissociation of dissolved CO2 into bicarbonate and a proton. Equilibrium constant is K6</pre>
          </body>
        </notes>
        <listOfReactants>
          <speciesReference species="CO2" stoichiometry="1" constant="true"/>
          <speciesReference species="H2O" stoichiometry="1" constant="true"/>
        </listOfReactants>
        <listOfProducts>
          <speciesReference species="HCO3" stoichiometry="1" constant="true"/>
          <speciesReference species="H" stoichiometry="1" constant="true"/>
        </listOfProducts>
        <kineticLaw>
          <math xmlns="http://www.w3.org/1998/Math/MathML">
            <apply>
              <times/>
              <ci> Vial </ci>
              <apply>
                <minus/>
                <apply>
                  <times/>
                  <ci> K6f </ci>
                  <ci> CO2 </ci>
                  <ci> H2O </ci>
                </apply>
                <apply>
                  <times/>
                  <ci> K6b </ci>
                  <ci> HCO3 </ci>
                  <ci> H </ci>
                </apply>
              </apply>
            </apply>
          </math>
```

```
    </kineticLaw>
   </reaction>
   <reaction metaid="COPASI66" id="TBA_Decarb" name="TBA Decarb" reversible="false" fast="false">
    <notes>
     <body xmlns="http://www.w3.org/1999/xhtml">
      <pre>Reaction for the decarboxylation of the tribromoacetate anion.</pre>
     </body>
    </notes>
    <listOfReactants>
     <speciesReference species="TBA" stoichiometry="1" constant="true"/>
    </listOfReactants>
    <listOfProducts>
     <speciesReference species="Br3C" stoichiometry="1" constant="true"/>
     <speciesReference species="CO2" stoichiometry="1" constant="true"/>
    </listOfProducts>
    <listOfModifiers>
     <modifierSpeciesReference species="H"/>
    </listOfModifiers>
    <kineticLaw>
     <math xmlns="http://www.w3.org/1998/Math/MathML">
      <apply>
       <times/>
       <ci> Vial </ci>
       <ci> k1 </ci>
       <ci> TBA </ci>
      </apply>
     </math>
     <listOfLocalParameters>
      <localParameter id="k1" name="k1" value="2.2e-05"/>
     </listOfLocalParameters>
    </kineticLaw>
   </reaction>
   <reaction metaid="COPASI67" id="CO2_Gas_Balance" name="CO2 Gas Balance" reversible="false" fast="false">
    <notes>
     <body xmlns="http://www.w3.org/1999/xhtml">
      <pre>The processing of CO2 off gassing from solution to the surrounding air. See notes on CO2g above.

The process is modelled as irreversible with a fitted constant. This is because
1) Atmospheric CO2 concentration will always be far lower than that in solution, and the vial is not a closed system. This is to avoid implementing the atmosphere as an additional compartment and including an equilibrium for CO2 solubility, which would be hard to get reliable numbers on, since:
2) CO2 off gassing is a complicated process (See great series of papers by Liger-Belair and coworkers on behaviour of CO2 in carbonated alcoholic beverages - a great read for general scientific interest), which depends on the size and shape of the vessel, the internal surface of the vessel, and a number of other factors that cannot be controlled for in this circumstance.

These assumptions both simplify the model and lead to reliable predictions. In all cases the rates are on the same order of magnitude (and all experiments are run in the same GPC vials).</pre>
     </body>
    </notes>
    <listOfReactants>
     <speciesReference species="CO2" stoichiometry="1" constant="true"/>
    </listOfReactants>
    <listOfProducts>
     <speciesReference species="CO2g" stoichiometry="1" constant="true"/>
    </listOfProducts>
    <kineticLaw>
```

```
      <math xmlns="http://www.w3.org/1998/Math/MathML">
       <apply>
        <times/>
        <ci> Vial </ci>
        <ci> k1 </ci>
        <ci> CO2 </ci>
       </apply>
      </math>
      <listOfLocalParameters>
       <localParameter id="k1" name="k1" value="0.00025"/>
      </listOfLocalParameters>
     </kineticLaw>
    </reaction>
    <reaction metaid="COPASI68" id="Asp_2nd_pKa" name="Asp 2nd pKa" reversible="true" fast="false">
     <notes>
      <body xmlns="http://www.w3.org/1999/xhtml">
       <pre>The second pKa of the polymer aspartic acid groups. The Ka is K9, from which forward and backward
values are derived by arbitrarily setting K9forward to be 10000.
K9 is set according to measured conductimetric pKa of the polymers.

K3 and K9 should be the same number. (They are implemented as separate numbers in case there was a clear first
and second deprotonation step if a different polymer is used)</pre>
      </body>
     </notes>
     <listOfReactants>
      <speciesReference species="AspH" stoichiometry="1" constant="true"/>
     </listOfReactants>
     <listOfProducts>
      <speciesReference species="Asp" stoichiometry="1" constant="true"/>
      <speciesReference species="H" stoichiometry="1" constant="true"/>
     </listOfProducts>
     <kineticLaw>
      <math xmlns="http://www.w3.org/1998/Math/MathML">
       <apply>
        <times/>
        <ci> Vial </ci>
        <apply>
         <minus/>
         <apply>
          <times/>
          <ci> K9f </ci>
          <ci> AspH </ci>
         </apply>
         <apply>
          <times/>
          <ci> K9b </ci>
          <ci> Asp </ci>
          <ci> H </ci>
         </apply>
        </apply>
       </apply>
      </math>
     </kineticLaw>
    </reaction>
    <reaction metaid="COPASI69" id="Water_Balance" name="Water Balance" reversible="true" fast="false">
     <notes>
      <body xmlns="http://www.w3.org/1999/xhtml">
       <pre>Self-ionization of water, equilibrium constant is Kw.</pre>
```

```
      </body>
    </notes>
    <listOfReactants>
      <speciesReference species="H" stoichiometry="1" constant="true"/>
      <speciesReference species="OH" stoichiometry="1" constant="true"/>
    </listOfReactants>
    <listOfProducts>
      <speciesReference species="H2O" stoichiometry="1" constant="true"/>
    </listOfProducts>
    <kineticLaw>
      <math xmlns="http://www.w3.org/1998/Math/MathML">
        <apply>
          <times/>
          <ci> Vial </ci>
          <apply>
            <ci> Constant_flux__reversible </ci>
            <ci> v </ci>
          </apply>
        </apply>
      </math>
      <listOfLocalParameters>
        <localParameter id="v" name="v" value="1e-14"/>
      </listOfLocalParameters>
    </kineticLaw>
  </reaction>
  <reaction metaid="COPASI70" id="TBA_Dimerization" name="TBA Dimerization" reversible="true" fast="false">
    <notes>
      <body xmlns="http://www.w3.org/1999/xhtml">
        <pre>Dimerization of the protonated TBA into hydrogen bonded dimers. Legacy reaction, has no bearing on model. Can be included if using a weaker acid with a known dimerization constant.</pre>
      </body>
    </notes>
    <listOfReactants>
      <speciesReference species="TBA_0" stoichiometry="2" constant="true"/>
    </listOfReactants>
    <listOfProducts>
      <speciesReference species="diTBA" stoichiometry="1" constant="true"/>
    </listOfProducts>
    <kineticLaw>
      <math xmlns="http://www.w3.org/1998/Math/MathML">
        <apply>
          <times/>
          <ci> Vial </ci>
          <apply>
            <minus/>
            <apply>
              <times/>
              <ci> KWf </ci>
              <apply>
                <power/>
                <ci> TBA_0 </ci>
                <cn> 2 </cn>
              </apply>
            </apply>
            <apply>
              <times/>
              <ci> KWb </ci>
```

```
            <ci> diTBA </ci>
           </apply>
          </apply>
         </apply>
        </math>
       </kineticLaw>
      </reaction>
    </listOfReactions>
  </model>
</sbml>
```

3.6. Acknowledgements

We acknowledge funding from the European Union's Horizon 2020 research and innovation program under the Marie Skłodowska-Curie grant agreement no. 812868. AW acknowledges funding via a Gutenberg Research Professorship underpinning his Life-Like Materials Program.

GF would like to thank Dr. Brigita Dúsz and Dr. Daniele Del Giudice for fruitful discussion regarding modelling of the TBA reaction system.

3.7. References

[1] Y. Mai, A. Eisenberg, Self-Assembly of Block Copolymers, *Chem. Soc. Rev.* **2012**, *41*, 5969.

[2] M. Karayianni, S. Pispas, Block Copolymer Solution Self-Assembly: Recent Advances, Emerging Trends, and Applications, *J. Polym. Sci.* **2021**, *59*, 1874.

[3] Y. Lu, J. Lin, L. Wang, L. Zhang, C. Cai, Self-Assembly of Copolymer Micelles: Higher-Level Assembly for Constructing Hierarchical Structure, *Chem. Rev.* **2020**, *120*, 4111.

[4] C. Charbonneau, C. Chassenieux, O. Colombani, T. Nicolai, Controlling the Dynamics of Self-Assembled Triblock Copolymer Networks Via the Ph, *Macromolecules* **2011**, *44*, 4487.

[5] X. Duan, J. Xiao, Q. Yin, Z. Zhang, H. Yu, S. Mao, Y. Li, Smart Ph-Sensitive and Temporal-Controlled Polymeric Micelles for Effective Combination Therapy of Doxorubicin and Disulfiram, *ACS Nano* **2013**, *7*, 5858.

[6] M. A. Würbser, P. Schwarz, J. Heckel, A. M. Bergmann, A. Walther, J. Boekhoven, Chemically Fueled Block Copolymer Self-Assembly into Transient Nanoreactor, *ChemSystemsChem* **2021**, *3*, e2100015

[7] X. Lang, U. Thumu, L. Yuan, C. Zheng, H. Zhang, L. He, H. Zhao, C. Zhao, Chemical Fuel-Driven Transient Polymeric Micelle Nanoreactors toward Reversible Trapping and Reaction Acceleration, *Chem. Commun.* **2021**, *57*, 5786.

[8] H. Che, S. Cao, J. C. M. van Hest, Feedback-Induced Temporal Control of "Breathing" Polymersomes to Create Self-Adaptive Nanoreactors, *J. Am. Chem. Soc.* **2018**, *140*, 5356.

[9] T. J. Martin, K. Procházka, P. Munk, S. E. Webber, Ph-Dependent Micellization of Poly(2-Vinylpyridine)-Block-Poly(Ethylene Oxide), *Macromolecules* **1996**, *29*, 6071.

[10] H. Dou, M. Jiang, H. Peng, D. Chen, Y. Hong, Ph-Dependent Self-Assembly: Micellization and Micelle-Hollow-Sphere Transition of Cellulose-Based Copolymers, *Angew. Chem. Int. Ed.* **2003**, *42*, 1516.

[11] A. Qin, M. Tian, C. Ramireddy, S. E. Webber, P. Munk, Z. Tuzar, Polystyrene-Poly(Methacrylic Acid) Block Copolymer Micelles, *Macromolecules* **2002**, *27*, 120.

[12] C. Sharma, I. Maity, A. Walther, Ph-Feedback Systems to Program Autonomous Self-Assembly and Material Lifecycles, *Chem. Commun.* **2023**, *59*, 1125.

[13] E. C. Edblom, Y. Luo, M. Orban, K. Kustin, I. R. Epstein, Systematic Design of Chemical Oscillators. 45. Kinetics and Mechanism of the Oscillatory Bromate-Sulfite-Ferrocyanide Reaction, *J. Phys. Chem.* **1989**, *93*, 2722.

[14] G. Wang, Y. Liu, Y. Liu, N. Xia, W. Zhou, Q. Gao, S. Liu, The Non-Equilibrium Self-Assembly of Amphiphilic Block Copolymers Driven by a Ph Oscillator, *Colloids Surf. A: Physicochem. Eng. Asp* **2017**, *529*, 808.

[15] E. Poros-Tarcali, J. Perez-Mercader, Concurrent Self-Regulated Autonomous Synthesis and Functionalization of Ph-Responsive Giant Vesicles by a Chemical Ph Oscillator, *Soft Matter* **2021**, *17*, 4011.

[16] T. Heuser, A. K. Steppert, C. M. Lopez, B. Zhu, A. Walther, Generic Concept to Program the Time Domain of Self-Assemblies with a Self-Regulation Mechanism, *Nano Lett.* **2015**, *15*, 2213.

[17] T. Heuser, E. Weyandt, A. Walther, Biocatalytic Feedback-Driven Temporal Programming of Self-Regulating Peptide Hydrogels, *Angew. Chem. Int. Ed.* **2015**, *54*, 13258.

[18] L. Heinen, T. Heuser, A. Steinschulte, A. Walther, Antagonistic Enzymes in a Biocatalytic Ph Feedback System Program Autonomous DNA Hydrogel Life Cycles, *Nano Lett.* **2017**, *17*, 4989.

[19] T. Heuser, R. Merindol, S. Loescher, A. Klaus, A. Walther, Photonic Devices out of Equilibrium: Transient Memory, Signal Propagation, and Sensing, *Adv. Mater.* **2017**, *29*, 1606842.

[20] C. Sharma, A. Walther, Self-Regulating Colloidal Co-Assemblies That Accelerate Their Own Destruction Via Chemo-Structural Feedback, *Angew. Chem. Int. Ed.* **2022**, *61*, 202201573.

[21] I. Maity, C. Sharma, F. Lossada, A. Walther, Feedback and Communication in Active Hydrogel Spheres with Ph Fronts: Facile Approaches to Grow Soft Hydrogel Structures, *Angew. Chem. Int. Ed.* **2021**, *60*, 22537.

[22] D. Del Giudice, E. Spatola, R. Cacciapaglia, A. Casnati, L. Baldini, G. Ercolani, S. Di Stefano, Time Programmable Locking/Unlocking of the Calix[4]Arene Scaffold by Means of Chemical Fuels, *Chem. Eur. J.* **2020**, *26*, 14954.

[23] C. Biagini, S. Albano, R. Caruso, L. Mandolini, J. A. Berrocal, S. Di Stefano, Variations in the Fuel Structure Control the Rate of the Back and Forth Motions of a Chemically Fuelled Molecular Switch, *Chem. Sci.* **2018**, *9*, 181.

[24] J. A. Berrocal, C. Biagini, L. Mandolini, S. Di Stefano, Coupling of the Decarboxylation of 2-Cyano-2-Phenylpropanoic Acid to Large-Amplitude Motions: A Convenient Fuel for an Acid-Base-Operated Molecular Switch, *Angew. Chem. Int. Ed.* **2016**, *55*, 6997.

[25] V. W. Liyana Gunawardana, T. J. Finnegan, C. E. Ward, C. E. Moore, J. D. Badjic, Dissipative Formation of Covalent Basket Cages, *Angew. Chem. Int. Ed.* **2022**, *61*, e202207418.

[26] E. Olivieri, B. Gasch, G. Quintard, J. V. Naubron, A. Quintard, Dissipative Acid-Fueled Reprogrammable Supramolecular Materials, *ACS Appl. Mater. Interfaces* **2022**, *14*, 24720.

[27] E. Olivieri, G. Quintard, J. V. Naubron, A. Quintard, Chemically Fueled Three-State Chiroptical Switching Supramolecular Gel with Temporal Control, *J. Am. Chem. Soc.* **2021**, *143*, 12650.

[28] D. Del Giudice, E. Spatola, M. Valentini, C. Bombelli, G. Ercolani, S. Di Stefano, Time-Programmable Ph: Decarboxylation of Nitroacetic Acid Allows the Time-Controlled Rising of Ph to a Definite Value, *Chem. Sci.* **2021**, *12*, 7460.

[29] D. Mariottini, D. Del Giudice, G. Ercolani, S. Di Stefano, F. Ricci, Dissipative Operation of Ph-Responsive DNA-Based Nanodevices, *Chem. Sci.* **2021**, *12*, 11735.

[30] Y. S. Jo, A. J. van der Vlies, J. Gantz, S. Antonijevic, D. Demurtas, D. Velluto, J. A. Hubbell, Raft Homo- and Copolymerization of N-Acryloyl-Morpholine, Piperidine, and Azocane and Their Self-Assembled Structures, *Macromolecules* **2008**, *41*, 1140.

[31] J. I. Solomun, L. Martin, P. Mapfumo, E. Moek, E. Amro, F. Becker, S. Tuempel, S. Hoeppener, K. L. Rudolph, A. Traeger, Ph-Sensitive Packaging of Cationic Particles by an Anionic Block Copolymer Shell, *J. Nanobiotechnology* **2022**, *20*, 336.

[32] T. Boursier, S. Georges, M. Mosquet, D. Rinaldi, F. D'Agosto, Synthesis of Poly(N-Acryloylmorpholine) Macromonomers Using Raft and Their Copolymerization with Methacrylic Acid for the Design of Graft Copolymer Additives for Concrete, *Polym. Chem.* **2016**, *7*, 917.

[33] B. de Lambert, M.-T. Charreyre, C. Chaix, C. Pichot, Poly(N-Tert-Butyl Acrylamide-B-N-Acryloylmorpholine) Amphiphilic Block Copolymers Via Raft Polymerization: Synthesis, Purification and Characterization, *Polymer* **2007**, *48*, 437.

[34] G. Fusi, D. Del Giudice, O. Skarsetz, S. Di Stefano, A. Walther, Autonomous Soft Robots Empowered by Chemical Reaction Networks, *Adv. Mater.* **2023**, *35*, e2209870.

[35] S. Hoops, S. Sahle, R. Gauges, C. Lee, J. Pahle, N. Simus, M. Singhal, L. Xu, P. Mendes, U. Kummer, Copasi--a Complex Pathway Simulator, *Bioinformatics* **2006**, *22*, 3067.

[36] G. Liger-Belair, M. Vignes-Adler, C. Voisin, B. Robillard, P. Jeandet, Kinetics of Gas Discharging in a Glass of Champagne: The Role of Nucleation Sites, *Langmuir* **2002**, *18*, 1294.

[37] A. L. Moriaux, R. Vallon, F. Lecasse, N. Chauvin, B. Parvitte, V. Zeninari, G. Liger-Belair, C. Cilindre, How Does Gas-Phase Co(2) Evolve in the Headspace of Champagne Glasses?, *J. Agric. Food. Chem.* **2021**, *69*, 2262.

Chapter

4 Autonomous Soft Robots Empowered by Chemical Reaction Networks

Preliminary Note: This Chapter is based on the journal article published in Adv. Mater. 35, 2209870. https://doi.org/10.1002/adma.202209870 (2023) by **G. Fusi**, D. Del Giudice, O. Skarsetz, S. Di Stefano and A. Walther.

4.1. Abstract

Hydrogel actuators are important for designing stimuli-sensitive soft robots. They generate mechanical motion by exploiting compartmentalized (de)swelling in response to a stimulus. However, classical switching methods, such as manually lowering or increasing the pH, cannot provide more complex autonomous motions. By coupling an autonomously operating pH-flip with programmable lifetimes to a hydrogel system containing pH-responsive and non-responsive compartments, autonomous forward and backward motion as well as more complex tasks, such as interlocking of "puzzle pieces" and collection of objects are realized. All operations are initiated by one simple trigger and the devices operate in a "fire and forget" mode. More complex self-regulatory behavior is obtained by adding chemo-mechano-chemo feedback mechanisms. Due to its simplicity, this method shows great potential for the autonomous operation of soft grippers and metamaterials.

4.2. Introduction

Traditional robots are typically built from hard materials and use electrical power and computer chips to operate. Even though they can perform a wide range of tasks, they face problems in manipulating delicate objects and lack biocompatibility. Soft robotics seeks to overcome these limitations by designing new classes of devices composed of soft functional materials, controllable through multiple stimuli. This will allow for robotic systems that more closely mimic the natural world, in both form and function.[1] At the core of every soft robotic system are soft actuators capable of changing their shape in response to an applied signal stimulus,[2] such as stimuli-responsive polymers, or pneumatics and hydraulics.[3] Hydrogels offer an interesting category of soft actuators due to their mechanical similarity to biological tissues, their biocompatibility and "wet" operation, which are advantageous for the development of bio-compatible and bio-interfaceable soft robots.[4-5] Hydrogel soft actuators operate through changes in swelling in one or more components in relation to an external stimulus, for instance heat, light, solvent, redox state and pH.[6] This stimuli-responsiveness has been exploited to develop actuating and shape-changing elements, such as linear pullers,[7] helical twisters,[7-8] bilayers and grabbers.[9-18] Unlike battery-powered and microchip-containing robotics,[19] these soft robotic systems are classically limited in the complexity of autonomous operations because they source their "instructions" and

energy for operation from an outside environmental stimulus. However, such environments do not typically undergo complex changes autonomously to pre-encode a behavior.

A pathway towards autonomous soft robotics devices capable of performing more complex tasks is through coupling chemical responsiveness to chemical reaction networks (CRNs) that can provide autonomous trajectories in chemical potential, such as transient or oscillating states with programmable temporal signatures.[20] In the field of oscillators, complex behavior has been achieved by coupling redox-sensitive gels to the Belousov-Zhabotinsky reaction.[21] Although pH oscillators have also been coupled to hydrogel (de)swelling, their autonomy is compromised as they require constant feeding of reactants.[11-12,22] Additionally, hydrogel relaxation was encoded using autocatalytic reaction/diffusion systems.[23] In general, despite the appeal of oscillators, they often require sophisticated chemistry expertise to master the multi-component cocktails, and, more importantly, the frequency and amplitude of the chemical potential can only be poorly controlled as the oscillations otherwise collapse. In contrast, we have recently shown how pH-feedback systems based on CRNs of acid- and base-producing enzymatic and non-enzymatic systems can be precisely controlled in their transient lifetime and pH amplitude.[24-25] We showed that such pH-feedback systems can be coupled to program transient self-assemblies,[26] molecular machines,[27-29] DNA devices,[30] hydrogelation[24,31-32] or photonics[33] with precise lifetimes. Two aspects are important when aiming to instruct soft robotic device with autonomous motion by CRNs. Firstly, due to the inverse relationship between size and response time in hydrogels, there should be excellent control over both the lifetime and the amplitude of the transient state of an autonomous pH-flip. Secondly, the system should be simple to operate.

Here, we introduce the first system-level integration of pH-feedback systems with compartmentalized hydrogel devices to encode autonomous operation of soft actuators. This is achieved by combining a particularly simple one-component acidic pH-flip based on a self-decarboxylating acid with actuators based on pH-responsive and non-pH-responsive hydrogel segments. To demonstrate the unique benefits of this actuator control mechanism, we design "fire and forget" gel devices capable of interlocking with each other and of capturing objects. Finally, we expand upon single-component fuels and couple the acid pH-flip with an antagonistic base-producing urea/urease reaction in a bilayer actuator to demonstrate higher level of chemo-mechano-chemo self-regulation.

4.3. Results and Discussion

4.3.1. Coupling a Self-Decarboxylating Acid to a Responsive Hydrogel

Figure 4.1 displays the basic operational principle of autonomous soft robotic devices using our one component transient pH-flip, based on activated carboxylic acids that display spontaneous pH-dependent decarboxylation in solution.[34] Upon injection of such an activated acid into an aqueous solution, the pH quickly acidifies, and subsequent decarboxylation leads to the formation of a carbanion, that quickly scavenges a proton from solution to increase the pH. The decarboxylation rate is dictated by the structure of the carboxylate, and occurs easily in the presence of electron-withdrawing groups in the *a* position, able to stabilize the resulting carbanion.[35] Although these acids have typically been used as fuels in non-aqueous solvents,[34] as hydrogen bonding with water prevents the crucial decarboxylation,[36] we found that they can also be successfully employed in aqueous systems containing small amounts of co-solvents (e.g.

DMSO, see section 4.5.3). We chose TBA (tribromoacetic acid)[37] as a one component pH-flip because the resultant transient acidic pH occurs on a suitable timescale (see section 4.5.3).

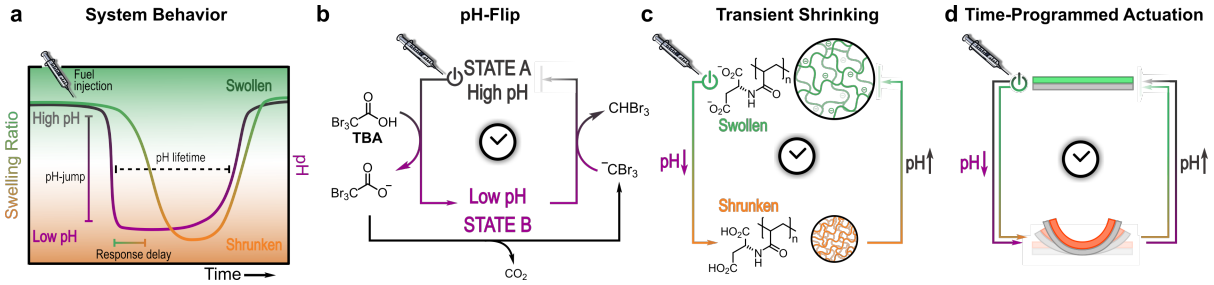

Figure 4.1: System integration of one-component pH-flips with pH-responsive hydrogels to reach autonomous actuators. (a) pH profile (purple line) and actuator response obtained by fueling with tribromoacetic acid. (b) Chemistry of the autonomous pH-flip after injecting TBA. (c) Transient isotropic hydrogel collapse of poly aspartic acid *N*-acrylamide hydrogels when coupled to the pH-flip. (d) Autonomous, time-programmed anisotropic actuation of a hydrogel bilayer device when coupled to the pH-flip.

The transient pH-flip can be readily controlled by injecting different quantities of TBA into a MOPS (morpholinopropane sulfonic acid) buffer at a starting pH of 7.2. Figure 4.2a-d summarizes the effect of injecting 3.5, 4.0 and 5.0 mM fuel into 2.5, 5.0, and 7.0 mM MOPS. Higher fuel/buffer ratios lead to larger and longer pH drops. Figure 4.2a shows that with a low buffer concentration, any of the three fuel amounts selected will lead to a large pH drop from 7.0 to 2.7-2.5. Lifetimes of the fueled state, given by the time for pH to regain ΔpH/2, show a clear upward trend with more fuel being added, with lifetimes of 40.5, 47.0 and 54.0 hours respectively. At higher buffer concentrations, the effect of fuel concentration is more pronounced. In 5.0 mM MOPS, the pH drops to 3.2, 3.0 and 2.9 – with corresponding lifetimes from 14 to 22 to 30 hours as fuel concentration increases. In 7.0 mM MOPS, the pH drops to 5.5, 3.8 and 2.8, with lifetimes of 17.5, 5.5 and 15.0 hours. Adding insufficient fuel to overcome the buffer (3.5 mM) leads to a small pH drop, and therefore an artificially long lifetime, as the pH quickly re-enters the buffered region. The CO_2 produced in the decarboxylation step is partially scavenged by water, leading to carbonic acid which dissociates to HCO_3^- and H^+, preventing the pH from being restored to its initial value. Apart from CO_2, a stoichiometric amount of bromoform is produced. As a high-boiling organic solvent that does not participate in acid-base equilibria, and given the small amount of fuel required to operate the pH flips, we expect it to have no effect on the observed pH profile.

In summary, the lifetime of the transient pH drop can be controlled on the timescale of a few hours to multiple days (Figure 4.2d) by the interplay of the concentrations of fuel and buffer; increasing fuel leads to deeper and longer pH drops, whilst increasing buffer has the opposite effect. Compared to commonly used pH-oscillators,[38-39] or other pH-feedback systems we have previously developed,[24,31] which rely on multi-component reactant systems and require a fine matching between the rates of the involved reactions, this system benefits from a clear simplicity, aiding its application-oriented use.

Next, we combined these pH-flips with a responsive hydrogel to understand how pH couples to shrinking and swelling kinetics on a larger length scale. Our hydrogels are based on aspartic acid *N*-acrylamide (A^3) crosslinked in a 50:1 molar ratio with poly(ethylene glycol)diacrylate, (PEGDA 6K; MW = 6000 g mol^{-1}). The hydrogel also includes rhodamine B, responsible for the orange color. The pK_a value of poly(A^3) hydrogels is at ca. 6.2. This fits into the pH range accessible by the TBA fuel system, and allows to access both swollen and unswollen states in our active gel.

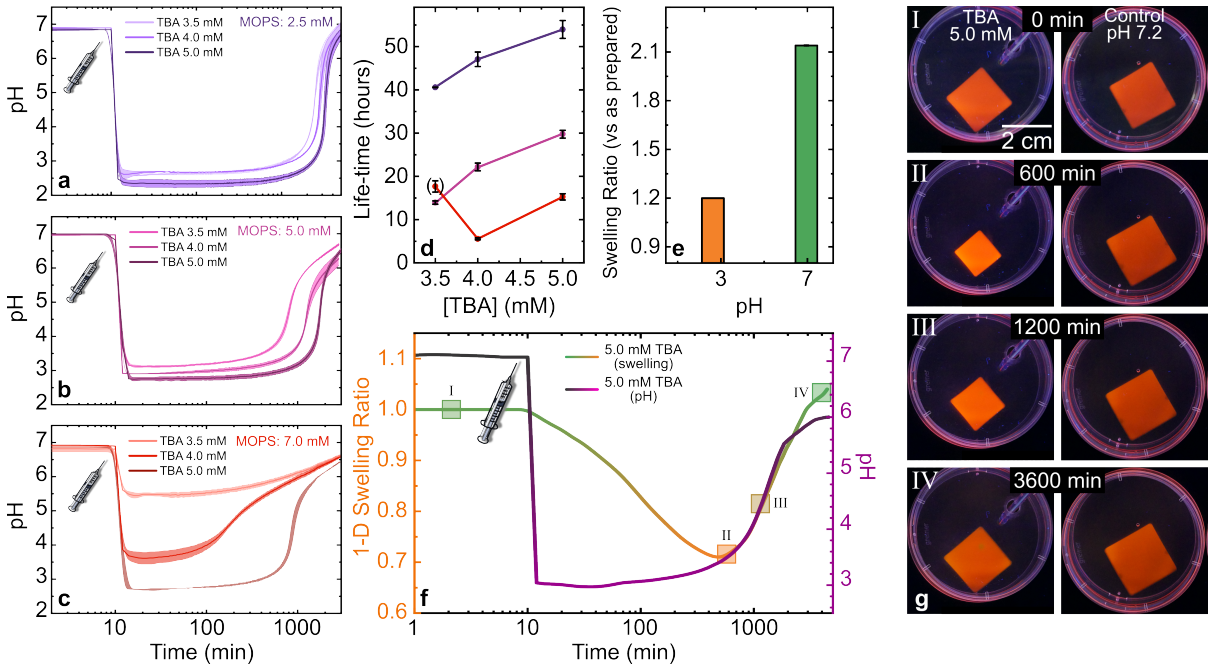

Figure 4.2: Tuning the pH-flip and coupling it to transient hydrogel deswelling. (a-c) pH curves of the TBA CRN at varying concentrations of TBA and MOPS in 70/30 v/v H_2O/DMSO. Shaded contours represent the standard deviation (n = 2 for a, c. n = 3 for b). (d) Corresponding lifetimes taken as the time for pH to regain ⊿pH/2. The lifetime for 3.5 mM TBA in 7.0 mM MOPS is outside the trend due to the small drop in pH. Error bars indicate the standard deviation (n = 3). (e) Equilibrium swelling ratio of the A³:PEGDA gel. Error bars indicate one standard deviation (< 0.4 %; n = 6). (f) Transient de-swelling of the gel in (g) alongside the pH experienced by the sample with 5.0 mM TBA fuel. (g) Photographs of transiently deswelling gel squares in 5.0 mM MOPS after injection of 5.0 mM TBA. A control is shown for comparison.

The drop in pH below the pK_a value of the gel leads to the progressive protonation of the carboxyl groups, and a shrinking of the gel network through a combination of lower electrostatic repulsion between chain segments and less favorable gel-solvent interactions. Indeed, the equilibrium swelling ratio, normalized to the specimen dimensions during synthesis in a mold, shows a decrease in 1-D swelling ratio from 2.2 at pH 7.0 to 1.2 at pH 3.0, hence a collapse to 45 % of the original volume (Figure 4.2e, see also section 0). To demonstrate coupling between pH flip and gels, we fueled gel squares of 2.0 × 2.0 × 0.5 cm in 5 mM MOPS buffer at pH 7.2 with 5.0 mM TBA (Figure 4.2f-g). The gel contraction reaches 70 % of the original dimensions when fueled. Due to the slow mass transport of water out of the gel, a significant lag time between reaching the lowest pH point and the maximum deswelling occurs, which underscores the importance of being able to tune the transient pH state over long periods.

4.3.2. Exploiting Transient Deswelling for Actuating Elements

In order to exploit this transient deswelling for autonomous motion, we paired the A³-gel with a non-responsive gel made of 2-acrylamido-2-methylpropane sulfonic acid (AMPS; crosslinked in a 50:1 molar ratio with PEGDA 6K) into bilayer devices. This hydrogel contains the fluoresceine dye responsible for the faint green color. Poly(AMPS) is a strong polyelectrolyte with a pK_a of 1.5,[40] and was selected as a passive layer due to its equilibrium swelling being close to that of the poly(A³) gel, while not displaying pH-responsiveness in the pH range of this study. The mechanical properties of both the active and passive gels are shown in the Supplementary Information. The bilayers are manufactured by partially photocuring each layer separately in a 30 × 2 × 2 mm PTFE mold, and overlaying them for a final photocuring step, ensuring robust interfacial adhesion

(Figure 4.3a). The bilayers are then soaked in 5.0 mM MOPS pH 7.2 to reach their final state, which is slightly bent due to smaller swelling of poly(AMPS). The bilayers are then cut shorter to 58 mm and mounted on a support before being attached to a container for fueling experiments.

To demonstrate the control over the magnitude and duration of the actuation, we fueled bilayers with 3.0, 5.0 and 7.0 mM TBA in 5.0 mM MOPS (Figure 4.3b-d). When fueled with 3.0 mM TBA, a pH drop from 7 to 3.5 with a duration of 250 minutes is observed. The active layer does not have enough time to equilibrate before the pH returns to its original value, leading to only minimal bending. This indicates the actuators require a threshold amount of fuel and transient lifetime to display motion. This threshold quantity is a function of the total size of the hydrogel device, as in a rod-like hydrogel, (de)swelling time scales with the radius squared.[41] In contrast, bilayers fueled with 5.0 mM and 7.0 mM TBA display a clear bending response, with more fuel leading to a longer and larger change in bending angle. Fueling with 5.0 mM TBA leads to a pH drop from ca. 7.0 to 3.0 and to a transient peak bending of 150 degrees. The bilayer fueled with 7.0 mM TBA experiences a pH drop from 7.0 to 2.0, and correspondingly a longer contraction of the active layer and a peak bending angle change of 160 degrees, demonstrating fuel-dependent actuator response.

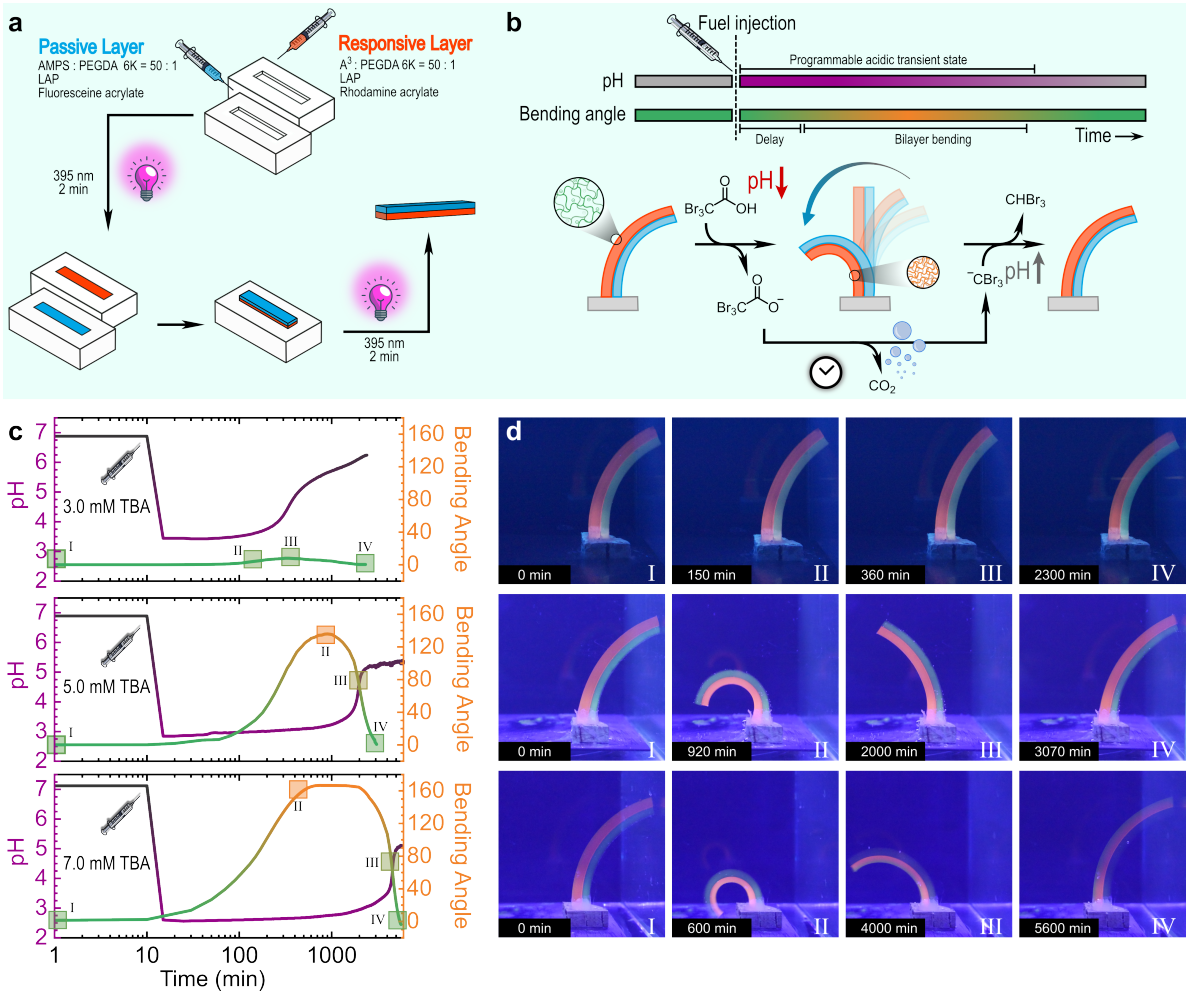

Figure 4.3: Autonomous bilayer actuators controlled by transient pH flips. (a) Fabrication of the bilayer devices by mold-casting and photocuring. Mold dimensions are 30 × 2 × 2 mm. Swollen active layer is 62 × 4 × 4 mm. AMPS layer shows lower swelling, leading to a curved conformation. (b) Schematic representation of the effect of the TBA CRN on the bilayer devices. (c) Effect of differing fuel concentrations on the magnitude and duration of the pH drop in 5.0 mM MOPS, and the corresponding change in bilayer angle. (d) Photographs of the corresponding bilayers at select time intervals.

4.3.3. Temporal Pre-Programming for Fire and Forget Devices

Next, we demonstrate the advantages of temporal pre-programming of these hydrogel actuators, as compared to classical responsive devices. These devices can operate in a "fire and forget" mode, where fueling leads to a predetermined actuation sequence. This can be interesting for systems where delivering successive external stimuli is not possible. For instance, we prepared complementary "puzzle piece" gels with responsive A^3 and unresponsive AMPS segments (Figure 4.4a). These complementary puzzle pieces are capable of interlocking but cannot be slid one into the other due to the width of the heads being larger than the gap between them (Figure 4.4b, panel I). On fueling with a critical amount of TBA, the orange active gel contracts. Since the gap is now big enough, the two puzzle pieces can be pushed together, and the active components interdigitate (Figure 4.4b panels II-III). As the acid fuel decarboxylates and the pH rises, the gels reswell, and are eventually fully interlocked, and cannot be pulled apart (Figure 4.4b panel IV). This operation is conditional on the amount of fuel in the system, as we have learned (Figure 4.3) that gel contraction occurs in a delayed fashion with respect to the pH-flip curve.

Secondly, fuel-mediated interlocking can also be exploited with just one active gel, as displayed by the gel harpoon (Figure 4.4c). The harpoon can be used to capture and move objects with an opening smaller than the unfueled head (Figure 4.4d, panel I). On fueling, the head, with a width of 14 mm, contracts and passes through a 10 mm hole drilled into a plastic cylinder (Figure 4.4d, panel II-III). Once the fueling cycle ends and the gel reswells, the harpoon can be lifted to take the captured load with it (Figure 4.4d, panel IV). In contrast to classical responsive devices that would require re-addition of chemicals, these devices are "fire-and-forget" and perform their autonomous operation without further user intervention, which allows for more flexible application scenarios and more complex interlocking of spaces that are poorly accessible from outside (e.g., the interior of the device captured by the harpoon).

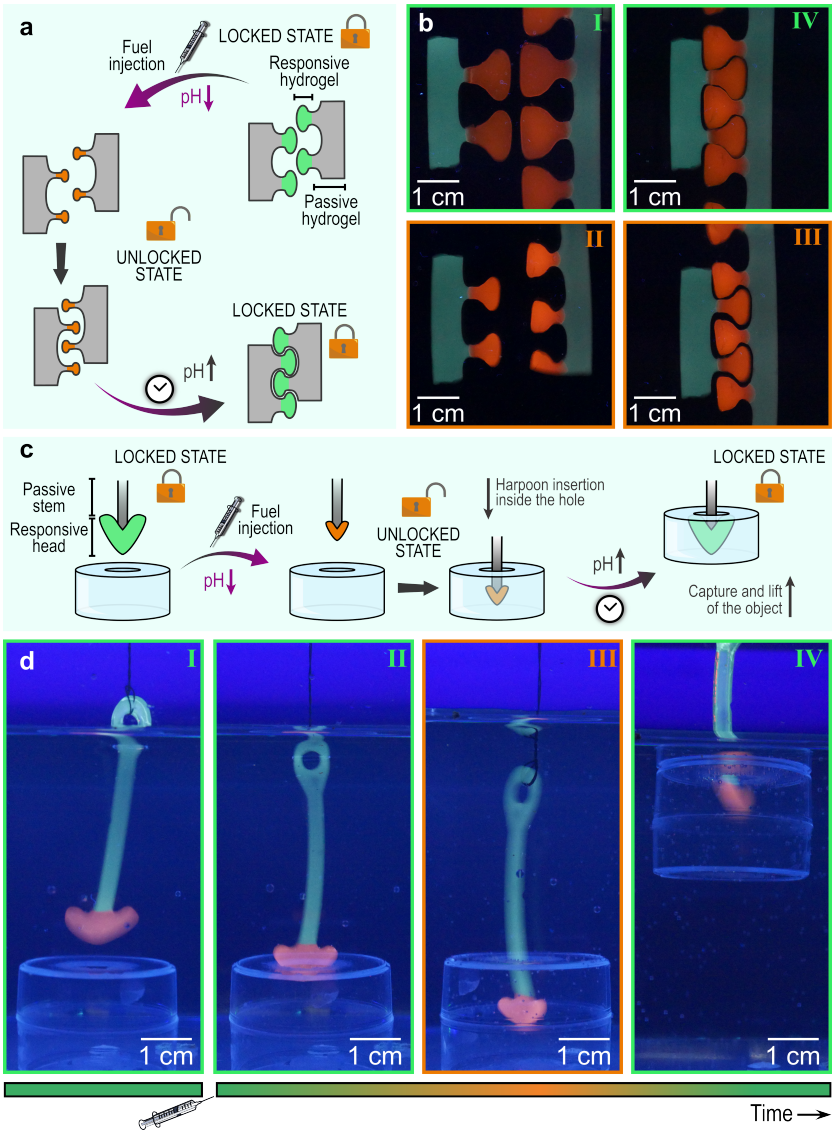

Figure 4.4: Autonomous interlocking of fueled gel devices and grabbing of objects with small orifices. (a) Scheme describing the operation of the smart "puzzle piece" gels. (b) Interdigitating complementary "puzzle piece" interfaces. The orange parts are composed of pH-responsive gel. I. Unfueled and incapable of interdigitating. II. Fueled and contracted heads. III. Interdigitated due to reduced size. IV. Reswollen to initial size. Carried out in 5.0 mM MOPS with 5.0 mM TBA fuel. (c) Scheme describing the operation of the "fire and forget" harpoon device for autonomous grabbing of objects with small orifices. (d) Harpoon device. From left to right: harpoon being lowered over opening, harpoon head resting on opening and unable to spear object, once fueled, head contracts and passes through opening, harpoon being lifted and taking object with it after re-expansion of head. Carried out in 5.0 mM MOPS with 5.0 mM TBA fuel.

4.3.4. Coupling to Urea / Urease Reaction for Chemomechanical Feedback

One of the key aspects of such autonomous devices enabled by CRNs is the possibility to add a higher-level autonomous control mechanism, by for instance embedding further antagonistic reaction modules at specific locations within the device. This multifunctionality enables chemomechanical feedback and self-regulation downstream of the initial fueling event. To demonstrate this, the TBA cycle is coupled to the urea/urease enzymatic reaction.[25,32] Urease is useful to couple to in this context, as it converts urea to ammonia and carbon dioxide, therefore leading to a rise in pH. As a device, we incorporated a cylindrical patch (h = 4 mm, r = 3.5 mm) composed of 25 wt% PEGDA 6K containing 10 mg mL^{-1} urease atop an A^3/AMPS bilayer like

those shown in Figure 4.3. This bilayer is then placed in a container containing a 100 mM urea solution in 5.0 mM MOPS, with an additional dodecane phase on top. Before fueling, the bilayer points out of the bottom aqueous phase and the urease-containing gel patch is located inside the dodecane top layer and cannot contact the urea. This avoids the enzymatic production of ammonia. Once fueled with 5.0 mM TBA, the bilayer bends, and brings the urease-containing patch into contact with the aqueous urea-containing solution. This initiates chemo-mechanical feedback by enzymatic conversion of urea into ammonia. This is in fact visible by the increased fluorescein fluorescence as the pH increases[42] in the passive gel next to the urease-containing block (Figure 4.5a,b). To quantify the effect of the added chemo-mechanical control mechanism, Figure 4.5c,d compares the pH profiles and the maximum bending angle of a system with a urease patch with an identical system without urease as a control. The maximum bending angles achieved are similar in both systems. However, the chemo-mechanical feedback begins raising the pH more quickly than the decarboxylation of the TBA could do alone, and hence significantly shortens the lifetime of the pH drop to less than 50%, from 16.5 hours 6 hours (Figure 4.5c). The added weight of the urease gel on top of the bilayer leads to some out of plane bending in the experiments, making the gel appear shorter in the final images. To confirm the effect of chemo-mechanical feedback, meaning the necessity of the urease patch to dive into the aqueous bottom layer and exclude urea diffusion though the bilayer to the urease-containing patch in the dodecane upper phase, we placed a non-bending homogenous AMPS post with a urease gel patch on top in the same two-phase system.

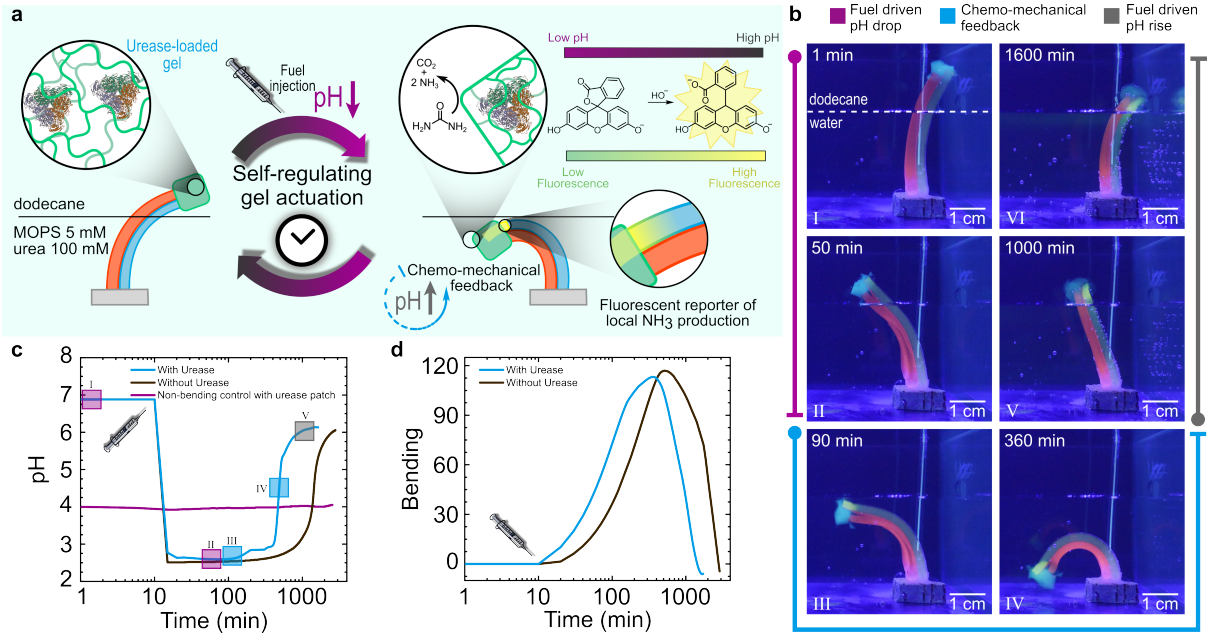

Figure 4.5: Chemo-mechanical feedback regulation of pH using the urea/urease enzymatic reaction. (a) Design of the urease-containing gel. A highly crosslinked gel containing urease is attached to the top of an A^3/AMPS bilayer. When the bilayer bends below the dodecane-water interface, the catalytic conversion of urea to ammonia begins. This can be visualized through the increased fluorescence (the apparent color changes from faint green to bright yellow) of the AMPS gel in proximity to the urease loaded gel. (b) Photographs showing the bilayer during a representative experiment. (c) pH profiles of the water phase in the experiment pictured in (b), a representative experiment without the urease-containing gel (both in 5.0 mM MOPS with 5.0 mM TBA fuel), and a control of an inert post holding the urease gel in the dodecane phase, with the water phase being 3.0 mM citrate. (d) Bending profiles of the bilayers mentioned in (c).

Figure 4.5c shows there is no change in aqueous phase pH over the course of the experiment. This confirms that no enzyme leakage occurs, and that the quicker pH feedback and chemo-mechanical return of the bilayer is indeed conditional on the urease patch diving into the fuel solution. Employing chemo-mechano-chemo feedback systems allows for higher self-regulation capacity, as the device can now sense externally present chemicals that are locally transduced into effectors.

4.4. Conclusion

In summary, this study has introduced a new method of autonomous control for soft robotic actuators by integrating autonomous chemical controllers in the form of transient pH-flips with pH-responsive hydrogels. In contrast to the complex cocktails often needed for other chemical controllers for autonomous systems,[43] specifically, CRNs suitable for polymers,[21,23,44] our system is particularly simple to operate due to the use of a one-component pH-flip. Indeed, it can be conveniently applied by a simple injection and allows a wide control over the lifetime and amplitude of the pH-flip. Compared to well-known clock reactions[38-39] or our earlier pH feedback systems,[24,31] this system can be operated with a reduced number of components and in a batch setting. Furthermore, the duration and amplitude of the pH-flip can be easily controlled by altering the amount of TBA fuel or buffer, rather than requiring fine-tuning of multiple component reactions. In addition to the control over bending angle of a bilayer as a function of the lifetime, we demonstrated applications where autonomous operation might be useful, e.g., for the autonomous interlocking of interfaces and for grabbing objects with small orifices where other stimuli would be difficult to apply. We also introduced how chemo-mechanical feedback can be included to achieve autonomous self-regulation of the device. On a fundamental level, this combination of responsive elements with advanced chemical control is vital for the transition from classical switchable materials to more life-like materials systems capable of autonomous, adaptive, and self-regulated behavior.[45]

Given that our simple one-component method to achieve autonomous control is compatible "out of the box" with pH responsive soft robot devices, we expect that this will "democratize" autonomous chemical controllers for material applications. Further research to find more environmentally benign self-decarboxylating acids will help to broaden the possible applications of this method. We further believe it is likely to be of great interest in systems where the delivery of successive fuels, complex fuel mixtures or physical stimuli is impractical, such as non-electronic, self-contained devices designed for autonomous operation, for example in microfluidic systems. The devices here shown, capable of "fire and forget" operation, could be used in smart implants, a growing interest in the biomedical field. Devices including chemomechanical feedback capabilities could lead to possible applications where fine control and feedback are necessary, such as prosthetics.

4.5. Supplementary Information

4.5.1. Instrumentation and Materials

Instrumentation

pH measurements in solution-phase experiments were carried out with 12-channel pH station (EA Instruments). pH measurements in the gel actuation experiments were carried out with a Mettler Toledo SevenCompact pH meter**.** Gel actuation experiments were imaged with a Panasonic Lumix G70 digital camera under UV light (400 nm). The UV irradiation was gated with an electrical socket timer to irradiate for 1 minute every 9 minutes. NMR spectra were measured on a Bruker 400 MHz spectrometer. Gel photopolymerisations were carried out in a commercially available nail curing lamp (4 × 9 W bulbs, maximum intensity wavelength 365 nm). Mechanical analysis was carried out on a Shimadzu EZ-LX tensile tester equipped with a 5 N force cell.

Materials

Acryloyl chloride (97%) and 4-dimethylaminopyridine (DMAP) (99%) were purchased from Alfa Aesar. Dicyclohexylcarbodiimide (DCC) (99%), acrylic acid (97%). Dichloromethane (≥99%), DMSO (≥99%), acetonitrile (≥99%), diethyl ether and NaOH (99%) were purchased from Fischer Scientific. Morpholinopropane sulfonic acid (MOPS) (99%) was purchased from TCI Europe. Citric acid (99%), trisodium citrate dihydrate (99%), urease (type III from Jackbean, *Canavalia ensiformis*), Fluorescein-*o*-acrylate, Perchloric acid (70% solution in water), Tribromoacetic acid, Tetramethylammonium hydroxide (25% solution in water) and Poly(ethyleneglycol) MW = 6000 g mol^{-1} (PEG 6K) were purchased from Sigma Aldrich. AMPS (99%) was purchased from Fluka. Acryloxyethyl thiocarbamoyl Rhodamine B was purchased from Polysciences. All chemicals were used as received, except for PEG 6K, which was dried as described below.

4.5.2. Synthesis Procedures

Synthesis of aspartic acid N-acrylamide (A^3)

In a typical procedure, aspartic acid (30 g, 225 mmol) and NaOH (31.5 g, 788 mmol) were dissolved in water (300 mL). The mixture was stirred vigorously and cooled to 0 °C, at which point acryloyl chloride (20 mL, 247 mmol) was added dropwise over the course of 30 minutes. The reaction was stirred at 0 °C for 3 hours, and then at room temperature for a further 4 hours. The aqueous mixture was extracted with EtOAc (3 × 500 mL). The aqueous phase was then adjusted to pH = 2 with conc. HCl and extracted with further EtOAc (9 × 500 mL). The combined organic layers were dried over $MgSO_4$, and their volume reduced in vacuo. A minimum amount of solvent was left to stand overnight for the product to crystallize from. The product was separated by filtration and washed once with minimum ice-cold EtOAc. The product was recovered as an off-white to faint pink solid (27.2 g, 145 mmol, 64% yield).

^{1}H NMR (400 MHz, D_2O, 25 °C, TMS): δ = 6.14 – 5.96 ppm (m, 2H; CH_2), 5.57 ppm (dd, ^3J = 9.7, 1.8 Hz, 1H; CH), 4.62 ppm (t, ^3J = 5.9 Hz, 1H, CH), 2.75 ppm (d, ^3J = 6.1 Hz, 2H; CH_2)

Synthesis of LAP photonitiator

Synthesis was carried out according to previously reported procedure.[46] Briefly, ethyl (2,4,6-trimethylbenzoyl) phenylphosphinate (5.693 g, 18 mmol) was dissolved in 2-butanone (100 mL). Lithium bromide (6.25 g, 72 mmol) was added, and the mixture heated to 50 °C for 10 minutes,

allowed to cool and left to stand overnight. The crystallized product was recovered by filtration, washed with ice-cold 2-butanone and dried in vacuo to yield LAP as a fine white powder in quantitative yield.

Synthesis of poly(ethylene glycol) (6000 g mol^{-1}) diacrylate (PEGDA 6K)

Poly(ethylene glycol) MW = 6000 g mol^{-1} (PEG 6K) (50 g, 8.3 mmol) was dried by heating to 80 °C in a vacuum overnight. To the dried and cooled PEG 6K, dry dichloromethane (200 mL), 4-dimethylaminopyridine (0.3 g, 2.5 mmol) and acrylic acid (3 g, 3.4 mL, 41.6 mmol) were added. The mixture was allowed to homogenize and cooled to 0 °C. Dicyclohexylcarbodiimide (12.8 g, 62.5 mmol) was added, and the mixture stirred for 4 hours at 0 °C, and at room temperature for 48 hours. The precipitated dicyclohexylurea was removed by filtration, the volume of the solvent was reduced in vacuo and the crude product precipitated out of Et_2O. The crude product was redissolved in MeCN, filtered twice to remove additionally precipitated dicyclohexylurea, and the product reprecipitated from Et_2O. The product was recovered as a white powder (42 g, 6.9 mmol, 84% yield).

Gel samples

Responsive gel components were made in water from 10 wt% A^3 monomer (equivalent to a 530 mM concentration), crosslinked with PEGDA 6K in a 50:1 molar ratio, including 0.05 mg·mL^{-1} LAP as photoinitiator, and acryloxyethyl thiocarbamoyl Rhodamine B as dye. Passive gel components were made in water from AMPS, crosslinked with PEGDA 6K, 0.05 mg mL^{-1} LAP photonitiator and fluorescein-*o*-acrylate as dye. Urease-containing gel components were made with 10 mg mL^{-1} urease, 25 wt% PEGDA 6K and 0.05 mg mL^{-1} LAP.

The solutions were then placed in PTFE molds and irradiated with 365 nm light for 3 minutes. Gel samples were then typically placed in 5 mM MOPS in 70/30 v/v H_2O/DMSO (pH = 7.2) to equilibrate.

4.5.3. pH measurements

A given volume (< 1.5 mL) of MOPS solution prepared at the experimental concentration, with added DMSO at the experimental amount, is placed in a 2.0 mL Eppendorf plastic tube and the initial pH was measured for at least 10 minutes using a pH electrode. A freshly prepared stock solution of fuel acid in MOPS was then added until the solution reached 1.5 mL, at the desired concentration of fuel. The measurements stood for at least 36 hours. Screening experiments (Figure 4.6, Figure 4.7) were run for shorter periods. pH readings in H_2O/DMSO mixtures were calibrated by making solutions of known proton concentration with perchloric acid and tetramethylammonium hydroxide and measuring the observed pH values. These values were then used to generate a calibration plot as previously described.[47]

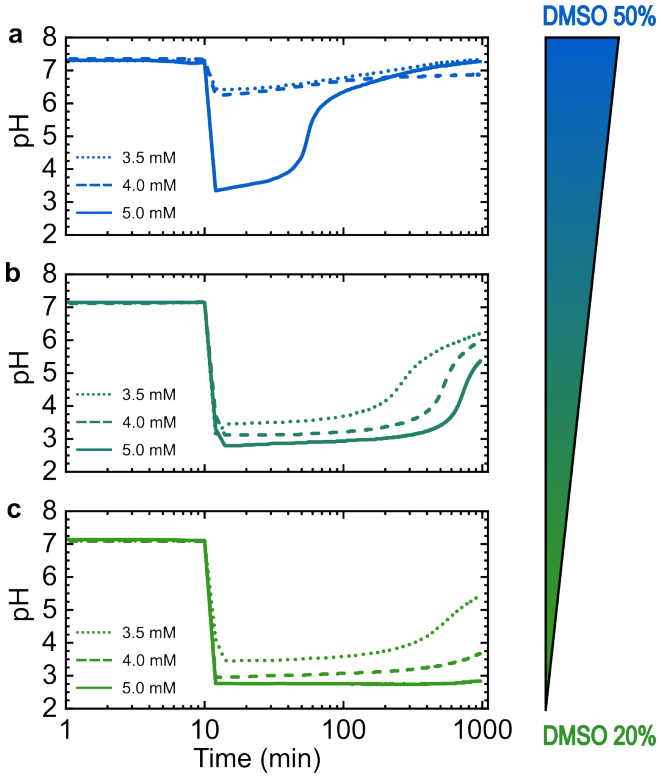

Figure 4.6: Effect of solvent mixture on pH-flip lifetime. pH profiles obtained by adding TBA (3.5, 4.0 and 5.0 mM) to 5.0 mM MOPS pH 7.2 in mixtures with (a) 50/50 v/v H_2O/DMSO, (b) 70/30 v/v H_2O/DMSO and (c) 80/20 v/v H_2O/DMSO. Increasing volume fraction of DMSO greatly shortens lifetime of the pH drop by increasing the rate of decarboxylation.

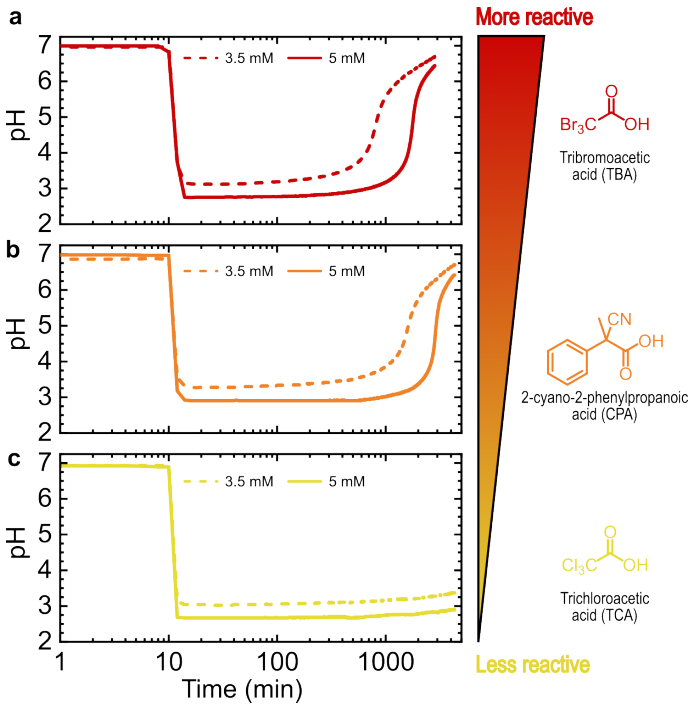

Figure 4.7: pH-flip lifetime in relation to acid. Screening of three self-decarboxylating acids investigated for this study. (a) Tribromoacaetic acid, (b) 2-cyano-2-phenylpropanoic acid, (c) trichloroacetic acid. Experiments carried out in 5.0 mM MOPS in 70/30 v/v H_2O/DMSO at pH 7.2, with 3.5 mM (dashed line) and 5.0 mM (solid line) of acid. Tribromoacetic acid was selected as one-component pH-flip due to the shorter lifetime of the fueled state.

4.5.4. Swelling and Fueling Experiments

After equilibration, gels and devices were placed in fresh 5.0 mM MOPS in 70/30 v/v H_2O/DMSO, and a freshly prepared TBA stock solution was added. 1-D swelling values were obtained by imaging gels from above and dividing the length at a given time by the equilibrium length. Bending angles were obtained by measuring the angle of the line described by the two extremities of the gel, along the interface between the two layers.

Equilibrium swelling values were taken by allowing gels and bilayers to equilibrate for 3 days in 5.0 mM MOPS, adjusted to given pH values (Figure 4.8).

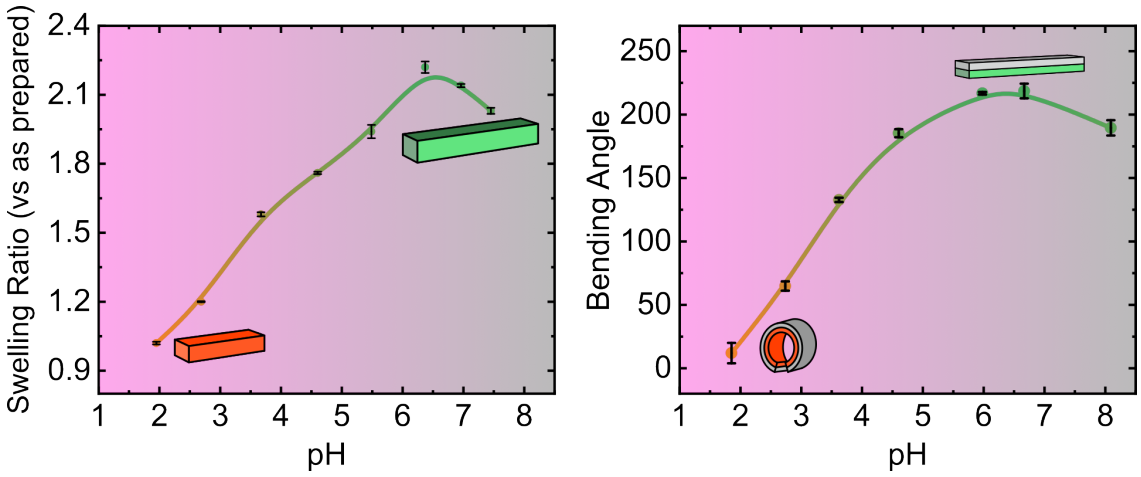

Figure 4.8: Effect of pH on equilibrium swelling of A³ gels and bending of A³/AMPS bilayers. Swelling ratios reported as 1-D ratios in comparison to dimensions as prepared in PTFE molds. Error bars indicate one standard deviation (n = 6). Bending angle taken as angle described by the two ends and midpoint of the bilayer. Error bars indicate one standard deviation (n = 6). All experiments run in 5.0 mM MOPS buffer adjusted to the given pH. With samples equilibrating for 3 days.

4.5.5. Mechanical Analysis of Gels

The aforementioned gels, prepared as dogbones in a 30×2×1 mm mold, were swollen in 5.0 mM MOPS pH 7.2 70/30 v/v H_2O/DMSO for 24 hours. The samples were then placed in a Shimadzu EZ-LX tensile tester equipped with a 5 N force cell, and measured until failure. Figure 4.9 displays the results.

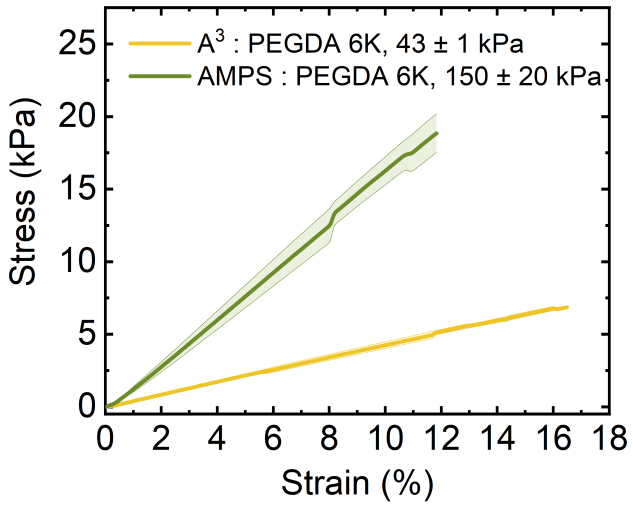

Figure 4.9: Tensile testing of pH-responsive (A³ : PEGDA 6K) and non-responsive (AMPS : PEGDA 6K). Measurements taken on gels swollen in 5.0 mM MOPS buffer, pH 7.2 in 70/30 v/v H_2O/DMSO. Error contours show one standard deviation, n = 4 for both samples.

4.5.6. Statistical Analysis

Data was gathered using the methods outlined above. pH data in H_2O/DMSO mixtures was corrected using the method previously described.[47] All data points featuring statistical analysis are presented as mean ± standard deviation. The sample size for each statistical analysis is reported in the relevant figure legend. Statistical analysis was carried out using Microsoft Excel and Origin Pro 2020.

4.6. Acknowledgements

We acknowledge funding from the European Union's Horizon 2020 research and innovation program under the Marie Skłodowska-Curie grant agreement no. 812868. AW acknowledges funding via a Gutenberg Research Professorship underpinning his Life-Like Materials Program. AW acknowledges funding by an ERC CoG (no. 101001638). DDG and SDS thank SupER project La Sapienza.

4.7. References

[1] G. M. Whitesides, Soft Robotics, *Angew. Chem. Int. Ed.* **2018**, *57*, 4258.

[2] N. El-Atab, R. B. Mishra, F. Al-Modaf, L. Joharji, A. A. Alsharif, H. Alamoudi, M. Diaz, N. Qaiser, M. M. Hussain, Soft Actuators for Soft Robotic Applications: A Review, *Adv. Intell. Syst.* **2020**, *2*, 2000128.

[3] J. Wang, D. Gao, P. S. Lee, Recent Progress in Artificial Muscles for Interactive Soft Robotics, *Adv. Mater.* **2021**, *33*, 2003088.

[4] M. Cianchetti, C. Laschi, A. Menciassi, P. Dario, Biomedical Applications of Soft Robotics, *Nat. Rev. Mater.* **2018**, *3*, 143.

[5] H. Banerjee, M. Suhail, H. Ren, Hydrogel Actuators and Sensors for Biomedical Soft Robots: Brief Overview with Impending Challenges, *Biomimetics* **2018**, *3*, 15.

[6] M. Ding, L. Jing, H. Yang, C. E. Machnicki, X. Fu, K. Li, I. Y. Wong, P. Y. Chen, Multifunctional Soft Machines Based on Stimuli-Responsive Hydrogels: From Freestanding Hydrogels to Smart Integrated Systems, *Mater. Today Adv.* **2020**, *8*, 100088.

[7] H. Arslan, A. Nojoomi, J. Jeon, K. Yum, 3d Printing of Anisotropic Hydrogels with Bioinspired Motion, *Adv. Sci.* **2019**, *6*, 1800703.

[8] R. M. Erb, J. S. Sander, R. Grisch, A. R. Studart, Self-Shaping Composites with Programmable Bioinspired Microstructures, *Nat. Commun.* **2013**, *4*, 1712.

[9] P. Techawanitchai, M. Ebara, N. Idota, T.-A. Asoh, A. Kikuchi, T. Aoyagi, Photo-Switchable Control of Ph-Responsive Actuators Via Ph Jump Reaction, *Soft Matter* **2012**, *8*, 2844.

[10] J. Y. Wang, F. Jin, X. Z. Dong, J. Liu, M. L. Zheng, Flytrap Inspired Ph-Driven 3d Hydrogel Actuator by Femtosecond Laser Microfabrication, *Adv. Mater. Tech.* **2022**, *7*, 2200276.

[11] C. Yang, F. Su, Y. Liang, W. Xu, S. Li, E. Liang, G. Wang, N. Zhou, Q. Wan, X. Ma, Fabrication of a Biomimetic Hydrogel Actuator with Rhythmic Deformation Driven by a Ph Oscillator, *Soft Matter* **2020**, *16*, 2928.

[12] C. Yang, F. Su, Y. Xu, Y. Ma, L. Tang, N. Zhou, E. Liang, G. Wang, J. Tang, Ph Oscillator-Driven Jellyfish-Like Hydrogel Actuator with Dissipative Synergy between Deformation and Fluorescence Color Change, *ACS Macro Lett.* **2022**, *11*, 347.

[13] X. He, Y. Sun, J. Wu, Y. Wang, F. Chen, P. Fan, M. Zhong, S. Xiao, D. Zhang, J. Yang, J. Zheng, Dual-Stimulus Bilayer Hydrogel Actuators with Rapid, Reversible, Bidirectional Bending Behaviors, *J. Mater. Chem. C* **2019**, *7*, 4970.

[14] X. Kong, Y. Li, W. Xu, H. Liang, Z. Xue, Y. Niu, M. Pang, C. Ren, Drosera-Inspired Dual-Actuating Double-Layer Hydrogel Actuator, *Macromol. Rapid Commun.* **2021**, *42*, e2100416.

[15] J. Liu, W. Xu, Z. Kuang, P. Dong, Y. Yao, H. Wu, A. Liu, F. Ye, Gradient Porous Pnipam-Based Hydrogel Actuators with Rapid Response and Flexibly Controllable Deformation, *J. Mater. Chem. C* **2020**, *8*, 12092.

[16] X. Wang, H. Huang, H. Liu, F. Rehfeldt, X. Wang, K. Zhang, Multi-Responsive Bilayer Hydrogel Actuators with Programmable and Precisely Tunable Motions, *Macromol. Chem. Phys.* **2019**, *220*, 1800562.

[17] Z. Jiang, M. L. Tan, M. Taheri, Q. Yan, T. Tsuzuki, M. G. Gardiner, B. Diggle, L. A. Connal, Strong, Self-Healable, and Recyclable Visible-Light-Responsive Hydrogel Actuators, *Angew. Chem. Int. Ed.* **2020**, *59*, 7049.

[18] L. Yang, T. Zhang, W. Sun, Construction of Biocompatible Bilayered Light-Driven Actuator Composed of Rgo / Pnipam and Pegda Hydrogel, *J. Appl. Polym. Sci.* **2020**, *137*, 49375.

[19] S. I. Rich, R. J. Wood, C. Majidi, Untethered Soft Robotics, *Nat. Electron.* **2018**, *1*, 102.

[20] R. Merindol, A. Walther, Materials Learning from Life: Concepts for Active, Adaptive and Autonomous Molecular Systems, *Chem. Soc. Rev.* **2017**, *46*, 5588.

[21] R. Yoshida, Self-Oscillating Gels Driven by the Belousov-Zhabotinsky Reaction as Novel Smart Materials, *Adv. Mater.* **2010**, *22*, 3463.

[22] T. Mikanohara, S. Maeda, Y. Hara, S. Hashimoto, Peristaltic Motion of Tubular Gel Driven by Acid-Autocatalytic Reaction, *Adv. Robot.* **2014**, *28*, 457.

[23] A. Paikar, A. I. Novichkov, A. I. Hanopolskyi, V. A. Smaliak, X. Sui, N. Kampf, E. V. Skorb, S. N. Semenov, Spatiotemporal Regulation of Hydrogel Actuators by Autocatalytic Reaction Networks, *Adv. Mater.* **2022**, *34*, e2106816.

[24] T. Heuser, E. Weyandt, A. Walther, Biocatalytic Feedback-Driven Temporal Programming of Self-Regulating Peptide Hydrogels, *Angew. Chem. Int. Ed.* **2015**, *54*, 13258.

[25] X. Fan, A. Walther, Autonomous Transient Ph Flips Shaped by Layered Compartmentalization of Antagonistic Enzymatic Reactions, *Angew. Chem. Int. Ed.* **2021**, *60*, 3619.

[26] C. Sharma, A. Walther, Self-Regulating Colloidal Co-Assemblies That Accelerate Their Own Destruction Via Chemo-Structural Feedback, *Angew. Chem. Int. Ed.* **2022**, *61*, 202201573.

[27] J. A. Berrocal, C. Biagini, L. Mandolini, S. Di Stefano, Coupling of the Decarboxylation of 2-Cyano-2-Phenylpropanoic Acid to Large-Amplitude Motions: A Convenient Fuel for an Acid-Base-Operated Molecular Switch, *Angew. Chem. Int. Ed.* **2016**, *55*, 6997.

[28] C. Biagini, S. Albano, R. Caruso, L. Mandolini, J. A. Berrocal, S. Di Stefano, Variations in the Fuel Structure Control the Rate of the Back and Forth Motions of a Chemically Fuelled Molecular Switch, *Chem. Sci.* **2018**, *9*, 181.

[29] D. Del Giudice, E. Spatola, R. Cacciapaglia, A. Casnati, L. Baldini, G. Ercolani, S. Di Stefano, Time Programmable Locking/Unlocking of the Calix[4]Arene Scaffold by Means of Chemical Fuels, *Chem. Eur. J.* **2020**, *26*, 14954.

[30] D. Mariottini, D. Del Giudice, G. Ercolani, S. Di Stefano, F. Ricci, Dissipative Operation of Ph-Responsive DNA-Based Nanodevices, *Chem. Sci.* **2021**, *12*, 11735.

[31] L. Heinen, T. Heuser, A. Steinschulte, A. Walther, Antagonistic Enzymes in a Biocatalytic Ph Feedback System Program Autonomous DNA Hydrogel Life Cycles, *Nano Lett.* **2017**, *17*, 4989.

[32] I. Maity, C. Sharma, F. Lossada, A. Walther, Feedback and Communication in Active Hydrogel Spheres with Ph Fronts: Facile Approaches to Grow Soft Hydrogel Structures, *Angew. Chem. Int. Ed.* **2021**, *60*, 22537.

[33] T. Heuser, R. Merindol, S. Loescher, A. Klaus, A. Walther, Photonic Devices out of Equilibrium: Transient Memory, Signal Propagation, and Sensing, *Adv. Mater.* **2017**, *29*, 1606842.

[34] C. Biagini, S. Di Stefano, Abiotic Chemical Fuels for the Operation of Molecular Machines, *Angew. Chem. Int. Ed.* **2020**, *59*, 8344.

[35] D. J. B. Lydia L. Lifongo, Peter Brimblecombe, Thermal Degradation of Haloacetic Acids in Water, *Int. J. Phys. Sci* **1992**, *Vol. 5(6)*, 738.

[36] D. Del Giudice, E. Spatola, M. Valentini, C. Bombelli, G. Ercolani, S. Di Stefano, Time-Programmable Ph: Decarboxylation of Nitroacetic Acid Allows the Time-Controlled Rising of Ph to a Definite Value, *Chem. Sci.* **2021**, *12*, 7460.

[37] V. W. Liyana Gunawardana, T. J. Finnegan, C. E. Ward, C. E. Moore, J. D. Badjic, Dissipative Formation of Covalent Basket Cages, *Angew. Chem. Int. Ed.* **2022**, *61*, e202207418.

[38] G. Rabai, I. Hanazaki, Ph Oscillations in the Bromate-Sulfite-Marble Semibatch and Flow Systems, *J. Phys. Chem.* **1996**, *100*, 10615.

[39] P. Warneck, The Formaldehyde-Sulfite Clock Reaction Revisited, *J. Chem. Educ.* **1989**, *66*, 334.

[40] H. Valle, J. Sánchez, B. L. Rivas, Poly(N-Vinylpyrrolidone-Co-2-Acrylamido-2-Methylpropanesulfonate Sodium): Synthesis, Characterization, and Its Potential Application for the Removal of Metal Ions from Aqueous Solution, *J. Appl. Polym. Sci.* **2015**, *132*, 41272.

[41] Y. Li, T. Tanaka, Kinetics of Swelling and Shrinking of Gels, *J. Chem. Phys.* **1990**, *92*, 1365.

[42] H. Che, B. C. Buddingh, J. C. M. van Hest, Self-Regulated and Temporal Control of a "Breathing" Microgel Mediated by Enzymatic Reaction, *Angew. Chem. Int. Ed.* **2017**, *56*, 12581.

[43] N. Singh, G. J. M. Formon, S. De Piccoli, T. M. Hermans, Devising Synthetic Reaction Cycles for Dissipative Nonequilibrium Self-Assembly, *Adv. Mater.* **2020**, *32*, e1906834.

[44] I. Piergentili, P. R. Bouwmans, L. Reinalda, R. W. Lewis, B. Klemm, H. Liu, R. M. de Kruijff, A. G. Denkova, R. Eelkema, Thioanisole Ester Based Logic Gate Cascade to Control Ros-Triggered Micellar Degradation, *Polym. Chem.* **2022**, *13*, 2383.

[45] A. Walther, Viewpoint: From Responsive to Adaptive and Interactive Materials and Materials Systems: A Roadmap, *Adv. Mater.* **2020**, *32*, e1905111.

[46] B. D. Fairbanks, M. P. Schwartz, C. N. Bowman, K. S. Anseth, Photoinitiated Polymerization of Peg-Diacrylate with Lithium Phenyl-2,4,6-Trimethylbenzoylphosphinate: Polymerization Rate and Cytocompatibility, *Biomaterials* **2009**, *30*, 6702.

[47] L. Baldini, R. Cacciapaglia, A. Casnati, L. Mandolini, R. Salvio, F. Sansone, R. Ungaro, Upper Rim Guanidinocalix[4]Arenes as Artificial Phosphodiesterases, *J. Org. Chem.* **2012**, *77*, 3381.

Chapter

5 Conclusions

5.1. Conclusions

Over the course of this thesis, we have demonstrated the use of polymeric materials based on the aspartic acid *N*-acrylamide (A^3) building block as a platform for the study of effect of polymeric architecture on dissipative, out-of-equilibrium material systems. We exploit its dual responsiveness to carbodiimide fuels and pH stimuli to operate both active material and active environment type chemical reaction networks. The former relies on the direct activation of A^3 aspartate units by N-ethyl-N'-(3-dimethylaminopropyl)carbodiimide) (EDC), leading to the formation of a 5-memebred intramolecular anhydride ring, with deactivation arising from hydrolysis of said anhydride. The latter CRN employs the self-decarboxylating tribromoacetic acid (TBA) as a single-molecule chemical fuel which drives a time-programmed pH drop by releasing a proton, decarboxylating to yield a carbanion, and scavenging released protons to return pH to the original value.

In **Chapter 2**, we employed EDC as a chemical fuel to drive the solution-phase self-assembly of block copolymers (BCPs) featuring a poly(*N*-acryloylmorpholine) (PNAM) hydrophilic segment and a switchable poly(aspartic acid *N*-acrylamide-*co-tert*-butylacrylamide) (A^3-*co*-*t*-BuAm). We examined the effects of multiple parameters on the lifetime and morphology of the resulting structures, in contrast to previous studies on EDC-fueled copolymer self-assembly.[1-2] Through turbidimetric observations and time-series dynamic light scattering (DLS) measurements, we showed that by altering the ratio of switchable A^3 monomer and the hydrophobic *t*-BuAm within the responsive block to include more hydrophobic monomer, we can exert control on the threshold concentration of fuel required for self-assembly, and we show increased fuel efficiency by demonstrating that significantly longer self-assembled lifetimes may be obtained while requiring less fuel. We attribute this behavior to increased overall hydrophobicity of the responsive block at higher *t*-BuAm content, requiring a smaller percentage of A^3 units to undergo EDC-fueled anhydride formations before the BCPs are driven to assembly. The significant increase in lifetimes observed is instead attributed to kinetic trapping of the polymer assemblies in a manner reminiscent of that observed in peptides.[3] By using a methylated analogue self-assembled *via* solvent exchange, we employed transmission electron microscopy (TEM) imaging to explore the effect of passive block length and responsive block composition on the morphology of the assemblies, which we rationalized through the effect of polymer structure on packing parameter. These observations were then used to contextualize DLS measurements showing the evolution of the fueled polymer assemblies over time. Finally, cryo-TEM imaging revealed the formation of polymersomes and elongated worm-like structures in fueled samples, confirming the observations made *via* DLS.

Ideally, future work would be able combine additional techniques to study the morphology of the polymer assemblies, such as small-angle x-ray scattering, with kinetic studies of fuel consumption[4] to further understand how these factors are influenced by polymer structure.

In **Chapter 3**, we went on to employ TBA as a chemical fuel to drive an active environment CRN, which controls the pH-dependent self-assembly of poly(NAM-*b*-(A^3-*co*-*t*-BuAm)) BCPs. By altering the ratio of pH-responsive A^3 to hydrophobic *t*-BuAm monomers in the responsive block, we showed through turbidimetric titrations that there is a significant increase in threshold assembly pH values as *t*-BuAm mole ratio increases. We likewise showed that increase in hydrophobic monomer leads to increased hysteresis between assembly and disassembly pH, and attribute this effect to reduced capacity for electrostatic stabilization of the solvated polymers and kinetic trapping of the polymer assemblies. We explored the lifetime of the assembled state as a function of fuel loading *via* turbidimetric measurements, and duration and magnitude of the pH drop through *in situ* pH measurements. We then employ this data to build a kinetic model of the TBA CRN, which is capable of accurately predicting the evolution of system pH over time as a function of both fuel loading and polymer composition, accounting for the buffering effects of the polymer and waste carbon dioxide on the system. This is, to our knowledge, the first report of the use of activated carboxylic acids as fuels for aqueous-phase self-assembly of polymeric materials. Our results demonstrate the ease of use of this fuel system as well as provide a blueprint for its application to self-assembly of polymers.

Building on the understanding gained of the TBA CRN and pH-responsiveness of the A^3 building block, in **Chapter 4** we apply the TBA CRN to control swelling of pH-responsive poly(A^3) hydrogels. We first demonstrated how the lifetime of the pH drop can be fine-tuned by altering fuel and buffer concentrations to match the kinetics of gel (de)swelling to achieve transiently deswelling hydrogels. We then coupled pH-responsive poly(A^3) and inert poly(2-acrylamido-2-methylpropane sulfonic acid) hydrogels to obtain bilayer devices whose actuation could be controlled in both magnitude and duration by altering TBA concentration. We subsequently demonstrated the unique benefits of such a batch-applicable CRN by employing it in applications where single-use autonomous operation might be desired, in self-interlocking interfaces and grabbing of perforated objects by means of a swelling harpoon. Finally, we introduced an additional layer of control by including the urea-urease reaction as a downstream, mechanically gated feedback module to shorten actuation lifetimes.

The results presented in this thesis establish design principles for designing dually-responsive polymeric materials to employ in both active material and active environment chemical reaction networks. By carefully designing the polymer material, the behavior of the active material CRN can be tailored, and the material's response to the out-of-equilibrium active environment modified. In particular, the results in **Chapters 3** and **4** show how, in contrast to the complex compositions often required for polymer-coupled CRNs,[5-7] the TBA CRN provides simple control over both the duration and amplitude of a widely applicable environmental stimulus, pH. This in particular sets it apart from previously employed pH-control mechanisms such as clock reactions,[8] dormant deactivator[9] or enzymatic[10-11] systems. Furthermore, by first employing the CRN in a solution-phase system, and then demonstrating control of macroscopic soft robotic aplications, a pathway from material and system design to applications is demonstrated

Given the broad applicability of pH as a stimulus in biological contexts, the great interest in polymeric assemblies as methods of controlled release,[12-13] and soft robotics in the context of bio-compatible and bio-interfaceable implants[14-15], activated-carboxylic acid CRNs hold great promise. Due to the low fuel requirements, waste generation is correspondingly low, half of that waste being aqueous CO_2, which living organisms already have the capacity to easily excrete. However, a key drawback of the system described here is the requirement of a non-aqueous co-solvent to modulate decarboxylation rate, and the toxicity of both the fuel molecule and haloalkane byproduct. The key challenge facing future work is therefore the discovery and design of new fuels that can be employed in conditions closer to those found in living organisms.

5.2. References

[1] X. Lang, U. Thumu, L. Yuan, C. Zheng, H. Zhang, L. He, H. Zhao, C. Zhao, Chemical Fuel-Driven Transient Polymeric Micelle Nanoreactors toward Reversible Trapping and Reaction Acceleration, *Chem. Commun.* **2021**, *57*, 5786.

[2] M. A. Würbser, P. Schwarz, J. Heckel, A. M. Bergmann, A. Walther, J. Boekhoven, Chemically Fueled Block Copolymer Self-Assembly into Transient Nanoreactor, *ChemSystemsChem* **2021**, *3*, e2100015

[3] B. A. K. Kriebisch, C. M. E. Kriebisch, A. M. Bergmann, C. Wanzke, M. Tena-Solsona, J. Boekhoven, Tuning the Kinetic Trapping in Chemically Fueled Self-Assembly, *ChemSystemsChem* **2022**, *5*.

[4] F. Schnitter, J. Boekhoven, A Method to Quench Carbodiimide-Fueled Self-Assembly, *ChemSystemsChem* **2020**, *3*.

[5] R. Yoshida, Self-Oscillating Gels Driven by the Belousov-Zhabotinsky Reaction as Novel Smart Materials, *Adv. Mater.* **2010**, *22*, 3463.

[6] A. Paikar, A. I. Novichkov, A. I. Hanopolskyi, V. A. Smaliak, X. Sui, N. Kampf, E. V. Skorb, S. N. Semenov, Spatiotemporal Regulation of Hydrogel Actuators by Autocatalytic Reaction Networks, *Adv. Mater.* **2022**, *34*, e2106816.

[7] I. Piergentili, P. R. Bouwmans, L. Reinalda, R. W. Lewis, B. Klemm, H. Liu, R. M. de Kruijff, A. G. Denkova, R. Eelkema, Thioanisole Ester Based Logic Gate Cascade to Control Ros-Triggered Micellar Degradation, *Polym. Chem.* **2022**, *13*, 2383.

[8] G. Rabai, M. Orban, I. R. Epstein, Systematic Design of Chemical Oscillators. 64. Design of Ph-Regulated Oscillators, *Acc. Chem. Res.* **1990**, *23*, 258.

[9] T. Heuser, A. K. Steppert, C. M. Lopez, B. Zhu, A. Walther, Generic Concept to Program the Time Domain of Self-Assemblies with a Self-Regulation Mechanism, *Nano Lett.* **2015**, *15*, 2213.

[10] T. Heuser, E. Weyandt, A. Walther, Biocatalytic Feedback-Driven Temporal Programming of Self-Regulating Peptide Hydrogels, *Angew. Chem. Int. Ed.* **2015**, *54*, 13258.

[11] L. Heinen, T. Heuser, A. Steinschulte, A. Walther, Antagonistic Enzymes in a Biocatalytic Ph Feedback System Program Autonomous DNA Hydrogel Life Cycles, *Nano Lett.* **2017**, *17*, 4989.

[12] R. A. Siegel, Stimuli Sensitive Polymers and Self Regulated Drug Delivery Systems: A Very Partial Review, *J. Controlled Release* **2014**, *190*, 337.

[13] S. Iqbal, M. Blenner, A. Alexander-Bryant, J. Larsen, Polymersomes for Therapeutic Delivery of Protein and Nucleic Acid Macromolecules: From Design to Therapeutic Applications, *Biomacromolecules* **2020**, *21*, 1327.

[14] M. Cianchetti, C. Laschi, A. Menciassi, P. Dario, Biomedical Applications of Soft Robotics, *Nat. Rev. Mater.* **2018**, *3*, 143.

[15] H. Banerjee, M. Suhail, H. Ren, Hydrogel Actuators and Sensors for Biomedical Soft Robots: Brief Overview with Impending Challenges, *Biomimetics* **2018**, *3*, 15.

Chapter

6 Acknowledgements